

**PHYSICS OF FOAM FORMATION ON A SOLID
SURFACE IN CARBONATED LIQUIDS**

A.F. Zuidberg

Promotor: Dr. A. Prins
hoogleraar fysika en fysische chemie van levensmiddelen
met bijzondere aandacht voor de zuivel

Co-Promotor: Dr. ir. H.J. Bos
universitair docent theoretische aerodynamica

WNO8201, 2290

PHYSICS OF FOAM FORMATION ON A SOLID SURFACE IN CARBONATED LIQUIDS

Antien Frances Zuidberg

Proefschrift

ter verkrijging van de graad van doctor
op gezag van de rector magnificus
van de Landbouwuniversiteit Wageningen,
dr. C.M. KarsSEN,
in het openbaar te verdedigen
op donderdag 19 juni 1997
des namiddags te half twee in de Aula.

WNO 8201 2290

CIP-DATA KONINKLIJKE BIBLIOTHEEK, DEN HAAG

Zuidberg A.F.

Physics of foam formation on a solid surface in carbonated liquids/

A.F. Zuidberg. - [S.l.: s.n.]

Thesis Wageningen. - with ref. -with summary in English and Dutch.

ISBN 90-5485-697-1

Subject headings:

Foam formation/ Bubble/ Solid surface/ Carbonated liquids/ Supersaturation

Druk: Ponsen & Looijen bv Wageningen

BIBLIOTHEEK
LANDBOUW/UNIVERSITEIT
WAGENINGEN

STELLINGEN

1. Een volume gas dat zich in een holte in een hydrofoob oppervlak bevindt kan thermodynamisch veel stabieler zijn dan wanneer het een hydrofiel oppervlak betreft.
Dit proefschrift
2. De convectiestroming veroorzaakt door het opstijgen van een zwerm bellen versnelt de schuimvorming op "actieve oppervlakken" in een oververzadigde oplossing.
Dit proefschrift
3. Om een homogeen schuim in een oververzadigde vloeistof te vormen is het van belang om een vlak "actief oppervlak" verticaal in de vloeistof te plaatsen.
Dit proefschrift
4. Bij het opleggen van een oscillerende beweging op een bel, die in een vloeistof aan een capillaire vastzit, kunnen, naast de traagheids-, viskeuze, opwaartse en capillaire krachten, de dynamische oppervlakte eigenschappen van de vloeistof een belangrijke invloed uitoefenen op de grootte van de loslatende bel.
Dit proefschrift
5. Onder nucleatie van gasbellen wordt in de literatuur behalve kiemvorming ook fasegroei verstaan hetgeen tot grote verwarring kan leiden.
6. Bij mensen die trachten af te vallen is het vaak de portemonee die het snelst in gewicht afneemt.
7. Het doen van gooien- en smijtproeven, ook lawaaioproefjes genoemd, zijn het meest succesvol voor het krijgen van fysisch inzicht als men zo onbezonnen mogelijk te werk gaat.
8. Als je spontaan bent heb je aan een half woord genoeg om het verkeerd te begrijpen.
9. De leus "een slimme meid is op haar toekomst voorbereid" wringt met de leus "een slimme meid heeft haar zwangerschap op tijd".
10. Bier uit een plastic beker zou beter smaken als het plastic niet hydrofoob was.

Stellingen behorende bij het proefschrift "Physics of foam formation on a solid surface in carbonated liquids" door A.F. Zuidberg. Wageningen 19 juni 1997.

“ In de wetenschap lijken wij op kinderen, die aan de oever der kennis hier en daar een steentje oprapen, terwijl de wijde oceaan van het onbekende zich voor onze ogen uitstrekt.”

John Newton (1725-1807)

Contents

1. Introduction	
1.1 Motivation	11
1.2 Aim of the project	13
1.3 Hypothesis	13
1.4 Outline of the thesis	14
References	15
2. General Theory	
2.1 Introduction	17
2.2 Bubble formation in gas supersaturated solutions	18
2.2.1 Terminology	19
2.2.2 Homogeneous nucleation theory	21
2.2.3 Heterogeneous nucleation and bubble formation	24
2.3 Effect of 'hinterland' volume on bubble growth at active sites	36
2.3.1 Theoretical approach	37
2.3.2 Bubble 'blow-up' instability	43
2.3.3 Retreat of the gas-liquid interface	44
2.3.4 Discussion	46
2.4 Solubility of CO ₂ in beer	47
2.5 Equilibrium and dynamic surface properties	50
2.6 Components contributing to the foaming properties and to the dynamic surface properties of beer.	53
2.7 'Skins' in beer	56
2.8 Conclusions	57
References	58
3. Bubble formation and growth on a capillary	
3.1 Introduction	63
3.2 Bubble size at detachment	63
3.2.1 Forces acting on a bubble attached to a solid surface	64
3.2.2 Effect of surface wetting on bubble size	65
3.2.3 Effect of variables on bubble size	69
3.3 Bubble growth rate	73
3.3.1 Diffusion driven bubble growth	73
3.3.2 Bubble growth models	75
3.4 Experimental	76
3.4.1 Materials	76
3.4.2 Methods	77
3.5 Results and Discussion	79
3.5.1 Bubble size at detachment	79
3.5.2 Bubble growth rate	86
3.6 Conclusions	96
References	97
Appendix III.1	99
Appendix III.2	104

4. Effect of motion and tilting angle on the bubble size	
4.1 Introduction	109
4.2 Theoretical	110
4.2.1 Bubble detachment at rest	111
4.2.2 Effect of the tilting angle ϕ	112
4.2.3 Oscillatory motion	112
4.2.4 Forces acting on a bubble in motion	114
4.3 Experimental	117
4.3.1 Materials	117
4.3.2 Methods	118
4.4 Results & Discussion	120
4.4.1 Tilting angle	121
4.4.2 Oscillatory motion	122
4.4.3 Surface rheology	129
4.5 Conclusions	132
References	134
5. Bubble rise	
5.1 Introduction	135
5.2 Theoretical	135
5.2.1 Terminal velocity of a gas bubble rising freely in a liquid	135
5.2.2 Bubble growth during rise	140
5.3 Experimental	143
5.3.1 Materials	143
5.3.2 Methods	144
5.3.3 Theoretical calculations	147
5.4 Results & Discussion	147
5.4.1 Terminal velocity of bubbles in beer and buffer	148
5.4.2 Rising bubbles in supersaturated beer and buffer solutions	149
5.4.3 Comparison between rigid sphere model and experimental results	152
5.4.4 Model calculations for bubble growth during rise	156
5.5 Conclusions	158
References	159
6. Tyvek: An ideal active surface?	
6.1 Introduction	161
6.2 Theory	163
6.2.1 Hypothesis of bubble formation	163
6.2.2 Effect of wetting and surface properties on bubble formation	164
6.3 Experimental	167
6.3.1 Methods	167
6.3.2 Materials	168
6.4 Results & Discussion	170
6.4.1 Wetting effect of beer on foamability of different surfaces	170
6.4.2 SEM and Cryo-SEM	172
6.4.3 Wetting of Tyvek in various liquids	176

6.4.4 Relation between wetting and foaming of Tyvek	179
6.4.5 Model active surface: wetting and foamability in beer	185
6.4.6 Size distribution of bubbles formed on Tyvek, in beer	187
6.4.7 Size of active sites in Tyvek material	188
6.5 Model calculation of foam produced on Tyvek surface	189
6.6 Conclusions	190
References	192
Appendix VI.1	193
7. Foam formation on Tyvek material	
7.1 Introduction	195
7.2 Literature	196
7.3 Experimental	198
7.3.1 Methods	198
7.3.2 Materials	204
7.4 Results & Discussion	206
7.4.1 Bubble size distribution	206
7.4.2 Effect of Tyvek manipulation	208
7.4.3 Effect of gas content	213
7.4.4 Quantifying the effect of concentration, Tyvek area and depletion on the foam height formation rate	215
7.5 Conclusions	219
References	220
Appendix VII.1	221
8. General Discussion and Conclusions	
General Discussion and Conclusions	223
References	225
Summary	227
Sammenvatting	231
Nawoord	235
Curriculum Vitae	236

INTRODUCTION

1.1 Motivation

The formation and subsequent stability of foams is a widely studied subject all over the world, and its application is found in a great many branches of industry. Not in all its applications, however, is bubble formation a popular phenomenon. For example, the cavitation of bubbles can generally be a problem in causing severe damage to ships propellers as well as to household boiling appliances (Apfel, 1970). Furthermore, in treating waste from for example, dairy plants (Wheatley *et al.*, 1988), the formation of foam causes a big problem. Similarly, in the dairy industry, quite often anti-foamers have to be used to restrict problems during the processing of whey. Deep sea divers can get a disease called the "bends" as a result of bubble formation in the blood stream, when depressurisation is not precisely controlled (Harvey *et al.*, 1944).

On the other hand, foam can also be very wanted and a lot of effort is being put to increasing its foam stability in for example aerated whipped cream (Wijnen, to be published). Other products such as foamed concrete (van Dijk, 1992) also profit from increased foam stability. Foams are increasingly used in very different kinds of applications: shaving cream, hair stabilisers, oil recovery, photographic films, ice cream, wafers, fire fighting foams, etc.. Some food products where the formation of foam is very wanted is bread (Kokelaar, 1994), and of course carbonated liquids such as beer (Ronteltap, 1989). In most of these cases, the formation and stability of bubbles is still not fully understood.

In general, bubbles can be produced in a liquid by agitating or whipping, by sparging or diffusing gas through a porous material, and by decreasing the pressure of a gas saturated liquid. In the latter case, the liquid becomes supersaturated following the pressure release, as a result of which bubbles can be formed. The supersaturation then has a large influence on the bubble formation, but specific details such as bubble size and amount of bubbles per unit time are mostly influenced by the solid surface at which the bubbles are formed. For example, carbonated liquid drinks form bubbles at the surfaces of the containers in which they are kept. In that case, the amount of bubbles formed and their size at detachment from the container wall is directly influenced by the physical properties of the surface of the container.

The recent study by Ronteltap (1989) shows that the initial bubble size distribution is, amongst others, a very important parameter which can have a large influence on the stability of foam against collapse. In supersaturated liquids such as beer, the surface at which the bubbles are formed plays a large role in determining that initial bubble size

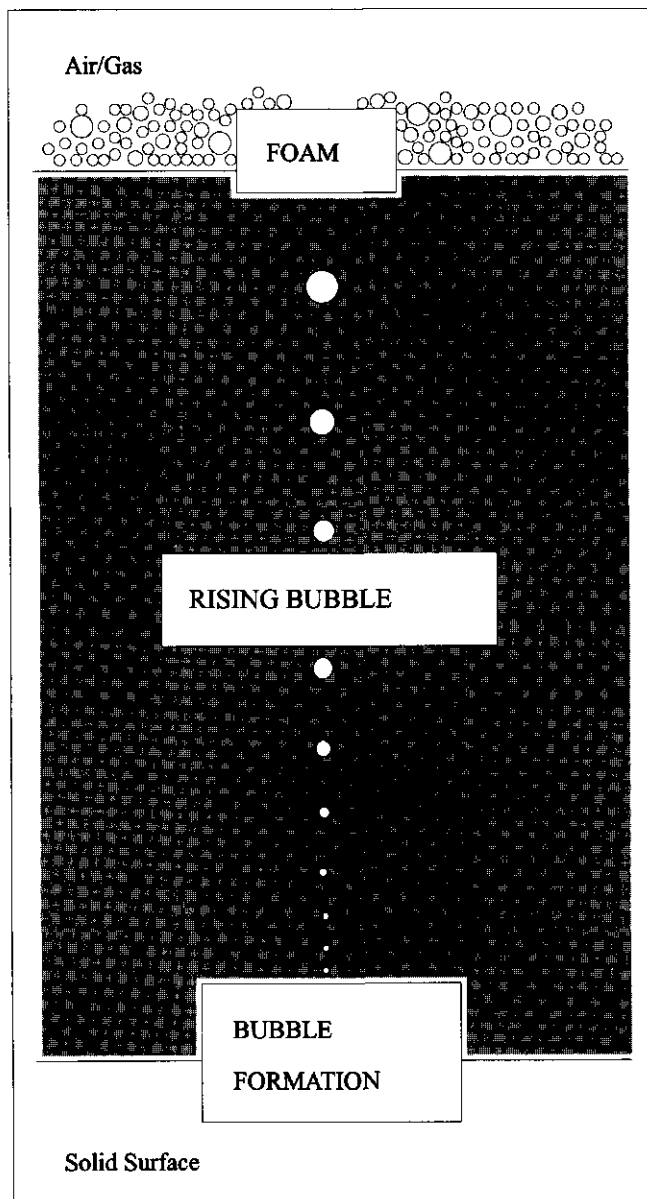


Figure 1.1 Schematic process of bubbles forming and growing at an active surface, detaching from the solid surface, and rising though the supersaturated liquid to join the foam layer.

distribution. For this reason, this investigation studies the effect of physical properties of the solid surface on a foam layer which is formed from that surface. To monitor foaming behaviour “active” surfaces are sometimes used in supersaturated liquids in order to produce the required amount and type of foam.

1.2 Aim of the project

By studying the physical mechanisms responsible for formation and growth of the bubbles that are produced on “active” surfaces and later found in the foam layer, we aim to find the relation between the physical properties of the solid surface and the liquid, and the foam behaviour of that liquid.

1.3 Hypothesis

The hypothesis of this work is that a bubble found in a foam layer has undergone a number of different processes before reaching its destination: formation at an “active” surface, growth at an “active” surface, detachment from an “active” surface and rise to the liquid surface (see figure 1.1). In the observed system, bubbles cannot be formed by homogeneous nucleation, since this would require an impractically large supersaturation level of gas in the liquid.

In the range of gas supersaturation used in the studied systems, heterogeneous bubble growth will only occur at catalytic sites on so called “active” surfaces, from a pre-existent nucleus or a solid surface in which a gas filled cavity is present. The physical properties of surface and liquid, such as the wetting conditions, determine whether a surface is catalytic or not, under set conditions. Nuclei will grow into bubbles only if physical parameters such as supersaturation and contact angle are suitable. The kinetics of growth depend on the gas concentration, on the gas transport rate through the liquid, on the pressure difference between the bubble and its surroundings, and on the surface properties of the bubble.

The maximum bubble size or volume depends on adhesion forces between the bubble and the solid surface (dynamic surface tension and contact angle) and the perimeter of contact with the surface. The bubble detaches when the buoyancy force exceeds the surface tension force. From the point of detachment, the bubble rises to the liquid surface to take part in the initial foam layer. The bubble size distribution in the initial foam then starts to affect the physical processes that occur during the ageing of the foam.

Studying the processes described above, the overall effect of the active surface can be found: we therefore assume that there is a relation between the physical properties of the active surface on which bubbles are produced, the physical properties of the supersaturated liquid and the physical properties of the resulting foam layer.

1.4 Outline of the thesis

A general literature review of available theory is presented in chapter 2. Due to lack of information on the physics of bubble formation at an active site from a supersaturated liquid, there was a need to perform model experiments of growth and detachment of individual bubbles at defined “active” sites. For this purpose, a glass capillary, which was closed on one end, was used to act as a model “active” site. In chapters 3 and 4, the effect of different properties of the solid surface on the formation and growth of bubbles was studied. In chapter 3, we varied the capillary radius, the hinterland volume, and measured the bubble size at detachment, as well as the growth rate at various supersaturation levels of the gas in the liquid. We attempted to predict the growth rates using several available calculation models. Uncontrolled depletion and convection were found to have a considerable effect on the growth rate of the bubbles. When bubbles grow for example at the wall of a glass of champagne, usually the liquid is agitated in some way. Furthermore the bubbles usually grow and detach from a vertical wall. For these reasons we studied the effect that tilting the capillary and that liquid flow has on the growth and detachment of the bubbles in chapter 4. Agitating a supersaturated solution, however, generally results in abundant, unwanted bubble formation, which would make it difficult to study one bubble in detail. It was therefore decided to move the bubble with the capillary in respect to the liquid, as opposed to the other way around.

When the bubble detaches from the surface and rises through the liquid, it is presumed to continue to grow until it reaches the foam layer. It was therefore decided to undertake the difficult task to measure the size of individual bubbles and their velocity during bubble rise, as shown in chapter 5.

With the results obtained from the bubble formation on a model “active” site, it was possible to define the requirements of an “active” surface that would produce a certain amount of bubbles of a certain size in a certain amount of time, even after a long period of storage in the supersaturated solution. We were successful in selecting a material suitable for the formation of enough bubbles in a supersaturated beer to form a layer of foam within seconds. This proved rather difficult, due to the good wetting properties of the supersaturated solution which we used. However, a suitable surface was found and tested on surface properties in chapter 6 and on foaming ability in chapter 7. From the results obtained from the growth of individual bubbles in the chapter 3, a simple predictive model of the foam formation on “active” surfaces in supersaturated liquids could be derived. Comparison with data from the foaming experiments with the “active” surface in chapter 7 showed that using a reasonably simple calculation method, it is possible to make a rough prediction of the amount of foam produced from a heterogeneous and reasonably defined “active” surface.

References

Apfel, R.E. (1970) The Role of Impurities in Cavitation-Threshold Determination *The Journal of the Acoustical Society of America* **48** (5), 1179-1186.

van Dijk, S. (1992) Schuimbeton: het andere beton als speerpunt in de bouw *De Ingenieur* **11**, p.48.

Harvey, E.N., Barnes, D.K., McElroy, W.D., Whitley, A.H., Pease, D.C. and Cooper, K.W. (1944) Bubble formation in animals, *J. Cell. and Comp. Phys.* **24** (1), 1-22.

Kokelaar, J.J. (1994) Physics of breadmaking, Ph. D. Thesis, Agricultural University Wageningen, The Netherlands, 129p.

Ronteltap, A.D. (1989) Beer Foam Physics, Ph. D. Thesis, Agricultural University Wageningen, The Netherlands, 133p.

Wheatley, A.D., Johnson, K.A. and Winstanley, C.I. (1988) Foaming in activated sludge plants treating dairy waste *Environmental Technology Letters* **9**, 181-190.

Wijnen, M.E. (to be published) Ph. D. thesis, Agricultural University Wageningen, The Netherlands.

GENERAL THEORY

2.1 Introduction

Foam formation is an important physical characteristic of carbonised beverages. In general such type of aerated drinks have a foaming behaviour which can be short-lived or transient, or of a somewhat more permanent nature. For producers of such drinks, it is a difficult task to keep the foaming properties and behaviour as constant as possible to satisfy the consumer. For example, the formation of foam in beer is of great importance in some countries, but reproducing a foam of constant quality is still found to be very difficult. To this end a better knowledge about the physical processes that determine the quality and quantity of the beer foam is a prerogative.

Until a few years ago, not so much was known about beer foam stability. Ronteltap (1989) observed beer foam behaviour in terms of physical processes that chiefly determine foam breakdown. Although the bubble formation process does not influence foam behaviour at first sight, this influence is quite pronounced. Very important factors for the stability of beer foam like gas content and composition, bubble size and bubble size distribution and bubble surface composition are determined during the bubble formation process. Ronteltap (1989) himself did not, however, go into the bubble formation processes.

In beer, the bubbles are formed as a result of an oversaturation of (usually) CO₂ gas, shortly before consumption. With the dispense of beer from a tap, bubbles are formed within the faucet and the beer and foam are poured together into a glass. When opening a can or bottle of beer the pressure is released and oversaturation occurs. However, this supersaturation does not necessarily lead to bubble formation within the container. Only in certain situations like shaking the bottle before opening will bubble formation occur after pressure release. This can be explained by the formation of small stable bubbles or nuclei during shaking which start to grow when the beer becomes supersaturated. In a quiescent situation, however, bubbles will not be formed until the beer is poured into a glass. More often than not, the produced foam will not be very stable due to the wide bubble size distribution in the foam and/or glass hygiene. In both methods of dispense, bubbles are formed on a solid surface, and presumably at those sites where gas is entrapped in small cracks, pits and grooves. For the tapped beer this happens within the faucet, for poured beer from a bottle or can this occurs at the wall of the drinking vessel and at the (dry) mouth of the bottle.

In the last years producers of beer have found ways to induce foam formation within the dispense container, after release of the pressure. Various forms of this kind of instant foaming devices are for example gas jetting and liquid jetting, as well as the application of active surfaces, i.e. insertion of solid surfaces filled with crevices and pores. These crevices can entrap gas, and supply the beer with a great number of nuclei, from which bubbles can be formed. This way, the formation of foam can be better controlled.

In this chapter, a review is presented of the literature relevant to the research on the bubble formation on active solid surfaces in relation to the stability of the resulting foam head.

We will discuss the different modes of bubble formation in gas supersaturated solutions. The presence of pre-existent nuclei in the bubble formation in beer will be shown to be of great importance for the formation of beer foam. Furthermore, the surface properties necessary for the long term stabilisation of pre-existent nuclei, such as wetting angle, surface roughness, and the formation of surface layers at the gas-liquid interface will be discussed in view of the formation of foam from an active surface (see chapter 6).

In supersaturated solutions, some knowledge is needed about the solubility of gas in the liquid in order to predict the rate of bubble formation (see chapter 3).

A review is presented of the components present which may influence the surface properties of beer, as well as the formation of foams in general. This knowledge is needed to understand the physical mechanisms during bubble detachment under influence of shear forces (see chapter 4) as well as understanding the rise behaviour of beer bubbles (see chapter 5).

2.2 Bubble formation in gas-supersaturated solutions

Bubbles in aqueous solutions can be formed when the solution becomes supersaturated with a gaseous phase, whether it be vapour or gas. Here we only describe the situation where the solution becomes supersaturated with a gas due to a decrease in pressure after having saturated the solution with gas. In literature two mechanisms of bubble formation are mentioned: homogeneous and heterogeneous nucleation. Homogeneous nucleation is the *de novo* formation of a new phase. It has been calculated that a bubble will be formed via this mechanism if the supersaturation level is a thousand-fold and when the liquid contains no catalytic surfaces. It is for this reason that in practical situations bubble formation in solutions with supersaturation degrees typical of carbonated beverages will most likely follow the heterogeneous nucleation mechanism.

Less activation energy is needed for the heterogeneous formation of a nucleus due to the presence of catalytic sites or pre-existent gas phase. A catalytic site is a place on a solid surface where a nucleus may form easily due to the energetically favourable surface

properties of the substrate. A pre-existent nucleus is a small gas mass which only needs energy and gas transfer in order to grow into a bubble. The latter is called heterogeneous bubble growth, as opposed to heterogeneous nucleation, where *de novo* formation is explicitly implied.

2.2.1 Terminology

In order to prevent misunderstandings concerning the terminology used and presented in this thesis, definitions of the various idioms are given here. In some cases, the definitions are literally copied from references, and in other cases where the available literature is rather vague a more detailed description of our thoughts on the subject is formulated.

As we find in some references, a distinction can be made between a nucleus and a bubble, both of which are gas masses, except that the nucleus is the first stage and the bubble the last stage during bubble formation. There is undoubtedly an arbitrary point in the growth of a nucleus at which it becomes a bubble, but it is practically impossible to define this point exactly, either in terms of size or shape. In this work, a large mass of gas in the liquid sticking to a solid surface (usually spherical) is called a bubble, whereas a minute invisible sphere of gas free in the liquid or situated at an interface is called a nucleus.

Two modes of bubble formation are defined in the literature: homogeneous and heterogeneous nucleation. Homogeneous nucleation occurs when during boiling superheating occurs, or in this case, when the gas supersaturation ratio is above a level characteristic for the system, where the energy barrier necessary to create new interface is low enough. Homogeneous nucleation is the term specifying a nucleus that is formed spontaneously in a liquid, and this *de novo* formation of bubbles (Harvey *et al.*, 1944) usually only occurs at very high gas supersaturation ratios (Wilt, 1986).

Heterogeneous nucleation is a process similar to homogeneous nucleation, but the *de novo* formation of bubbles takes place at a solid surface in contact with the liquid phase. Due to energy-barrier-lowering effects, heterogeneous nucleation may occur at lower supersaturation ratios than homogeneous nucleation.

The two most important energy-barrier-lowering effects are the presence of 'catalytic sites' and the presence of 'pre-existent nuclei' (also called Harvey nuclei by Lubetkin (1989a) among others). Analogous to the definition of a 'catalytic impurity' that can facilitate fast crystallization (Prins *et al.*, 1986), a catalytic site can be defined as a place on a solid surface where the free activation energy for nucleation is lower than in the bulk liquid, i.e. due to the geometry of the site or due to the wetting properties of the substrate and the surface tension of the liquid phase.

A **pre-existent nucleus** is a volume of gas molecules grouped together to form a gas-liquid interface. The term pre-existent refers to the fact that the nucleus is already present, i.e. the new interface has already been created, so that the activation energy necessary for bubble formation is very low or even negative. This means that a pre-existent nucleus can grow immediately by diffusion if it is present in sufficiently supersaturated solution and a bubble may be rapidly formed. Without supersaturation, the growth of the gas phase depends on the curvature of the gas-liquid interface. Such a process is comparable to the addition of a crystal to a super-cooled or supersaturated solution, with two differences: (1) only crystals of the same substance or an isomorphic can act as 'seeds', whereas any gas mass, even a cavity filled with water vapour, will serve to start a bubble; (2) growth on a crystal is continuous until the supersaturation of the solution disappears, whereas growth of a gas mass may be temporary due to thermodynamic instability. A pre-existent nucleus attached to a solid surface may start to enlarge but only after certain critical conditions are met will the growth continue indefinitely, limited only by the amount of available gas.

In this last case we cannot speak of heterogeneous nucleation since, as we mentioned above, the nucleation process is avoided. In this work, growth of bubbles from pre-existent nuclei at alien surfaces will be called 'heterogeneous bubble growth' in contrast to 'heterogeneous nucleation', which is the *de novo* formation of nuclei after which heterogeneous bubble growth can occur. In the situations where it is unclear which process is referred to, we will use the general term 'heterogeneous bubble formation'.

Pre-existent nuclei may be present in the bulk solution or at solid surfaces, in cavities and cracks. These nuclei may have been trapped in cavities when liquid is poured into a vessel, or entrained into the liquid by a liquid jet (Detsch and Sharma, 1990). According to some authors, very small bubbles called micro-bubbles may exist over a long period of time, due to their great stability. Others are convinced that 'bubble ghosts' (Ronteltap and Prins, 1990) may act as catalytic sites for heterogeneous nucleation or even as nuclei for bubble growth. Bubble ghosts are created where the surface active material accumulated at a bubble interface forms an insoluble skin or layer after the bubble has disappeared due to dissolution of the gas.

Assuming no micro-bubbles or bubble ghosts are present, pre-existent nuclei are usually attached to a solid surface at the catalytic sites. Depending on the physical properties of the substrate and the site, and intrinsic properties of the liquid and gaseous phases, the pre-existent nuclei grow into bubbles or dissolve. When bubble growth is apparent, the catalytic site with nucleus is called an active site. An active surface is a solid surface in which is present an amount of active sites. In the situation that the active surface is submerged in a liquid, and the nuclei are removed from the active sites, we call the site deactivated. If no nuclei are left the surface has become inactive.

The following paragraph constitutes the classical nucleation theory. Ward and his colleagues have created a model which is a generalisation of the Gibbs' model. It enables us to determine the critical radius of a nucleus formed due to gas supersaturation of a liquid solution as well as the nucleation rate J (Ward *et al.*, 1970). In the following paragraph heterogeneous nucleation and formation is described. The last paragraph in this section is devoted to what we call heterogeneous bubble growth from active sites. Here we will show how nuclei can stay stable in cracks and cavities in solid surfaces, and what influence wetting and size of the cavity may have on bubble growth.

2.2.2 Homogeneous nucleation theory

Classical nucleation theory for an ideal gas, makes the assumption that bubble nucleation can be described in terms of bulk thermodynamic properties. A definite amount of energy is associated with the reversible formation of a vapour bubble submerged in the liquid. The formation of a nucleus of volume V , where $V = (4/3)\pi R^3$, requires work PV , where P is the pressure of the liquid. When a liquid is under a negative pressure the work PV is negative. However the formation of the new liquid-vapour interface of area A , where $A = 4\pi R^2$, requires work equal to γA , where γ is the liquid-vapour interfacial tension. The overall work required to fill the nucleus or bubble reversibly with vapour, at pressure P_b , is negative and equal to $-P_b V$. The net amount of work, W , associated with the reversible formation of a spherical nucleus of radius R at constant temperature and pressure is therefore:

$$W = \gamma A + PV - P_b V = \gamma A - (P_b - P)V \quad (2.1)$$

In equilibrium the pressure inside the bubble P_b and the pressure in the liquid P are related by the Laplace equation (Ward *et al.*, 1970):

$$\Delta P = P_b - P = \frac{2\gamma}{R_c} \quad (2.2)$$

where R_c is the radius of the bubble. Here, for homogeneous nucleation, R_c is the equilibrium or critical radius. The energy necessary for the creation of a nucleus of a radius nearing R_c or the change in Helmholtz function as a result of the formation of a nucleus as given by equation (2.1) now becomes:

$$W = \Delta F = 4\pi R_c^2 \gamma - \frac{2\gamma}{R_c} \frac{4}{3}\pi R_c^3 = 4\pi R_c^2 \gamma \left(1 - \frac{2}{3} \frac{R_c}{R_c} \right) \quad (2.3)$$

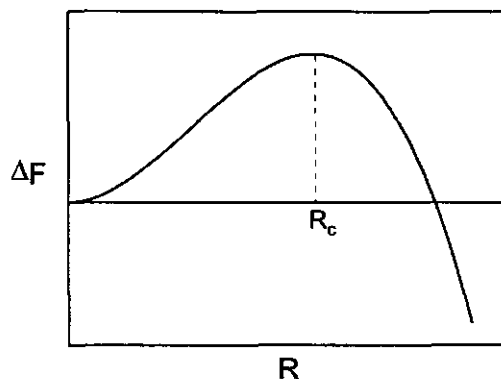


Figure 2.1 The Helmholtz function as a function of the radius of a spherical bubble for homogeneous nucleation (see equation (2.3)).

For isothermal solutions the formation of gas bubbles occurs in order to relieve solution supersaturation. For a case such as carbonated beverages, where a solution is bottled under pressure, when the pressure is released, supersaturation of the gas in solution occurs and gas bubble formation will take place.

The supersaturation is defined as:

$$\alpha = \frac{C}{C_s} \quad (2.4)$$

where C is the concentration of gas in solution and C_s is the saturated gas concentration in solution both at pressure P .

The energy change required for the homogeneous nucleation of a gas bubble as a function of the bubble radius R is shown in figure 2.1. ΔF goes through a maximum, after which the volume increase makes up for the increase in surface. Nucleation, like ordinary chemical kinetics need an activation process leading to the formation of unsteady intermediates known as embryo's. Depending on the activation process an embryo of a certain size will be produced. If this embryo is smaller than the thermodynamically unstable nucleus with critical radius R_c , it will necessarily decrease in size, whereas a nucleus larger than critical size will grow until the supersaturation is alleviated.

The maximum free energy required in order for nucleation to proceed occurs when $R = R_c$ or when $(\delta \Delta F / \delta r)_{T, \alpha} = 0$. The work necessary to create a bubble of critical size follows from equation (2.3):

$$W = \frac{4}{3} \pi \gamma R_c^2 \quad (2.5)$$

From equation (2.2) in which P_b is constituted by the vapour pressure of the solvent and the partial pressure(s) of the gas(es) present, the critical radius of a nucleus in a weak solution of gas dissolved in a liquid is found to be:

$$R_c = \frac{2\gamma_{LG}}{\eta P_v + \alpha P - P} \quad (2.6)$$

where P_v is the vapour pressure of the pure solvent; γ_{LG} is the surface tension of the liquid-gas interface; and η is the correction of the vapour pressure for a concave interface (usually close to unity) defined by the equation:

$$\eta = \exp \left[\frac{\nu_1 (P - P_v)}{k T} - \frac{C_2}{C_1} \right] \quad (2.7)$$

In this expression ν_1 is the specific volume of the pure solvent and k is the Boltzmann constant. The subscripts 1 and 2 refer to the properties of the solvent and solute respectively.

The critical size of the nucleus is thus sensitive to the supersaturation as well as the surface tension and the pressure. The amount of energy needed to make this critically sized nucleus is therefore extremely sensitive to the degree of supersaturation (see equation (2.3)).

According to the analysis leading to the equation (2.6), a nucleus of radius slightly larger than R_c will grow while under the same conditions a nucleus slightly smaller than this size will dissolve; hence the radius R_c is termed the critical radius.

A second important parameter calculated by Ward *et al.* (1970) is the nucleation rate. The rate of nucleation J is the number of nuclei with radius R_c created in time within a certain volume of liquid due to thermal fluctuations or Brownian motion:

$$J = Z \exp \left(-\frac{\Delta F}{kT} \right) = Z \exp \left(\frac{-4\pi \gamma R_c^2}{3kT} \right) \quad (2.8)$$

The constant Z depends on the system at hand but is generally given by (Wilt, 1988):

$$Z = N_G \left(\frac{2\gamma}{\pi m} \right) \quad (2.9)$$

where m is the mass of one molecule, and N_G is the amount of moles/m³ gas. According to Ward *et al.* (1970) Z is found to be very large for pure liquids. We use the same equation to

estimate Z for a gas in liquid solution. Due to the exponential factor, however, Z hardly affects the nucleation rate.

In order to give an idea of the orders of magnitude of these values, R_c and J are calculated for bubbles in a low supersaturated carbonated solution such as beer: $\gamma \approx 45 \text{ mNm}^{-1}$, $\eta \approx 1$, $P = 10^5 \text{ Pa}$, $\alpha = 3$, and P_v is neglected, which gives for equation (2.6):

$$R_c = 0.45 \mu\text{m}.$$

A bubble with a critical radius of this size is not visible by eye. Increasing the supersaturation ratio will decrease the critical radius. A nucleus with a radius larger than R_c will grow out into a bubble.

The constant Z estimated with equation (2.9) is found to be around 10^{36} , but with the large number in the exponential, this gives for the nucleation rate:

$$J = e^{-12550223} \approx 0$$

This rough estimate shows that homogeneous nucleation will not likely occur in a low supersaturated beverage such as beer, after the pressure is released. From calculations of the nucleation rate, Wilt (1986) also shows that supersaturation ratios of 1100 to 1700 would be required for homogeneous nucleation to occur at room temperature, which supports the theory that bubble formation in carbonated beverages occurs always heterogeneously.

Ward and Tucker (1975) give the differential equation governing the radius of the bubble as a function of time, where again it is clear that if $R > R_c$, dR/dt is positive, i.e. the nucleus grows. On the other hand, when $R < R_c$, continued dissolution will occur, as was demonstrated experimentally in the same article.

2.2.3 Heterogeneous nucleation and bubble formation

As mentioned in the introduction, heterogeneous nucleation is the creation of new interface between gaseous and liquid phases at a lower free activation energy than homogeneous nucleation. The energy-lowering effects can be (a) catalytic sites and (b) pre-existent nuclei. We speak of a catalytic site on a solid surface or substrate when the three-phase contact angle at that site or the radius of curvature of the gas-liquid interface is such that a gas nucleus with a critically sized radius can be stable. Thermodynamically speaking, this is where a nucleus with radius R_c has a lower surface to volume ratio than in the homogeneous situation. This is the case when a nucleus is situated inside a cavity or crevice.

We speak of a pre-existent nucleus when the gas phase necessary for bubble growth is already present, either in the bulk solution or at a catalytic site. The orientation and the value of the radius of curvature of the gas-liquid interface determines whether the gas mass will grow. The rate of growth (or dissolution) is determined by the supersaturation level of the gas in the liquid. The free activation energy for bubble formation (read growth) is much lower or even negative in some cases because the new interface is already formed. Heterogeneous nucleation needs a lower amount of energy and can therefore occur at a lower degree of supersaturation than homogenous nucleation. Analogously, heterogeneous bubble formation or growth from a pre-existent gas mass, with $R > R_c$, can occur at even lower supersaturations. In fact, with the presence of pre-existent nuclei gas bubble formation can be spontaneous when the liquid is supersaturated with gas.

2.2.3.1 Contact angle, surface roughness and heterogeneity

With heterogeneous bubble formation the effect of an additional phase must be taken into account, which is that of a solid surface. Attraction and repulsion forces between liquid and solid will be of great importance whether or not bubble formation will occur and whether or not the bubble or nucleus once formed will be stable. Therefore a brief explanation about liquid-gas-solid interaction is given in this paragraph.

A drop of liquid in space is drawn into a spherical shape by the magnitude of its surface tension, but brought into contact with a solid surface, will modify its shape until equilibrium is reached between the relative forces of adhesion and cohesion with the solid surface (Morra *et al.*, 1990). The visible value attached to this effect is the contact angle, which is the equilibrium angle at the three phase boundary, measured across the liquid interface (Lyklema and Koopal, 1984). In the case that the liquid 'wets' a surface, the liquid will spread to a small or even zero contact angle on the solid surface; analogously when the contact angle is large, the drop stays more or less in a spherical shape, in which case the liquid is called 'non-wetting'. Frequently when an aqueous liquid wets a surface this surface is called 'hydrophilic' and if not, the surface is called 'hydrophobic'. This can, however, be misleading when talking about non-polar liquids, which can wet 'hydrophobic' surfaces quite well.

The contact angle is the equilibrium result of the three relative interfacial tensions, as described by the Young equation:

$$\gamma_{sg} - \gamma_{sl} = \gamma_{lg} \cos\theta \quad (2.10)$$

where γ_{sg} is the interfacial tension of the solid in equilibrium with the vapour and gas phase, γ_{sl} is the interfacial tension between solid and liquid, γ_{lg} is the surface tension between liquid and vapour and gas phase, and θ is the equilibrium contact angle for a drop of the liquid on the solid. In figure 2.2 the contact angle is shown for a drop of liquid on a

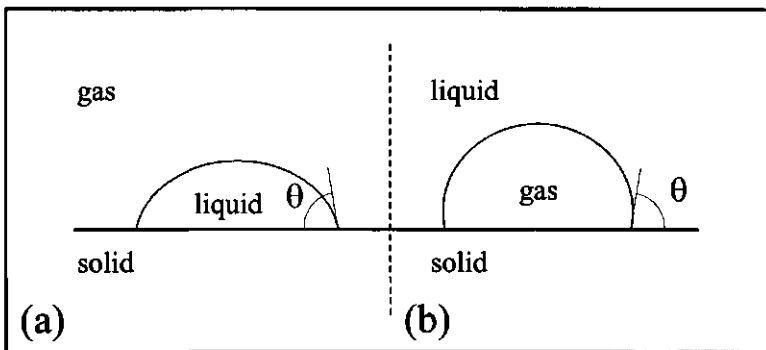


Figure 2.2 (a) Drop of liquid on a solid surface; (b) Gas bubble on a solid surface.

solid surface as well as for a bubble attached to a solid surface submerged in a liquid, which is the situation found in bubble formation on solid surfaces. As shown the contact angle is always defined across the most dense phase of the two 'fluids'.

The Young's equation is valid for ideal flat solid surfaces, i.e. smooth and characterised by a well defined value of the surface tension of the material, and the wetting liquid must not interact chemically or physically with the solid. More often than not, these surfaces are not found in practical systems so that the equilibrium contact angle as defined by Young does not have much practical value. The measured value of the contact angle can vary greatly due to surface properties, liquid properties or due to interactions between liquid and surface. There are two limiting cases: the maximum or advancing contact angle θ_a , which occurs when the liquid drop is advancing over a dry clean surface and the minimum or receding contact angle θ_r , which occurs when the meniscus is receding from a previously wetted surface. Moving a drop of liquid on an inclined surface gives both angles: the advancing angle will be apparent at the front of the drop and the receding angle at the rear end. Generally the equilibrium contact angle will lie between advancing and receding contact angles. The large difference that can occur between advancing and receding contact angles is called contact angle hysteresis, and is mainly due to properties like surface roughness, heterogeneity, adsorption kinetics and so forth.

A second important effect is the roughness of the surface. The ideal situation of a microscopically smooth surface is not a practical one. The roughness of a surface is often in the range of microns, and can have a large effect on the measured macroscopic contact angle. Cornell (1982) studied the effect of contact angle hysteresis due to roughness and surface heterogeneity, and found that a certain degree of roughness (or heterogeneity) should be present in hydrophilic surfaces in order to trap a stable gas nucleus at that surface. Hydrophobic cavities give a concave meniscus (to the aqueous phase) which makes the trapping as well as the stability of the trapped gas mass more plausible (see figure 2.3). But even for hydrophobic surfaces there are situations where no nucleation will occur. Ryan and Hemmingsen (1993) did not find heterogeneous bubble formation at

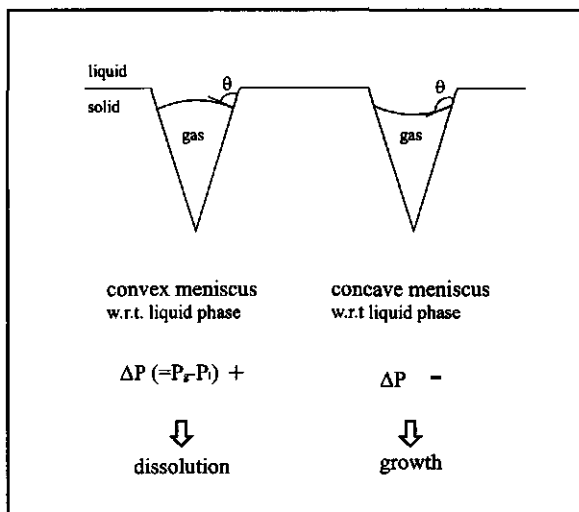


Figure 2.3 The gas-liquid interface in a conical cavity (adapted from Cornell, 1982).

smooth hydrophobic surfaces. Cavities and other inhomogeneities are obviously of vital importance for the trapping and stability of gas masses at surfaces.

Heterogeneous surfaces (surfaces of varying chemical composition, or local contamination's) can also cause contact angle hysteresis. One very important example is the irreversible adsorption of surface active material onto surfaces, which can cause surfaces which initially were 'hydrophobic', or not well wetted by aqueous polar liquids, to be coated by a 'hydrophilic' layer (well wetted by aqueous polar liquids). In that case the surface has changed and different contact angles will be measured. This can also happen by chemical changes such as oxidation of surfaces. Yet another example is the change in surface due to uptake of liquid by the surface.

It is these surface properties that can facilitate the formation of a nucleus at a solid interface (or a second fluid interface). Heterogeneous nucleation was first observed in nucleate pool boiling. It can occur when either the contact angle is greater than 0° , or when the surface is rough so that the nucleation can take place in a crevice. In order for heterogeneous nucleation to occur at a planar interface the surface should have a contact angle larger than 0° . By increasing the contact angle, the energy barrier for nucleation can be decreased considerably (Hilton, 1992).

Any surface which has not been specially treated will contain imperfections such as pits, grooves, scratches and projections. Sizes and shapes of these sites can influence the nucleation barrier as well as the nucleation rate.

Harvey *et al.* (1944) observed that heterogeneous nucleation is a distinctly different situation from homogeneous nucleation. The size of a critical spherical nucleus (equation (2.6)) is determined by the radius of curvature, whereas the size of a stable nucleus at the surface is also determined by the geometry of the surface, the shape of the gas-liquid-solid

junction, the advancing and receding contact angles between gas phase and surface, the surface tension and the Laplace pressure difference. With these considerations, spherical nuclei grow above a critical size, whereas attached nuclei grow above a critical pressure difference. This is because the pressure in spherical nuclei only depends on its size, whereas in attached nuclei the pressure also depends on the solid surface, not only on the size.

Blander (1979) has reviewed theoretical considerations and experiments concerning heterogeneous bubble formation in pool boiling, as has Cole (1974). The basis for the theoretical analysis is the classical nucleation theory, used to calculate nucleation rates. The nucleation rate equation (equation (2.8)) was applied to the several cases of heterogeneous nucleation, such as on a smooth planar surface, and in conical and spherical shaped cavities. Blander concludes that a smaller cavity radius increases the probability of nucleation occurring, and that, in the case of conical cavities, the contact angle must be greater than the apex angle of the cavity β (half the angle between the diagonal sides, see figure 2.4).

Ward *et al.* (1983) extended the critical radius and rate of nucleation theory in finite volume for the heterogeneous nucleation within a conical shaped cavity. They analysed the growing of the nucleus as it emerges from the cavity. They found that in the case of $\theta > \beta$, the radius of curvature would limit the emergence of the bubble from the cavity. As the bubble emerges from the cavity the radius goes through a minimum. The bubble can then either grow further if $R > R_c$, or not emerge and maybe dissolve. A different situation not sketched by Ward *et al.* is when the contact angle is so large that the contact base of the bubble spreads across the outer surface as soon as the bubble emerges from the cavity (for very hydrophobic surfaces). In this case R does not go through the minimum as described by Ward, and can grow further without hindrance. In the case of $\theta < \beta$ (only for very hydrophilic surfaces), R does not go through a minimum either, and the bubble grows on if

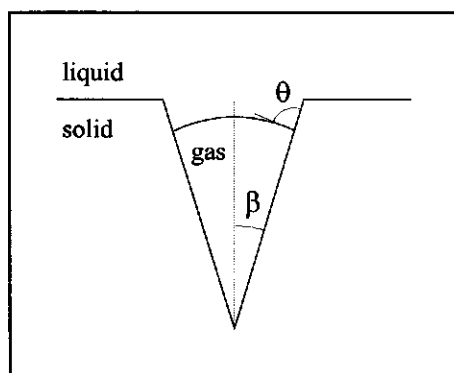


Figure 2.4 A nucleus situated in a conical cavity; β is half the apex angle of the cavity and θ is the contact angle.

$R > R_c$. However when the bubble detaches, the cavity will be flooded and no further bubble formation takes place unless by nucleation.

Griffith and Wallis (1960) also studied reservoir type cavities (the opening of the cavity is less wide than the cavity), which will be even more effective in trapping gas and holding a stable nucleus, due to the flip-over of the meniscus as the cavity curves inwards. The meniscus is then concave with respect to the liquid phase, which is an important stabilising mechanism, as then the pressure difference across the interface is reversed. The gas phase will then tend to grow as opposed to a convex interface. However, the likelihood that such cavities exist in practical surfaces is very small.

Wilt (1986, 1988) extended Blander's work (1979) and Ward's and his colleagues' work (1983) for heterogeneous bubble formation in supersaturated CO_2 /water solutions for various simple solid surface geometry's such as conical cavities, conical projections, spherical cavities and spherical projections. Calculations show that unusually large contact angles ($\sim 175^\circ$) are necessary to make heterogeneous nucleation occur from carbonated solution at a smooth planar interface ($\alpha = 5$). For conical cavities, Wilt calculates that observable nucleation rates are predicted for physically realistic contact angles. For example if the supersaturation ratio is 5, nucleation should occur at a conical cavity with apex angle $\beta = 5^\circ$, contact angle $\theta = 95^\circ$, and surface tension $\gamma = 65\text{mN/m}$. Spherical cavities have been analysed by Ciholas and Wilt (1988). The calculations predict that nucleation is possible only for very large contact angle ($\theta \approx 130^\circ$) and very small cavity mouth radius ($r_c \approx 10^{-9} \text{ m}$). Smaller contact angles are theoretically possible but the radius of the cavity mouth should then be so small that it is disputable whether the volume of the nucleus (about 1 or 2 CO_2 molecules) should be considered a gaseous phase, with a gas-liquid interface. From a theoretical point of view it is therefore not possible for nucleation to occur at spherical cavities. Furthermore, no nucleation is predicted to occur at spherical or conical projections in low supersaturated solutions.

Generally according to theoretical predictions, nucleation should occur preferentially at conical cavities or reservoir type cavities. Cavities such as grooves and very steep ridges are more likely to occur at practical surfaces, but bubble formation may well be explained with these model calculations. It is, however, wise to notice how small changes in contact angle and cavity geometry and size can influence the probability of bubble nucleation.

2.2.3.2 Experimental investigations of bubble formation at solid surfaces

Very few nucleation experiments have been reported in literature, mostly due to the rigorous experimental procedures needed to achieve reproducible results. Even then discrepancy factors of several orders of magnitude may be found between experimental results and theoretical predictions. (Katz, 1992). The applications of these experiments are

found in nucleate boiling (Judd and Lavdas, 1980), Sgheiza and Myers (1985), Griffith and Wallis (1960), bubble formation in humans due to decompression sickness otherwise known as ‘bends’ (Yount, and Strauss, 1976, 1979), bubble formation in sea water, vital to the convection of micro-organisms (D’Arrigo (1984)) and bubble formation in carbonated beverages (Lubetkin, 1988, 1989; Bisperink and Prins (1994)). Most experiments are conducted by heating liquids or saturating liquids with gasses at high pressures, and then releasing the pressure isothermally. Other than pressure, supersaturation of gases in liquid may be achieved by chemical reactions (Rubin and Noyes, 1987; Hilton, 1992). Other methods of bubble formation without supersaturation and therefore not discussed here include whipping, agitation, sparging gas through orifices (Ronteltap, 1989; Lin *et al.*, 1994).

Methods of measurement include measurement of the decrease in pressure at bubble breakout (Finkelstein and Tamir, 1985), counting of bubbles as a function of time by various methods (acoustical: Lubetkin (1989); light scattering: Hilton (1992), photographic: Yount and Strauss (1976), Judd and Lavdas (1980), infrared camera: Sgheiza and Myers (1985)). By far the largest part of experimental studies were done to study vapour bubble formation in pool boiling. We are mostly interested in bubble formation from supersaturated solutions at isothermal conditions, however the effect of nucleation sites and site interactions has been further explored in the pool boiling field than in any other. It is for this reason that this literature is also reported.

Most investigations are concerned with bubble nucleation, and therefore the process is treated and analysed as a random event. However effects that ease bubble nucleation are found to be equally valid in bubble formation from pre-existent nuclei. These effects include:

a) the degree of gas supersaturation; an increase in supersaturation is found to increase the number of bubbles formed as well as the rate of formation. Lubetkin found that, at supersaturations typical of a carbonated beverage, the rate of bubbles released from the surface was a good measure of nucleation rate, as long as the surface was hydrophilic (1988, 1989). The nucleation rate predicted by a simplified version of Wilt’s equation (1986) for heterogeneous nucleation of bubbles at conical cavities, was found to agree well with experimental results. Hilton’s results showed an increase in number of bubbles formed with an increase in supersaturation, as well as an increase in growth rate of the bubbles (1992).

b) the contact angle of the liquid on the solid surface; increasing the contact angle may increase the number of bubbles formed, but can lead to a lower detachment rate. Lubetkin (1989) found that the rate of bubbles released from the solid surface was much lower at surfaces with large contact angles. He proposed that the nucleation rate was the same as on a surface with small contact angle, but that the detachment of the bubble is the rate determining step on a non-wetting surface. Hilton (1992), observing only very short time scales in bubble formation (130 ms), found that increasing the contact angle of the surface led to a large increase in the number of bubbles formed and that bubble formation

occurred at a lower critical supersaturation than on surface with a small contact angle. Ryan and Hemmingsen (1993) found that a large wetting angle is not enough to induce heterogeneous nucleation, a certain degree of roughness is imperative. Wang and Dhir (1993) showed in nucleate pool boiling that increasing the degree of oxidation of a copper surface increased the effective amount of nucleation sites. Even so, only 1-10% of the cavities present at the surface were active when the surface contact angle was 90°.

c) the presence of cavities at the solid surface; Inhomogeneities are found to increase the nucleation rate, especially when the contact angle is also increased. This latter effect is due to the larger probability of gas being trapped in these cavities. In literature, however, often no distinction is made between heterogeneous nucleation and heterogeneous bubble formation from pre-existent nuclei. This is due to the fact that the presence of minute nuclei at surfaces or in the liquid is not easily traceable. The best check is to measure the pressure at which bubble formation occurs and to compare these results with nucleation theory. If the bubbles are formed at relatively low supersaturation then it stands to reason that the formation of bubbles is made favourable by the presence of nuclei.

Among many others, Clark *et al.* (1959) and Wang and Dhir (1993) observed clearly that nucleation, when it occurred, originated from pits and grooves at the surface. Clark *et al.* (1959) measured the size of the active pits and found them to be roughly in the range of 0.1 μm to 10 μm .

d) the size and geometry of cavities at the surface; The shape and size of the cavity can decrease the critical pressure at which bubble formation occurs and the mouth radius of the cavity can influence size at detachment (Clark *et al.*, 1959). Griffith and Wallis (1960) proposed that the radius of the cavity mouth was important with respect to the critical superheat required for vapour bubble formation, and that the shape determined the stability of the bubble once it is nucleated.

Wang and Dhir (1993) calculated the size distribution of active sites in practical surfaces and found that this could be well described by a Poisson distribution, as was also found by Judd and Lavdas (1980) and Sgheiza and Myers (1985).

e) the density of cavities at the solid surface; Judd and Lavdas (1980) showed that bubbles forming at active sites in liquid pool boiling are able to mask neighbouring potential active sites temporarily. Besides the physical overlapping of bubbles, depletion of gas in the liquid surrounding a growing bubble may prevent new bubbles to grow at neighbouring sites.

f) the presence of pre-existent nuclei at these surfaces; Yount and Strauss (1976) used gelatin solutions to observe bubble formation as a function of compression and decompression cycles. They found that pre-existing nuclei accounted for almost all bubbles formed by decompressing the supersaturated solution, and that most of these nuclei were present in the water before adding the gelatin. These nuclei could be crushed by a rapid compression. Hilton (1992) found critical supersaturation degrees of CO_2 in water at which bubbles were formed which could not be explained by nucleation. She proposes that the

bubbles were mostly formed at the solid surface due to the presence of pre-existent gas nuclei. Even on hydrophilic surfaces single bubble events were found to occur.

g) the viscosity of the supersaturated liquid: Hilton (1992) observed CO₂ bubble formation in salt solutions with and without 25 % v/v glycerol, and found that the amount of bubbles was the same in both cases, but that the growth of bubbles in the liquid with higher viscosity is slower. This can be explained with the diffusional gas transport, which is a slower process when the viscosity is increased.

Although the literature does show the trends of the effects that may influence bubble formation, there is still a lot to be learned, especially when bubble formation on practical solid surfaces is concerned. There are enough theories for nucleation, but experimental studies show how difficult the nucleation rate is measured, especially when the bubbles do not detach from the surface (Lubetkin, 1989). Furthermore it is very likely that bubble formation in practical systems such as beer and champagne is caused by pre-existent nuclei, present at the solid surfaces in contact with the supersaturated solution (Hilton, 1992). Whether or not bubble growth is seen, depends on the supersaturation ratio, and indirectly on the critical radius of curvature of the pre-existent nuclei. In the next paragraph we show how pre-existent nuclei have been found to be stable for longer periods of time in a solution or at an interface. Furthermore the effect of shape and the size of the cavity on the possibilities of gas entrapment are discussed.

2.2.3.3 Pre-existent nuclei

Numerous authors have suggested that bubble formation may often be caused by a pre-existing gas phase (Yount *et al.* 1976, D'Arrigo, 1978). Experiments have shown that bubble formation was found at considerably lower gas supersaturations than the threshold pressure from theory indicates, which implies that bubble formation must be initiated by processes other than the application of modest pressure and random motion of the liquid and gas molecules. By degassing liquids, or by pre-application of high pressures, the low bubble formation threshold can be increased significantly. It is found that the early onset of bubble formation is caused by the presence of pre-existent nuclei, although their origin and mechanism of stabilisation is still not well understood.

Pre-existent nuclei need an extra stabilising mechanism: bubbles larger than 1 μm will rise to the surface of a standing liquid, whereas smaller ones will dissolve rapidly due to the high internal pressure inside the gas nucleus (see equation (2.2)). Several stabilising models have been proposed over the years. Harvey *et al.* (1944) described how a gas mass could be stabilised if situated inside a crack or cavity at a solid surface. If the radius of curvature is concave or flat, the gas phase will grow or be stable, as the gas pressure in the gas phase is then equal or lower than the ambient pressure. As long as R is large, the nucleus can persist indefinitely. In practical situations only very steep cavities of

hydrophobic nature satisfy the constraints needed for this stabilising mechanism. According to Yount *et al.* (1977), although maybe some of the larger nuclei are associated with crevices in solid impurities, the vast majority of nuclei are not.

Additional stabilising mechanisms described in literature are elastic forces in surrounding media, gas-impermeable organic skins (Fox and Herzfeld, 1954), ionic surfaces and the latest and most actual mechanism was described by Yount *et al.* (1977). Yount *et al.* founded their idea on the experimental discovery that the stabilisation of gas phases in water is always attributable to the presence of surface active agents. Yount (1979) postulates that 'elastic films or skins' are formed at the interface which can be impermeable to gas during compression, but become permeable when a large decompression occurs. D'Arrigo (1984) goes further by proposing that these surface active compounds are mostly hydrophobic surfactants. More specific the micro-bubble surfactant in question was found to a glycopeptide-lipid-oligosaccharide complex, reversibly held together by both hydrogen bonding and non-polar interactions.

Manley (1960) found with bubble dissolution experiments that as the radius decreased in size, the rate of dissolution was considerably reduced. He calculated a lower diffusion coefficient for the latter part of the dissolution, and attributed the effect to the formation of a (partly) impermeable skin at the surface. Ronteltap and Prins (1990) found that compression of a bubble surface could result in a considerable decrease in surface tension, which is the driving force in the Laplace equation (equation (2.2)). For systems with low surface viscosity the gas bubble could dissolve quite rapidly, whereas a system with high surface viscosity could decrease the rate of dissolution considerably. Furthermore a 'skin' was found to form around the dissolving bubble. Whether this skin had impermeable properties was not investigated. In sea water these 'skins' are also found to be formed around dissolving bubbles (Johnson and Cooke, 1980). Lucassen (1981) showed that, when the surface elasticity is larger than half the surface tension and when the surface is purely elastic, the decrease in bubble size can be stopped. After this, the bubble can stay stable over very long periods of time. This is a credible possibility for the situation of large molecules that do not readily desorb from a bubble surface. This situation can persist during compression of the surface, when the forming 'skin' becomes a mechanical barrier to further compression. The 'elastic network' formed at the surface can then only be removed when a very fast expansion and /or compression cycle is applied. In paragraph 2.7 we will go into more detail of surface rheological aspects of the system used in this thesis, and the formation of insoluble 'skins' at interfaces.

When Harvey *et al.*'s (1944) cavity model is combined with one or more of these surface stabilising mechanisms, stable nuclei can survive in cavities and crevices over extremely long times. It is found however that the cavity stabilises a nucleus best if internal surface of the cavity is not well wetted by the liquid phase.

2.2.3.4 Gas Entrapment at solid surfaces

The mechanism by which the gas nuclei may be entrapped inside crevices at a solid surface was described by Harvey *et al.* (1944), Bankoff (1958), Cole (1974), Apfel (1970) and Winterton (1977).

The spreading of a liquid over a surface containing grooves and cavities has been considered by Bankoff (1958). For simplicity only spreading in one direction is considered. Figure 2.5(a) illustrates the conditions for entrapment of gas in the advance of liquid across a groove. It is apparent that if the contact angle θ is greater than the apex angle 2β , the advancing liquid will meet the opposite wall of the cavity before it has completed its advance down the nearest wall. Hence the condition for entrapment of gas (for conical shaped cavities and grooves) is:

$$\theta > 2\beta \quad (2.11)$$

which is usually the advancing contact angle.

Figure 2.5(b) illustrates the condition of liquid displacement from a groove by the retreating gas-liquid interface. It is apparent that if the contact angle θ is less than $\pi - 2\beta$, the gas-liquid interface will reach the opposite side of the cavity before the liquid is drained from the cavity, analogous to the situation in figure 2.5(a). Thus the condition for failure to displace liquid from the conical groove is

$$\theta < \pi - 2\beta \quad (2.12)$$

which is usually the receding contact angle.

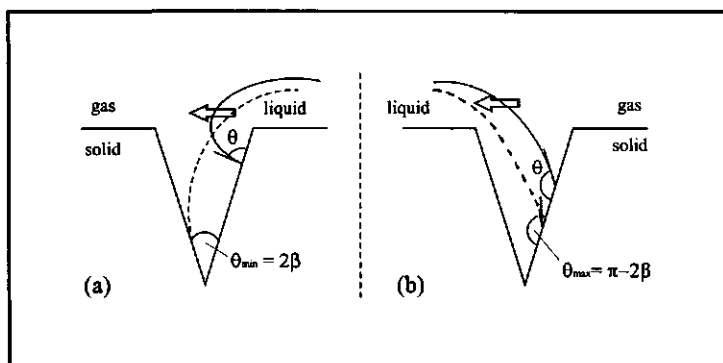


Figure 2.5 (a) Advance of liquid over a gas-filled cavity or groove; (b) Retreat of liquid from a liquid-filled cavity or groove (adapted from Bankoff, 1948).

Bankoff (1958) divided the cavities into 4 categories:

- a) those that obey the first inequality, but not the second (only gas entrapment). These are steep cavities that are poorly wetted.
- b) those that obey the second inequality, but not the first (only liquid entrapment). These are steep cavities that are well wetted.
- c) those cavities that obey both inequalities (both gas and liquid entrapment). These are shallow cavities which are poorly wetted.
- d) those that obey neither inequality (no entrapment of either gas or liquid). These cavities are shallow and are well wetted.

It seems that those cavities that have the best possibility of acting as nucleation sites and which are preferred for stabilising a gas nucleus, are just those cavities that have the greatest tendency to entrap gas and vapour.

Rounded grooves were found to be very much less effective in trapping gas or vapour, as the liquid spreads easily into the cavity, as is the case for shallow cavities.

The stability of the gas phase once trapped in a cavity was described in the previous paragraph, and depends mostly on the pressure difference across the gas liquid interface , as described by Harvey *et al.* (1944).

One last aspect to be taken into account is the stability of the active site, when bubbles start to be formed. It can be the case that a cavity can entrap a nucleus, but that the gas left behind in the cavity is slowly reduced in volume by the repeated formation of new bubbles. After a bubble detaches from the mouth of a wetted cavity, the liquid penetrates the cavity by capillary attraction, at the same time releasing a little gas that was originally in the cavity. The liquid penetration stops when the capillary pressure is balanced by the gas saturation pressure in the liquid (Griffith and Wallis, 1960). For example, if surface active components from the liquid adsorb at the retreating interface, the gas nucleus can eventually be completely removed due to higher capillary pressure. This phenomenon is found to occur in the washing action of detergents, only then the phase to be removed is liquid. The chance of the slow (each bubble removes a little) removal of nuclei in cavities is much lower when the cavity is not well wetted by the liquid, where the capillary pressure will be lower or negative.

2.3 Effect of 'hinterland' volume on bubble growth at active sites

When a bubble is growing from a gas supersaturated solution at the opening of a cavity or, in this case a cylindrical capillary, the growth rate of the bubble depends on the gas transport characteristics from the liquid phase to the gas phase and vice versa. An influence on the bubble growth rate can be found when the capillary holds a sizable finite 'hinterland' volume filled with compressible gas. This influence which can be accounted for by the change in volume of the gas phase as a function of the change in pressure. The pressure in the gas phase P_g will determine the volume of that phase V_g , as described by Boyle's law (assuming isothermal conditions):

$$P_g V_g = \text{constant} \quad (2.13)$$

The pressure inside the gas phase is given by the Laplace equation for spherical bubbles P_b with radius R (see equation (2.2)):

$$P_b = P_0 + \Delta P = P + \frac{2\gamma}{R} \quad (2.14)$$

where ΔP is the Laplace pressure difference and P_0 is the ambient pressure. In order to understand the pressure change which a bubble goes through during growth, the radius of the bubble must be followed: Assuming the interface of gas-liquid is flat at the mouth of the capillary when the bubble starts to grow, the radius of curvature has to decrease from infinity until the bubble has reached a hemispherical state. At this point the radius of curvature has reached a minimum value equal to the radius of the capillary.

Correspondingly the pressure has reached a maximum, $\Delta P_{\max} = b$. After this point the bubble radius increases with growth, therefore the pressure inside the bubble decreases. Due to drop in the pressure the gas phase expands, making the bubble grow, which increases the radius and results in a further pressure drop, and so forth.

The effect described above will always take place, but can go unnoticed when the hinterland volume is negligible, since the gas phase volume then only consists of the bubble volume. The hinterland volume is no longer negligible when the expansion is large enough to result in the unstable 'blowing up' of the bubble until detachment from the surface.

The hinterland effect described above was also found by Liggieri *et al.* (1990) during surface tension measurements using a drop volume method, where the drop growth on a nozzle was found to be unstable due to the accidental presence of small compressible gas bubbles in the liquid phase. When the drop was increasing in size the pressure dropped inside the drop phase. This caused the small gas bubbles to inflate, and thus suddenly cause the drop to be released.

In order to be able to predict whether the 'hinterland' volume, or the volume of the cavity, will affect the growth rate of the bubble, certain assumptions must be made; for the sake of simplicity the bubble is assumed to be spherical, and the contact angle with the solid is 0° for a well-wetted surface; however at the point of detachment an apparent contact angle (of the gas-liquid interface with the surface) of 90° with the horizontal is assumed, which seems justified by experiments (see chapter 3 and 4); the vertical capillary has a cylindrical shape with the opening facing upwards; the surface tension is assumed to be constant and equal to the equilibrium surface tension; furthermore the influence of friction on the gas flow within the capillary is neglected and pressure fluctuations are assumed to be stabilised immediately under the hypothesis of ideal gas behaviour.

Apart from its ability to increase the rate of bubble growth the presence of a hinterland volume can lower the frequency of multi-bubble formation. After a bubble detaches from a capillary a small gas phase is left behind, which then proceeds to grow into a new bubble. Under conditions that the liquid meets the inside part of the cavity after bubble detachment, the convex meniscus (with respect to the liquid phase) creates a higher gas pressure in the cavity than at the moment that the bubble detaches from the cavity. This results in a retreat of the meniscus into the capillary creating a certain distance Δh between the interface and the bulk liquid (see figure 2.12). The retreat results in a much slower gas transport from the bulk solution to the remaining gas pocket in the cavity.

2.3.1 Theoretical approach

In order to calculate the effect of the expanding and compressing hinterland on bubble growth and bubble formation frequency, a bubble on a capillary is made to grow from the hemispherical shape ($R=r$) with added steps of volume. When the bubble reaches a hemispherical shape the bubble pressure is at a maximum. Any further increase in bubble volume causes a decrease in the bubble curvature, hence also in the bubble pressure. The gas phase expands, making the bubble grow and thereby further decreasing the pressure, and triggering a process which will stop when the pressure decrease with bubble growth has become negligible.

For a situation just before and after a bubble reaches hemispherical shape, the volume of the gas as a function of bubble growth can be derived analogous to Liggieri *et al.*'s (1990) approach. The volume of a spherical bubble V (larger than hemisphere) perched on a capillary can easily be found if the radii of both capillary r and bubble R are known (see figure 2.6):

$$V = V_{sphere} - V_{segment} = \frac{4}{3}\pi R^3 - \frac{1}{6}\pi a(a^2 + 3r^2) \quad (2.15)$$

where:

$$a = R - \sqrt{R^2 - r^2} \quad (2.16)$$

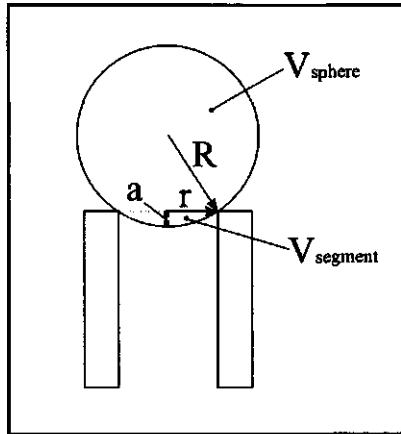


Figure 2.6 Schematic presentation of a spherical bubble perched on a cylindrical capillary; r is the radius of the capillary, R is the radius of the bubble curvature and a is the height of the segment of the bubble imbedded in the capillary.

On the other hand, the bubble volume may also be described by a hemispherical shape which is increased in volume by diffusional gas transport ΔV_d and expanded volume ΔV_e (by pressure decrease):

$$V = \frac{2}{3}\pi r^3 + \Delta V_d + \Delta V_e \quad (2.17)$$

where according to Boyle's law (equation (2.13)) (see figure 2.7):

$$\Delta V_e = V_b - V_a = \frac{V_a P_a}{P_b} - V_a \quad (2.18)$$

V_a is the total volume of gas at maximum pressure b . In our case V_a is defined by the volume of the hinterland V_b and the hemispherical form perched on the capillary:

$$V_a = V_b + \frac{2}{3}\pi r^3 \quad (2.19)$$

By combining equations (2.15) and (2.17) we can now define $f = \Delta V_d$. For the situation where the bubble is growing past the hemispherical state we find f :

$$f = \Delta V_d = \frac{4}{3}\pi R^3 - \frac{1}{6}\pi a (a^2 + 3r^2) - \frac{2}{3}\pi r^3 - \Delta V_e \quad (2.20)$$

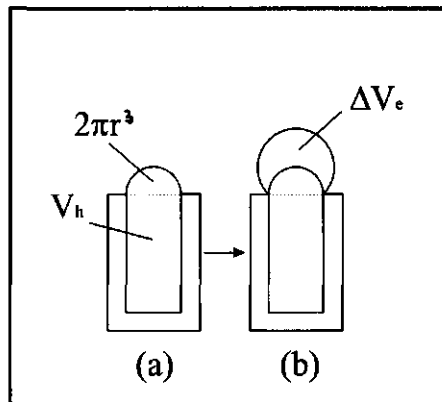


Figure 2.7 (a) Situation where bubble has reached the hemispherical state. Growth induces an expansion to (b) where ΔV_e is the expansion volume.

We can rewrite f_i as a function of ΔP and b ($= \Delta P_{max}$) :

$$f_i = \frac{\pi}{3} r^3 \frac{2 \Delta P_{max}^2 + \Delta P^2}{\Delta P^3} \sqrt{\Delta P_{max}^2 - \Delta P^2} + \frac{16}{3} \pi \frac{\gamma^3}{\Delta P^3} - \frac{2}{3} \pi r^3 \left(V_h + \frac{2}{3} \pi r^3 \right) \left(\frac{\Delta P_{max} - \Delta P}{\Delta P + P_0} \right) \quad (2.21)$$

The same function can be derived for a spherical cap which has not yet reached its hemisphere, f_2 :

$$f_2 = -\frac{\pi}{3} r^3 \frac{2 \Delta P_{max}^2 + \Delta P^2}{\Delta P^3} \sqrt{\Delta P_{max}^2 - \Delta P^2} + \frac{16}{3} \pi \frac{\gamma^3}{\Delta P^3} - \frac{2}{3} \pi r^3 \left(V_h + \frac{2}{3} \pi r^3 \right) \left(\frac{\Delta P_{max} + \Delta P}{\Delta P + P_0} \right) \quad (2.22)$$

As can be seen from figure 2.8, f_2 (change in bubble volume by diffusion from a flat interface until the hemispherical state) increases as the pressure increases until the bubble has reached its half-spherical state. At this point the pressure reaches the maximum $b = \Delta P_{max}$, after which the radius increases and therefore the pressure decreases (f_i). For very small hinterland volumes, f_i (change in bubble volume from the hemispherical state until detachment) increases with pressure decrease. However if the hinterland volume is large enough, f_i is first seen to drop below zero, reaches a minimum and then proceeds to a stable increase. At $f_i = 0$, there are two states for ΔP , but only b is a meta-stable state and the hemispherical form is preserved.

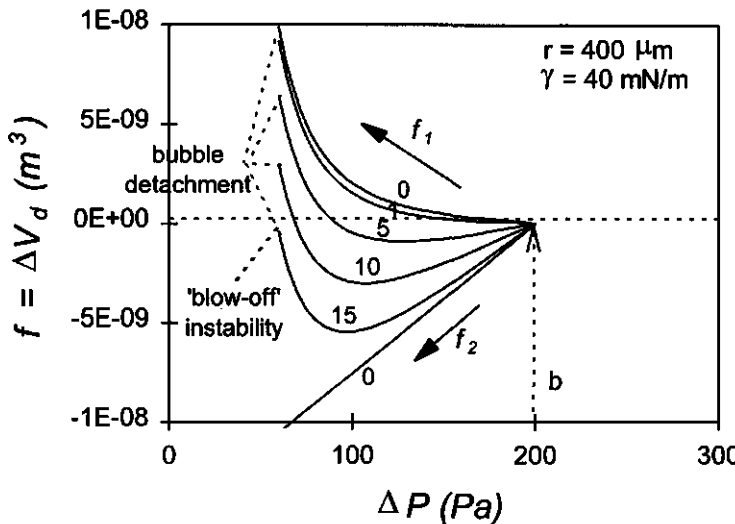


Figure 2.8 The functions f_1 and f_2 in relation to ΔP for $r = 4.10^{-4}$ m, and for increasing hinterland length $h = 0, 1, 5, 10$ and 15 m; b is the maximum pressure at hemispherical state; $\gamma = 40$ mN/m.

Growth of a bubble from a flat interface, a jump in the bubble pressure is found (corresponding to a sudden increase in the volume of the gas) after which growth is once more stable (see figure 2.9(a)). Making a bubble shrink in the same situation, the volume decreases until the minimum is reached, after which the pressure increases with a jump until the bubble is smaller than the hemispherical state and only then decreases monotonously (figure 2.9(b)).

To calculate the stability conditions, it is useful to evaluate the influence of the various parameters (capillary radius, hinterland volume, surface tension and ambient pressure) on the derived functions f_1 and f_2 . Figures 2.10(a) and 2.10(b) show $\Delta V(f)$ as a function of ΔP for different capillary radii for capillary length $h = 0$ and $h = 13$ m respectively.

As has been mentioned before f_1 increases monotonously for negligible hinterland volumes (figure 2.10(a)) but shows a minimum for high hinterland volumes (figure 2.10(b)). The value of this minimum decreases with increasing hinterland volume (figure 2.8), and the latter results in a larger 'blow-up' of the bubble. Furthermore, the effect of the hinterland volume becomes more pronounced when the hinterland volume is larger than the maximum bubble volume at detachment.

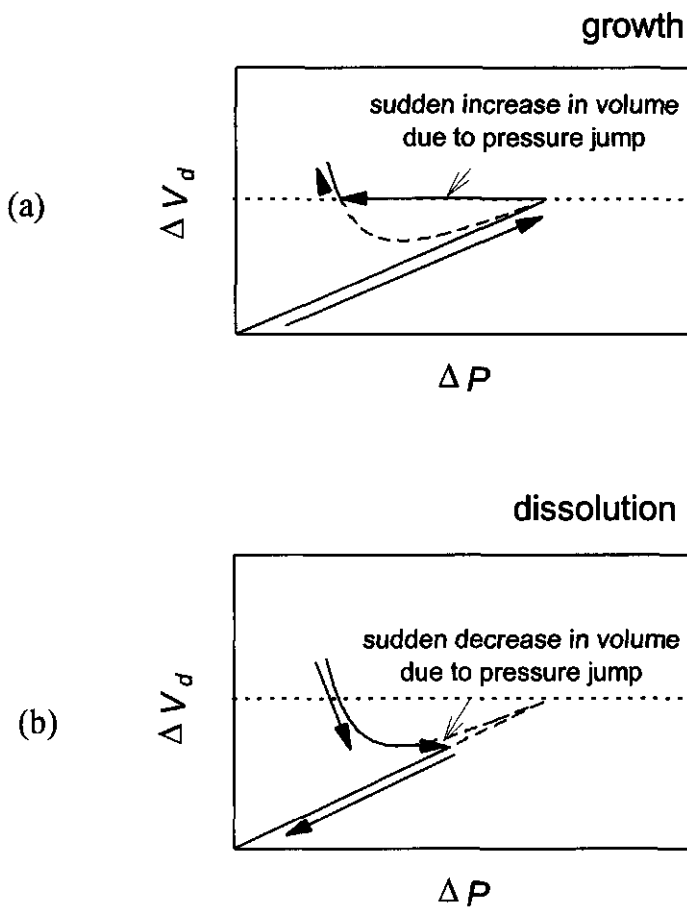


Figure 2.9 Change in bubble volume as a function of the bubble pressure, which follows for the curvature of the bubble interface (a) path followed for a growing bubble, and (b) for a dissolving bubble.

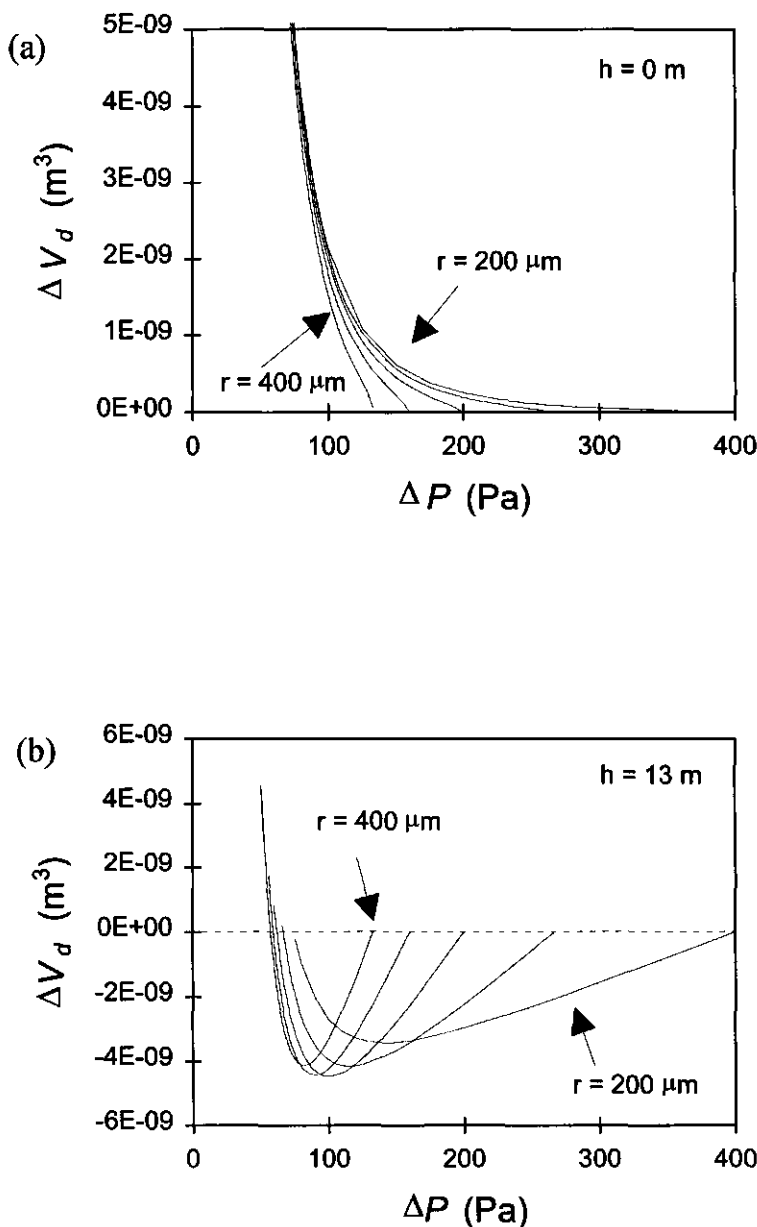


Figure 2.10 The function f_i in relation to ΔP for $r = 2, 3, 4, 5, 6 \cdot 10^{-4} \text{ m}$, and for (a) $h = 0 \text{ m}$ and (b) $h = 13 \text{ m}$; $\gamma = 40 \text{ mN/m}$.

2.3.2 Bubble 'blow-up' instability

The jump in the bubble volume only takes place for $f_i < 0$; rewriting equation (2.21) gives:

$$\frac{\left(2r^3 + \frac{3V_h}{\pi}\right) * \left(\frac{\Delta P_{\max} - \Delta P}{\Delta P + P_0}\right) + 2r^3}{(2R^2 + r^2) * \sqrt{R^2 - r^2 + 2R^3}} > 1 \quad (2.23)$$

or

$$V_h > \frac{\pi}{3} \left(\frac{(2R^2 + r^2) * \sqrt{R^2 - r^2} + 2R^3 - 2r^3}{\left(\frac{\Delta P_{\max} - \Delta P}{\Delta P + P_0}\right)} - 2r^3 \right) \quad (2.24)$$

Simplifying equation (2.23) by assuming $P_0 \gg \Delta P_{\max}$ ($= b$), V_h above which an expansion effect can be noticed can be calculated for every r and R .

For non-existent hinterland volumes ($V_h = 0$) the equation could never be greater than one since $r \leq R$, therefore no growth instability will arise in the situation where no hinterland volume is present.

The next step would be to find out under what conditions the jump in bubble growth exceeds the volume of the bubble at detachment V_{det} , since in this situation the bubble would be 'blown off' the capillary. At detachment, R is the radius of the bubble in equilibrium with the surface tension force according to Archimedes' law (see also chapter 3):

$$R = \sqrt[3]{\frac{3r\gamma}{2\Delta\rho g}} \quad (2.25)$$

Figure 2.11 shows the inequality in equation (2.24) V_h as a function of r . All points above the line show situations where bubble growth is unstable. The second Y-axis gives the length of the cylindrical hinterland h corresponding to V_h for each r . As can be seen, the length of the hinterland needed to blow off a bubble is much larger than would be encountered in practical situations.

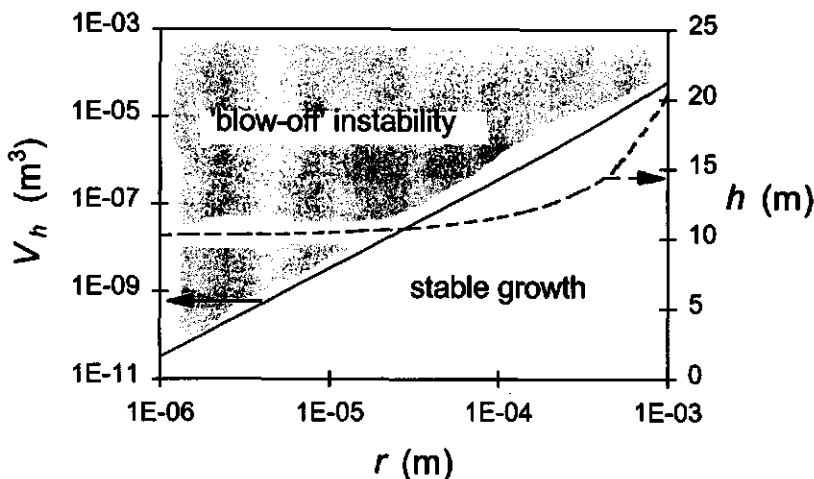


Figure 2.11 Hinterland volume V_h and length h as a function of capillary radius r ; $\gamma = 40$ mN/m.

2.3.3 Retreat of the gas-liquid interface

A second effect we discussed earlier is the retreat of the interface into the capillary: in order to calculate the retreat for a perfectly wetted capillary, there are two assumptions to be made: 1) the bubble left on the capillary after detachment has volume $2\pi r^3$ with pressure $2\gamma/R + P_o$, and 2) the radius of curvature stays equal to r when the volume of gas retreats into the capillary as for perfect wetting conditions (see figure 2.12).

We derive with Boyle's law (equation (2.13)):

$$(\Delta P + P_o) * \left(\frac{2}{3} \pi r^3 + V_h \right) = (\Delta P_{\max} + P_o) * \left(\frac{2}{3} \pi r^3 + V_h - \Delta V \right) \quad (2.26)$$

where $\Delta V = \Delta V_c$ is the change in volume due to compression, becoming:

$$\Delta V_c = \left(\frac{2}{3} \pi r^3 + V_h \right) * \left(\frac{\Delta P_{\max} - \Delta P}{\Delta P_{\max} + P_o} \right). \quad (2.27)$$

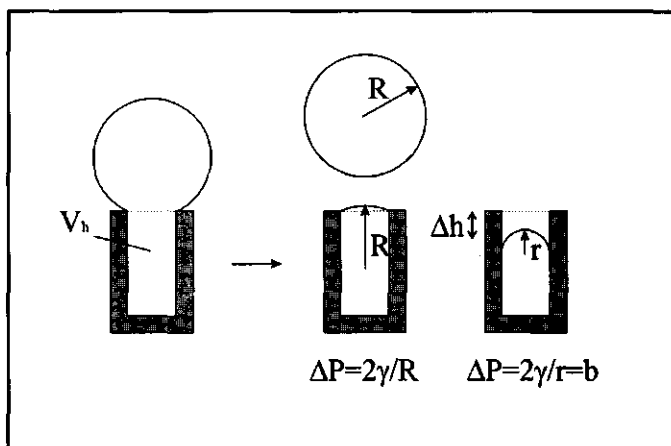


Figure 2.12 Schematic presentation of the situation before and after bubble detachment, resulting in a retreat of the gas-liquid interface in a well-wetted capillary.

Since the cavity under observance is a cylindrical capillary the retreat can also be calculated as a distance Δh where:

$$\Delta h = \frac{\Delta V_c}{\pi r^2} \quad (2.28)$$

Figure 2.13 shows the length of the capillary h necessary to 'blow' the bubble off the capillary, as well as the resulting distance of retreat of the gas-liquid interface into that same capillary. As can be seen Δh (retreat into the capillary) can become quite large for small capillary radii, but becomes negligible for large capillary radii.

With the help of the penetration theory for diffusion of gas to the retreated interface (see also section 2.5):

$$h = \sqrt{\pi D t} \quad (2.29)$$

we can roughly estimate that renewed bubble growth will be delayed by a factor h^2 , which means by a factor $1/r^4$. This effect can have a much more serious influence on the rate of bubble formation than the 'blow-up' instability.

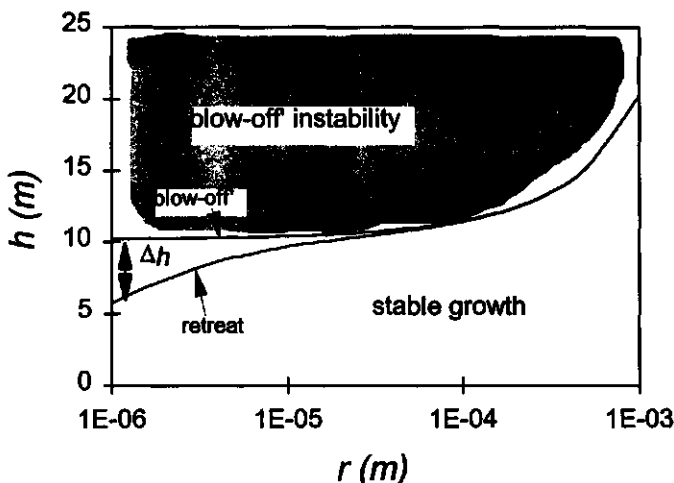


Figure 2.13 Length of retreat of gas-liquid interface h after bubble ‘blow-up’ instability as a function of the capillary radius r . Δh is the effective retreat of the gas liquid interface.

2.3.4 Discussion

The previous calculation of the hinterland volume which can influence the stability of bubble growth is an academic one. First of all, the model cavity geometry used here is cylindrical, and these cylindrical cavities should be at least 10 m for bubbles to be ‘blown off’, which is not a very realistic value. Secondly the gas will undergo friction as it expands, and will therefore not have enough time to expand before the bubble grows any further by diffusion: it is therefore imperative that time scales are taken into account. For different geometry’s where wall effects will not influence the expansion too much, the above calculations are closer to the truth.

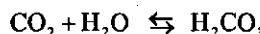
It should be noted that we made these calculations for a perfectly wetted capillary. When the bubble detaches from a non-wetted capillary, the equilibrium radius of curvature is much larger than r . Consequently less or no compression is needed to reach equilibrium, and the retreat of the interface will be of much less consequence. In this situation the bubble growth will not be affected by either ‘blow-up’ instability or by the retreat of the gas-liquid interface.

To conclude, bubble growth on a capillary can be accelerated by the presence of a large hinterland volume but if the surface of the capillary is well wetted, the consequential retreat of the interface back into the capillary has much more influence on the deceleration of renewed bubble growth driven by diffusion.

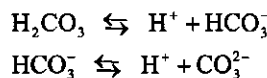
2.4 Solubility of CO₂ in aqueous solutions

In this work we will observe the formation of carbon dioxide bubbles in gas-supersaturated aqueous solutions. The supersaturation (equation (2.4)) of the gas in a liquid depends on its solubility in the liquid, and on its association with the liquid. This association is also a function of the ambient temperature and pressure. For example, the maximum solubility of CO₂ is about 50 times larger than that of N₂. This means that in order to get the same concentration of gas in a liquid, the applied pressure to achieve this concentration should be 50 times higher for nitrogen than for carbon dioxide.

Carbon dioxide reacts with water to produce a simple addition product, carbonic acid H₂CO₃, according to the equation:



This acid reacts further to produce:



Hence there could be up to four different carbon dioxide products present in the solution, if all these reactions were to occur. In practice, when CO₂ is added to unbuffered water, most of the carbon remains in the form of unreacted CO₂, that is, none of the reactions take place to any appreciable content. To begin with, only about 0.35% of the undissociated species are in the form of H₂CO₃ at 25°C. Secondly, the lowering of pH accompanying the ionic dissociation reactions shifts the point of equilibrium to the left. That is, the first dissociation is strongly suppressed and the second practically does not occur. The presence in beer of a natural buffer system further ensures that almost 100% of the carbon dioxide content is present in the form of solubilised CO₂.

Another special consideration to be invoked when discussing CO₂ solubility is the non-ideality of the gas. For many gases at ordinary temperatures and pressures, it is possible to use the ideal gas approximation when trying to explain relationships between gas pressure and dissolved gas concentration at equilibrium. But interactions among CO₂ molecules are sufficiently strong to cause the effective pressure exerted by the gas to be slightly lower from the applied pressure, under typical conditions in a beverage application. At 25°C this means that the fugacity (gas pressure) is 5% lower than the applied pressure.

King (1969) showed that experimental data on the pressure dependence of solubility's of real gases which react with the solvent (including that for CO₂) could be represented by a linear relation between the fugacity and the concentration of undissociated

Table 2.1 Henry's law constant for the solubility of CO₂ in water as a function of temperature. (Janssen en Warmoeskerken, 1987)

Temp. (°C)	H _{CO₂} (Pa)
0	7.62
5	9.16
10	10.9
15	12.8
20	14.8
25	17.1

gas molecules, also called Henry's law:

$$x = \frac{P}{H} \quad (2.30)$$

where x is the mole fraction of the gas in water (mol/mol), P is the partial pressure of the solute gas (Pa), and H is Henry's law constant (Pa), which increases with temperature (see table 2.1)

The temperature dependence of the solubility of CO₂ in water can also be found with the empirical relation for a partial pressure of 1 bar, valid between 273 and 353 K.

$$x = \exp\left(\frac{4.184}{R}\left(A + \frac{B}{T} + C \ln T + DT\right)\right) \quad (2.31)$$

where R is the gas constant (8.31 J/mol.K), A , B , C and D are empirical constants and T is the temperature (K). For CO₂ in water, the constants $A = -317.658$, $B = 17371.2$, $C = 43.0607$ and $D = -0.00219107$. It has been found empirically that the solubility of CO₂ in beer is about 4% lower than in pure water (private communication), yielding the same constants except for $A = -306.84$.

The mole fraction x can then be converted to concentration units using the following formulae for dissolved gas in pure water:

$$c_1 \left[\text{mol / kg} \right] = \frac{1000 \cdot x \cdot P}{18,0153 (1-x) P_{atm}} \quad \left[\frac{(\text{g H}_2\text{O / kg})(\text{Pa})}{(\text{g / mol H}_2\text{O})(\text{Pa})} \right]$$

$$c_2 \left[\text{vol / vol} \right] = c_1 \cdot V_m \cdot \rho \quad \left[\frac{(\text{mol / kg})(\text{m}^3 \text{ gas / mol})}{(\text{kg / m}^3 \text{ H}_2\text{O})} \right]$$

$$c_3 \left[\text{g / kg} \right] = c_1 \cdot M_m \quad \left[\frac{(\text{mol / kg})(\text{g / mol})}{(\text{mol / kg})(\text{g / mol})} \right]$$

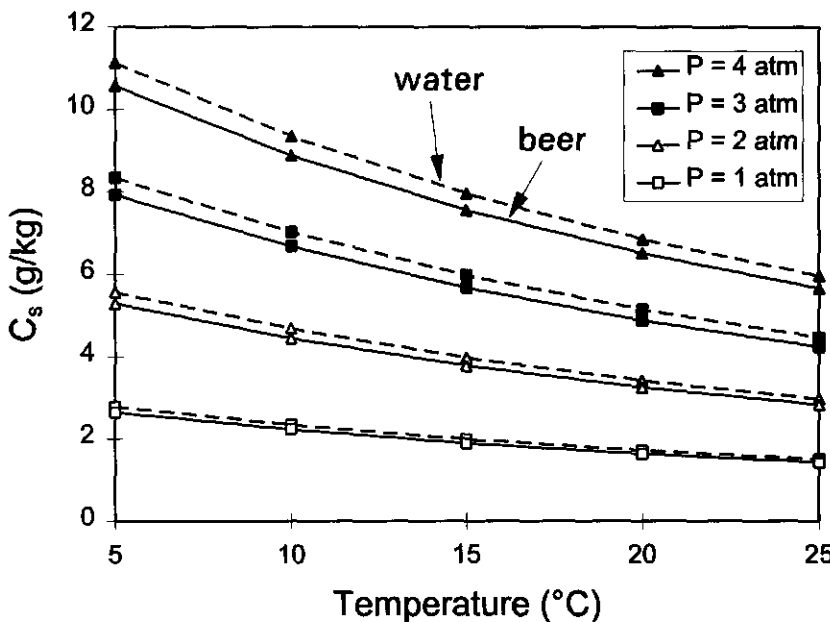


Figure 2.14 Saturation concentration of CO_2 dissolved in water (dotted line) and beer (full line) for 4 ambient pressures, as a function of ambient temperature, using equation (2.31)

where V_m is the molar volume of the gas phase, ρ is the density of water, and M_m is the molar mass of the gas. The solubility in g CO_2 /kg liquid is calculated by means of equation (2.31) for the liquids water and beer, and plotted as a function of temperature for ambient pressures of 1, 2, 3 and 4 bar in figure 2.14. A value of 4400 g/mol is found empirically for the molar mass of beer (private communication).

In figure 2.14 we find a non-linear relationship between the dissolution concentration and temperature, as was predicted. The difference between beer and water is minimal, when the pH is buffered equally in both systems.

2.5 Equilibrium and dynamic surface properties

Before discussing the effect of surface rheological properties on the behaviour of foams in more detail, a short discussion to surface physical chemistry of surfactant solutions will be given.

All condensed phases (solids and liquids) have a surface tension. This surface tension γ is caused by the fact that a certain amount of free energy G is needed in order to enlarge the surface of such a system by the unit of surface area A . Since from a thermodynamical point of view, all systems strive to reach the lowest value of free energy, the surface area will be kept as small as possible. This explains why a bubble will try to retain a spherical shape.

According to the definition of the surface tension given above its dimension is energy per unit area, or force per unit length, N/m (Prins, 1990). This indicates that the surface tension can be considered a force which acts in a surface over a unit length. For a given temperature and pressure the surface tension depends on the nature of the system: the surface tension is a characteristic property of a system. One of its most important properties is that the surface tension of a liquid can be changed by addition of surface active components. When a component like a surfactant or soap is present in water it adsorbs at the gas-liquid surface and by doing that, it lowers the surface tension of the water from 72 mN/m (pure water) to, say, about 35 mN/m.

Adsorption of low molecular weight surfactants to air-water surfaces at low concentrations can be derived by measuring the decrease of the surface tension with concentration increase, by the use of Gibbs' law. The basis of the Gibbs equation is a dynamic equilibrium between adsorbed and dissolved surfactant molecules; the adsorption is therefore reversible. Due to their extremely high surface activity, macromolecules are very hard to desorb by lowering the bulk concentration. Therefore Gibb's law is in general not applicable to adsorption of macromolecules. Apart from this, desorption of macromolecules such as proteins is slow, the more so if the molecular weight is high. In practice, then, proteins may be adsorbed almost irreversibly. They may become even more so by cross-linking reactions occurring between the molecules (within minutes up to days), as their concentration is extremely high in an adsorbed layer (Walstra, 1989).

Apart from pressure and temperature the surface tension of a surfactant solution can be varied when the surface is expanded or compressed, as can and will happen abundantly in practical situations (for example during a process of dispersion such as foaming or emulsifying). Since in this situation there is no equilibrium between the surface coverage and the concentration in the bulk liquid, the surface tension is called the dynamic surface tension. The rate at which the surface is compressed/expanded and the total relative compression/expansion of the surface can have different influences on the effective, dynamic surface tension. The way the surface tension adjusts to new situations such as expansion or compression is characteristic of the type of molecules adsorbed at the surface.

In order to be able to understand the behaviour of systems such as the rupture of liquid films, spreading of immiscible liquids over each other, disproportionation of bubbles and slow drainage of foams requires knowledge of the relation between the rate (or amount) of deformation and the change in surface tension. The relation, which is generally used, is based on the suggestion of Boussinesq (1913), according to which the excess surface tension $\Delta\gamma$ of an expanding (or compressed) surface element is simply proportional to the relative rate of deformation $d\ln A/dt$:

$$\Delta\gamma = \eta_s \frac{1}{A} \frac{dA}{dt} = \eta_s \frac{d\ln A}{dt} \quad (2.32)$$

where $\Delta\gamma$ is the increase (or decrease) in surface tension with respect to the equilibrium value, η_s is the proportionality factor, also known as the surface dilational viscosity (Prins, 1986, 1988; van Voorst Vader *et al.*, 1964), dA is an infinitesimal increase in surface area in time dt , and $d\ln A/dt$ is the relative rate of deformation at which the surface area A is increased (or decreased).

In solutions of low-molecular-weight surfactants, the surface dilational viscosity accounts for the fact that, on enlarging the surface area, transport of surfactant to the depleted surface takes a finite time because surfactant molecules have to move through the liquid across a certain distance. When mass transport is dictated by diffusion, the required time can be estimated from the penetration length:

$$l = \sqrt{\pi ID t} \quad (2.33)$$

where l represents the distance over which diffusion takes place (m), and ID is the diffusion coefficient (m^2/s). For a surfactant concentration c and an adsorbed amount Γ , the distance over which diffusion has to take place is of the order of Γ/c . This means that t can be described as a function of Γ and c using equation (2.33). This gives the relevant time-scale as a function of surfactant concentration. For high-molecular-weight surfactants such as proteins and polysaccharides, the same line of reasoning also applies, but an additional time is needed for the conformational changes which the macromolecules need to undergo in order to be able to adsorb at the surface.

It should be pointed out that η_s is not a constant. Its value decreases as the value of $d\ln A/dt$ increases. It is found (Prins, 1986), for liquid foodstuffs such as beer and milk, that η_s falls from ca. 1.10^3 mNs/m to 5 mNs/m as $d\ln A/dt$ increases from 10^{-2} to 1 s^{-1} (see also chapter 4).

The practical significance of the surface dilational viscosity in food related surfactants is that, due to the time needed for re-equilibration processes, surface tension gradients can occur when a liquid flows along a surface. This can have influence on for example the rate of drainage in a foam, but also the rise of bubbles in liquids. The stress

imparted on the surface by the flowing fluid is in mechanical equilibrium with a constant surface tension gradient (Prins, 1990):

$$\left(\frac{dv_x}{dz} \right)_{z=0} = \frac{d\gamma}{dx} \quad (2.34)$$

where η is the bulk liquid viscosity (Ns/m^2), v_x the velocity of the liquid parallel to the surface, z the coordinate perpendicular to the surface, and $z=0$ is the position of the interface. The extent to which the surface lags behind the moving liquid depends on the stiffness of the surface as expressed by the value of η_s . In the extreme case of purely elastic surfaces (an insoluble monolayer), the interface can be completely motionless, as a result of the surface tension gradient.

In bubbles rising through a liquid this can have a great effect on the velocity of rise. For a rigid surface, the rise velocity is impeded by the friction caused by the immobile interface. If the surface is freely moving with the liquid, not only does the rise velocity increase (see chapter 5), but the bubble will start to move in zigzag motion (Duineveld, 1994).

A different practical effect that surface rheology can have on practical processes is the continuous expansion or compression of a surface. We find an example of expansion in bubble growth, of compression when bubbles shrink due to diffusional gas transport. In a foam both growth and shrinkage of bubbles occur as a result of disproportionation or Ostwald ripening (Prins, 1990). When two bubbles of different size are present in a liquid, the pressure difference between the two bubbles (see the Laplace equation (2.2)) will result in the growth of the larger bubble at the expense of the smaller one. Ronteltap and Prins (1990) showed that the shrinking rate of bubbles could be greatly reduced when the surface dilational viscosity was measured to be high, i.e. the surface tension decreases considerably with the compression of the surface. Model calculations (Ronteltap *et al.* (1990) showed that incorporation of dynamic surface properties could account for this decrease in shrinking rate: a bubble with constant surface tension disappears within finite time, but when the surface dilational viscosity is taken into account, a considerable slowing down is observed after a certain radius is reached.

The above relates to bubble surfaces which behave visco-elastically, so the disproportionation process can only be slowed down, not completely stopped. As shown by Lucassen (1981), however, the process can be stopped completely if the bubble surface behaves in a purely elastic way, i.e. if the following relation is satisfied:

$$E_s \geq \frac{\gamma}{2} \quad (2.35)$$

where E_s is the surface dilational elasticity or modulus. The surface dilational elasticity is a parameter of the surface close to equilibrium as opposed to the surface dilational viscosity,

and is defined as the infinitesimal change in (dynamic) surface tension as a result of an infinitesimal change in surface area:

$$E = \frac{Ad\gamma}{dA} = \frac{d\gamma}{d \ln A} \quad (2.36)$$

Apart from surface dilation, surface shear can also affect the effective surface properties. Surface shear imparts a change in the shape of the surface but not in size. Surface properties can be influenced by surface shear in situations when the adsorbed molecules interact with each other, forming a network or 'skin' layer. The molecules are then more or less attached to one another and cannot move freely past each other. In practice, however, it is difficult to indicate whether shear or dilation plays the dominant role in the deformation. Generally surface deformations will be a mixture of both. There are, however, still many unanswered questions concerning the effect of surface rheological properties on practical processes such as foaming and emulsifying as a whole.

2.6 Components contributing to the foaming properties and dynamic surface properties of beer

In carbonised beverages, the presence of foam can be desired or not, depending on the consumer acceptance of this foam. A formation of a desired aqueous foam, such as that found in dutch beer, requires the presence of a surfactant in solution, which can stabilise the increase in surface area as a result of the formation of bubbles. Once the foam is formed, it will immediately start to collapse. This is because foams are thermodynamically unstable, and will tend towards the state of minimum free energy, or, in this case, surface area. Foam collapse initially occurs by drainage of liquid from the films or lamellae between gas bubbles due to gravitational forces as well as Laplace suction from the plateau borders (Sebba, 1987).

The rate of drainage is also governed by the surface viscosity of the liquid phase of the foam. A high surface dilational viscosity is desirable for foam stability (Morris, 1984) in that the liquid films are more difficult to deform. Furthermore, liquid films in foams stabilised by proteins are found to be quite rigid, so that the liquid flow between the two interfaces is much slower than when the interfaces move freely.

When the liquid films are still quite thick, their stability is determined by the Gibbs-Marangoni effect. Generally speaking this is the prevention of the formation of a local thinning in the film, and can only occur if surfactants are present. A foam under dynamic conditions is subject to local extensions and compressions which, in the presence of surfactants, cause local increases and decreases in surface tension. The reparation

mechanism for this destabilisation is called the Gibbs-Marangoni stabilisation. It's mechanism is that, due to the presence of a surface tension gradient, a rapid lateral movement of adsorbed molecules takes place from surfactant-rich parts of the film to surfactant-poor parts of the film (Gibbs elasticity). The movement of the surface drags liquid along to the thinner part of the film (Marangoni effect), thereby repairing the film.

Drainage between the two interfaces will continue until the disjoining pressure becomes large enough to withstand the plateau border suction. At this point the film is in equilibrium, and can withstand any deformation, unless evaporation simply causes the film to desintegrate. Without the stabilising mechanisms of Gibbs-Marangoni, the film ruptures easily as a result of surface deformation and two bubbles coalesce. The coalescence of bubbles results in the bubbles becoming fewer and larger. This usually takes place in the top of the foam where the films are the thinnest. As a result the foam height decreases and eventually disappears.

Two other influences can play an important role in the stability of foams. The diffusion of gas from small to large bubbles, called Ostwald ripening or disproportionation, occurs due to a pressure difference between the bubbles. This effect can be reduced if the bubbles are more uniform in size. The disproportionation mechanism can have large effects on the stability of beer foam containing chiefly carbon dioxide gas. As a result the foam can coarsen rapidly, i.e. the distribution of bubble sizes becomes wider. This effect can, however, be minimised by the use of a gas with a lower solubility, such as nitrogen (Morris, 1984). Ronteltap (1989) gave a comprehensive review of the physics of the stability of beer foams.

When other surface active components such as fatty acids are present in the film, spreading of this phase on the film surface can cause the film to rupture and the bubbles to coalesce. The spreading particle mechanism has been researched in depth by Bisperink (1997), who shows that the main reason for spreading of for examples fatty acid droplets in beer foams, is due to the difference in surface tension.

Using the criteria listed above for a stable foam, beer is an non-ideal solution of surfactants. It has a reduced surface tension (about 40-45 mN/m) which is due to the adsorption of surface active material. It contains a great variety of surface active materials, but not all contribute in a positive way to foam stability, as will be described in the following paragraph. The presence of non-surface active dextrans and glucans (Bamforth, 1985) give beer an increased bulk viscosity, which is known to slow down the process of drainage.

The surfactants in beer have been divided historically (Pierce, 1978; Whitear, 1978; Roberts, 1975; Morris, 1984; Bamforth, 1985) into foam positive agents (those promoting foam formation and stability) and foam negative agents (those which destabilise foam). Whilst the contribution of many separate compounds to the formation and stability of beer foam have been observed, researchers are still “ no nearer to answering the question whether stable foams are irretrievably linked to the absence in beer of one or a few special

types of foam active substances or alternatively whether the balance of a greater or lesser number of compounds of diverse chemical structure determines foam stability" (Bamforth, 1985). The potential foam active substances found in beer can be listed in the following way:

foam positive agents:

- proteins, or more specific polypeptides
- hop resins, in particular isohumulones
- melanoidins
- glycoproteins, glycolipids
- carbohydrates
- metal ions, in particular nickel
- ethanol

foam negative agents:

- lipids, free fatty acids, phospholipids, glycerides, sterols and esters
(to a lesser extent monoglycerides)
- nitrogenous material (peptides) $< 5000\text{D}$
- detergent in glasses and dispensers

The reader can refer to either of the references listed in this paragraph for a more detailed description of what effect each component will have on foam stability. We limit ourselves to mentioning a few characteristics properties of the foam stabilising mechanisms.

According to most of the authors, beer essentially has more than enough foam positive material. The amount of foam negative species present in the beer determines, or rather, limits the foamability and stability. It seems that mostly the larger hydrophobic polypeptides are stabilising the interface, complexed or not with carbohydrates (glycoproteins) or with isohumulones, which also can have hydrophobic side-chains. The generally accepted mechanism of the destabilising action of foam negative agents is believed to be a disruption of a type of cross-linked network of foam positive agents adsorbed at the surface. The types of interactions between various foam stabilising species are thought to be cross-linking, ionic bonding, hydrophobic interactions and hydrogen bonding.

Maeda *et al.* (1991) found that the foam stability increased as also the surface (shear) viscosity increased. They found that the beer protein fraction MW $> 40\text{kD}$ was most effective in stabilising foam, in decreasing the surface tension and was also the most hydrophobic fraction of proteins. Perhaps these types are the most effective in complexing with other species. Clark *et al.* (1991) found evidence of cross-linking between hop acids and adsorbed model proteins, resulting in a decrease of the liquid drainage from these films.

All evidence found suggests that some complexing process of adsorbed material at beer bubble surfaces results in a network formation of some kind which can be quite strong. Morris (1978) observed that solid material was found to be present in collapsed foam from hopped beer as opposed to unhopped beer, proposed to be complexes of isohumulone, glycoproteins and metal ions such as nickel, bound by ionic or weak hydrophobic interaction. This leads us on to the next paragraph, which will deal with the phenomena of surface layers, networks or 'skins', and what effect this phenomenon may have on mechanisms as bubble shrinkage, growth, detachment, bubble rise and drainage of liquid from foam.

2.7 'Skins' in beer

As described in paragraph 2.2.3.3, pre-existent nuclei may be stabilised by macroscopical surface layers or 'skins'. Morris (1978) observed the formation of solid material in collapsed foam made from hopped beer. In sea water the 'skins' found to form around dissolving bubbles contain proteins, fatty acids, sterols and fatty alcohol's (Johnson and Cooke, 1980). We have found that during the degassing of beer, specks of dark material are formed at the junctions between collapsed bubbles. In the past, these 'skins' have also been found at the bottom of the falling liquid films which can be studied in the overflowing cylinder and with the falling film apparatus. It seems that these solid surface layers only form after an expansion and a compression of the surface. From literature it is known that an expansion/compression cycle will induce the formation of some kind of network at the interface (Yount, 1979; D'Arrigo, 1984). The formation of such a layer can have a large effect on surface rheological properties, and hence on the dynamic processes of drainage and disproportionation. Ronteltap and Prins (1990) observed a decrease in bubble dissolution, and accounted this phenomenon to 'skin' formation, as did Manley (1960). Later Bisperink and Prins (1994) found that, in bubble formation at a capillary, there is a threshold for bubble growth by diffusion that is unaccountable to geometrical influences. It is very possible that before the bubble really starts to grow, the surface is covered by a surfactant layer, which possesses a yield stress which should first be reached in order to 'break' the surface layer before bubble growth can continue.

It seems, then, that there is enough evidence of the formation of some kind of surface layer at gas-liquid interfaces in surfactant solutions. The surface layer has surface rheological properties which can influence the stability of gas bubbles in liquids. The implications of this surface layer or 'skin' in the detachment and the rise velocity of beer bubbles is discussed in chapter 4 and 5.

2.8 Conclusions

In literature, a large amount of theory is available for the calculation of nucleation rates in gas-supersaturated liquids. In low supersaturated solutions such as beer, however, bubble growth generally occurs due to the presence of pre-existent nuclei, which can be entrapped at cavities in the solid, depending on its physical properties. Small cavities and hydrophobic surfaces make bubble formation easier, but it is still unclear how practical surfaces may be predicted to show a certain yield of bubble formation

The geometry of cavities used in theory are often conical or cylindrical in shape, but in practice mostly grooves and slits will be present in solid surfaces. The entrapment of gas at surfaces is imperative for the bubble formation described in this thesis, as well as the stability of the entrapped nuclei over a longer period of time. The curvature of the nucleus determines whether it will dissolve or not, but the liquid surface rheological properties can also play a large role in mechanically slowing down or stopping the dissolution of the nucleus.

Growth of the bubbles mostly occurs by diffusive and convective gas transport as will be described in the next chapter, but 'blow-up' instability of the bubble growth can occur at sufficiently large hinterland volumes. In bubble formation from cavities, however, this effect will be rather small, due to the huge hinterland volume needed for this instability. More importantly, the retreat of the gas-liquid interface once the bubble has detached from the solid surface can slow down the onset of growth of the next bubble at the same site.

References

Apfel, R.E. (1970) The Role of Impurities in Cavitation-Threshold Determination *The Journal of the Acoustical Society of America* **48** (5), 1179-1186.

D'Arrigo, J.S. (1978) Improved Method for Studying The Surface Chemistry of Bubble Formation *Aviation, Space, and Environmental Medicine* **49** (2), 358-361.

D'Arrigo, J.S. (1984) Surface Properties of Microbubble-Surfactant Monolayers at the Air/Water Interface *J. Colloid Interface Sci.* **100** (1), 106-111.

D'Arrigo, J.S. and Imae, T. (1992) Physical characteristics of Utrastable Lipid-coated Microbubbles *J. Colloid and Interface Sci.* **149** (2) 592-595.

Bamforth, C.W. (1985) The foaming properties of beer *J. Inst. Brew.* **91**, 370-383.

Bankoff, S.G. (1958) Entrapment of Gas in the Spreading of Liquid Over a Rough Surface *A.I.Ch.E. Journal* **4** (1), 24-26.

Bisperink, C.G.J. and Prins, A. (1994) Bubble growth in carbonated liquids *Colloids and Surfaces A: Physicochemical and Engineering Aspects* **85**, 237-253.

Blander, M. (1979) Bubble nucleation in liquids *Adv. Colloid and Interface Sci.* **10**, 1-32.

Boussinesq, M. (1913) *Ann. Chim. Phys.* **29**, 567.

Clark, D.C., Wilde, P.J. and Wilson, D.R. (1991) The effect of pre-isomerised hop extracts on the properties of model protein stabilised foams *J. Inst. Brew.* **97**, 169-172.

Clark, H.B., Strenge, P.S. and Westwater, J.W. (1959) Active Sites for Nucleate Boiling *Chemical Engineering progress Symposium Series no 29* **55**, 103-110.

Cole, R. (1974) Boiling Nucleation, in *Advances in Heat Transfer* Irvine, T.F. Jr. and Hartnett, J.P. (eds), Vol 10, Academic Press, New York, 85-166.

Cornwell, K. (1982) On boiling incipience due to contact angle hysteresis *Journal of Heat and Mass Transfer* **25** (2), 205-211.

Detsch, R.M. and Sharma, R.N. (1990) The critical angle for gas bubble entrainment by plunging liquid jets, *Chem Eng. J.* **44**, 157-166.

Duineveld, P.C. (1994) Bouncing and coalescence of two bubbles in water, Ph. D. Thesis, Universiteit Twente, The Netherlands, 160p.

Finkelstein, Y. and Tamir, A. (1985) Formation of Gas Bubbles in Supersaturated Solutions of Gases in Water *American Institute of Chemical Engineering Journal* **31** (9), 1409-1419.

Fox F.E. and Herzfeld K.F. (1954) Gas Bubbles with Organic Skin as Cavitation Nuclei *The Journal of the Acoustical Society of America* **26** (6), 984-989.

Griffith, P. and Wallis, J.D. (1960) The Role of Surface Conditions in Nucleate Boiling *Chemical Engineering Progress Symposium Series. Heat Transfer-Storrs* **56**, 49-63.

Harvey, E.N., Barnes, D.K., McElroy, W.D., Whitley, A.H., Pease, D.C. and Cooper, K.W. (1944) Bubble formation in animals, *J. Cell. and Comp. Phys.* **24** (1), 1-22.

Hilton, A.M. (1992) The Formation and Growth of CO₂ Gas Bubbles from Supersaturated Solutions, Ph. D. Thesis, University of Nottingham, The United Kingdom, 177p.

Janssen, L.P.B.M. and Warmoeskerken, M.M.C.G. (1987) *Transport Phenomena Data Companion*, Edward Arnold, Delftse Uitgevers Mij., London, p.137.

Johnson, B.D. and Cooke, R.C. (1980) Organic particle and aggregate formation resulting from the dissolution of bubbles in seawater *Limnol. Oceanogr.* **25** (4), 653-661.

Judd, R.L. and Lavdas, C.H. (1980) The nature of nucleation site interaction *J. Heat Transfer* **102** (3), 461-464.

Katz, J. L.(1992) Homogeneous nucleation theory and experiment - A survey *Pure and Appl. Chem.* **64** (11), 1661-1666.

King, M.B. (1969) *Phase Equilibrium in Mixtures* Pergamon, Oxford.

Liggieri, L., Ravera, F. and Passerone, A.. (1990) Drop Formation Instabilities Induced by Entrapped Gas Bubbles *J. Colloid Interface Sci.* **140** (2), 436-443.

Lin, J.N., Banerji, S.K. and Yasuda, H. (1994) Role of Interfacial Tensions in the formation and the Detachment of Air Bubbles 1. A Single Hole in a Horizontal Plane Immersed in Water *Langmuir* **10**, 936-942.

Lubetkin, S.D. and Blackwell, M. (1988) The nucleation of bubbles in supersaturated solutions, *J. Colloid and Interface Sci.* **126** (2), 610-615.

Lubetkin, S.D. (1989a) Measurement of bubble nucleation by an acoustic method, *J. Appl. Electrochem.* **19** (5), 668-676.

Lubetkin, S.D. (1989b) The nucleation and detachment of bubbles, *J. Chem. Soc., Faraday Trans.* **85** (7), 1753-1764.

Lucassen, J. (1981) Dynamic Properties of Free Liquid Films and Foams, in *Anionic Surfactants: Physical Chemistry of Surfactant Action* (ed. Lucassen-Reynders, E.H.), Marcel Dekker, New York, 217-265.

Lyklema, J. and Koopal, L.K. (1984) *Inleiding tot de grensvlakchemie*, Landbouwuniversiteit Wageningen, The Netherlands, 221p.

Maeda, K., Yokoi, S., Kamada, K. and Kamimura, M (1991) Foam Stability and Physicochemical Properties of Beer *A.S.B.C. Journal* **49** (1), 14-18.

Manley, D.M.J.P. (1960) Change in size of air bubbles in water containing a small dissolved air content *British J. Appl. Phys.* **11**, 38-42.

Morra, M., Occchiello, E., and Garbassi, F. (1990) Knowledge about polymer surfaces from contact angle measurements *Adv. Colloid and Interface Sci.* **32**, 79-116.

Morris, K.S. (1984) The stability of foam *Brewers Guardian* **dec**, 11-13.

Pierce, J.S. (1978) The role of positive and negative factors in head retention *Institute of Brewing Australian and New Zealand Section Proceedings of the 15th Convention*, 51-65.

Prins, A. (1986) Theory and Practice of Formation and Stability of Food Foams , in *Food Emulsions and Foams* , Dickinson, E. (ed.), Royal Society of London, Leeds, 30-39.

Prins, A. (1988) Principles of Foam Stability, in *Advances in Food Emulsions and Foams*, Dickinson, E and Staynsby, G. (eds), Elsevier Applied Science, 91-122.

Prins, A. (1990) Liquid flow in foams as affected by rheological surface properties: A contribution to a better understanding of the foaming behaviour of liquids, in *Hydrodynamics of Dispersed Media* , Hulin, J.P., Cazabat, A.M. Guyon, E. and Carmona, F. (eds.), Elsevier Science Publishers B.V., North Holland, 5-15.

Prins, A., van Vliet, T., and Walstra, P. (1986) Inleiding in de levensmiddelennatuurkunde Landbouwuniversiteit Wageningen, The Netherlands, 238p.

Roberts, R.T. (1975) Glycoproteins and beer foam *European Brewery Convention Proceedings of the 15th Convention, Nice*, 453-464.

Ronteltap, A.D. (1989) Beer Foam Physics, Ph. D. Thesis, Agricultural University Wageningen, The Netherlands, 133p.

Ronteltap, A.D. and Prins, A. (1990) The Role of Surface Viscosity in Gas Diffusion in Aqueous Foams. II. Experimental *Colloids and Surfaces* **47**, 285-298.

Ronteltap, A.D., Damsté, B.R., Gee, M. de and Prins, A. (1990) The Role of Surface Viscosity in Gas Diffusion in Aqueous Foams. I. Theoretical *Colloids and Surfaces* **47**, 269-283.

Ronteltap, A.D., Hollemans, M. Bisperink, C.G.J. and Prins, A. (1991) Beer Foam Physics, *M.B.A.A. Technical Quarterly* **28**, 25-32.

Rubin, M.B. and Noyes, R.M. (1987) Measurements of Critical Supersaturation for Homogeneous Nucleation of Bubbles *J. Phys. Chem.* **91**, 4193-4198.

Ryan, W.L. and Hemmingsen, E.A. (1993) Bubble Formation in water at smooth hydrophobic surfaces *J. Colloid Interface Sci.* **157**, 312-317.

Schafer, N.E. and Zare, R.N. (1991) Through a Beer Glass Darkly, in *Physics Today*, oct, 48-52.

Sebba, F. (1987) Polyhedral Gas Foams, in *Foams and Biliqid Foams* , John Wiley and Sons, 47-62.

Sgheiza, J.E. and Myers, J.E. (1985) Behavior of Nucleation Sites in Pool Boiling *A.I.Ch.E. Journal* 31 (19), 1605-1613.

Voorst Vader, F. van, Erkens, Th.F. and Tempel, M. van den (1964) Measurement of Dilatational Surface Properties *Trans Faraday Soc.* 60, 1170-1177.

Walstra, P. (1989) Principles of Foam Formation and Stability, in *Foams: Physics, Chemistry and Structure*, Wilson, A.J. (ed.), Springer-Verlag, London, 1-15.

Wang, C.H. and Dhir, V.K. (1993) Effects of Surface Wettability on Active Site Density During Pool Boiling of Water on a Vertical Surface *J. Heat Transfer* 115, 659-669.

Ward, C.A., Balakrishnan, A. and Hooper, F.C. (1970) On the thermodynamics of nucleation in weak gas-liquid solutions *J. Basic Eng.* 92, 695-704.

Ward, C.A. and Tucker, A.S. (1975) Thermodynamic theory of diffusion-controlled bubble growth or dissolution and experimental examination of the prediction *J. Appl. Phys.* 46 (1), 233-238.

Ward, C.A., Kohnson, W.R., Venter, R.D., Ho, S., Forest, T.W. and Fraser, W.D. (1983) Heterogeneous bubble nucleation and conditions for growth in a liquid-gas system of constant mass and volume *J. Appl. Phys.* 54 (4), 1833-1844.

Wilt, P.M. (1986) Nucleation Rates and Bubble Stability in Water-Carbon Dioxide Solutions *J. Colloid and Interface Sci.* 112 (2), 530-538.

Wilt, P.M (1988) Nucleation Rates in Water-Carbon Dioxide Solutions: The Spherical Cavity Case *J. Colloid and Interface Sci.* 123 (1), 296-298.

Winterton, R.H.S. (1977) Nucleation of boiling and cavitation *J. Phys. D: Appl. Phys.* 10, 2041-2056.

Whitear, A. L. (1978) Basic factors that determine foam stability *Institute of Brewing Australian and New Zealand Section Proceedings of the 15th Convention*, 67-75.

Yount, D.E. and Strauss, R.H. (1976) Bubble formation in gelatin: A model for decompression sickness *J. Appl. Phys.* 47 (11), 5081-5089.

Yount, D.E. , Kunkle, T.D., D'Arrigo, J.S., Ingle, F.W., Yeung, C.M. and Beckman, E.L. (1977) Stabilization of Gas Cavitation Nuclei by Surface-Active Compounds *Aviation, Space and Environmental Medicine* 48 (3), 185-191.

Yount, D.E. (1979) Skins of varying permeability: A stabilization mechanism for gas cavitation nuclei *The Journal of the Acoustical Society of America* 65 (6), 1429-1449.

BUBBLE FORMATION AND GROWTH ON A CAPILLARY

3.1 Introduction

From the hypothesis formulated in chapter 2, bubbles can grow on active surfaces from gas supersaturated solutions because they are helped by the presence of gas pockets or nuclei that are situated in cavities in the solid wall of the active surface. From the active surface, a great number of bubbles are formed which rise through the liquid and after accumulation at the surface they form a foam layer such as can be found in beer. The quality of the foam, or better said the stability of the foam against collapse is influenced by the individual rate of bubble formation and by the size distribution of the bubbles in the foam (Ronteltap, 1989). In order to understand better the properties of foam formed on active surfaces, it is useful to observe the individual formation of bubbles at single active sites in gas supersaturated solutions. To this end, we have used a glass capillary which is closed at one end. The open-ended side of the capillary will retain a small amount of gas when immersed in the supersaturated liquid, and can therefore act as a model nucleus for bubble growth.

By using a model active site for the observation of individual bubble growth we could manipulate certain factors which were thought to influence bubble size at detachment. For example factors such as the internal perimeter of the capillary and the wetting angle, as well as the surface tension of the liquid and its wetting properties could be varied in order to produce bubbles of various sizes. The bubble growth was recorded with a photographic technique, and the bubble volume was measured by the use of image analysis; the experimental values were then compared to theoretical predictions.

The growth rate of individual bubbles was also measured as a function of gas concentration, to observe whether the best suitable growth model (Bisperink, 1994) is valid for the supersaturations used in this work. It will be shown that it is extremely difficult to create experimental conditions where all the parameters are completely under control, at least in our situation, where the gas concentration in the liquid is very important to the bubble growth.

3.2 Bubble size at detachment

In this paragraph, we look at the factors which determine the bubble size at detachment from solid surfaces. The forces which can influence this size are described in the following section.

3.2.1 Forces acting on a bubble attached to a solid surface

At very low growth rates, the theoretical bubble volume at detachment can be obtained by equating the surface tension force with the buoyancy force, where factors such as the difference between the density of gas and liquid, wetting characteristics of the liquid on the solid surface (contact angle and surface tension) and the perimeter of plane contact between bubble and solid surface chiefly determine the size of the bubble at detachment. Bubble growth on a capillary ends as the bubble detaches, when the upward forces become greater than the downward forces (see figure 3.1). The quantitative expressions for various forces are given below, where the perimeter of the contact base in equation (3.2) is defined by the perimeter of a circular shaped cavity opening:

$$\text{buoyancy force} \quad F_1 = V(\rho_l - \rho_g)g \quad (3.1)$$

$$\text{surface tension force} \quad F_2 = -P_c \gamma \sin\theta \quad (3.2)$$

where $P_c = 2\pi r_c$ is the perimeter of the cavity opening, V is the bubble volume (m^3), ρ is the density of the liquid l or the gas phase g (kg/m^3), g is the acceleration due to gravity (m/s^2), r_c is the radius of the cavity opening (m), γ is the equilibrium surface tension (N/m) and θ is the dynamic contact angle ($^\circ$).

When bubble growth is very fast, forces associated with the expansion velocity of the bubble influence the bubble size at detachment. The bubble expands at a definite rate

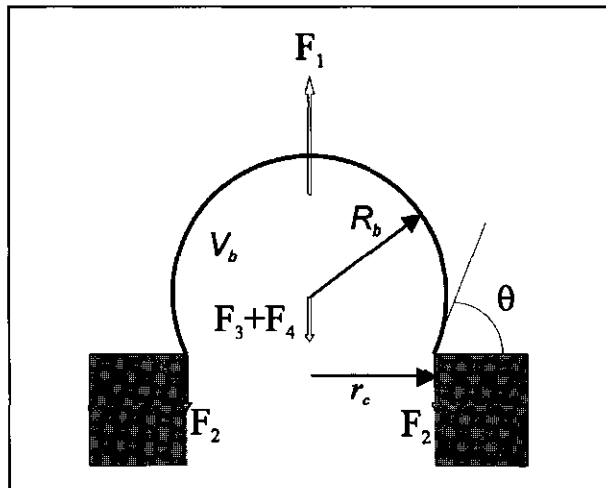


Figure 3.1 Forces acting on a bubble perched on a solid surface; see text for a description of the symbols.

thereby giving rise to a viscous drag and an inertial force. Both these forces add to the surface tension force in trying, as it were, to keep the bubble attached to the solid surface. The viscous force F_3 is described here for a rigid sphere, also known as Stokes' law:

$$\text{viscous drag} \quad F_3 = -6\pi R_b \eta v_m \quad (3.3)$$

where R_b is the bubble radius (m), η is the liquid viscosity (Pa.s) and v_m is the velocity of bubble movement (m/s).

The inertial force F_4 depends mostly on the volume of displaced liquid and the radial velocity of bubble growth (Chesters, 1979):

$$\text{inertial force} \quad F_4 = -\rho_l V \frac{d(v_m)}{dt} \quad (3.4)$$

As can be seen in figure 3.1, F_1 is positive and directed upwards, whereas the other forces are directed downwards, hence the negative sign. The forces are balanced at detachment with:

$$F_1 + F_2 + F_3 + F_4 = 0 \quad (3.5)$$

and the maximum bubble volume V_{max} prior to detachment can be calculated.

For each situation that arises, different forces dominate, and some may be neglected in certain cases. For example when a bubble is formed very rapidly, the rise of the bubble leading to detachment is impeded by inertia of the surrounding liquid and slowed down by drag forces. Therefore the bubble grows to a greater size before detaching (Chesters, 1979). For large enough growth rates, F_2 is small enough compared to F_1 and F_4 to be neglected. On the other hand, if bubble growth is slow and liquid viscosity low, F_3 and F_4 can be neglected and F_1 is the sole attaching force.

At the small rates of bubble growth employed in this chapter both viscous and inertial forces can be neglected (Chesters, 1979). However in another situation where liquid motion relative to the capillary is present (see chapter 4), the effect of viscosity F_3 and inertia F_4 can become increasingly important.

3.2.2 Effect of surface wetting on bubble size

When observing bubble growth the bubble may be floating freely in a liquid, attached to a flat smooth surface, or to a cavity embedded in a solid surface. In this work we are limited to the latter case where the bubble grows by diffusional gas transport from the gas-supersaturated liquid to a pre-existent nucleus that is trapped within a cavity, and where the bubble detaches when it reaches a specific size.

Some investigators have examined the effects of the nature of the solid surface on bubble growth and bubble size at detachment in the study of nucleation (Leiner and Böhmisch, 1984; Nesis and Komarov, 1975, Jańczuk, 1983; Lubetkin, 1989; Hilton, 1993). Lin *et al.* (1994a) varied the contact angle of an orifice plate and measured the size of bubbles detaching from the orifice in a sparging experiment. In all cases the bubble volume increased with reduced wettability or increased contact angle of the surface.

In the preceding paragraph, the forces are defined which influence the detachment of the bubble from the surface. The contact base of the bubble is limited by the radius of the cavity opening, as is the case for a hydrophilic surface where the contact angle between solid, liquid and gas phase is small. As will be described in section 2), the contact base is not limited by the cavity opening when the contact angle becomes larger than 90°.

1) hydrophilic surface or small wetting angle

In the situation of a well wetted surface, the bubble contact base does not expand beyond the rim of the cavity with radius r_c (3.2(a)). The reason for this is that the components of the interfacial tensions parallel to the solid surface keep the base from expanding, as will be explained in the next section.

The detachment of the bubble occurs at a critical or maximum bubble volume. The volume of spherical bubbles detaching under equilibrium conditions (low growth rates) at the horizontally positioned surface can be predicted theoretically from the balance between the buoyancy force F_1 pulling the spherical gas bubble up from the surface and the surface tension force F_2 holding the bubble attached to the surface, as described by equations (3.1) and (3.2):

$$F_1 = F_2$$

or:

$$V_{max} = \frac{2\pi r_c \gamma \sin\theta}{\Delta\rho g} \quad (3.6)$$

where V_{max} is the maximum bubble volume at detachment, $\Delta\rho$ is the difference in density between the liquid and the gas phase. As can be seen from equation (3.6) the volume of the detaching bubble or the maximum volume is defined by the difference in density, the perimeter of the contact base and vertical component of the surface tension. The surface tension is equal to the equilibrium surface tension since the surface dilation during bubble growth in these experiments is very small (see section 3.4.2). At low surface expansion rates, it is generally accepted that no surface tension gradients are present in the bubble surface (Chesters, 1979).

The inclusion of the contact angle at this stage is only justified from a theoretical point of view since experimental work (this work; Chesters, 1979; Lin *et al.*, 1994a; Jańczuk, 1983; Pinczewski, 1981; Hayes *et al.*, 1959; Kumar and Kuloor, 1970) has shown that an extended neck appears to form between the bubble and the surface before detachment (see figure 3.2). Although very short lived, the formation of the neck can be seen to occur in some of the frames (see figure 3.3). It is therefore reasonable to consider that the dynamic apparent contact angle θ just before the bubble detaches from the surface is 90° to the horizontal plane. This is probably due to the local geometry of the edge of the cavity, as discussed in more detail in chapter 4. Equation (3.6) then becomes:

$$V_m = \frac{2\pi r_c \gamma}{\Delta \rho g} \quad (3.7)$$

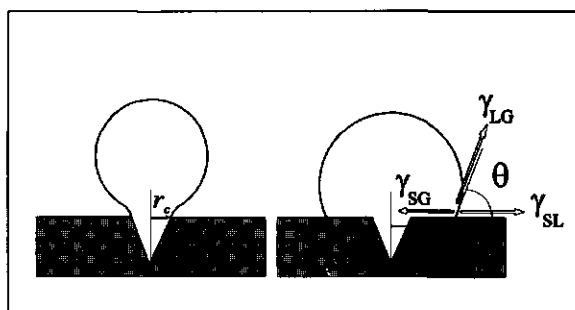


Figure 3.2 (a) bubble growing from a cavity on a hydrophilic surface and (b) bubble growing from a cavity on a hydrophobic surface.

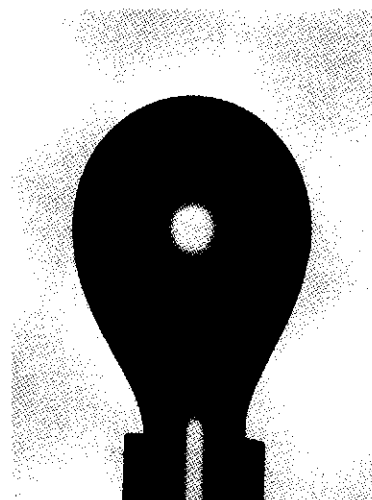


Figure 3.3 Photograph taken of a bubble growing on a capillary prior to detachment.

2) hydrophobic surface or large wetting angle

In contrast to the hydrophilic surface, the detachment volume of bubbles growing on a cavity surrounded by hydrophobic surface is defined largely by the wetting properties of the solid surface. The nature of the solid surface and of the liquid phase define the contact angle which presides at the bubble contact base. If the angle is larger than about 50° (Lin *et al.*, 1994a), the net horizontal force will induce the contact base to expand beyond the rim of the cavity (figure 3.2(b)).

The balance of interfacial tensions (in equilibrium) parallel to the solid surface at the three phase contact point is given by Young's equation:

$$\gamma_{SL} + \gamma_{LG} \cos\theta = \gamma_{SG} \quad (3.8)$$

where γ_{SL} and γ_{SG} are the interfacial tensions between solid-liquid and solid-gas phases respectively and where $\gamma_{LG} \cos\theta$ is the horizontal component of the surface tension between the liquid and the gas phase.

We now define a new force which works radially parallel to the surface, the net expansion force F_s :

$$F_s = 2\pi r_c (\gamma_{SL} + \gamma_{LG} \cos\theta - \gamma_{SG}) \quad (3.9)$$

Note that at $\theta=90^\circ$, $\cos\theta=0$ and γ_{SL} and γ_{SG} are equal to one another, so that F_s becomes zero. This means that the contact base does not expand unless θ is larger than 90°.

If the liquid does not wet the solid surface the contact angle is large and the contact base will expand from r_c to r_e , as shown in figure 3.2 (Leiner and Böhnisch, 1984; Chesters, 1979; Lin *et al.*, 1994a) and the bubble volume at detachment becomes:

$$V_{max} = \frac{2\pi r_e \gamma \sin\theta}{\Delta\rho g} \quad (3.10)$$

where again $\sin\theta$ becomes 1 just before detachment.

Several researchers found a maximum bubble volume for hydrophobic surfaces as a function of the wetting angle. Fritz (1935) found a semi-empirical relation for the maximum bubble size attached to a smooth hydrophobic surface:

$$R_b = 0.0105\theta \sqrt{\frac{\gamma}{\Delta\rho g}} \quad (3.11)$$

Nesis and Komarov (1974) found an analytical relation for the maximum radius:

$$R_b = \sqrt{\frac{1}{4}} \sin \frac{\theta}{2} \sqrt{\frac{\gamma}{\Delta \rho g}} \quad (3.12)$$

which can also be derived when inserting the equality $R_b = r_c$ (the maximum obtainable bubble radius where the bubble has the shape of half a sphere) and $\theta = 90^\circ$ into the original force balance $F_i = F_z$ (equation (3.10)). When the bubble is a half-sphere, V_{max} becomes:

$$V = \frac{1}{2} \pi R_b^3 \quad (3.13)$$

The maximum radius then becomes:

$$R_b = \sqrt{\frac{3\gamma}{\Delta \rho g}} \quad (3.14)$$

which is the same relationship as derived by Lubetkin (1989) and Nesis and Komarov (1974) for a 90° contact angle. Equation (3.14) yields a radius which is twice as large as equation (3.12) due to the fact that we assume the bubble to have the volume of a half sphere prior to detachment, whereas equations (3.11) and (3.12) calculate the radius of a full sphere. For water ($\gamma = 70 \text{ mN/m}$) we find $R = 4.6 \text{ mm}$, and for beer ($\gamma = 40 \text{ mN/m}$) we find $R = 3.5 \text{ mm}$.

Concluding, the size of bubbles growing on hydrophilic surfaces are limited by the radius of the cavity to which they are attached. Bubbles growing on hydrophobic surfaces can expand beyond the rim of the cavity and detach at a larger size, unaffected by the cavity radius and chiefly dependent of the wetting properties of the solid surface. This means that bubbles growing on a hydrophobic surface can become very large in size ($R > 3 \text{ mm}$). Moreover, the bubble size can vary greatly on a practical material due to local variations in surface wetting characteristics.

3.2.3 Effect of variables on bubble size

The maximum size of bubbles at detachment from a cavity in a solid surface has been reviewed in the former paragraph as a function of wetting characteristics of the solid surface. Two modes of bubble detachment can be distinguished; hydrophilic where the bubble volume depends on the cavity size, and hydrophobic where the bubble volume is limited by surface wetting properties.

Various authors in literature concern themselves either with bubble growth by sparging gas through an orifice (figure 3.4(a)), or with heterogeneous bubble nucleation

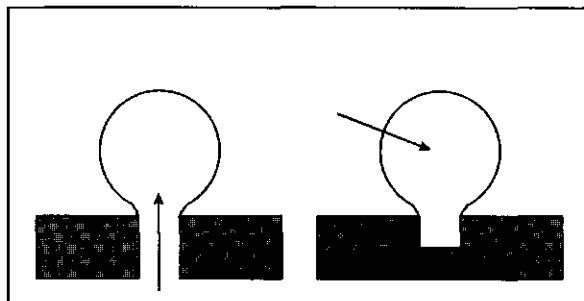


Figure 3.4 Sketch of an orifice-formed bubble and a diffusion-formed bubble.

and growth by applying a supersaturation in the liquid (see figure 3.4(b)). In either case, bubbles are formed at solid surfaces. The bubble growth rate in gas sparging is driven by the flow rate of gas through an orifice, whereas the latter process (heterogeneous bubble growth) is driven by diffusional gas transport from the liquid bulk phase to the bubble-liquid interface.

In either situation the influence of various variables on the size of the bubble formed will be more or less the same at equal growth rates. It seems however that more researchers have observed influences on bubble size with "orifice-formed" bubbles than with "diffusion-formed" bubbles. In this paragraph we have therefore tried to give a short review about the effects of various variables on bubble size, formed either by gas flow from an orifice or by gas diffusion on a cavity. We have used a categorical approach as used by Kumar and Kuloor (1970).

1. Solid surface variables

cavity or orifice diameter

As was discussed in paragraph 3.1.3 the volume of the bubble is proportional to the diameter of the orifice for hydrophilic surfaces, and independent of the orifice diameter for hydrophobic surfaces.

plane/capillary

Kumar and Kuloor (1970) pointed out that bubbles formed at a plane surface have a larger size at detachment than if they are formed on capillaries, although this is not explained. It would seem that this would only be of consequence for low wettability, where the contact base radius expands beyond the edge of the cavity/orifice. In the case of a capillary, the expansion is then limited by the edge of the outer diameter, whereas the bubble can expand further on a plane surface.

cavity or orifice geometry

Most authors have used circular openings for orifices as well as cavities. Any other geometry will influence and distort the axis-symmetry of the bubble formed. When the

shape of the cavity mouth deviates from circularity, the effective perimeter will be an average of the radii of circumference, as the bubble will try to assume a shape of smallest interfacial area.

inclination or orientation of the bubble contact base

Bubbles detaching from a hydrophilic surface can be greatly reduced when the angle of inclination is increased (Datta *et al.*, 1950; Kumar and Kuloor, 1970). This does not need to be the case for surfaces of low wettability (Lin *et al.*, 1994b). This aspect will be dealt with in greater detail in chapter 4, where experiments were performed to observe the effect of the angle of inclination on the maximum bubble volume.

chamber or hinterland volume

For orifice-formed bubbles the volume of the gas chamber situated behind the orifice opening can influence the size of detaching bubbles. At low flow rates a zero chamber volume (negligible compared to the bubble volume) will not affect the bubble volume. Enlarging the chamber volume from zero results in an increase in the size of the detaching bubble; However, when the pressure gradient is very large over the whole length of the chamber (e.g. for narrow and long capillaries) a zero chamber volume is effected and no increase in bubble volume is found.

Diffusion-formed bubbles are formed at cavities, therefore the analogue of a chamber volume is the hinterland volume (see section 2.3). If the hinterland volume is large enough, it will affect the rate of bubble growth (Zuidberg and Prins, 1995).

2. System variables

surface tension

For orifice-formed bubbles the bubble volume will only be proportional to the surface tension at small flow rates (Datta *et al.*, 1950). Diffusion-formed bubbles in our work have low growth rates, therefore the relation between the (equilibrium) surface tension and the bubble volume at detachment is linear as given in equation (3.7). This has been confirmed by Hayes *et al.* (1959), Chesters (1979) and Lin *et al.* (1994a). At high growth rates, the large expansion rate of the bubble surface can result in an increase in effective or dynamic surface tension due to slow relaxation processes of surface active compounds. Hence the size of a bubble at detachment can become larger as a result of surface rheological phenomena.

contact angle

The contact angle has a very large influence on bubble size since it determines whether the bubble contact base is limited by the rim of the orifice or the cavity or not. In the case of large contact angle the bubble will detach at a considerably larger but limited size than at small contact angle, as discussed in paragraph 3.2.2.

Viscosity and *density* of the liquid phase are only important at very large growth rates, and are therefore not investigated here (Chesters, 1979; Kumar and Kuloor, 1970)

3. Operating variables

bubble growth rate

In general the growth rate of diffusion-formed bubbles is relatively slow at the low supersaturation levels employed in this work, unless a convective mass-transport is included as a result of liquid movement. At the low growth rates found in this work, the size of the bubble is nearly independent of the transport rate, and is determined primarily by previously mentioned parameters as cavity diameter, surface tension and liquid density. The growth rates found in the diffusion-driven bubble growth will be reviewed in the next paragraph.

The size of orifice-formed bubbles can be considerably affected by a large flow rate of gas (Davidson and Amick, 1957; Hayes *et al.*, 1959; Kumar and Kuloor, 1970). Increasing the flow rate from zero the bubble volume remains constant whereas the frequency of bubble detachment increases. Further increase in the flow rate increases the bubble volume at detachment, because inertial and drag forces become more important.

temperature and pressure

Bubbles formed from injected air are not really affected by temperature or pressure unless indirectly due to a resulting change in liquid density, viscosity or surface tension. However, diffusion rates are directly under influence of the solubility of the gas in the liquid which has a nearly linear relationship with temperature and pressure at low concentrations (see section 2.4). Increasing the temperature would increase the gas supersaturation and therefore bubble growth, whereas a rise in pressure decreases the supersaturation and so reduces the driving force for bubble growth.

liquid velocity

Although this is not an aspect that has been reviewed in detail in literature, it has been observed that liquid movement parallel to the solid surface decreases maximum bubble size, as well as when the liquid moves in the same direction as the buoyancy (Cho *et al.*, 1990). When the liquid moves against the buoyancy force the bubble can remain attached to the solid surface for a longer period of time, resulting in a larger bubble volume at detachment. This subject will be further elucidated in chapter 4.

3.3 Bubble growth rate

3.3.1 Diffusion driven bubble growth

When bubbles can be formed at solid surfaces as a result of a supersaturation of gas in the liquid, the rate at which they grow depends on the rate of diffusion and convection of gas molecules through the liquid phase. Diffusion is the displacement of matter driven by Brown motion. Convection or convective mass transport is displacement of matter as a result of displacement of the bulk fluid (in this case liquid). The rate of diffusion is driven by a concentration gradient between the bulk liquid and the bubble-liquid interface. The concentration at the bubble interface is usually lower than in the liquid bulk and follows from Henry's law (see section 2.4). In models for bubble growth driven by diffusion, equilibrium in the bubble interface between the bubble pressure and the respective gas concentration in the surrounding liquid is assumed. Far from the interface, the liquid has a bulk gas concentration. The resulting gradient drives the diffusional gas transport. The gas transport is therefore limited by resistance to diffusion in the liquid and possibly in the interface. A resistance to mass transport in the interface could for example be effected by a surface layer at the bubble interface in which the gas is less soluble. This however is a factor which we have left out of consideration in this chapter.

In literature, many studies involving bubble growth driven by diffusional gas transport can be found. One of the simpler systems which has often been considered is that of one dissolving (or growing) stationary isolated spherical gas bubble in an infinite liquid. Frank (1950) provided an analytical solution for the growth of a sphere from zero initial size with no radial convection in the liquid surrounding the sphere. The model was extended by Scriven (1959) to the general case where transfer of gas across the gas-liquid interface also results in a radial convection term.

Epstein and Plesset (1950) presented an approximate analytical solution in the "quasi-stationary" model, in which both convective transport and interface motion were neglected. Tao (1978) accounted for radial motion of the bubble boundary, but ignored the resulting convective transport in the surrounding liquid. Subramanian and Weinberg (1980) pointed out that Tao's theory leads to an underestimation of the rate of gas transport. Better would be to ignore all boundary motion such as in the quasi-stationary approximation of Epstein and Plesset (1950).

Ward, Rizk and Tucker (1982) used the statistical rate theory to show that the assumption of local equilibrium at the gas-liquid boundary overestimates dissolution (growth) rates at high driving forces (large under- or supersaturation). Weinberg (1980) and Cable and Frade (1988) showed that the surface tension can play a significant role at very low growth or dissolution rates. Perhaps this phenomenon may be viewed as a kind of surface elasticity, as described in section 2.5. In growth, this inhibition could lead to an induction period before bubble growth rate follows parabolic growth.

However, at fast growth rates, convection becomes a much more important factor, and the surface tension may be neglected, analogous to bubble formation at solid surfaces as described in the previous section.

Manley (1960), as well as recently Hey *et al.* (1994), used Epstein and Plesset's approximation, since it is easily applicable and comparable to experimental results. However care must be taken in the interpretation of growth curves with this method at longer time scales.

One of the few growth models found in literature that predicts growth rates of bubbles attached to a solid surface has recently been developed by Bisperink and Prins (1994). They present a growth model based on Fick's diffusion law, which takes into account the changes in the boundary layer (or concentration profile) surrounding the bubble: (a) a decrease in layer thickness is accounted for by the stretching of the bubble surface: a semi-convective term and (b) an increase in boundary layer is accounted for by depletion of gas in the surrounding liquid, as described by the penetration theory (see section 6.4). Furthermore, the surface tension and the influence of the bubble internal pressure on the interfacial gas concentration are taken into account. One of the simplifications used in their model is the assumption of a linear concentration profile across the bubble boundary layer (figure 3.5), and no account is taken of a resistance to mass transport in the interface.

This model is expected to be applicable in our case since Bisperink's model accounts for the fact that part of the bubble surface is shielded by the presence of the solid surface to which the bubble is attached, as is the case in our experiments.

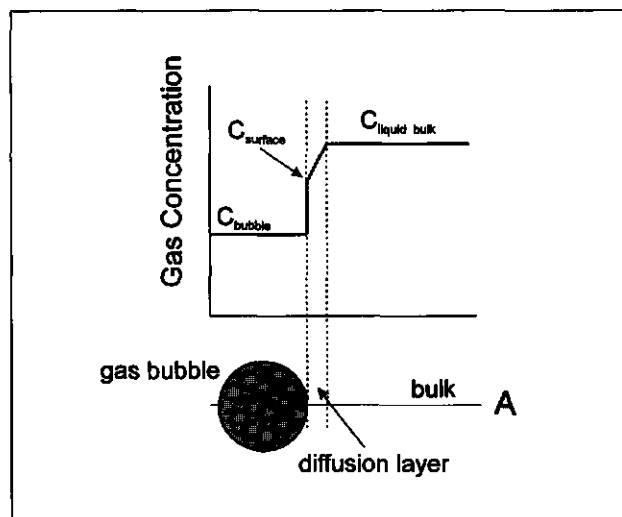


Figure 3.5 Sketch of the concentration profile across the boundary layer between bubble interface and bulk liquid, for a supersaturated liquid.

3.3.2 Bubble growth models

From literature, various approaches are used to describe the growth rate of bubbles in supersaturated solutions. Scriven (1959) solved the growth rate of bubbles floating freely in supersaturated solution analytically from zero bubble size. Van Stralen (1979) derived an analogous relation for mass transport from Scriven's theory:

$$R^2 = \left(\frac{12}{\pi}\right) \frac{(c_i - c_s)^2}{\rho_g^2} IDt \quad (3.15)$$

where c_i is the concentration of dissolved gas in the supersaturated solution (kg/m^3), c_s is the gas concentration in a saturated solution, R is the radius of the bubble (m) and ID is the diffusion coefficient (m^2/s). Scriven's relation takes into account a radial convection term as a result of boundary movement.

Solving the diffusion equation, where convective effects as well as surface tension effects are neglected, a time dependent expression is obtained for the concentration gradient around the bubble. With further simplification by assuming that a steady state gradient is reached the following approximate expression for the growth rate can be obtained (Epstein and Plesset (1950), Manley (1960), Hey, Hilton and Bee(1994)):

$$\frac{dR}{dt} = \frac{ID(c_i - c_s)}{\rho_g R} \quad (3.16)$$

Integration with $R=R_0$ at $t=0$ gives:

$$R^2 = R_0^2 + \frac{2(c_i - c_s)IDt}{\rho_g} \quad (3.17)$$

Equation (3.17) does not account for radial convection, and effectively assumes a boundary layer of size R , which increases as the bubble grows.

As mentioned in the previous section, Bisperink and Prins (1994) developed a model for diffusive growth of bubbles attached at a capillary. They used Fick's diffusion law as the basis for gas transport:

$$\Phi = ID \frac{dc_i}{dx_i} \quad (3.18)$$

where Φ is the gas flux across the interface ($\text{m}^3 \text{m}^{-2} \text{s}^{-1}$), ID is the diffusion coefficient of the oversaturated gas in the liquid ($\text{m}^2 \text{s}^{-1}$), and dc_i/dx_i is the concentration gradient between

the bubble surface and the liquid bulk at time $t=i$ (s). The equation for the conservation of mass is introduced:

$$A_i \Phi_i = \frac{dV}{dt} * \frac{P_{i+1}}{P_i} \quad (3.19)$$

where A_i is the area of available interface (m^2) at time i , P_{i+1}/P_i is the ratio representing the change of pressure as a result of the change in bubble curvature during growth (also defined in the equation of Laplace, section 2.2). In their model, Bisperink and Prins let the bubble grow on a capillary with finite steps in volume. For each step the time taken for the volume increase is calculated as well as the boundary layer thickness needed to provide enough gas molecules for that volume increase. An increase in bubble radius results first of all in a decrease in the layer thickness surrounding the interface because the boundary layer must expand. On the other hand, the boundary layer becomes thicker due to the depletion of gas from the liquid surrounding the bubble. Therefore the boundary layer is corrected for the increase in bubble area and also for the excess concentration in the supersaturated liquid. The only real disadvantage of this method is that a linear concentration profile is used, thereby probably overestimating the growth rate of the bubble.

In all the models discussed above the bubble grows primarily by diffusional gas-transport, where bubble growth simplifies to parabolic growth, corrected for the circumstances under which the growth is described.

3.4 Experimental

3.4.1 Materials

Capillaries

The four capillaries used varied ranging from 25 to 1000 μm in diameter. The large model active sites (ca. 1 mm internal diameter) were made from glass capillary tubes (Hirschmann Laborgeräte) which were filled from one end up to a certain point with glue (Bison-Combi, Perfecta Chemie). This way the internal volume of the gas-pocket could be controlled as well as ensuring the continuity of bubble formation during experiments due to the hydrophobicity of the internal glue coating. The smaller capillaries were made of fused silica tubing (Chrompack; 25, 100 and 160 μm internal diameter). The silicon coating was first removed using a Bunsen burner in order to create a hydrophilic external surface, after which the extremely fragile tubing was carefully glued into a larger 'holder capillary'. The capillaries were scratched with a diamond knife after which they were carefully broken. This method ensures a clean break and prevents scratches at the internal

edge of the capillary mouth. A perfect cutting edge is essential for the precision of the measurements. The internal diameter of the capillaries were measured before use with a stereo microscope (Zeiss, magnification 80x).

Supersaturated solutions

The solutions to be supersaturated were beer (pilsener, 11.5° Plato original gravity) and a buffer solution of sodium acetate/acetic acid at pH 4. Beer is naturally buffered at around pH 4 and was supersaturated with CO₂ at various pressures and temperatures. At first, we used a piece of equipment called the Foam Generator (see section 7.3), which was especially designed to equilibrate beer with gas at a set temperature and pressure with the use of a micro-porous hydrophobic membrane. One of the problems encountered when using this method was that the maximum sample volume was 4 litres, which could not be kept microbiologically stable longer than one day. In order to be able to use samples from the same batch for each measurement, a cask of beer was equilibrated for one week at an absolute pressure of 4 bar and a temperature of 23°C, after which all measurements were done with this batch. The concentration is found to be about 0.16 mol/l.

The supersaturated buffer solution was prepared with equal volumes of a 1 M HAc/NaAc buffer at pH 3.95 and 0.32 mol/l Na₂CO₃ (anhydrous, Merck), which when mixed together gives a 0.16 mol/l carbonated solution which is equivalent to the saturation concentration of CO₂ in water at an absolute pressure of 4 bar and a temperature of 20°C. The surface tension of beer and buffer solutions were measured in equilibrium using the Wilhelmy plate technique, and were found to be 46 mN/m and 70 mN/m respectively. The difference between gas and liquid density $\Delta\rho$ is about 1000 kg/m³, and g is 9.8 m/s².

3.4.2 Methods

Apparatus

The experimental set-up is described schematically in figure 3.6. The apparatus consists of a thermostated measuring vessel with a pressure reducer valve, a light source, a light diffuser, and a video camera (Sony 3CCD) with accessories (macro lens Tamron 35-80 and extension tubes). Images of the growing bubbles were transferred on line to an image analyser (Quantimet 570, Leica) where bubble volumes were calculated (see Appendix III.1) with a sample frequency of 0.5 s⁻¹.

Measurement

During experiments it was found that bubbles were formed at microscopic crevices on the outer walls of the capillary. The detachment and rise of these “parasite” bubbles were found to influence gas transport to the bubble considerably by inducing upward liquid convection. In order to compare results between consecutive measurements the

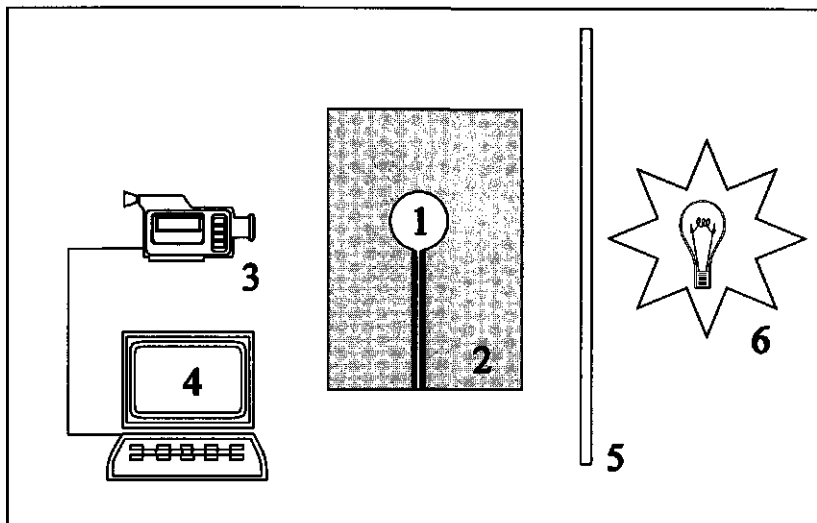


Figure 3.6 Diagram of the apparatus set-up, where 1 is the growing bubble perched on the capillary, 2 is the supersaturated liquid, 3 is the video camera, with 4 the image grabber, 5 the light diffuser, and 6 the light source.

formation of these parasite bubbles had to be avoided. It was found that the best way to prevent parasitic bubble formation was to pre-wet the external part of the capillaries in the measuring solution for one day or so.

Shortly before the measurement the pre-wetted capillaries were introduced into the thermostated vessel ($20^{\circ}\text{C} \pm 1^{\circ}\text{C}$). For the experiment using the buffer solution the CO_2 supersaturation was reached by mixing 250 ml of both the Na_2CO_3 and Acetate buffer solutions under pressure in the thermostated container. For the experiments with beer, 500 ml beer was transferred from the casket (equilibrated at 4 bar) into the measuring vessel at a slightly lower pressure (3.9 bar), ensuring the least possible loss of gas from the liquid before starting the experiment.

Both the beer and buffer solutions are saturated at 4 bar absolute pressure and 23°C , after which pressure is decreased until respectively 2, 1.5 and 1 bar absolute pressure. In order to set the excess concentration or supersaturation, the pressure is (partly) released. The resulting excess concentrations found in table 3.1 are calculated as follows:

$$C_e = C_s (T = 20^{\circ}\text{C}, P = 4 \text{ bar}) - C_s (T = 20^{\circ}\text{C}, P = \text{measurement pressure})$$

The bubble growth rates were measured at absolute pressures of 2 bar, 1.5 bar and 1 bar, at an ambient temperature of $20^{\circ}\text{C} (\pm 1^{\circ}\text{C})$. The resulting excess concentrations are listed in table 3.1.

Table 3.1 Calculated excess concentrations of CO_2 in beer and in buffer ($P_{sat} = 4$ bar) at various measuring pressures and at a temperature of $20^\circ C$, assuming phase equilibrium.

Systems	P_{meas} (bar)	C_s (g/kg)	C_e (g/kg)
saturation	4	5.65	0
C1	1	1.4	4.14
C2	1.5	2.12	3.43
C3	2	2.83	2.830

After releasing the pressure to the pressure reducer valve (which controls the vessel pressure) bubbles begin to be formed one by one at the tip of the capillary. The bubble growth at the capillary is followed by video and image analysis until detachment.

3.5 Results & Discussion

3.5.1 Bubble size at detachment

Effect of cavity diameter on bubble volume

The maximum bubble volume prior to detachment from capillaries of various internal diameter was measured with the computer analysis described in Appendix III.1. The calculated bubble volume is given as a function of the capillary radius (measured in beer) in figure 3.7. The points show the experimental data, whereas the line represents the theoretical relationship as given by equation (3.7), using the equilibrium surface tension measured by Wilhelmy plate technique. From the good fit found by equation (3.7) for all capillary radii except the largest one it seems that the assumption of a detaching contact angle of 90° is valid.

The volume of the largest bubbles are found to deviate about 25% from the theoretical calculated values. In all these cases the volume is smaller than would be expected from theory. A few reasons can be given for this relative decrease in bubble size:

- the gas bubbles attached to the cavity are deformed considerably at this size and elongated to such a degree that they can become mechanically unstable and so detach at an earlier stage;

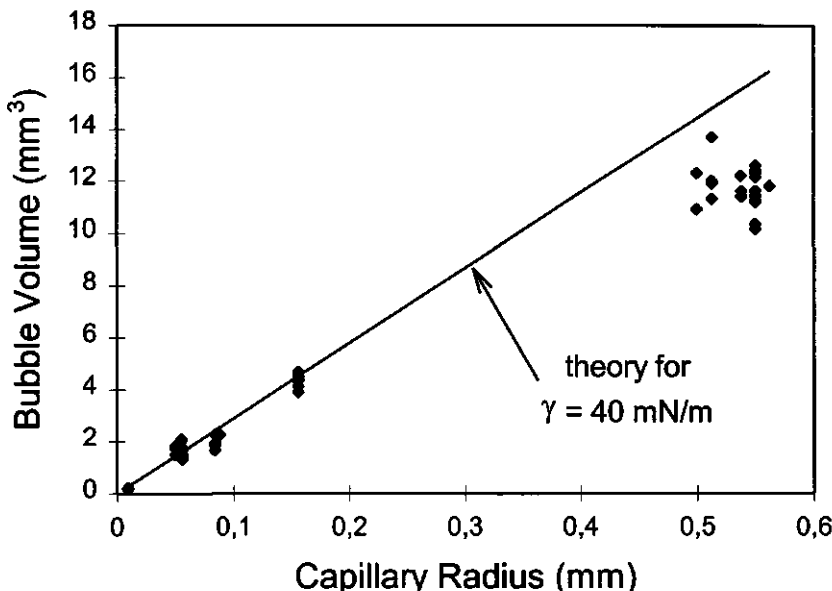


Figure 3.7 Maximum bubble volume in beer as a function of capillary radius; the data points represent experimental values, the line represents equation (3.7).

- parasite bubbles formed at the external wall of the capillary produce slight vibrations and also a small shear force which could induce the large bubbles formed at the tip of the capillary to detach at an earlier stage;
- a significant error can be made in the “effective” perimeter of the capillary opening: prior to detachment, a neck starts to form, which has a smaller perimeter than the cavity opening. This can induce an earlier detachment than predicted.
- errors in the measurement of the radius of the cavity opening are not large enough to give such a large decrease in bubble volume at detachment;
- the image analysis assumes axis-symmetry of the bubbles. This gives rise to some error in the data, as discussed in Appendix III.1. However, an analysis of the calculation of bubble volume shows that errors are usually smaller than 10 %.

Effect of surface tension on bubble volume

The maximum bubble volumes measured in beer are compared to bubbles growing on the largest capillary in a supersaturated buffer solution in table 3.2. The theoretical maximum bubble volume in buffer is calculated using the measured equilibrium surface

Table 3.2. Theoretical and experimental values for the maximum volume at detachment on a capillary with $r_c = 0.55$ mm in beer and in buffer solution.

	theoretical volume	experimental volume
beer ($\gamma = 46$ mN/m)	15.9 mm ³	11.60 ± 0.94 mm ³
buffer sol. ($\gamma = 70$ mN/m)	24.2 mm ³	17.52 ± 0.37 mm ³

tension of 70 mN/m. This value is very close to that of pure water, and it indicates it contains only a minimal amount of contaminants.

As can be seen in table 3.2, the maximum bubble size found in buffer (for the largest capillary only) also deviates from the predicted value. The percentage deviation of the average of all the largest bubbles growing in beer is 27.0 %, whereas in the buffer solution the sizes are 27.8 % smaller than the predicted values. These deviations may be similar by chance, but it may also indicate that surface rheological properties do not play an important role. If surface rheology was the chief cause for the earlier detachment of bubbles in beer, the bubbles growing in buffer should be unaffected by this phenomenon. Furthermore, the bubbles would become larger instead of smaller as a result of dynamic surface properties. The buffer solution contains little or no surfactant molecules and should behave like pure water. The fact that the bubbles in buffer are also smaller at detachment suggests that some kind of mechanical instability occurs.

The conditions for mechanical break-up of an elongated bubble can be estimated. When a volume of liquid is elongated into a cylinder-shaped form, there is a limit to the length of elongation (Raleigh instability). The cylinder will break up into one spherical bubble of equal volume. For a given cylinder with radius R_{cyl} and length l (see figure 3.8(a)) the volume V_{cyl} and surface area A_{cyl} are respectively:

$$\begin{aligned} V_{cyl} &= \pi R_{cyl}^2 l \\ A_{cyl} &= 2\pi R_{cyl} l \end{aligned} \quad (3.20)$$

When the cylinder breaks off, the resulting spherical bubble with radius R_b has volume V_b and surface area A_b (see figure 3.8(b)):

$$\begin{aligned} V_b &= \frac{4}{3}\pi R_b^3 \\ A_b &= 4\pi R_b^2 \end{aligned} \quad (3.21)$$

The volume of gas bubbles before and after break-up have roughly the same value: $V_{cyl} = V_b$ and the break-up theoretically occurs when $A_{cyl} > A_b$. This inequality leads to the critical break point where:

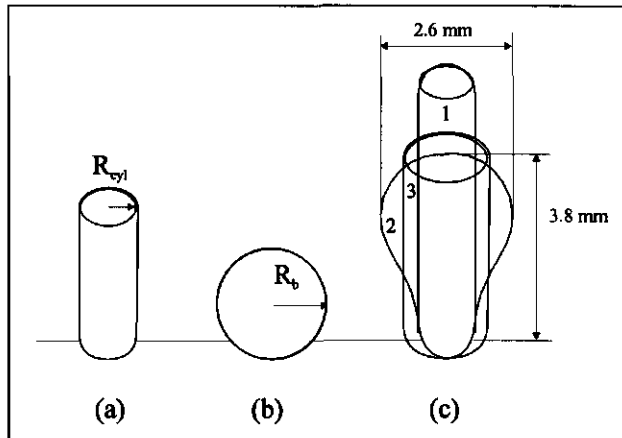


Figure 3.8 Sphere of volume V_b and surface area A_b , (a), and equivalent cylinder (b) with volume V_{cyl} and surface area A_{cyl} , of maximum length L . in (c) 1 is the cylinder, 2 is the real bubble and 3 is the average fitting cylinder.

$$R_b < \sqrt{\frac{R_{cyl}l}{2}} \quad (3.22)$$

Inserting this inequality into equation (3.21) and by equating eq. (3.20) to (3.21), it can be calculated that a (cylindrical) bubble breaks off when its length reaches a critical size:

$$l_{crit} > 4.5 R_{cyl} \quad (3.23)$$

If we insert the capillary radius $r_c = 0.55$ mm for R_{cyl} , the maximal length of the elongated cylindrical bubble before instability occurs will be $l_{crit} = 2.5$ mm (see 1 in figure 3.8(c)). This length would be critical for the theoretical situation of a cylinder-shaped bubble. In practice, the bubbles forming at these large capillaries reach a typical maximum width of 2.6 mm (radius = 1.3 mm) and a maximum length of 3.8 mm (see 2 in figure 3.8(c)). It is no surprise this maximum length is not equal to the critical length, as in practice, the detaching bubble does not have the shape of a cylinder.

However, using the average width of the bubble (the average between R_{cyl} and the maximum radius of the bubble) as the radius of the cylinder $R = 0.9$ mm (see 3 in figure 3.8(c)), a critical length of 4.2 mm is calculated, which is only slightly larger than the measured 3.8 mm length.

Following this line of thinking, the assumption that a mechanical instability is the cause of the earlier detachment is therefore plausible. Possibly small vibrations and necking may help the process toward earlier detachment. A more precise method to

calculate whether instability is the cause for the earlier detachment is to calculate the surface area of the elongated bubble prior to detachment, and compare it to the surface area after detachment.

These measurements for $r_c = 0.55$ mm are given in Appendix III.1 (see table III.3) and show that the numerically calculated surface area is the same before and after detachment. However, the numerically measured bubble size is indeed much closer to the line in figure 3.7 than the measured one by image analysis. We therefore presume that when the bubbles are very elongated, which is the case here for larger bubbles, the image analysis is no longer an adequate tool for measuring the bubble volume.

Effect of hinterland volume on bubble volume

As discussed in section 2.3, an increase in bubble growth rate can be predicted as a result of the pressure decrease in the bubble during growth. A large amount of gas present in the hinterland can expand relatively more than if the gas volume is limited to only the bubble. This expansion is independent of diffusional gas transport. According to literature this small increase in bubble growth rate should not influence the bubble size at detachment. Figure 3.9 shows the bubble volumes at detachment for various hinterland volumes for two different capillary radii (A: $r_c = 0.05$ mm and B: $r_c = 0.55$ mm). It can be seen that the experimental error is larger than a possible influence of increased hinterland volume. This is especially well observable for the largest capillary of $r_c = 0.55$ mm over a wide range of hinterland volumes. No significant change in maximum bubble volume is found with increasing hinterland volume.

The effect of hinterland volume on the growth rate is discussed in section 3.4.2.

Effect of growth rate on bubble volume

In section 3.1, it was postulated that bubble growth in this work is too slow to affect the maximum bubble volume at detachment. Figure 3.10 shows the detachment volume of bubbles formed at 2 different capillaries in beer and 1 capillary in buffer as a function of the bubble formation time (A: $V_b = 2$ mm³, B: $V_b = 12$ mm³, C: $V_b = 18$ mm³). The data in figure 3.10 show that the measured volume is unaffected by the differences in bubble formation time, and is therefore not influenced by inertial or viscous forces, which is to be expected. From literature, bubble volumes increase in size above typical formation frequencies of 100 Hz as a result of viscous and inertia effects (Kumar and Kuloor, 1970).

The increase in growth rate may, however, influence the surface tension locally at the bubble interface. For gas-liquid interfaces that are stabilised by surfactants, an increase in the surface expansion rate as a result of faster growth can increase the dynamic surface tension of that interface. The force keeping the bubble attached to the surface is then higher than before (see equation (3.2)), and the bubble can grow to a larger size before it

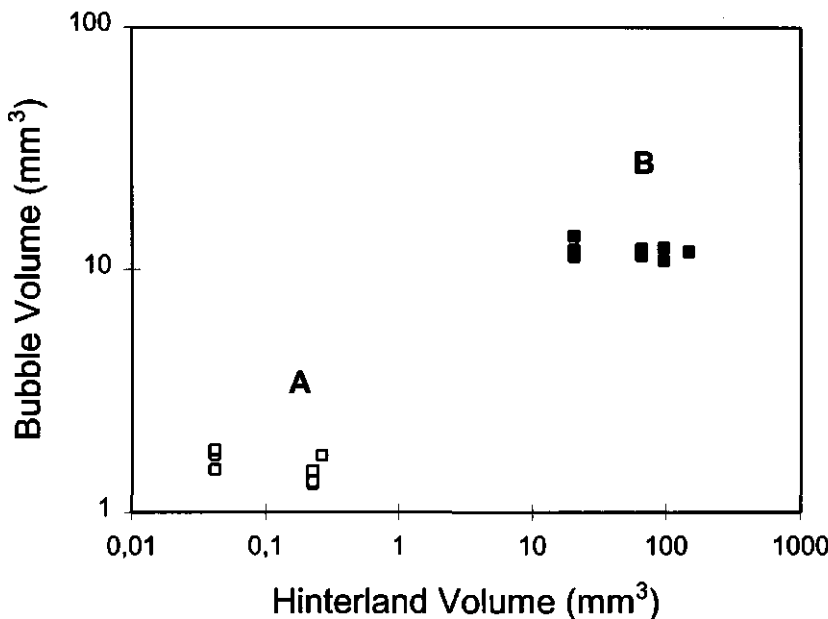


Figure 3.9 Maximum bubble volume as a function of hinterland volume; (A) $r_c = 0.05$ mm ; (B) $r_c = 0.55$ mm.

detaches. In order to investigate this effect, the relative expansion rate $d\ln A/dt$ was calculated for bubbles growing at various bubble formation rates.

Figure 3.11 gives the relative surface expansion rate of a bubble growing at three bubble formation rates found in the experiments (0.1, 0.03 and 0.01 bubbles per second). It is clear that $d\ln A/dt$ is relatively low at bubble formation rate below 0.1 s^{-1} . If we use the power law given in Appendix III.2 to calculate the increase in surface tension due to the surface expansion as a result of the surface dilational viscosity, we find (with $m = -0.82$ and $n = -1.98$) that the surface tension should be increased by about 7 mN/m in the first 40 seconds of bubble formation at 0.1 s^{-1} due to the relative expansion rate of the bubble surface.

The values of m and n were measured in Appendix III.2 for degassed beer, in which it is reasonable to assume that most of the alcohol has also been removed. Calculating again using the constants for degassed beer with an addition of 4% alcohol, the increase in surface tension reaches about 4 mN/m.

It should be noted that the equilibrium surface tension measured in the Langmuir trough experiments in Appendix III.2 were somewhat lower (42 - 43 mN/m) than the ones measured in this chapter (46 mN/m).

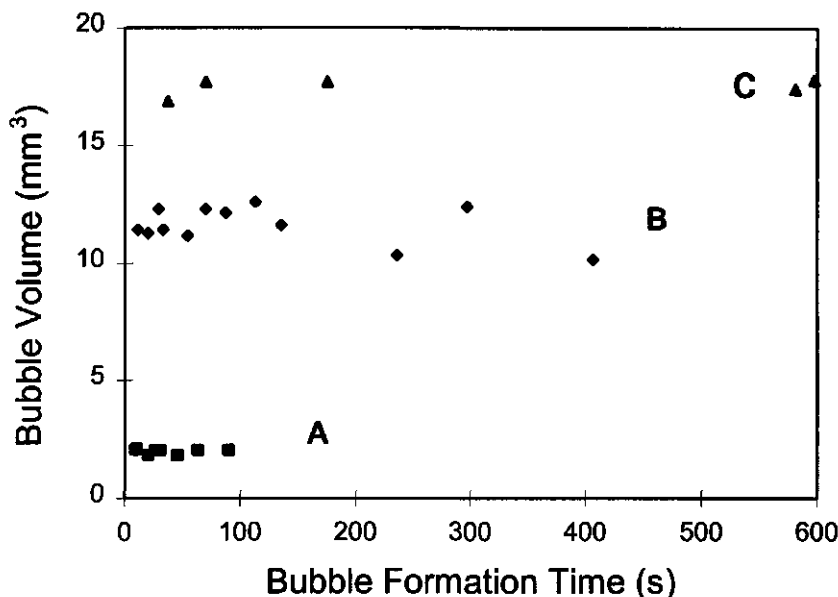


Figure 3.10 Maximum bubble volume as a function of bubble formation time for small and large bubbles: (A) $V_b = 2 \text{ mm}^3$, (B) $V_b = 12 \text{ mm}^3$, and (C) $V_b = 18 \text{ mm}^3$.

Concluding, there may be a slight increase in the surface tension due to the expansion of the surface, but the surface tension will not exceed 48 - 50 mN/m. Inserting these values into equation (3.7), the theoretical bubble volume at detachment would become 1.1 times larger than predicted by the line in figure 3.7. We can therefore safely say that the bubble size at detachment in the range of bubble formation rates used here are not affected by the formation rate.

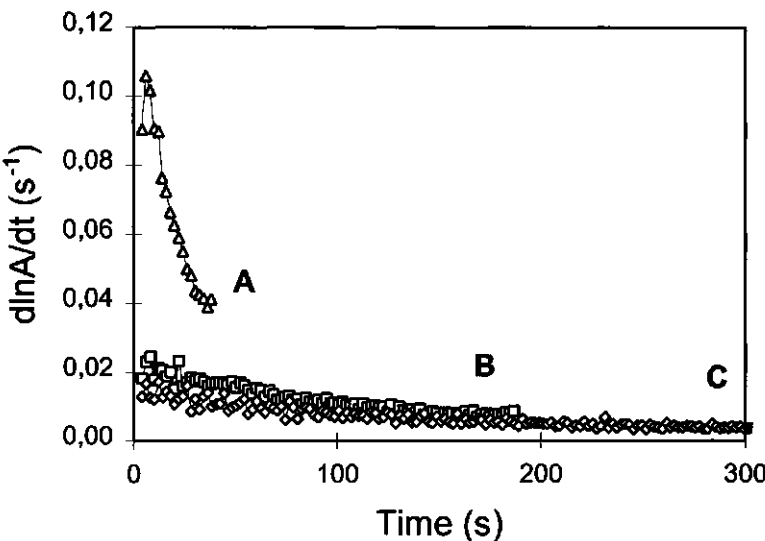


Figure 3.11 Relative expansion rates for the bubble interface as a function of time at the average bubble formation rate of (A) 0.1 s^{-1} , (B) 0.03 s^{-1} and (C) 0.01 s^{-1} .

3.5.2. Bubble growth rate

Effect of liquid supersaturation on bubble growth rate

The growth rate of bubbles growing on 2 capillaries of different internal radius was measured at three excess CO_2 concentrations in beer (C1, C2 and C3, see table 3.1). When first starting experiments it was found that various factors besides the concentration, temperature and pressure could influence the growth rate of a bubble at a solid surface:

- 1) convective gas transport due to the formation of parasite bubbles at high excess gas concentration;
- 2) depletion of the gas concentration at low excess gas concentration.

ad 1) One of the most difficult tasks was to eliminate the growth of bubbles at sites other than at the capillary mouth. The growth and rise of these undesired “parasite” bubbles were found to induce liquid movement and therefore mixing of the originally quiescent liquid. This in turn led to an increase in bubble growth rates as the diffusion layer or boundary layer surrounding the growing bubble was effectively diminished in size. In order to observe the effect of the gas excess concentration it was therefore imperative to get rid of the “parasitic” growth sites. Immersing the capillary over a period of a few days in a wetting liquid such as beer successfully removed all bubble sites, sometimes including

the capillary mouth itself. Ignoring this precaution, however, could lead up to a five-fold increase in bubble growth rate, as will be shown in the next paragraph. Serious attempts were made to keep the formation of "parasite" bubbles to a minimum, but unfortunately this was not possible in all cases and the reproducibility of the results suffered somewhat from this unwanted effect.

ad 2) A different factor that was found to influence bubble growth rates at low excess gas concentration was depletion of gas. Figure 3.12 shows the growth curves of 5 consecutively formed bubbles at one capillary at the lowest excess CO_2 concentration (C3). As can be seen, the time needed for a bubble to grow at this low concentration increases during time. This is most probably due to a local depletion of CO_2 gas from the liquid. The liquid movement due to the rise of each bubble after detachment is obviously not sufficient to restore the initial boundary layer of the first bubble. The boundary layer is further depleted with every consecutive bubble and increases in size, resulting in a longer growth time for the next bubble growing at the capillary. This effect is found in a lesser degree at higher concentrations.

Figures 3.13 shows the bubble growth rates at the 3 effective CO_2 concentrations given in paragraph 3.3.4, for beer (r_c is 0.55 mm and 0.05 mm) and buffer solution (r_c is 0.55 mm). The curves represent the average growth of the first three bubbles, all from

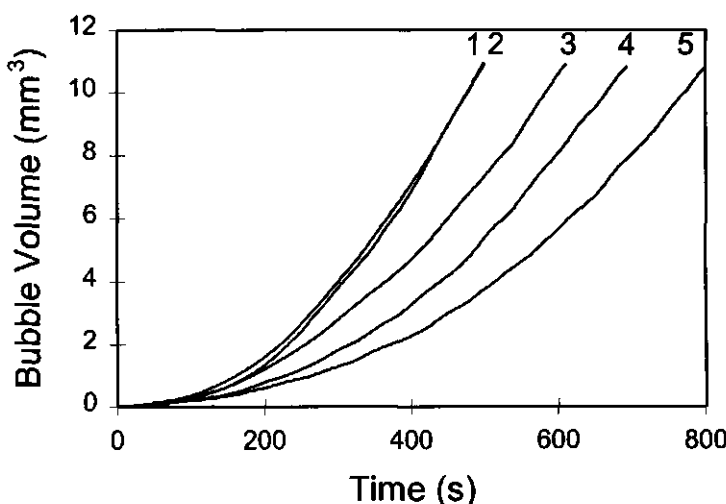


Figure 3.12 Effect of gas depletion on the growth rates of bubbles consecutively formed at a capillary; CO_2 excess concentration is C3. The end of the curve indicates the detachment of the bubble from the capillary.

However in order to keep this irreproducibility to a minimum the average formation rates of only the first three measured bubbles are shown in the figures.

single measurements. In each following experiment, an increasing amount of "parasite" bubbles were formed, which were found to have a large influence on the rate of bubble growth as will be shown in the next section.

In the figures, the curves start from the point where the bubble is only a half sphere, as it protrudes from the capillary and end at the point where the bubble detaches from the capillary. The values of the bubble size at detachment were discussed in detail in the former section. It must be noted, that although the bubbles formed at the different capillary radii have different detachment volume, the kinetics of growth rate should be fairly similar. Figure 3.13 shows that at the same gas concentration, the slope of the curves do not all fall together. On the contrary, the slope for the buffer solution deviates considerably from the other two slopes (in beer) at concentration C2. This could easily be due to an increase in the formation of parasite bubbles in one experiment than in the next. As a rule, however, the slopes are reasonably consistent with one another for the three gas concentrations.

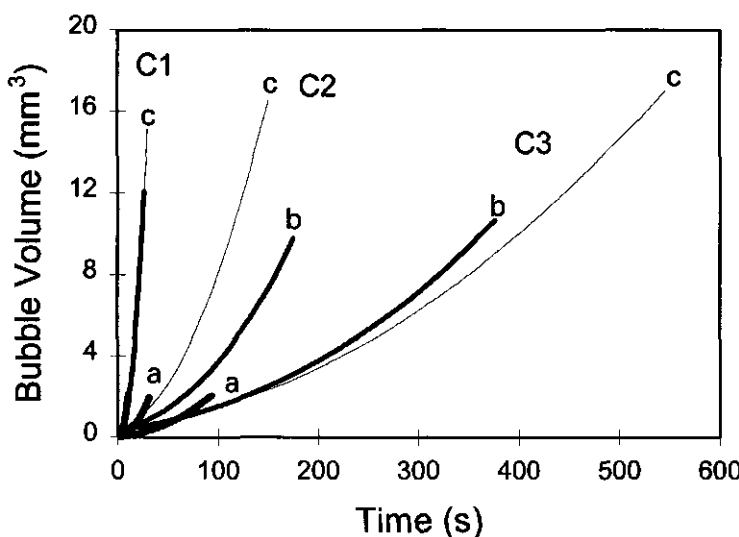


Figure 3.13 Experimental growth rates of bubbles in a (a) beer solution, $r_c = 0.05$ mm, (b) beer solution, $r_c = 0.55$ mm and (c) buffer solution, $r_c = 0.55$ mm at excess concentrations C1, C2 and C3.

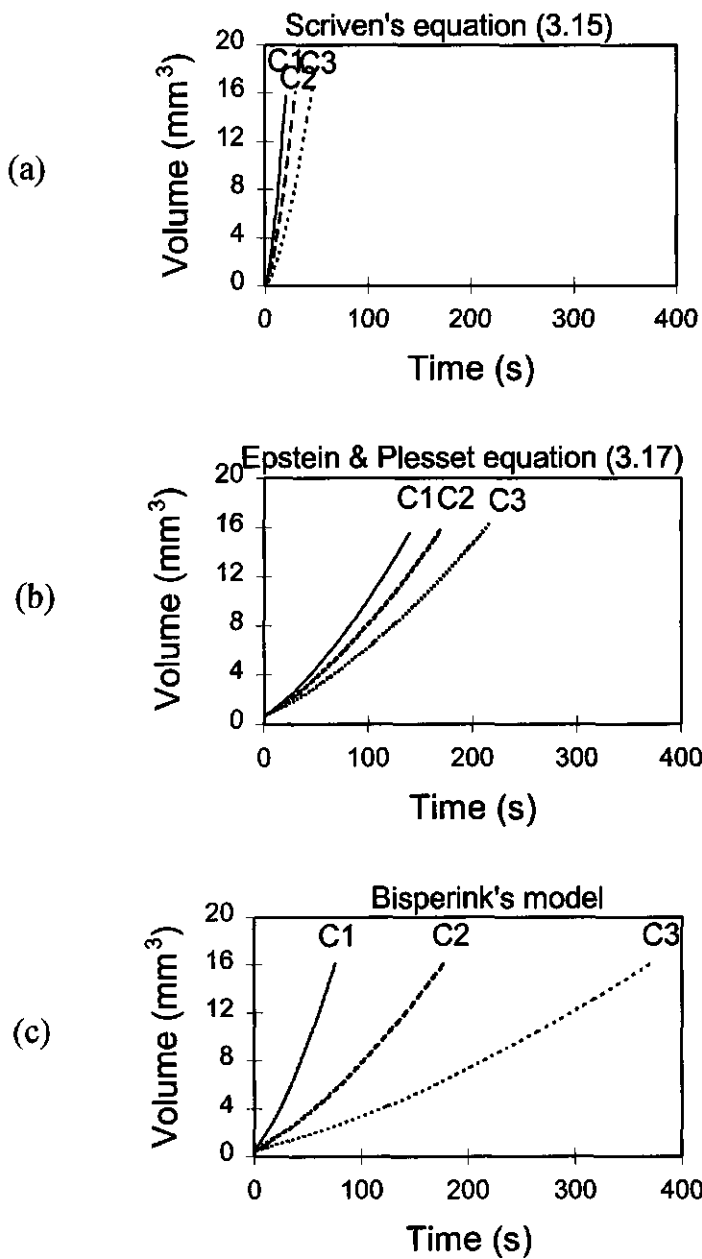


Figure 3.14 Theoretical growth rates of bubbles for
 (a) Scriven's equation (3.15), C1, C2 and C3
 (b) Epstein & Plesset's equation (3.17) C1, C2 and C3
 (c) Bispenink's model ; C1, C2 and C3 ; $r_c = 0.55$ mm and $\gamma = 46$ mN/m

In order to be able to compare some of the growth models used in literature, theoretical bubble growth curves for equations (3.15) and (3.17), as well as the bubble growth rate calculated with Bisperink's model for the 3 excess concentrations used in the experiments is shown in figure 3.14.

As seen in figure 3.14(a), equation (3.15) describes a relatively fast growth rate which is not duly affected by the differences in concentration. Equation (3.20), shown in figure 3.14(b), describes a much slower growth rate. This is expected as this model does not account for boundary layer movement. Again the concentration does not have a large influence on the growth rate. Bisperink's model shown in figure 3.14(c) predicts slow growth at the lowest concentration, and fast convective growth at the highest concentration, spanning a much larger range of bubble growth rates than found for equations (3.15) or (3.17) at the used gas concentrations. It must be noted that both Scriven's (3.15) and Epstein and Plesset's (3.17) equations are valid for spherical bubbles in an unbounded liquid, whereas Bisperink's model was developed for a bubble, although also spherical, which is partially imbedded into the capillary to which it is attached.

In figure 3.15 the growth rate according to Bisperink's model for the 3 concentrations used is shown for the smallest capillary size. Included is also the build-up of the boundary layer δ as a function of time, given as a layer of liquid surrounding the bubble. At the lowest concentration C_3 , the bubble takes the longest time to grow, and the boundary layer is the thickest. Although not clear from the figure, the boundary layer at the end of the curve has a larger total volume than the bubble itself. At the highest concentration C_1 , the bubble boundary layer is still smaller than the bubble volume at the end of the curve. It is clear therefore that at the lowest concentration, depletion of gas from the surrounding liquid is occurring, possibly affecting the growth of the next bubble on the capillary. So at a low gas concentration, the build-up of the boundary layer gives an extra decrease in bubble growth rate.

When comparing the values in figure 3.15 to values calculated for a larger capillary, the trends in bubble growth and in boundary layer build-up are the same. However the bubble growth on a larger capillary shows a slower increase in time than for a small capillary. This is probably due to the fact that at the beginning of bubble growth the interfacial area through which diffusion can take place is different for different sized capillaries: for the small capillary the interfacial area at the start of bubble growth (area for a half-sphere) is 0.0157 mm^2 , whereas for the large capillary the area at the beginning is 1.9 mm^2 , which is 121 times larger.

A cursory glance at the experimental data (figure 3.13) and the three models (figure 3.14) shows that Bisperink's model fits the wide range of bubble growth rates better than the other two models, as was expected. We have therefore only made comparisons with Bisperink's model.

In figures 3.16(a), (b) and (c) the experimental results from figure 3.13 are plotted together with the theoretical curves of Bisperink's model for the excess concentrations used. Figure 3.16(a) shows bubble growth in beer on a small capillary, figure 3.16(b) for

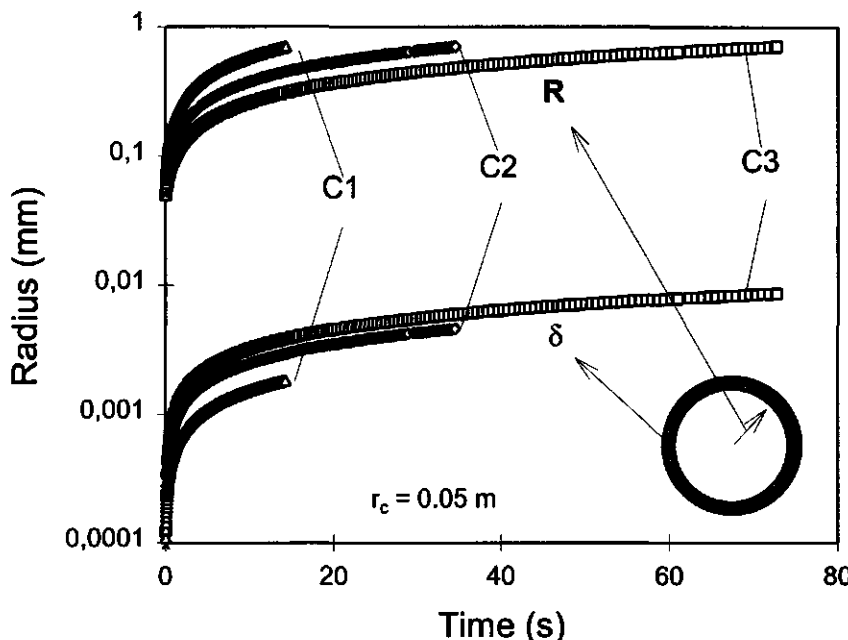


Figure 3.15 Theoretical change in bubble radius and boundary layer δ as a function of time calculated with Bisperink's model for a beer solution, $r_c = 0.05$ mm at excess concentrations C1, C2 and C3.

the large capillary, and figure 3.16(c) gives bubble growth rates in buffer solution on the large capillary. Figure 3.16(a) shows good agreement with theoretical prediction. From figure 3.16(b) a considerable discrepancy is found between the experimental results and the theoretical curves. The buffer experiments (figure 3.16(c)) give good agreement with Bisperink's theory except for the lowest concentration, which showed much slower growth than predicted.

The theoretical curves lie sometimes to the left, sometimes to the right of the experimental curve. Generally, it seems that, for the highest concentration C1, the growth is underestimated by theory, whereas for the lower concentrations the theory is mostly correct or overestimates the bubble growth. It is our belief that the values of gas concentrations used for the theoretical calculations may in some cases be overestimated. In the experiments the time needed to set up the capillary after opening the measuring vessel could not be reproduced very well and part of the dissolved gas dissipated from the liquid, naturally lowering the gas concentration in the liquid. After inserting the capillary the pressure was once more elevated to the saturation pressure and equilibrated for 30 minutes. Despite this precaution, errors were probably made in the setting of saturation

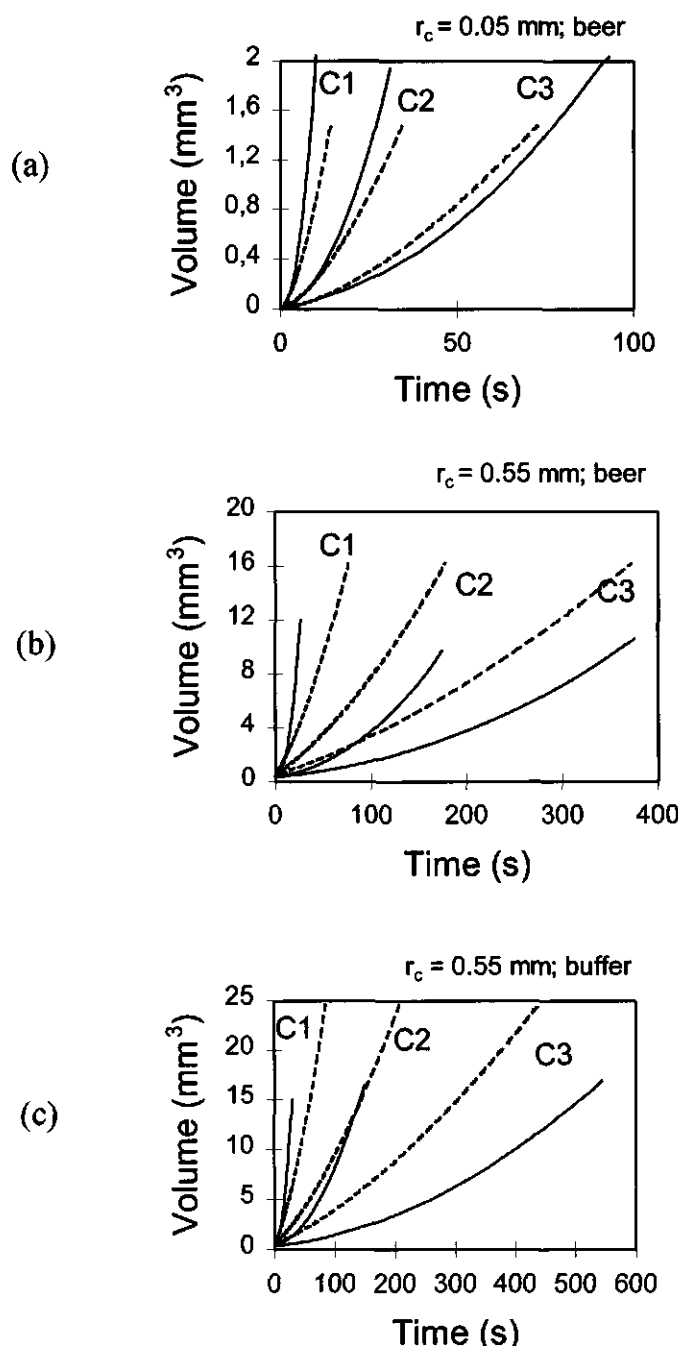


Figure 3.16 Experimental (full line) and theoretical (dotted line) growth rates (Bisperink's model) of bubbles (a) beer solution, $r_c = 0.05 \text{ mm}$ at C1, C2 and C3, (b) beer solution, $r_c = 0.55 \text{ mm}$ at C1, C2 and C3, and (c) buffer solution, $r_c = 0.55 \text{ mm}$ at C1, C2 and C3.

concentrations. This effect should result in an overestimation of the growth as sometimes found for the lower concentrations.

In some cases, the higher concentrations gave rise to the growth of numerous "parasite" bubbles which can increase transport rates considerably. Although this phenomenon also results in a more rapid depletion of gas from the liquid, in first instance this effect will lead to faster growth than predicted by theory.

Taking into account all the possible phenomena that can occur in these experiments it is rather difficult to conclude why the experimental results are not always in agreement with the theory. It was however found that the measurements of consecutive bubbles growing on the capillary are very reproducible.

Effect of liquid convection on bubble growth rate

As was mentioned in former paragraphs the influence of "parasite" bubbles was found to increase growth rate kinetics by up to a factor five. Figure 3.17 shows different measurements of the bubble growth rate on the largest capillary at supposedly the same CO_2 concentration in beer. During the experiments it was observed that in the measurements 1-4 an increasing amount of "parasite" bubbles were produced on the external wall of the capillary. This same effect is observed in figure 3.17 where the bubble growth is increased considerably in that same order by a factor 5. It seems therefore that

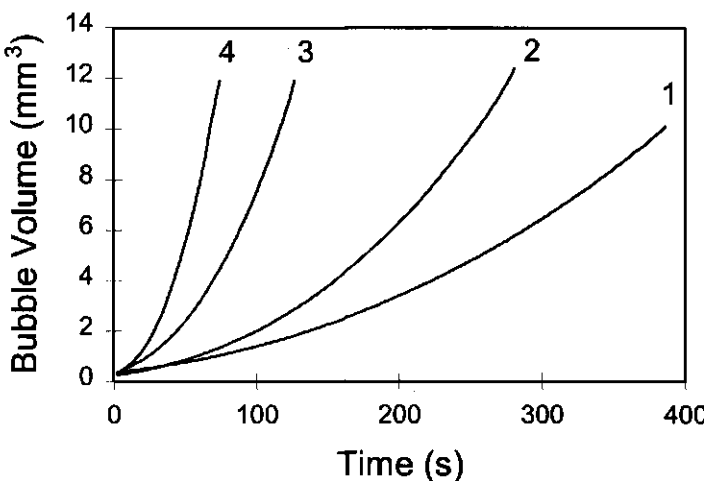


Figure 3.17 Experimental growth rates of bubbles at excess concentration C3 in a beer solution for 4 consecutive measurements carried out in the order 1-4; $r_c = 0.55$ mm.

the prolific growth and rise of these bubbles entrains a certain amount of liquid into movement, thereby presumably considerably decreasing the boundary layer thickness surrounding the bubble under observation.

An extra reason for the increase in bubble growth could be the heating up of the liquid during the measurements due to the continuous back-lighting of the vessel. Although care was taken to ensure a constant temperature of 20°C, the bubble formed on the capillary acts as a lens thereby increasing the temperature locally. However it is not expected that this would have such a great effect on the bubble growth.

Fitting the curves with Bisperink's model gave "effective" concentrations roughly varying between C1 and C3. Since the concentrations were not varied, the boundary layer must have been thinner where convection took place, and wider where depletion was occurring.

Effect of hinterland volume on bubble growth rate

As explained in the theory in section 2.3, the size of bubbles at detachment is hardly affected by a finite hinterland volume. The bubble growth rate can however be increased by the pressure-driven expansion of the hinterland gas volume. A secondary and more important effect is that the frequency of bubble formation can be greatly reduced under conditions of a large hinterland. For example, when a bubble detaches from the capillary, the gas that remains behind in the capillary is again compressed to its original pressure (due to the smaller radius of curvature). This original pressure depends on the wettability of the internal capillary surface. For a small contact angle, the original pressure is high and the gas is compressed in such a way that the liquid-gas interface must retreat into the capillary. For a large contact angle, the pressure does not increase so much and the retreat of the interface is less pronounced.

In the former case of the wettable surface the retreat of the interface can stop further bubble formation; the length of diffusion is now the rate determining parameter for the time before a new bubble is formed. As a result the next bubble is formed after a considerable lag time. This is shown in figure 3.18, where bubble growth is shown on a capillary with r_c is 0.15 mm, where the hinterland volume is set at 2 (figure (a)-(c)) and 22 μl (figure (d)-(f)). Figure 3.18 shows various moments in the cycle of bubble growth and detachment. Figures (a) and (d) are taken at the moment after bubble detachment. As can be seen the retreat is larger for the larger hinterland volume. The second stage (b) and (e) is when the bubble starts to protrude outside the capillary. Note the difference in elapsed time between (b) and (e). It has taken the bubble in (e) more than twice the time to reach the same stage of bubble growth. In the next stage (c) and (f) the bubbles grow at approximately the same rate, although the growth of the bubble on the capillary with the large hinterland is 1.5 times faster.

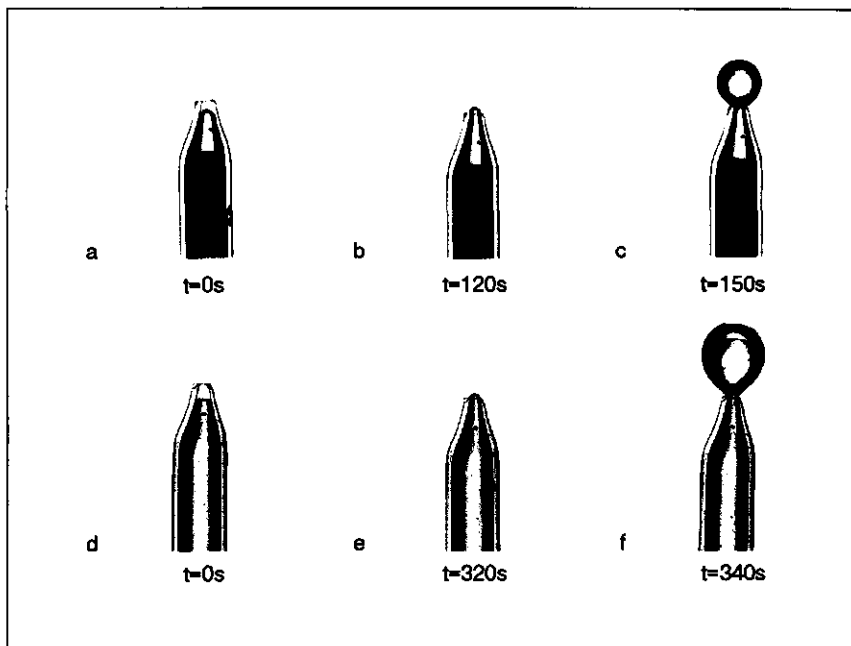


Figure 3.18 Photographs of the cycle of a bubble growing on a capillary. (a), (b) and (c) hinterland volume = $2\mu\text{l}$; (d), (e) and (f) hinterland volume = $22\mu\text{l}$. Note the time indicated below the individual photographs

The bubble growth on a capillary with a large hinterland volume is faster than on a capillary with a negligible hinterland. At the same time the frequency of the formation of consecutive gas bubbles can be greatly reduced when the internal surface of the cavity is well wettable. For a relatively small hinterland volume, both effects become less pronounced: the growth rate and frequency of bubble formation will then be solely governed by gas diffusion and convection. In a practical situation this would mean that a large hinterland volume would more or less stop bubble formation, despite the increased growth rate of the bubble once formed. When bubble formation is preferred at a high frequency, care must be taken to keep the hinterland volume to a minimum (a too small hinterland volume can create the danger of completely loosing the active site due to wetting) or to keep the internal capillary walls hydrophobic.

3.6 Conclusions

With bubble formation on capillaries we can distinguish between size of a bubble at detachment, the bubble growth rate of one bubble from the start up to detachment and the frequency of bubble formation.

We have found that the size of bubbles at detachment can be well predicted with the available theory for the relatively slow growth encountered in the experiments performed in this chapter. The size was found to be dependent of the cavity size, the surface tension of the liquid and the buoyancy force only, where care was taken to ensure a hydrophilic situation. It was also observed that the largest bubbles detached at a smaller size than predicted by theory. It is possible that this is due to small mechanical instabilities.

In this chapter we have tried to check the only available model for the growth rate of a bubble growing on a capillary up to detachment. It was found that in comparison to other well-known methods, Bisperink's model gave the best fit over the range of gas concentrations and the time scales observed. The experimental data were sometimes found to deviate from the theory. The bubble growth rates were found to change slightly during time, but most important, the experimental conditions were such that "parasite" bubbles could not always be avoided: as a result a mixing of the liquid was induced, probably decreasing the bubble boundary layer and resulting in an increase in growth rate.

The frequency of the bubble detachment could be decreased considerably by increasing the hinterland volume at well wetted conditions. If care was taken to keep the hinterland volume small, the frequency of bubble detachment was only dependent of growth kinetics and bubble size at detachment.

The experimental conditions used here were such that extra factors influencing gas transport mechanisms such as depletion and convective movement were always present, making it impossible to model gas bubble growth in detail.

References

Bisperink, C. G. J. and Prins, A. (1994) Bubble growth in carbonated liquids *Colloids and Surfaces A: Physicochemical and Engineering Aspects* **85**, 237-253.

Cable, M. and Frade, J. R. (1988) The influence of surface tension on the diffusion-controlled growth or dissolution of spherical gas bubbles *Proc. R. Soc. Lond. A* **420**, 247-265.

Chesters, A. K. (1979) Bubble Sizes in Nucleate Pool Boiling in Boiling Phenomena vol I and II, chapter 26, 879-99.

Cho, S. C. and Lee, W. K. (1990) A model for steam bubble formation at a submerged orifice in a flowing liquid *Journal of Chemical Engineering of Japan* **23** (2), 180-5.

Datta, R. L., Napier, D. H. and Newitt, D. M. (1950) The properties and behaviour of gas bubbles formed at a circular orifice *Trans. Inst. Chem. Eng.* **28**, 14-26.

Davidson, L. and Amick, E. H., Jr. (1957) Formation of gas bubbles at horizontal orifices *A.I.Ch.E. Journal* **2**(3), 337-342.

Epstein, P. S. and Plesset, M. S. (1950) On the stability of gas bubbles in liquid-gas solutions *J. Chem. Phys.* **18**, 1505-9.

Frank, F. C. (1950) Radially symmetric phase growth controlled by diffusion *Proc. R. Soc. Lond* **201A**, 586-99.

Fritz, W. (1935) Berechnung des maximal Volume von Dampfblasen *Phys Z.* **36**, 379.

Hayes, W. B., Hardy, B. W. and C. D. Holland (1959) Formation of Gas Bubbles at Submerged Orifices *A.I.Ch.E. Journal* **5** (3), 319-324.

Hey, M. J., Hilton, A. M. and R. D. Bee (1994) The formation and growth of carbon dioxide gas bubbles from supersaturated aqueous solutions *Food Chemistry* **51**, 349-357.

Hilton, A. M. (1992) The Formation and Growth of CO₂ Gas Bubbles from Supersaturated Aqueous Solutions Ph.D. Thesis, University of Nottingham, United Kingdom.

Jańczuk, B. (1983) Detachment Force of Air Bubble from the Solid Surface (Sulfur or Graphite) in Water *J. Colloid Interface Sci.* **93** (2), 411-418.

Kumar, R. and Kuloor, N. R. (1970) The formation of bubbles and drops *Adv. Chem. Eng.* **8**, 255-368.

Leiner, W. and Böhnisch, S. (1984) Study of bubble growth at conical nucleation sites with reduced wettability *Wärme- und Stoffübertragung* **18**, 231-235.

Lin, J. N., Banerji, S. K. and H. Yasuda (1994) Role of Interfacial Tension in the Formation and the Detachment of Air Bubbles. I. A Single Hole on a Horizontal Plane Immersed in Water *Langmuir* **10**, 936-942.

Chapter 3

Lin, J.N., Banerji, S. K. and H. Yasuda (1994) Role of Interfacial Tension in the Formation and the Detachment of Air Bubbles.2. A Single Orifice on an Inclined Plane Immersed in Water *Langmuir* **10**, 943-948.

Lubetkin, S. D. (1989) The Nucleation and Detachment of Bubbles *J. Chem. Soc., Faraday Trans. 1* **85** (7), 1753-1764.

Manley, D. M. J. P. (1960) Change of size of air bubbles in water containing a small dissolved air content *Brit. J. Appl. Phys.* **11**, 38-42.

Nesis, E. I. and Komarov, V. I. (1975) Detachment of bubbles from a wetted solid surface *Colloid J. USSR* **37**, 721-4.

Pinczewski, W.V. (1981) The formation and growth of bubbles at a submerged orifice *Chemical Engineering Science* **36**, 405-411.

Polytechnisch Zakboekje (1990) 44th edition , (Eds) M.R. Creemers [et al.], PBNA, Arnhem.

Ronteltap, A. D. (1989) Beer Foam Physics Ph.D. Thesis , Agricultural University of Wageningen, The Netherlands.

Scriven, L. E. (1959) Dynamics of phase growth *Chem. Eng. Sci* **10**, 1-13.

Stralen, van S. (1979) Growth rate of vapor and gas bubbles , in *Boiling Phenomena*, vol I, Cole, R. (ed), Hemisphere, Washington, 197-271.

Subramanian, R. S. and Weinberg, M. C. (1980) The role of convective transport in the dissolution or growth of a gas bubble *J. Chem. Phys.* **72** (12), 6811-13.

Tao, L. N. (1978) Dynamics of growth or dissolution of a gas bubble *J. Chem. Phys.* **69** (9), 4189-94.

Ward, C. A., Rizk, M. and Tucker, A. S. (1982) Statistical rate theory of interfacial transport. II. Rate of isothermal bubble evolution in a liquid-gas solution *J. Chem. Phys.* **76** (11), 5606-14.

Weinberg, M. C. (1981) Surface tension effects in gas bubble dissolution and growth *Chem. Eng. Sci.* **36**, 137-141.

Zuidberg, A.F. and Prins, A. (1995) Bubble Growth on an Active Site: Effect of the Cavity Volume *Proceedings of the Conference "Food Macromolecules and Colloids"* held in Dijon, 23-25 March 1994, E. Dickinson and D. Lorient (Eds), The Royal Society of Chemistry, 316-318.

Appendix III.1 Calculation of the bubble volume using image analysis (I.A.)

In order to calculate the volume of the bubbles by photographic means, a calibration is needed. In this chapter, the external diameter of the largest capillary (external diameter is 1.5 mm) was used as a calibration length. The error made by flat photography of a curved object is more or less compensated by making the same error with the calibration of a curved capillary.

The bubbles which are sampled are spherical when small but as the growth progresses and the bubble volume increases the bubbles elongate (elongation factor = length/breadth). In most literature, the volume of spherical obloids is obtained by measuring the planar area and calculating an equivalent radius for a circle of that area. From there an equivalent volume for a sphere of that radius can be calculated. Using this method, the radius of a perfect sphere of steel was overestimated by about 1%. Using the same method, the radius of detached bubbles was underestimated by about 1 %. For elongated bubbles, the error made is much larger. Another method therefore had to be found for the calculation of the volume of elongated bubbles.

Since the bubbles are assumed to be axis-symmetrical, the relationship for a 'rotational body' can be used (*Guldin's rule, Polytechnisch zakboekje, 1994*). With this relation the bubble volume is calculated from the planar area on either side of the axis of symmetry and the shortest distance between the centre of gravity of that area and the boundary or the axis of symmetry L_i , so that:

$$V = \text{Area} \times L_i \times 2\pi \quad (\text{III.1})$$

In order to check the validity of the calculation, two steel spheres of known size were measured. The results are given in table III.1. For spheres 1 and 2 the radius R_o , measured with a caliper rule, is given in column 2. The volume is measured with image analysis (I.A.) according to equation (III.1) and from there the curved surface area and radius R_i are calculated assuming spherical shape. As can be seen the radius found by I.A. comes within 1.2-1.8 % of the measured value.

Table III.1 *Size of 2 steel ball bearings, measured by caliper rule and measured by image analysis.*

	size	Image analysis		
		R_o (mm)	V (mm^3)	A (mm^2) sphere
sphere 1	1.58	15.61	30.21	1.55
sphere 2	3.21	143.3	132.4	3.25

In order to compare the spherical images to elongated bubbles the volume of a bubble prior to and just after detachment was also measured, and is given in table III.2 (figures III.1(a) and (b)). Before detachment, the large bubble is elongated up to about 140% (small bubble 125%) into a pear shape, and after detachment the bubble is an oblate spheroid.

The first column shows the elongation factor, the second column shows the capillary radius at which the bubble is formed. Column three shows the radius of a spherical bubble at detachment calculated with equation (3.7). The fourth column shows the volume by calculated with I.A. R_s is simply the equivalent radius of a sphere with volume V .

Table III.2 *Size of 2 bubbles before and after detachment from the capillary, calculated with equation (3.7), and measured by image analysis. $\gamma=40\text{mN/m}$.*

	Elongation factor	r_c	Eq. (3.7)	Image Analysis	
	(%)	(mm)	R_s (mm)	V (mm ³)	R_s (mm) sphere
1 attached	125	0.05	0.92	3.22	0.92
1 detached	84	0.05	0.92	3.57	0.95
2 attached	140	0.55	1.49	12.16	1.43
2 detached	97	0.55	1.49	11.78	1.41

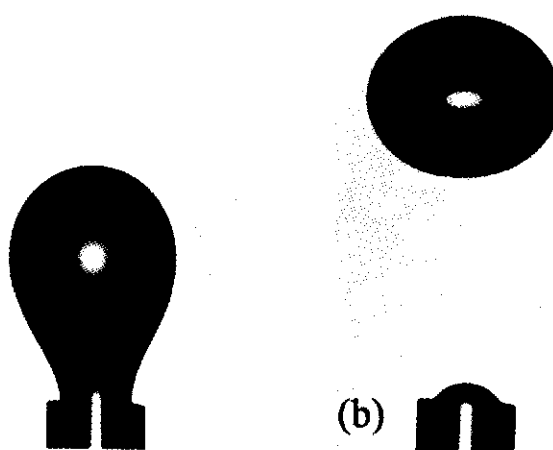


Figure III.1 Photographs of bubble 2 (a) prior to detachment and (b) after detachment from the capillary.

The consecutive images of the bubbles (attached to capillary and detached) have volumes that differ somewhat. For bubble 1 the detached volume is larger than before detachment, whereas for bubble 2, the detached volume is smaller than when it was attached. It was expected that the volumes would be more or less the same since the images are taken with a time interval of 0.2 seconds in which almost no growth is expected. The values found for R_v were found to be within 0-5.4% of R_o .

A different method was used to calculate the real surface area and volume independently, and to check the validity of the image analysis technique, using numerical calculations. From the outline curve of the bubbles (see figure III.2), a numerical calculation can be made for a 'rotational body', using the following integrals:

$$= \pi \int_{x_1}^{x_2} f(x)^2 dx \quad (III.2)$$

$$A = 2\pi \int_{x_1}^{x_2} f(x) \sqrt{1 + f'(x)^2} dx \quad (III.3)$$

where $f(x) = ax + b$, and $f'(x) = a$ or the slope of the line between each point.

Table III.3 shows the values for image analysis and the numerical calculations of the same images. For sphere 1 (see also table III.1), the numerical calculation gives a 3% larger area and a 4% larger volume than measured by I.A.. For the elongated bubble the volume calculated numerically is 5% larger than measured by I.A., whereas the area is 9%

Table III.3. *Size of a steel ball bearing and one bubble, before and after detachment, calculated with equation (3.7) or measured by caliper rule, measured by image analysis, and calculated by a numerical method. $\gamma = 40 \text{ mN/m}$.*

	Eq. (3.7)	Image Analysis			Numerical Calculation			
		R_o (mm)	V (mm ³)	A (mm ²) sphere	R_v (mm) sphere	V (mm ³) eq. III.2	R_v (mm) sphere	A (mm ²) eq. III.3
sphere 1	1.58	15.61	30.21	1.55	16.23	1.57	31.16	1.58
b1 attached	1.49*	12.16	24.62*	1.43*	12.79	1.45*	27.06- 0.95	1.49*
b2 detached	1.49	11.78	25.03	1.41	13.02	1.46	27.04	1.47

* the value is calculated assuming a spherical shape, which is not the case.

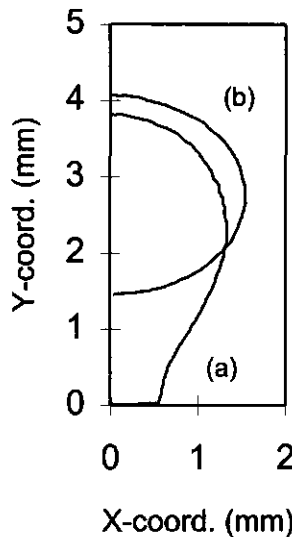


Figure III.2 Left and right bubble contours of bubble 2 (a) prior to detachment and (b) after detachment. The X and Y co-ordinates are given in mm.

larger. This latter is not strange as the area of a sphere is smaller than that of an elongated bubble. The area calculated numerically is corrected for the area of the base of the elongated bubble.

For the detached bubble, the numerical method shows a 10% larger volume and a 7.5% larger area. Table III.3 also gives the radius calculated with equation (3.7) R_o , radius of a sphere calculated from the volume from I.A. R_i , and radius of a sphere calculated from numerically calculated volume R_v and area R_A . As can be seen the numerical calculation gives radii which are closer to the predicted value R_o than R_i .

The differences in bubble volume before and after detachment are not very large. With I.A. there is a 3% smaller volume after detachment which could be explained by the left-over gas in the capillary after detachment. However, the numerical calculation gives a 1.8% larger volume after detachment, which could only be due to growth or error in the image analysis.

The numerical calculation does not show a larger surface area for the elongated bubble than for the detached bubble. We expected this as the bubbles formed on these large capillaries showed a smaller size at detachment than predicted. When we compare R_o with R_i , indeed we see a discrepancy. However, this discrepancy is not found between R_o

and R_v or R_s . This means that the error is in the Image analysis and not in the real bubble volume.

Although small differences between bubble volumes will fall within the uncertainty of the method (5-10 %), the image analysis seems an efficient tool to rapidly measure the volumes of elongated bubbles in a rough way, if they are not too big. The radius of bubbles can only be given for spherical images, and the equivalent surface area of elongated bubbles give a 10% error from image analysis compared to the numerical results. This is probably due to edge effects of the analysed images.

Appendix III.2 Measurement of the surface rheology of beer at relatively large deformations, far from equilibrium.

In order to know the state of the surface and of the surface tension during bubble growth and at detachment, surface rheological experiments are carried out with a rectangular Langmuir trough, equipped with a caterpillar belt with six barriers (see figure III.3). In this method, (Prins, 1986) the surface is continuously expanded or compressed at a constant rate. The measurements were carried out with relative compression and expansion rates varying between 10^{-4} and 10^{-1} s $^{-1}$. During compression or expansion the surface tension is measured with the Wilhelmy plate technique, at constant temperature and pressure. The surface is deformed uni-axially and if surface active components are present, the surface tension changes depending on the rate of expansion, respectively compression. After a certain time, the surface tension becomes constant at a steady state condition. The change in surface tension between equilibrium and deformation conditions can be used to calculate the surface dilational viscosity η_s^d with equation (1.33):

$$\eta_s^d = \frac{\Delta\gamma}{\frac{d \ln A}{dt}} \quad (\text{III.4})$$

The value of the deformation rate ($d \ln A/dt$) is defined to be positive for expansion and negative for compression. Experimental results have shown that the surface dilational viscosity depends strongly on the surface deformation rate. At higher rates the viscosity of the surface decreases, showing a "shear thinning" behaviour (Prins, 1976). Experiments done on with practical systems show that a power-law relationship exists between surface dilational viscosity and the relative expansion rate (Prins, 1988, Ronteltap, 1993):

$$\log \eta_s^d = m \log \frac{d \ln A}{dt} + n \quad (\text{III.5})$$

where m and n are power-law constants. The absolute value of the surface dilational viscosity depends strongly on the value of n . The shear thinning behaviour of the surface is mainly characterised by m (Ronteltap, 1989). According to Ronteltap, this relationship should be valid for expansion as well as for compression. However using practical systems like beer it is not unthinkable that adsorption rates are quite different from desorption rates.

For beer, the surface dilational viscosity is measured in compression and in expansion at various rates. For practical purposes the beer should be completely degassed, which entails a logical decrease in alcohol content. In order to see the effect of such a decrease a second measurement was carried out with the same beer to which 4% alcohol

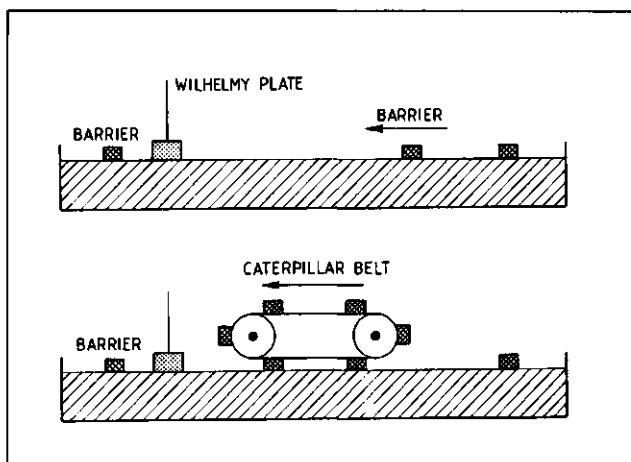


Figure III.3 The Langmuir trough equipped with a caterpillar belt (from Ronteltap, 1989).

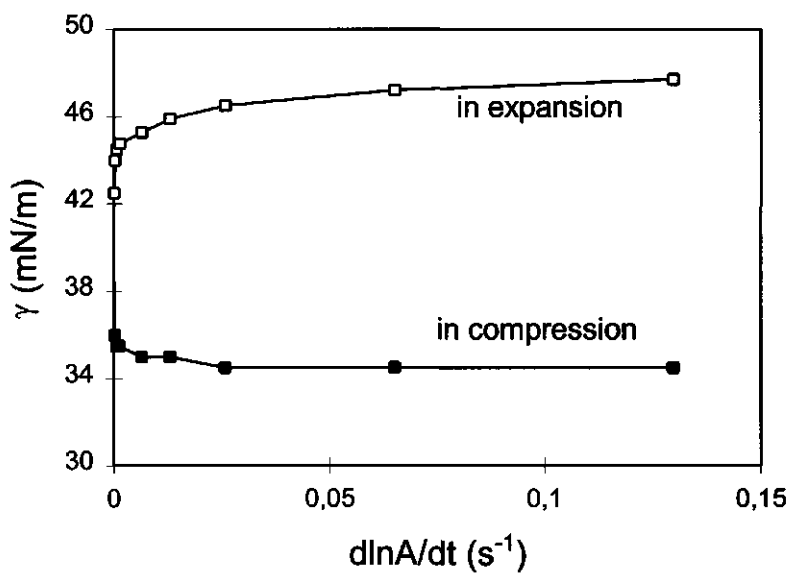


Figure III.4 Measured surface tension of the beer surface in expansion and in compression, as a function of the relative surface deformation rate.

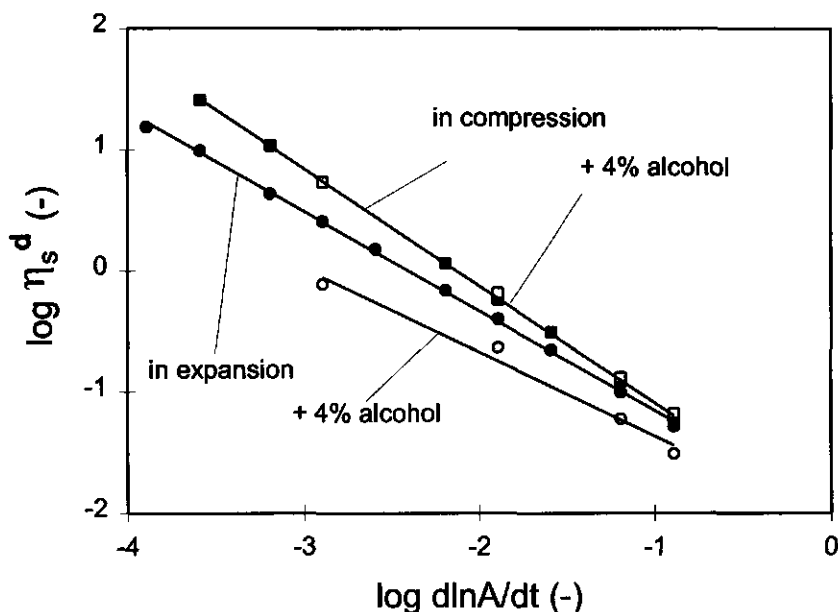


Figure III.5 The log-log plot of the surface dilational viscosity against the relative surface deformation rate of beer, for compression (■) and expansion (●) of degassed beer, and for compression (□) and expansion (○) of degassed beer with added alcohol.

was added. Figure III.4 shows the change in surface tension as a function of the relative deformation rate for compression as well as for expansion. The surface tension decreases in compression and increases in expansion.

Figure III.5 shows the log-log plot of the surface dilational viscosity versus the relative deformation rate. The resulting m and n values are shown in table III.4. As can be seen in the figure, the compression leads to a higher surface viscosity than expansion, as would be expected for surface filled with proteins and other macromolecules. The expansion curve for the beer containing extra alcohol shows a comparable line with beer in compression, but in expansion the addition of the alcohol leads to a relatively lower dilational viscosity. It could be that in compression the surface is filled with macromolecules, whereas in expansion the alcohol molecules have a chance to get to the surface and "relax" it when gaps start to fall in the surface layer.

Table III.4. *m and n values calculated with the powerlaw (equation III.5) from the lines in for compression and expansion of degassed beer, and expansion of degassed beer with an added amount of alcohol, as shown in figure III.5.*

	<i>m</i>	<i>n</i>
compression (with and without alcohol)	-0.9671	-2.0506
expansion	-0.8231	-1.9784
expansion (+ 4% alcohol)	-0.6946	-2.0619

DETACHMENT OF BUBBLES FROM A CAPILLARY: EFFECT OF TILTING ANGLE AND OSCILLATORY MOTION

4.1 Introduction

Bubbles formed in carbonised beverages, such as beer or champagne, often originate from the vertical glass wall of the container holding the liquid. The bubbles are generally formed at cracks and cavities in the solid surface that hold an amount of entrapped gas and which are in contact with the supersaturated liquid. Driven by diffusion and convection, gas is transported from the supersaturated solution to the gas-liquid interface, where the gas mass or nucleus can then grow into a bubble. As the bubbles detach from the vertical wall and rise to the foam layer, liquid is entrained parallel to the glass surface. This liquid motion in turn can introduce an extra detaching force on the bubble as a result of which smaller bubbles can be formed than in a situation where no motion is present.

The aim of this work is to understand what effect tilting of the solid surface has on the bubble volume at detachment. Furthermore the effect of motion (here oscillatory) of the solid surface relative to the quiescent liquid on the growing bubble is investigated. The reason for this investigation can be found in the formation of aqueous foams. Foam formed in the process of sparging, but also in supersaturated liquids, is the total product of the continuous formation of single bubbles. The quality of the foam or, better said, the stability of the foam against collapse can be seriously influenced by the bubble size and by the bubble size distribution in the foam. Three important mechanisms involved in the collapse of foam are drainage, coalescence and disproportionation, all of which are directly influenced by bubble size and bubble size distribution in the foam (Ronteltap, 1989). A better control of the bubble size at detachment from the solid surface can therefore be a tool by which the characteristics and the stability of the produced foam can be influenced.

The size of bubbles detaching from a motionless horizontal solid surface is dictated by a number of factors such as the density difference between gas and liquid, the surface tension, the perimeter of the contact line between the bubble and the solid surface and the wettability of the surface. The bubbles detach from the solid surface when the buoyancy force exceeds the forces which keep the bubble attached to the surface (see section 3.2; Bisperink and Prins, 1994).

Two factors that have been found to be able to decrease bubble size at detachment are the tilting angle of the solid surface and liquid motion relative to the solid surface, which are the main subjects of this chapter.

From literature there is a lack of quantitative knowledge of the effect of the tilting angle on the forces which influence the detaching mechanism, although Lin *et al.* (1994b) showed that, inclining the angle of the surface at which the bubble is attached, decreases the size of the bubble at detachment, depending also on the wettability of the surface (see also chapter 3). Earlier investigations by Sullivan *et al.* (1964) showed only small effects of the angle of inclination on bubble formation. However, these authors only analysed the frequency of the bubble formation, assuming a constant volume region. Strangely enough, the size of the orifices which they employed was large compared to those used here, which would result in a larger effect.

Effects of liquid motion parallel to the solid surface on the detachment of decane droplets were studied by Mahé *et al.* (1988), but only shear forces were taken into consideration. In the investigation done here, the shear forces are of relatively small importance, as will be shown in the theoretical section. Cho and Lee (1990) found that upward liquid movement perpendicular to the surface helped bubbles to detach at a smaller size than when the liquid was quiescent, but did not investigate liquid motion parallel to the surface. In emulsification processes using porous glass membranes, this effect is observed: a liquid phase is introduced into a second immiscible fluid phase (water in oil for example) by forcing it through a glass porous membrane. Within the tubular membrane the continuous phase has a finite velocity, which is found to make the droplets detach at a smaller size than if the liquid would be quiescent (Muschiolik and Dräger, 1995). These effects could mostly be explained by the shear force exerted by the streaming continuous phase on the droplets at the wall of the membrane.

On the effect of oscillatory motion on bubble or droplet detachment no literature references at all were found. In the following paragraph some of the applicable theory is presented concerning the detachment of bubbles at rest, under influence of a tilting angle and when the oscillation is applied to the capillary during bubble growth.

4.2 Theoretical

In this theoretical part the forces that influence bubble detachment from a single capillary are described. The cases considered are: bubble detachment at rest, detachment of bubbles from a tilted capillary and bubble detachment under the influence of oscillatory motion of the capillary relative to the liquid.

Bubbles are formed at cavities in the form of a glass capillary (the opening is circular) which is held in a vertical position unless otherwise specified.

4.2.1 Bubble detachment at rest

A bubble growing on a horizontal solid surface detaches when the vertical buoyancy force exceeds the surface tension force holding the bubble attached to the circular rim of the cavity. There is one important assumption that has to be made in order to predict the bubble volume at detachment. When the bubble grows beyond the mouth of the capillary, it is imperative that the glass edge is sharp in order to prevent the contact base from spreading, as mentioned already in section 3.2. As the bubble grows the contact angle is small at first, as would be expected for a wetted solid (see section 2.2). However, as the bubble grows, the bubble is pulled away from the solid surface by buoyancy. Due to the sharp edge the contact angle can adjust to the force pulling on it. As a result, the 'apparent' contact angle will reach 90° with the horizontal plane at the moment of bubble detachment, where the force of attachment (the vertical component of the surface tension) reaches a maximum (see figure 4.1(a)).

The bubble volume at detachment can be found with the following force balance (see also equation (3.6)):

$$V(\rho_l - \rho_g)g = 2\pi r\gamma \sin\theta \quad (4.1)$$

where V is the volume of the bubble (m^3), ρ_l and ρ_g are the liquid and gas density (kg/m^3), and g is the acceleration due to gravity (m/s^2); $2\pi r$ is the perimeter of the contact base with radius r between bubble and solid surface (m), γ is the surface tension (N/m) and θ is the

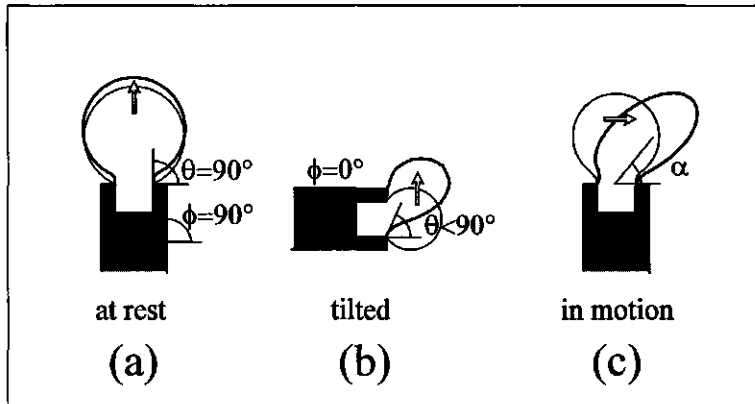


Figure 4.1. Schematic representation of a bubble growing on a capillary; (a) at rest, (b) at an inclined angle and (c) imparted with oscillatory motion. θ is the apparent contact angle, ϕ is the tilting angle and α is the maximum angle of inflection of the bubble as a result of the oscillatory motion.

apparent contact angle ($^\circ$) between the gas-liquid interface and the horizontal surface plane. As a rule the angle becomes 90° before detachment which results in $\sin\theta$ equals 1 (Bisperink and Prins, 1994; Lin *et al.*, 1994a).

It should be noted that normally the contact angle is the angle between the solid surface and gas-liquid interface, measured across the liquid phase. Here, however, where the angle of attachment adjusts itself to each situation around the pivot point of the edge of the cavity, the angle used is measured from the horizontal plane. This method was also applied for the tilting angle investigation.

4.2.2 Effect of tilting angle ϕ

When the surface on which the bubble is formed is inclined at an angle, the bubble can detach at a smaller size (Cho and Lee, 1990; Lin *et al.*, 1994b) due to the smaller effective surface tension force acting on the bubble. Figure 4.1(a) shows the bubble on a capillary which is held vertically, at an inclination angle of $\phi = 90^\circ$. In figure 4.1(b), the capillary is tilted sideways, and $\phi = 0^\circ$. The bubble size at detachment in (b) will be smaller than in (a).

In order to keep the same force balance valid, equation (4.1) now becomes:

$$\begin{aligned} (\rho_l - \rho_g)g &= 2\pi r\gamma \cos(\theta - \phi) \\ &= 2\pi r\gamma (\cos\theta \cos\phi + \sin\theta \sin\phi) \end{aligned} \quad (4.2)$$

where ϕ is the angle of inclination. When inserting $\phi = 90^\circ$ for a vertical capillary, equation (4.2) becomes equation (4.1) once again. According to Lin *et al.* (1994b) the apparent contact angle θ will always become 90° with the horizontal plane before detachment due to stretching of the surface in the process of neck formation. As mentioned before, this can also be explained by the sharp pivot point of the edge of the cavity. This means that, at an inclination angle of 90° (vertical position), $\cos(\theta - \phi)$ becomes 1, and when the tilting angle is 0° (horizontal position), $\cos(\theta - \phi)$ becomes 0. Theoretically speaking therefore, a zero bubble volume would be expected at a zero tilting angle. Due to this effect, the effect of the surface tension on the bubble size is decreased in absolute sense as the capillary is tilted from $\phi = 90^\circ$ to 0° .

4.2.3 Oscillatory motion

In this section we attempt to study the effect of liquid motion on the detachment of a growing bubble from a solid surface. Along the same line of investigation as in the previous chapter, the bubbles are formed on a glass capillary, growing by diffusion and convection from a gas-supersaturated aqueous solution. The most straight-forward method to observe the effect of motion would be to let liquid flow past the site where the bubble grows. However, as was observed earlier in chapter 3, motion of supersaturated solution introduces the formation of extra 'parasite' bubbles. In order to avoid 'parasite' bubble formation, the liquid was held motionless while the capillary (with the bubble) underwent an oscillatory motion.

Oscillatory motion, however, is a wave motion which causes alternating viscous and inertial forces; these forces are therefore never constant during the growth of the bubble. This makes the analysis of the results rather difficult. Furthermore, the forces affecting the capillary are assumed to be fully imparted onto the bubble attached to the capillary. It is unsure whether this is a reasonable assumption. Also, as can be seen in figure 4.9, the bubbles can be considerably deformed. For the sake of simplicity, however, they are assumed to be spherical in the theoretical considerations.

In spite of all these anomalies, an attempt was made in the following section to analyse the forces at play in oscillatory motion, and how they may affect the detachment of a growing bubble attached to a capillary.

The periodic motion that is imparted to the capillary, and thus to the attached bubble, results in a change in displacement, velocity and acceleration as a function of time (or phase angle) as can be seen in figure 4.2. Figure 4.1(c) shows that the bubble is deformed and is inflected as a result of the forces, as will be explained further on. This leads to an earlier detachment of the bubble than when the capillary is motionless. The displacement s , velocity v and acceleration a can be described as:

$$s = Amp \sin(2\pi f t) = Amp \sin(2\pi \frac{t}{T})$$

$$v = \frac{ds}{dt} = 2\pi f Amp \cos(2\pi f t)$$

$$a = \frac{dv}{dt} = -4\pi^2 f^2 Amp \sin(2\pi f t)$$

where Amp is the amplitude (m) and f is the frequency of the oscillation (1/s); t is the time (s) and T is the time taken by one oscillation (s).

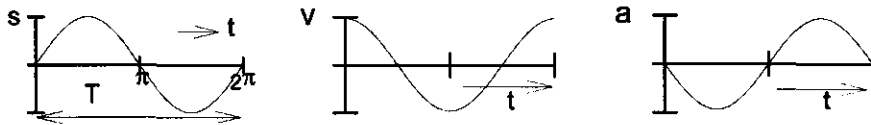


Figure 4.2. Schematic representation of the relations between displacement s , velocity v and acceleration a in simple oscillatory motion.

The velocity and acceleration in figure 4.2 are maximal during different stages in the oscillatory motion and have a value of:

$$s_{\max} = Amp \quad \text{at } \frac{1}{2}\pi \text{ and } 1\frac{1}{2}\pi \quad (4.3a)$$

$$v_{\max} = 2\pi f Amp \quad \text{at } 0, \pi \text{ and } 2\pi \quad (4.3b)$$

$$a_{\max} = -4\pi^2 f^2 Amp \quad \text{at } \frac{1}{2}\pi \text{ and } 1\frac{1}{2}\pi \quad (4.3c)$$

4.2.4 Forces acting on bubble during motion

When moving a bubble attached to a capillary in a periodic motion, various forces have to be taken into account. In all cases, we inserted the maximum values of the forces exerted on the bubble into the equations, which occur at the maximum values of the velocity and the acceleration (see equations 4.3(a), (b) and (c)).

The buoyancy force F_B , which is always present in the direction perpendicular to the oscillatory motion, can be described by (see also the left-hand side of equation (4.1)):

$$F_B = V(\rho_l - \rho_g)g \quad (4.4)$$

As a result of the bubble motion relative to the liquid, a shear force F_s is imparted to the bubble parallel to the oscillatory motion which is supposed here to be equal to the Stokes equation, under the assumption that the bubble interface is rigid (Goldman *et al.*, 1967; Mahé *et al.*, 1988):

$$F_s = 6\pi\eta R v \quad (4.5)$$

where η is the liquid viscosity (Pa s), R is the radius of the bubble (m) and v is the maximum velocity of the oscillatory motion (m/s).

An inertial force F_I arising due to periodic changes in velocity may be described by Newton's second law, also parallel to the oscillatory motion:

$$F_I = (m + m')a \quad (4.6)$$

where $(m + m')$ is the virtual mass of the bubble containing m the mass of the bubble (kg) and m' the added or hydrodynamic mass of displaced liquid; a is the acceleration of motion (m/s^2). For a sphere moving in an unbounded fluid the added mass $m' = \frac{1}{2}m$ (Milne-Thompson, 1968) which for the inertial force translates into:

$$F_I = \left(\frac{4}{3} \pi R^3 \rho_g + \frac{2}{3} \pi R^3 \rho_l \right) a \approx \frac{2}{3} \pi R^3 \rho_l a \quad (4.7)$$

where the density of the gas phase is neglected in comparison to that of the liquid phase. The resultant force F which combines buoyancy, viscous and inertial forces is shown in figure 4.3 and can be described as:

$$F = \left(F_B^2 + (F_S + F_I)^2 \right)^{\frac{1}{2}} \quad (4.8)$$

where F_B , F_S and F_I are given by equations (4.4), (4.5) and (4.7) respectively.

The resultant force F is found to be more or less equal to $F_B + F_I$. However, F_B is independent of the oscillation. The maxima therefore depend on $|F_I|$, which results in a

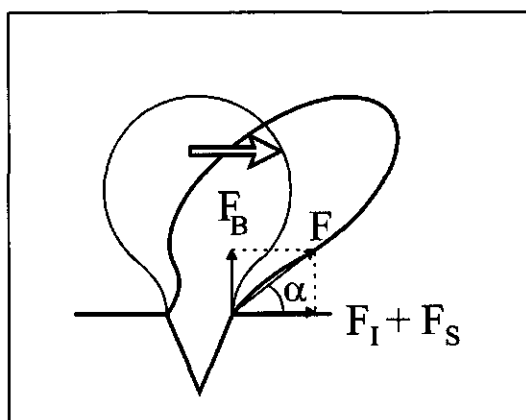


Figure 4.3. Vectorial representation of the forces acting on a bubble growing on an oscillating capillary.

maximum detaching force at every turning point of the oscillation (see equation (4.7) and (4.3c)). As a result of bubble growth, both the buoyancy as well as the inertial force will increase independent of the oscillations. The maxima in force F are found at the same point in the oscillation as where the bubbles are most deformed, and where they supposedly detach from the capillary.

The resultant force F is balanced by the surface tension force working on the perimeter of the contact base of the bubble with the capillary (see also the right-hand side of equation (4.1)). Equating these two net forces results in the mechanical equilibrium balance for the detachment of a bubble on an oscillating capillary (see figure 4.3):

$$F = 2\pi r\gamma \sin\alpha \quad (4.9)$$

where $\sin\alpha$ is:

$$\sin\alpha = \frac{F_B}{F} \quad (4.10)$$

α is the angle at which the resultant force acts on the bubble contact plane, and also the angle at which the bubble is inflected due to the applied horizontal forces of shear and inertia as shown in figure 4.1(c). Combining equations (4.9) and (4.10) gives:

$$F^2 = 2\pi r\gamma F_B \quad (4.11)$$

The effect of the forces of buoyancy, surface tension, shear and inertia on the bubble size at detachment was simulated using equation (4.11) and inserting equation (4.8). In order to study the effect of these forces the maximum velocity of motion and the maximum acceleration given by equations (4.3b) and (4.3c) were used. It should be noted that the maximum shear force acts on the bubble as it passes through the equilibrium point ($Amp=0$) whereas the maximum inertial force is found where the amplitude is maximal (see also figure 4.2). A study of the course of the resultant force F showed that for the chosen frequency and amplitude range the shear force F_s can be neglected compared to the inertial force F_i . Hence from here on, only the inertial force on the bubble is taken into account, which leads to a simplification of the resultant force F in equation (4.8) so that equation (4.11) becomes:

$$F_B^2 + F_i^2 = 2\pi r\gamma F_B \quad (4.12)$$

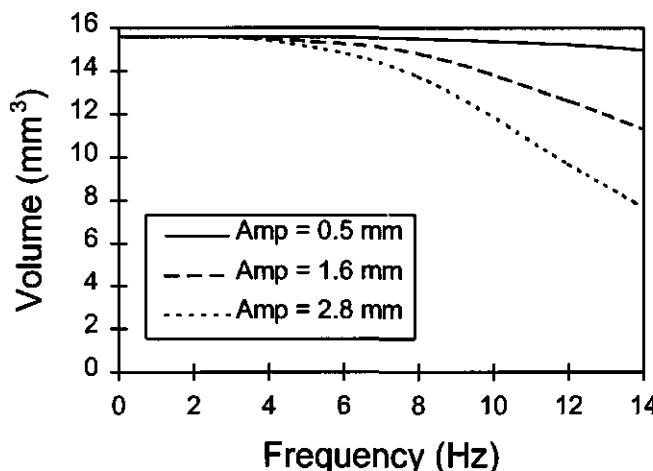


Figure 4.4. Theoretical volume of bubbles prior to detachment as a function of applied frequency for $r_c = 0.553$ mm, $\gamma = 40$ mN/m and (—) $Amp = 0.5$ mm, (---) $Amp = 1.6$ mm, and (---) $Amp = 2.8$ mm.

The theoretical (spherical) bubble volume at which detachment occurs can now be easily calculated for each capillary size, frequency and amplitude. Figure 4.4 shows the calculated values for the largest capillary, at three amplitudes and various frequencies.

4.3 Experimental

4.3.1 Materials

Supersaturated liquid

The liquid used was beer (lager, 11.5° Plato original gravity) supersaturated with an absolute concentration of 0.12 mol CO₂ / l liquid at a temperature of 20°C and at atmospheric pressure (4.4 g/kg excess concentration).

The surface tension of the beer solution was measured in equilibrium using the Wilhelmy plate technique and was found to be 46 mN/m.

Capillaries

Bubble growth was induced on glass capillaries (Hirschmann Laborgeräte, Chrompack) holding a cavity filled with gas, as used by Bisperink and Prins (1994) (see also figure 4.5). The largest capillary is melted on one end. For the two smaller capillaries, one end of the capillary is partly filled with a hydrophobic glue (Bison-Combi, Perfecta Chemie) in order to keep the liquid from wetting the cavity. The internal diameters of the capillaries were measured before use with a stereo microscope (Zeiss, magnification 80x). The three glass capillaries used in this work have an internal radius of respectively 0.550 mm, 0.155 mm and 0.050 mm.

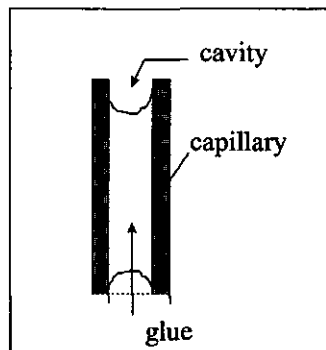


Figure 4.5. Schematic presentation of the capillary, partly filled with glue. The cavity at the top side is used as the bubble formation site.

4.3.2 Methods

Tilting

The three capillaries were tilted at angles varying between $\phi = 90^\circ$ (vertical position) and $\phi = 0^\circ$ (horizontal position).

Oscillatory motion

Movement of the capillary was created by applying a horizontal sinusoidal oscillation to the vertically positioned capillary. The glass capillary was attached to two speakers such as can be seen in figure 4.6. The speakers are soldered together at a 90° angle in order to be able to move the capillary at a controlled amplitude and frequency.

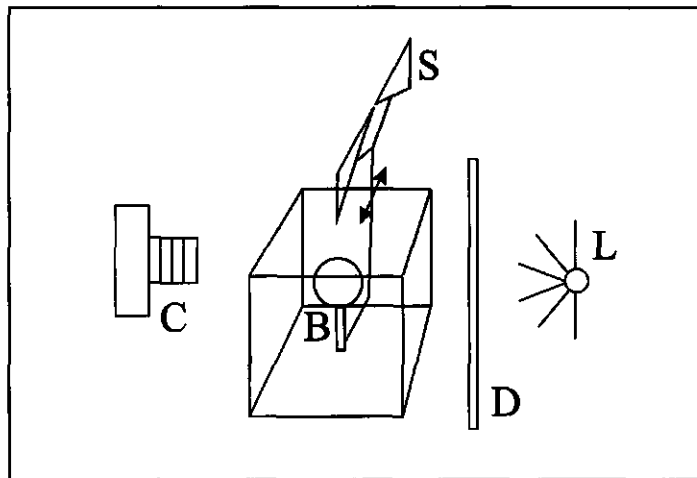


Figure 4.6. Schematic side view of the experimental set-up; C = Camera, S = oscillating Speakers, B = Bubble, D = Diffuser, L = Lamp

Setting the signal to the cones of the speakers in phase induces a vertical movement of the capillary, whereas when the cones move out of phase the motion of the capillary is horizontal. The latter setting was applied here. The speakers are connected to a signal generator (DSG2, Farnell) with which both amplitude and frequency could be varied. The amplitudes used were around 0.5 mm, 1.8 mm and 3 mm. These amplitudes were generally found to decrease slightly over the range of frequencies used; the decrease was found to be 4 %, 13 % and 12 % for the three respective amplitudes at the maximum frequency. The applied frequency range was kept between 0 and 14 Hz, where already a considerable influence on the bubble size prior to detachment was found. These frequencies are below the resonance frequency of bubbles of this size (Minnaert, 1933).

Photography

The last stages of bubble growth and detachment at the capillary tip were monitored by taking photographs at consecutive time intervals of 0.2 seconds, using a photo camera (Nikon F801) with macroscopic lens and accessories and a flash light (Metz 60 CT1) as back lighting.

To obtain high quality photographs external light sources were eliminated by covering the sides of the vessel. An optical diffuser was placed between the light source and the vessel in order to obtain exposures of better resolution.

Image Analysis

The last exposure prior to bubble detachment was used to measure bubble volume at detachment. This was done by measuring a planar area with an image analyser (Joyce-Loebl, Magiscan), and calculating the volume using the following equation, as already described in Appendix III.1:

$$V = 2\pi \delta \frac{1}{2}A \quad (4.13)$$

in which $\frac{1}{2}A$ is half the planar area of the bubble on either side of the axis of symmetry (m^2) and δ is the shortest distance from the centre of gravity of the area $\frac{1}{2}A$ to the axis of rotation or symmetry (m). This equation gives accurate results for bodies of revolution such as spheres. In chapter 3 we have shown that in the case of bubbles growing in a vertical position without applied motion the results are very reasonable for not too large bubbles. When the capillary is tilted or when motion is applied the bubbles are deformed and the described method is less accurate. However, we have found that the acquired values are quite reproducible and are therefore viewed as reasonable approximations of the bubble volume. For example, during these experiments, the bubbles were photographed in various positions of deformation and the values found with image analysis were well reproducible in the different positions.

4.4 Results & Discussion

Apart from the obvious influences of tilting angle and motion on the bubble volume at detachment investigated in this work, it should be noted that the radius of the capillary sets an important limit to the maximum bubble volume when the bubble is growing at rest, i.e. when no motion is applied. This is also true for the surface tension. Equation (4.1) gives a linear relationship between the volume and the capillary radius and surface tension. This means in the experiments that bubbles detaching from capillaries of decreasing radius contain a reduced volume of gas. In the same analogy, the bubble volume decreases with decreasing surface tension. In the experiments the surface tension is not varied but, as will be explained at a later stage, it is highly plausible that, due to expansion and compression of the surface, the surface tension is not constant over the surface of the bubble.

In several figures the volume of detaching bubbles are scaled to the bubble volume found in the vertical, motionless position ($\phi = 90^\circ, f = 0 \text{ Hz}, \text{Amp} = 0 \text{ mm}$) in order to compare results.

4.4.1 Tilting angle

Figure 4.7 shows two photographs taken of a bubble prior to detachment from the largest capillary at two different tilting angles. The measured volume of bubbles prior to



Figure 4.7. Two photographs of a bubble detaching from an inclined capillary.

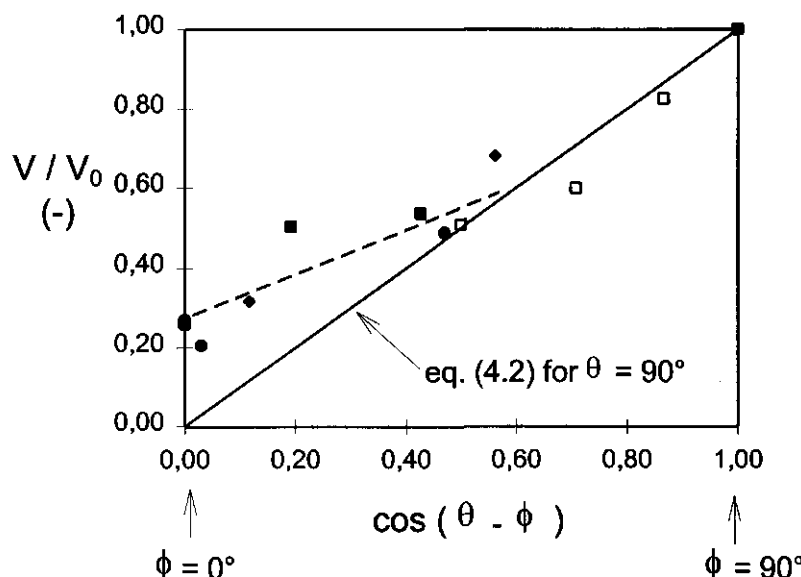


Figure 4.8. Relative volume of bubbles prior to detachment growing on a capillary held at various tilting angles (■) $r_c = 0.055$ mm, (◆) $r_c = 0.155$ mm, (●) $r_c = 0.553$ mm, (□) data from Lin *et al.* (1994b) $r_c = 0.275$ mm and (—) shows equation (4.2).

detachment on capillaries held at various inclined angles is plotted in figure 4.8 for the three different capillary sizes as a function of the cosine of the apparent contact angle θ minus the tilting angle ϕ , as found in equation (4.2).

The y-axis denotes the relative volume, i.e. the volume of the detaching bubble divided by the bubble volume at a 90° inclination angle (vertical position). The line shown in figure 4.8 is the theoretical relation given by equation (4.2), also scaled to the initial volume of detachment. Increasing the inclination angle ϕ from 90° to 0° ($\cos(\theta - \phi)$) goes from 1 to 0) reduces the relative volume of the detaching bubble. This reduction is rendered independent of capillary size by making the volume relative as can be seen in figure 4.8. Data from Lin *et al.* (1994b) of bubbles formed at an orifice plate at low contact angles are included in figure 4.8, showing a similar relationship. According to equation (4.2) the relative volume should approach zero when $\cos(\theta - \phi)$ approaches 0. This would mean that when the capillary is tilted to 0° (horizontal position), the bubble should detach before a finite volume is reached.

It can be seen however that this situation is not reached, indicating that the apparent contact angle is smaller or greater than 90° . From figure 4.8 we calculate a maximal discrepancy of about 15° , suggesting that when the capillary is gradually tilted to a horizontal position the apparent contact angle will be gradually decrease from 90° to about 75° with the horizontal. The photograph in figure 4.7 also shows that the apparent contact angle θ is now not at a 90° angle with the surface, as suggested by Lin *et al.* (1994b). Furthermore we can see that the gas-liquid interface partly retreats into the capillary resulting in an increase of the perimeter of contact base. This could effectively increase the bubble volume at detachment (see equation (4.2)).

It seems fair to say that the apparent contact angle cannot reach 90° when the capillary is tilted to the horizontal position. This is not very strange as the pivot or hinge point on the edge of the glass capillary is then at its limit. Equation (4.2) is therefore only valid when the variation in the apparent contact angle with the inclination angles is taken into account.

4.4.2 Oscillatory motion

Figure 4.9 shows photographs of bubbles attached to an oscillating capillary prior to detachment in a frequency range from 0 to 14 Hz at an amplitude of circa 2.8 mm. The measured volume of bubbles prior to detachment on oscillating capillaries is plotted in figures 4.10(a), (b) and (c) for the three different capillary sizes. In figures 4.10(a), (b) and (c) the absolute volume is plotted as a function of the frequency, each line representing a different amplitude. Each point represents an average of three individual measurements, and the error bars show the maximum deviation from the average value.

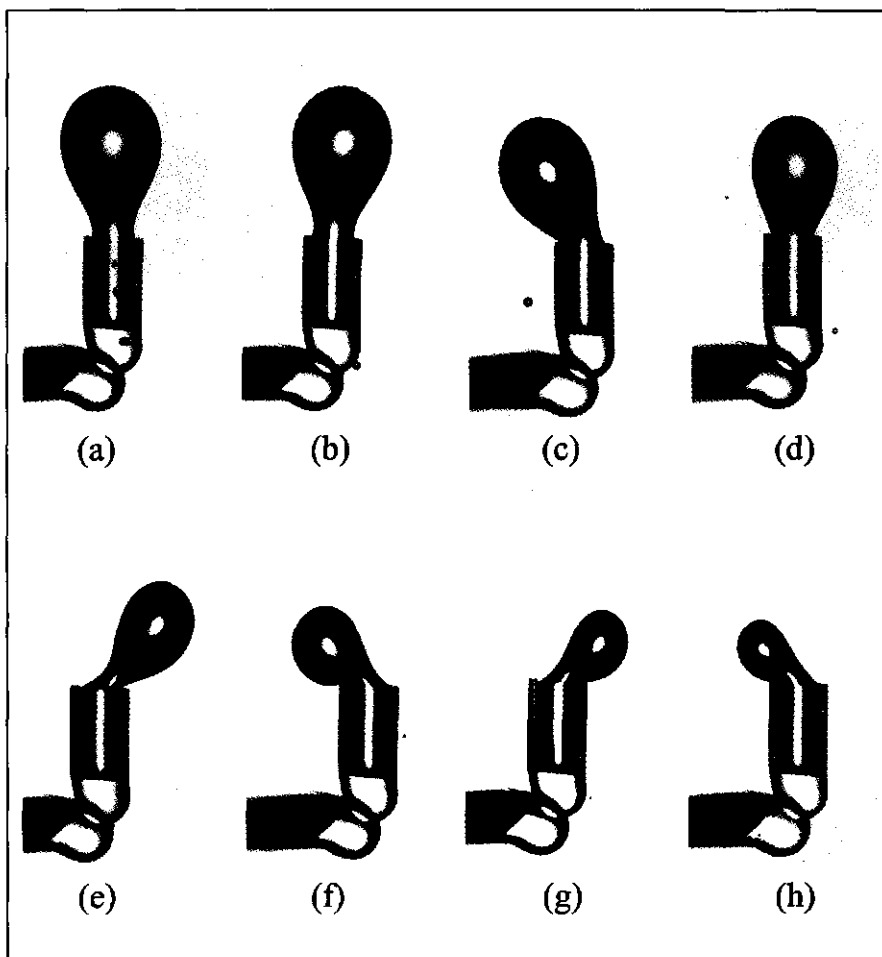


Figure 4.9. Photographs of bubbles detaching from a capillary which is going through oscillatory motion with an amplitude of 2.8 mm ; (a) $f = 0$ Hz, (b) $f = 2$ Hz, (c) $f = 4$ Hz, (d) $f = 6$ Hz, (e) $f = 8$ Hz, (f) $f = 10$ Hz, (g) $f = 12$ Hz and (h) $f = 14$ Hz.

It is clear from all three figures that the bubble size at detachment is increasingly lowered by the increase in both the amplitude and the frequency of the oscillatory motion. Furthermore, the value of the applied amplitude seems to be of less consequence to the detachment volume of the bubble as the frequency is increased to 14 Hz. The bubble volume is expected to approach zero with further increase in both amplitude and frequency. The figures suggest that bubbles growing on a larger capillary, i.e. larger bubbles, are less

affected by the amplitude of the motion than the bubbles growing on a smaller capillary. This is probably misleading, as the applied amplitudes do not scale with the used capillary radii, see table 4.1. Probably if this scaling had been used to select the amplitudes to be applied on the three capillaries, there would have been a smaller difference between the figures 4.10(a), (b) and (c). This influence can be shown graphically as well: Figure 4.11(a) the dimensionless volume as a function of the frequency alone. When the volume is set as a function of the frequency multiplied with the scaling factor (figure 4.11(b)), the lines lie much closer to one another, confirming the effect of the scaling factor.

Table 4.1 *Scaling factor of the amplitude with the capillary radius (Amp / r_c).*

Amp / r_c	0.050 mm	0.155 mm	0.550 mm
0.5 mm	10	3.226	0.909
1.8 mm	36	11.61	3.273
3.0 mm	60	19.35	5.455

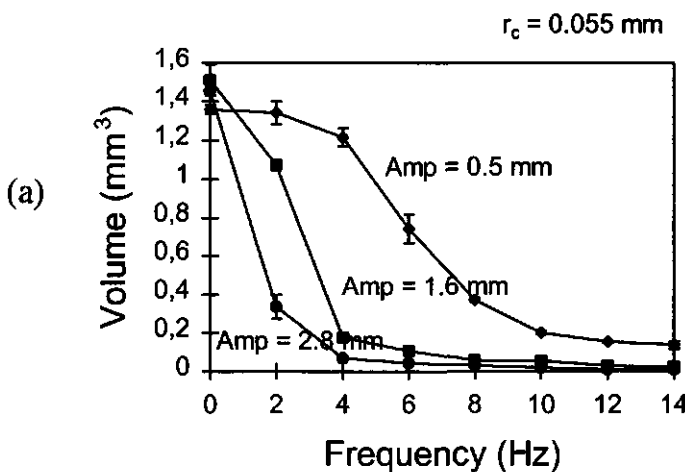


Figure 4.10 a Measured volume of bubbles prior to detachment as a function of applied frequency (a) $r_c = 0.055$ mm, (b) $r_c = 0.155$ mm, (c) $r_c = 0.553$ mm (see next page) and (◆) $Amp = 0.5$ mm , (■) $Amp = 1.6$ mm and (●) $Amp = 2.8$ mm.

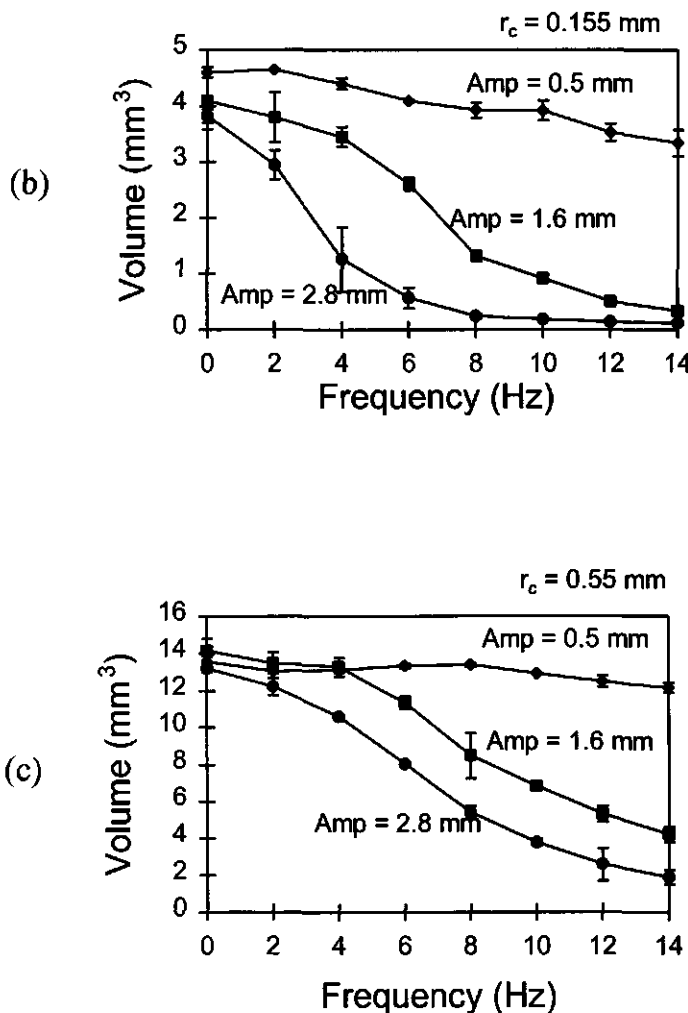


Figure 4.10 b and c. Measured volume of bubbles prior to detachment as a function of applied frequency (c) $r_c = 0.553 \text{ mm}$ and (◆) $\text{Amp} = 0.5 \text{ mm}$, (■) $\text{Amp} = 1.6 \text{ mm}$ and (●) $\text{Amp} = 2.8 \text{ mm}$.

Figure 4.4 shows the calculated volumes of bubbles detaching from the largest capillary, using the theory described in paragraphs 4.2.3 and 4.2.4. A comparison between figure 4.4 and figure 4.10(c) shows that the decrease in bubble volume at detachment as a result of the buoyant and inertial forces acting on the bubble is not sufficient to explain the experimental results. In fact, the measured volumes are smaller than the calculated ones.

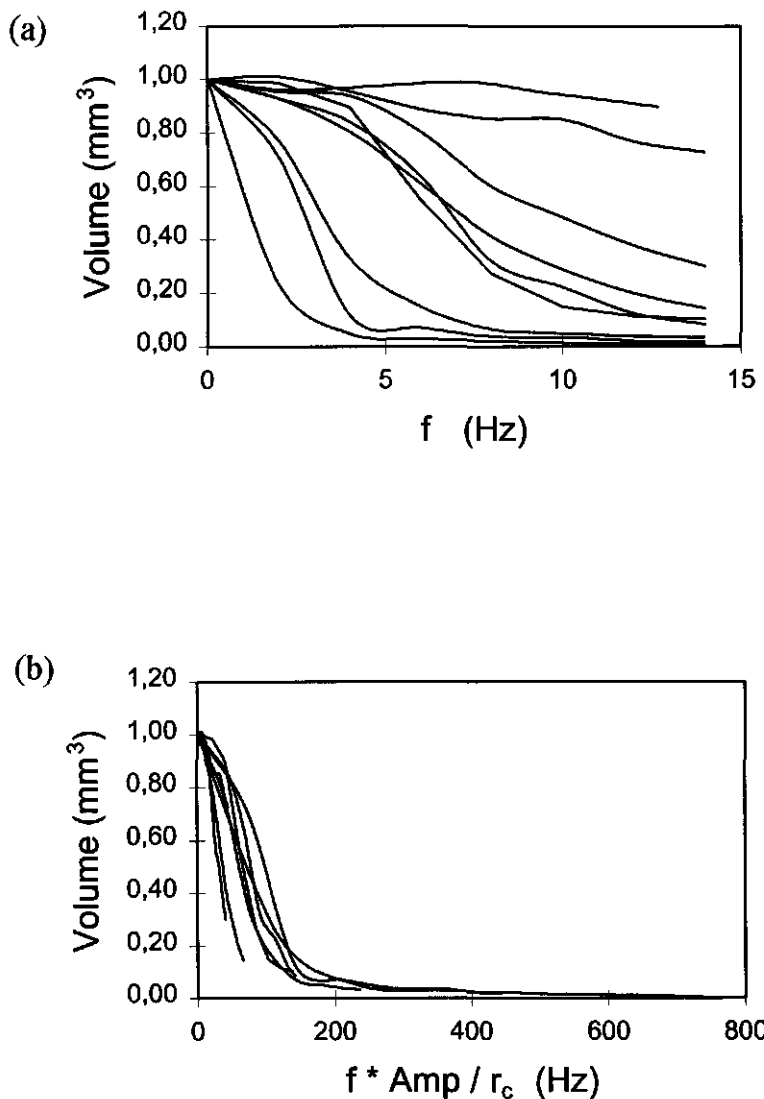


Figure 4.11. Dimensionless measured volume of bubbles prior to detachment as a function of (a) the frequency, and (b) the frequency, multiplied by the scaling factor. The lines in the figure are all measured systems, as shown in figure 4.10.

Although not shown here, the same conclusions could be taken from the calculations for the smaller capillaries. This suggests that there are other or additional factors which influence the detachment mechanism of bubbles growing on an oscillating capillary.

In the calculations the forces determining the detaching volume of the bubble are the buoyancy force and the inertial force. The buoyancy only depends on the volume and the density difference and therefore cannot be influenced by the applied motion. Therefore, a more detailed analysis of the inertial force is in order. F_i is a function of mass m and acceleration a , where the acceleration is applied by the oscillatory motion and is therefore a set value. The value used for the added mass m' of entrained liquid in this work is $\frac{1}{2}m$ which is valid for a sphere. However, we observed that the bubbles deform considerably during the motion and, furthermore, the bubble is attached to a cylindrical capillary. From Milne-Thompson (1968) the added mass for a cylinder is found to be m . It seems plausible therefore that m' lies somewhere between $\frac{1}{2}m$ and m , effectively resulting in a larger calculated inertial force acting on the bubble.

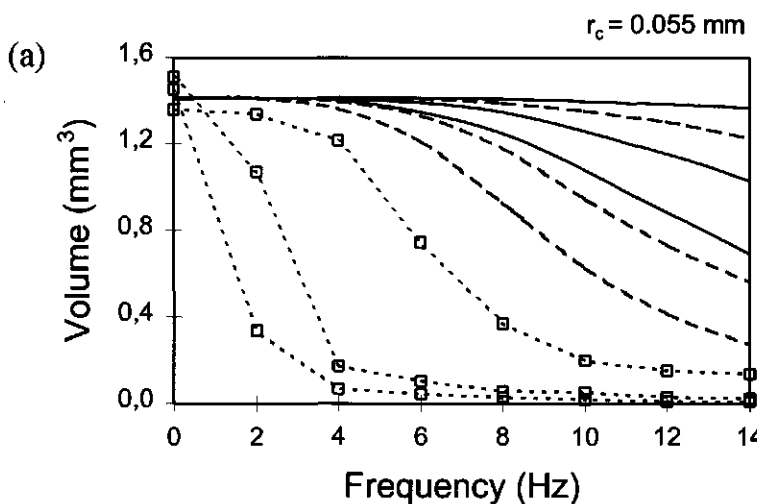


Figure 4.12.a Comparison between experimental values and theory for bubble volume at detachment for the three amplitudes as a function of applied frequency. (a) $r_c = 0.055$ mm, (b) $r_c = 0.155$ mm, (c) $r_c = 0.553$ mm (see next page); (..□..) experimental values, (—) theory with added mass $\frac{1}{2}m$ and (---) theory with added mass m .

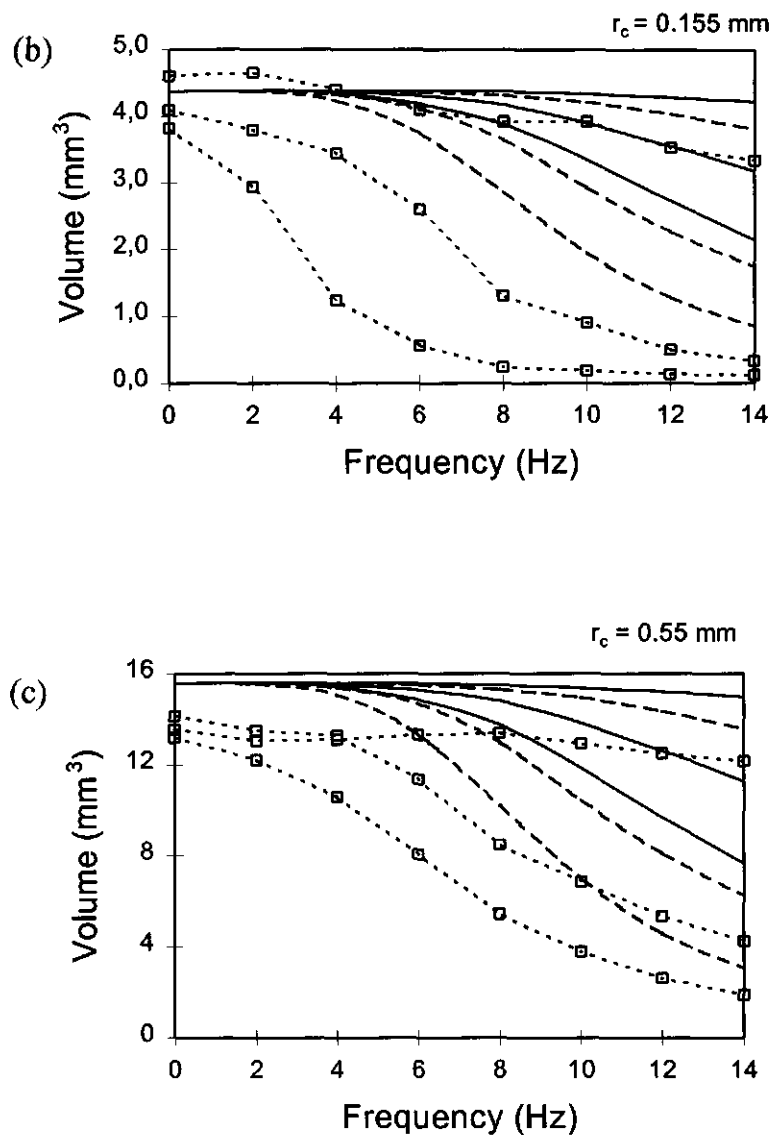


Figure 4.12 b and c. Comparison between experimental values and theory for bubble volume at detachment for the three amplitudes as a function of applied frequency. (b) $r_c = 0.155 \text{ mm}$ and (c) $r_c = 0.553 \text{ mm}$ (..□..) experimental values, (—) theory with added mass $\frac{1}{2}m$ and (---) theory with added mass m .

Figure 4.12(a) to (c) shows the experimental results (..□..), the values calculated with the theory using added mass = $\frac{1}{2}m$ (---), and the values calculated by theory using added mass = m (—). As can be seen from figures 4.12(a), (b) and (c), the theory approaches the experimental values better when the added mass = m , but F_I is still not large enough to force the bubbles to detach at a smaller volume. What may be noticed, however, is that the difference between theoretical calculations and experimental values is smaller for the larger capillary. One of the possible reasons for this effect, described in the following section, is that the surface tension decreases at the bubble interface as a result of the dynamic conditions applied to the bubble. It must be noted that the suggestions put forward are speculative and can only at this moment be dealt with in a qualitative manner.

4.4.3 Surface Rheology

In our experiments we found that the bubble volume at detachment is reduced with increasing velocity of motion. This effect cannot be explained by buoyancy and inertial forces alone. The only other explanation we can think of, for now, is that the surface tension decreases so that the adhesion force of the bubble to the capillary is lowered (see equation 4.1).

From the experiments it is clear that a greater relative decrease in bubble volume with frequency and amplitude of motion is found for smaller bubbles than for the larger ones. In this paragraph we will try to explain the observed effects with dynamic surface phenomena.

In this work we have looked at growth and detachment of bubbles in gas-supersaturated beer. The fermented product contains all kinds of surface active materials such as proteins, hop residues, polysaccharides and lipids and probably many more species (Bamforth, 1970), some of which play an important role in the stabilisation of the gas-bubble interface. The rheological behaviour of a beer surface causes the surface tension to vary with the dynamic conditions imparted upon it.

Ronteltap (1989) showed that the surface tension of a beer surface can be lowered considerably by compressing the surface continuously. In his work a flat surface is compressed by a barrier. Here, it is imaginable that the liquid flowing past the bubble applies a shear force to the surface, by which the surface is expanded at the front and compressed at the back (see figure 4.13 (b)). Macromolecular surface active components will adsorb quite readily onto the surface when it is expanded (at the front). However, some species, such as proteins, will not desorb very fast, if at all, from the compressed area at the

back. Both a high surface coverage as well as a compression can give rise to extremely low surface tensions. Ronteltap (1989) measured surface tension values below 10 mN/m in compressed beer surfaces. Apart from the low surface tension, the expansion and compression cycle can in some cases give rise to the formation of a solid 'skin' at the interface (see section 2.7)

We now propose a model for the mechanism that might lead to the earlier detachment of the bubbles from an oscillating capillary. The shear stress applied by the liquid movement relative to the bubble surface is balanced mechanically at the surface by a counter-acting opposite surface tension gradient, as a result of which the surface is rendered more or less immobile:

$$\sigma = \frac{d\gamma}{dx} = \eta \left(\frac{dv_x}{da} \right)_{a=0} \quad (4.14)$$

where σ is the shear stress, $d\gamma/dx$ is the surface tension gradient along the surface of the bubble, η is the liquid dynamic viscosity, and dv_x/da is the velocity gradient in the radial direction from the surface outwards ($a = 0$ indicates the position of the interface).

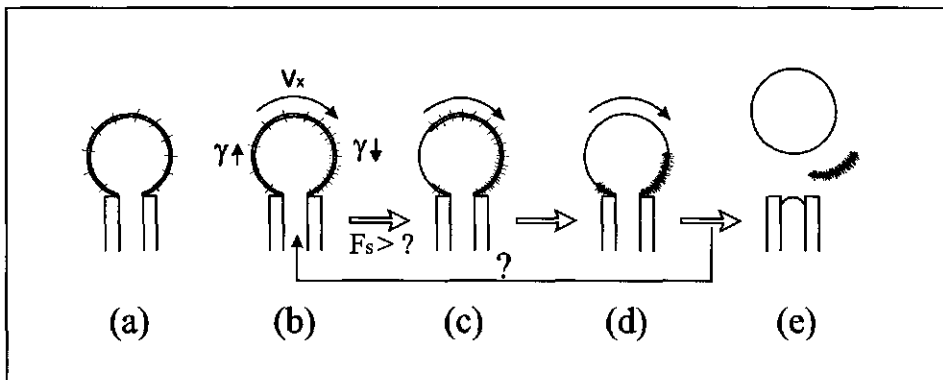


Figure 4.13. Schematic representation of the presented mechanism of the rupture of the surface layer and the subsequent detachment of the bubble. (a) capillary motionless, (b) capillary in motion and build-up of a surface tension gradient, (c) rupture and (d) compression of the surface layer and (e) detachment of the bubble. The transition between (b) and (c) occurs when F_s is larger than the intermolecular forces holding the surface components together as a 'skin'.

The maximum velocity is defined by equation (4.3b) and the shear force on a rigid particle by equation (4.5), assuming Stokes to be valid for a rigid interface. The shear stress σ can also be described as:

$$\sigma = \frac{F_s}{A} = \frac{6\pi\eta R (2\pi f Amp)}{4\pi R^2} = 3\pi\eta f \frac{Amp}{R} \quad (4.15)$$

where A is the surface area of the spherical bubble. As can be seen the shear stress scales with Amp/R , which can also be interpreted as an indirect scaling of the amplitude with the capillary radius, since the radius of the detaching bubble R and the capillary radius r_c are related to a certain extent.

Figure 4.13 shows (a) a bubble growing on a motionless capillary, (b) when the capillary is in motion. In figure 4.13(b) the velocity gradient is balanced by a surface tension gradient, where the surface tension is high at the front of the bubble (extended part) and low at the back (compressed part).

During bubble growth the bubble radius R increases, which increases the shear force pulling at the rigid interface. It is our hypothesis that, when a certain yield force is reached, the 'skin' surrounding the bubble will break. The force at which the surface layer yields will be related to the force necessary to break the cohesive bonds between the adsorbed molecules that hold the surface 'skin' together. The new bubble surface is extremely mobile, compressing the 'skin' rapidly to the back. Figure 4.13(c) and (d) show the compression of the broken surface 'skin'. It is not necessarily true that at this point the bubble detaches from the capillary. It is possible that this mechanism occurs several times before the situation arises where the bubble is detached from the capillary (figure 4.13(e)). The reason for bubble detachment could be that (1) the surface tension is lowered considerably at the back of the bubble decreasing the attachment force and (2) the rupture of the 'skin' and the subsequent rapid compression can give rise to a mechanical instability leading to detachment of the bubble from the solid surface.

From previous investigations, it is known that these kind of surface layers can be formed at interfaces stabilised by proteins, after a cycle of expansion and compression (D'Arrigo, 1984; Yount, 1979). Previous work was carried out to observe the mobility of the surface of egg white solutions in a flowing channel (Prins *et al.*, 1996), where the surface was found to more or less immobile at shear stresses of about 0.001 N/m^2 which do not surpass those found here. Surface layers were also found to occur in the overflowing cylinder with β casein solutions (Prins *et al.*, 1996). Further evidence from Prins and co-workers show that there is a transition in the relative expansion rate of surfaces of β casein and bovine serum albumin (BSA) solutions, from a more or less immobile surface to a more mobile surface as the shear rate of the surface is increased. This suggests that there is a shear rate, stress or force at which the surface layer yields.

It should be noted that this hypothesis is very speculative and no hard evidence is available at the moment to confirm it. An estimation of the surface tension at which the bubbles detach (using equation (4.1)) tells us that the surface tension should indeed in some cases be very low ($\sim 1\text{mN/m}$). The shear stress at which the surface yields can be calculated using equation (4.14). Interestingly, in every case measured, the surface is found to become mobile at a shear stress of roughly 0.01 N/m^2 . It is therefore our belief that this yield value depends on the type of adsorbed molecules and the cohesion that exists between them and which also depends on the shear rate imparted on the layer.

A good check of this model would be the measurement of the detachment behaviour of bubbles in a pure liquid, where the absence of surface active components will prevent the formation of a surface tension gradient. If our hypothesis holds, the bubbles growing on an oscillating capillary in a pure liquid will detach at a later stage than found here, as a result of the resultant forces only. Unfortunately, this experiment could not be carried out here due to the limited time available.

However, if the break-up mechanism described above holds, there could be implications for other fields of research such as in the break-up of emulsion droplets where similar surface active components are used.

4.5 Conclusions

The size of bubbles detaching from a solid surface can be decreased by increasing the tilting angle and also by increasing the frequency and the amplitude of an applied oscillatory motion. When applying a tilting angle, the volume of the bubble at detachment decreases with decreasing radius of capillary with a scaling factor which depends on the apparent contact angle as well as on the angle of inclination. As the inclination angle varies from 90° to 0° with the horizontal plane, the apparent contact angle is estimated to decrease slightly from 90° to circa 75°.

The decrease found in the bubble size at detachment when the capillary is oscillated cannot be explained alone by the buoyant, inertial or shear forces which act on the bubble as a result of the density difference between gas and liquid and of the applied movement. A qualitative explanation is presented, which accounts for the effect of the shear force on the rigid interface of the bubble. A hypothesis is presented where the bubble is surrounded by a macromolecular surface layer, or 'skin' which ruptures when the shear force is larger than the cohesive intra-molecular forces. After surface rupture, the surface tension can decrease considerably locally and the bubble is easier to detach. Furthermore it is possible that the sudden compression of the surface layer may destabilise the bubble, resulting in an earlier detachment. An interesting phenomenon is that the magnitude of the amplitude of the motion relative to the bubble size plays an important role in the surface rupture. If this is low then no surface rupture occurs, whereas the likelihood for surface rupture increases with increasing amplitude.

It seems clear then, that the mechanism of bubble detachment when the capillary is tilted is not comparable to the situation where the capillary is oscillated (at least when surface active components are present), although both effects result in the decrease of the bubble at detachment. Both methods can be effective in the formation of a foam with a population of very fine bubbles, although with the oscillation method the bubble can be varied over a larger range of sizes.

References

D'Arrigo, J.S. (1984) Surface Properties of Microbubble-Surfactant Monolayers at the Air/Water Interface *J. Colloid Interface Sci.* **100** (1), 106-111.

Bisperink, C.G.J. and Prins, A. (1994) Bubble growth in carbonated liquids *Colloids and Surfaces A: Physicochemical and Engineering Aspects* **85**, 237-253.

Cho, S.C. and Lee, W.K. (1990) A model for steam bubble formation at a submerged orifice in a flowing liquid *Journal of Chemical Engineering of Japan* **23**, 180-185.

Dussan V., E.B. and Tao-Ping Chow, R. (1983) On the ability of drops and bubbles to stick to non-horizontal surfaces of solids *J. Fluid Mech.* **137**, 1-29.

Goldman, A.J., Cox, R.G. and Brenner, H. (1967) Slow viscous motion of a sphere parallel to a plane wall - Motion through a quiescent liquid *Chem. Eng. Sci.* **22**, 637-651.

Lin, J.N., Banerji, S.K. and Yasuda, H. (1994) Role of Interfacial Tensions in the Formation and the Detachment of Air Bubbles. 1. A Single Hole in a Horizontal Plane Immersed in Water *Langmuir* **10**, 936-942.

Lin, J.N., Banerji, S.K. and Yasuda, H. (1994) Role of Interfacial Tensions in the Formation and the Detachment of Air Bubbles. 2. A Single Orifice on an Inclined Plane Immersed in Water *Langmuir* **10**, 943-948.

Mahé, M., Vignes-Adler, M., Rousseau, A., Jacquin, C.G. and Adler, P.M. (1988) Adhesion of Droplets on a Solid Wall and Detachment by a Shear Flow I. Pure Systems *J. Colloid Interface Sci.* **126**, 314-328.

Milne-Thompson, L.M. (1968) *Theoretical Hydrodynamics*, Macmillan, London.

Minnaert, M. (1933) On Musical Air-Bubbles and the Sounds of Running Water *Phil. Mag.* **16**, 235-248.

Prins, A., Jochems, A.M.P., van Kalsbeek, H.K.A.I., Boerboom, F.J.G., Wijnen, M.E. and Williams, A. (1996) Skin formation on liquid surfaces under non-equilibrium conditions, *Progr. Colloid Polym. Sci.* **100**, 321-327.

Ronteltap, A.D. (1989) Beer Foam Physics, Ph.D. Thesis, Wageningen Agricultural University, The Netherlands.

Sullivan, S.L., Hardy, B.W. and Holland, C.D. (1964) Formation of Air Bubbles at Orifices Submerged Beneath Liquids *A.I.Ch.E. J.* **10** (6), 848-854.

Yount, D.E. (1979) Skins of varying permeability: A stabilization mechanism for gas cavitation nuclei *The Journal of the Acoustical Society of America* **65** (6), 1429-1449.

BUBBLE RISE

5.1 Introduction

In previous chapters, we observed the growth of gas bubbles whilst being attached to a capillary. After detachment, the bubbles rise to the foam layer between the liquid and the gas phases. During the time in which the bubbles rise, they have ample opportunity to continue to grow, increasing in size and therefore increasing in rise velocity, in mass transport and so forth.

This effect is difficult to observe visually as the bubbles rise with relatively high velocities. For this reason, a high speed camera is used to record the rise of bubbles in various liquids, as well as the bubble size before and after rise. The rise of these bubbles is observed when the liquid is in equilibrium with the gas in the bubble, and when the liquid is supersaturated with that gas. In the experiments, the rise of bubbles was observed in 6 systems: three levels of carbon dioxide gas in beer and in a buffer solution. Beer is known to contain a multitude of surface active materials which may affect the surface reology of the bubble, and therefore influence the rise velocity and the mass transfer to the bubble. Comparison was therefore made with rise of bubbles in water, buffered with acetic acid to the same pH as beer.

5.2 Theoretical

The theoretical section first deals with the rise velocity of bubbles of constant volume, which depends on a) difference in density and viscosity of the two phases, b) volume of the bubble and c) surface properties, and for large bubble sizes d) the shape of the bubble. When a) and b) are constant at constant T and P, both the surface properties and the shape of the bubble can influence the drag or the friction force exerted on the bubble interface and also the motion of the liquid surrounding the moving bubble. As described by Archimedes' law (see also section 3.2.1), the size and density difference of the bubble determines the buoyancy force, and the interface and the liquid surrounding it determines the bubble's resistance to the movement. In the steady state, the buoyancy force is opposite and equal to the resistance to the movement.

The second part of the theory goes on to describe the effect of the increase of bubble size on the rise velocity. The growth velocity of the bubble is dependent of the mass transfer coefficient of the gas transport from the liquid to the bubble, which in turn may depend on the rise velocity and on the dynamic surface properties.

5.2.1 Terminal velocity of a gas bubble rising freely in a liquid

Drag forces on a sphere

The stationary rate of rise of a bubble is calculated by assuming its apparent weight to be equal to the resistance force, the former being nothing more than :

$$\frac{4}{3}\pi R^3 \Delta \rho g \quad (5.1)$$

where R is the radius of the bubble (m), $\Delta \rho$ is the difference in density between gas and liquid phases (kg/m^3) and g is the force of gravitation (m/s^2). The resistance force depends on the flow of the liquid around the bubble. The flow around a single sphere, or around a gas bubble with a rigid or immobile interface, is influenced by the dimensionless Reynolds number, Re , defined as :

$$Re = \frac{2Rv_b \rho}{\eta} \quad (5.2)$$

where v_b is the bubble rise velocity (m/s), ρ is the density of the liquid (kg/m^3) and η is the dynamic viscosity of the fluid (Pa.s). With the Reynolds number, a value can be found for the drag coefficient C_w from the standard drag curve for rigid spheres (figure 5.1) and the resistance drag force F can be calculated:

$$F = \frac{1}{2} C_w \pi R^2 \rho v_b^2 \quad (5.3)$$

where C_w is the drag coefficient (-).

At highly viscous flow, $Re < 1$, no inertial effects occur and the streamlines of the liquid converge behind the sphere or bubble (Beek and Mutzall, 1975). For this case, the drag force can be calculated from $C_w = 24 / Re$, and becomes Stokes' law:

$$F = 6 \pi \eta R v_b \quad (5.4)$$

At higher values of Re ($Re > 20$, Clift *et al.*, 1978) both the friction resistance and the geometric resistance play a role in the drag force as eddy's start to appear at the rear end of the bubble. At even higher Re numbers, $10^3 < Re < 10^5$, also known as the Newton Regime, C_w becomes a constant 0.44.

At intermediate ranges, $1 < Re < 10^3$, which is most often encountered, only a numerical solution is possible. The force balance is found empirically (Beek and Mutzall, 1975; Perry, 1963) and is written in the following two dimensionless forms:

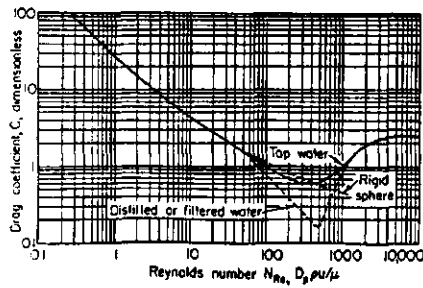


Figure 5.1 The drag coefficient for air bubbles rising in water at room temperature (Perry, 1963)

$$C_w \cdot Re^2 = 32/3 \cdot \frac{R^3 \rho \Delta \rho g}{\eta^2} \quad (5.5)$$

or :

$$\frac{C_w}{Re} = \frac{4g\eta\Delta\rho}{3\rho^2 v_b^3} \quad (5.6)$$

In this range of Re numbers, C_w can also be approximated as:

$$C_w = \frac{24}{Re} (1 + 0.14 Re^{0.7}) \quad (5.7)$$

If the bubble rise velocity or the bubble radius is known, $C_w Re^2$ or C_w/Re can be calculated and from numerical tables (Perry, 1963), the relevant Reynolds number can be found, through which the radius or the velocity can be calculated as well as the drag coefficient. The stationary velocity can be calculated, equating the apparent weight (equation (5.1)) to the resistive force (equation (5.3)), and inserting C_w from equation (5.6), so that it becomes:

$$v_b = \frac{\eta \cdot Re}{2 \rho \cdot R} \quad (5.8)$$

which is the same equation as equation (5.2). These equations are based on the assumption that the bubble has a spherical shape and a rigid interface.

Deviation from spherical shape

According to Perry (1963), a gas bubble can remain spherical until $Re = 1-100$. At higher Re numbers, the bubble is so large that it can be easily deformed and it can assume a flattened shape normal to the direction of the flow, which is accompanied by an increase in drag.

Eddies start to appear in the converging streamline at $Re > 20$, which also decrease the rise velocity. Motion of such deformed bubbles is generally unstable and subject to oscillations. Speaking in terms of bubble sizes, this generally means that gas bubbles with $d < 0.8$ mm are spherical (Beek and Mutzall, 1975). In a liquid of higher surface tension, bubbles can remain spherical up till larger sizes, due to the relatively higher Laplace pressure inside that bubble.

Although not clearly described in literature, the shape that a fluid bubble takes also depends on the surface rigidity of the surface. When surface active material is present in the liquid, it can adsorb to the surface and at least partly immobilise the surface. Some surfactants can even completely immobilise the surface. The rigidity of the surface can, up to a certain point, retain the spherical shape of the bubble to a larger bubble size than found in pure liquids. Edge and Grant (1972) showed that the bubble size at which oscillations start to occur (a sign that the bubble is no longer spherical) becomes larger as the surfactant concentration in the liquid is increased.

Mobility of the gas-liquid interface

Rigidity can be defined in two ways: resistance against deformation of spherical shape, which acts perpendicular to the bubble surface, and resistance against shear, which acts parallel to the surface. Due to a lower surface tension in a solution of surface active material, the formed bubbles are smaller (see chapter 3) and this increases the Laplace pressure difference which can help the bubble to resist against deformation of the spherical shape. A too low surface tension, however, decreases the Laplace pressure difference, resulting in a low resistance against shape deformation.

The presence of surface active material can help to immobilise the bubble surface due to the formation of a surface tension gradient which resists the shear exerted by the liquid passing the bubble interface. This effect can result in stopping internal circulation inside the bubble and giving it a rigidity that makes the bubble behave like a solid sphere. This means that the bubble rise velocity is retarded in comparison to fully mobile surfaces, such as found with pure liquids with no contaminant present. Depending on their size, the bubbles rise according to the drag that resists their upward motion. In practical situations it is almost impossible to work with completely clean and pure liquids (Duineveld, 1994), as a result of which it is expected that the surface of a rising bubble will be partly immobilised at least. It is well established in literature (e.g. Griffith, 1962; Levan and Newman, 1976) that the surface of a bubble can be immobilised by contaminants and surfactants. Bachhuber and Sanford (1974) even showed a dependence of the rise velocity

on the history or "age" of the bubble. Bubbles just released into the "pure" liquid were still relatively free of surfactants and rose as if in a pure liquid. After a certain rising distance the rise velocity was retarded, apparently due to the collection of surface active material onto the bubble surface along the way. This explains the differences found in the rise velocity of bubbles in so-called "pure" water found in literature.

The generally used criterion for predicting the transition from solid sphere to fluid sphere behaviour is given by Beek and Mutzall (1975), where gas bubbles are found to be rigid as long as the buoyancy force is smaller than the shear force acting along the surface as the bubble rises, which can be rewritten as:

$$d < 2 \sqrt{\frac{\gamma}{\Delta \rho g}} \quad (5.9)$$

where d is the critical diameter (m) and γ is the surface tension (N/m). Thus, air bubbles in for example pure water are rigid if $d < 2.6$ mm. At larger diameters the bubble surface becomes mobile and the bubble starts to oscillate during rise. The stationary rate of rise in the direction of the motion is then given by (Beek and Mutzall, 1975):

$$v_b = \sqrt{\frac{\gamma}{\rho R} + \frac{\Delta \rho g R}{\rho}} \quad (5.10)$$

For systems with known surface properties (see chapter 4), a surface velocity can be estimated for known radius and shape. With this surface velocity the retardation of rise velocity of the spherical bubble can be calculated with known values of C_w and Re .

Levich (1962) was the first to provide a satisfactory explanation of the retardation of the velocity of a rising bubble caused by surface-active solutes in the medium. He postulated that adsorbed surfactant is not uniformly distributed on the surface of a moving bubble. The surface concentration on the upper part of the bubble is lower than the equilibrium surface load, while that on the lower part is greater than equilibrium. This disequilibrium of the concentrations is brought about by the viscous drag of the liquid acting on the surface, which in turn creates a surface tension gradient across the vertical length of the bubble. The interface then tries to flow (Marangoni flow) from the region of lower tension to that of higher tension, effectively decreasing the surface mobility; when the surface mobility is completely inhibited, the terminal velocity of rise is reduced to that given by equation (5.8).

Boussinesq (1913) offered the explanation that the surface dilatational viscosity of the interface is enhanced by the presence of surface-active material in the liquid, which seems to be in agreement with Levich's theory, as long as the definition of a high surface viscosity is that, with a given gradient in surface tension $\Delta\gamma$, the relative surface

deformation is very small, meaning that the surface is nearly immobile, or in different words, rigid (see also section 2.5 and equation 5.29).

In literature there are systems found where the terminal velocity was reduced, yielding a drag coefficient C_w nearly equal to that of a solid particle. Kok (1989) found that upon addition of a nonionic surfactant at low concentration, a slight decrease in terminal velocity was found, whereas addition of a hundred-fold concentration contaminant resulted in the rise velocity for a solid sphere of equal volume. Another result which he found was that, at higher surfactant concentration, bubbles do not coalesce upon collision but "bounce", which gives an indication of the rigidity of the surface.

5.2.2 Bubble growth during rise

Mass transfer coefficient

So far, we have elucidated the terminal rise velocity of bubbles of constant volume. In our case, however, we are interested in the rise velocities of bubbles that are increasing in size. For the moment we are assuming that the bubbles are spherical, have a rigid surface and reach terminal velocity momentaneously, as described by the standard drag curve for rigid spheres. Accordingly, the velocity will increase proportionally to the bubble growth.

In order to be able to describe this bubble growth, the mass transfer of the gas from the dissolved state in the liquid to the gaseous state in the bubble must be known.

Using the equation for the conservation of mass, we find:

$$\Phi = \text{gas}_{in} - \text{gas}_{out} = \frac{\rho_g}{MA} \frac{dV}{dt} = K_L \Delta c \quad (5.11)$$

Where $\text{gas}_{out} = 0$, Φ is the molar flux in mol/m²s, M is the molar mass of the gas (kg/mol), A is the surface area through which transport takes place, dV/dt is the increase in bubble volume as a result of the mass transport, Δc is the concentration gradient which exists between liquid bulk and bubble surface and K_L is the mass transfer coefficient (m/s), in which all mass transfer phenomena are included (van 't Riet and Tramper, 1991).

Equation (5.11) can be rewritten as:

$$K_L \Delta c = \frac{\rho_g}{M} \frac{dR}{dt} \quad (5.12)$$

or:

$$\frac{dR}{dt} = \frac{K_L M \Delta c}{\rho_g} \quad (5.13)$$

The concentration difference Δc (see also figure 3.5) is taken to be linear and can be described by:

$$\Delta c = C_{bulk} - C_{surface} = C_{bulk} - \frac{1000}{M_{H_2O}} \left(\frac{P_b}{H} \right) \quad (5.14)$$

where C_{bulk} is the gas concentration in the liquid, $C_{surface}$ is the surface concentration of the gas, P_b is the bubble pressure, H is Henry's constant in Pa (Janssen and Warmoeskerken, 1987) and M_{H_2O} is the molar mass of water (kg/mol).

In order to get an indication of the growth velocity of the bubble, a value for the mass transfer coefficient is needed. Van 't Riet and Tramper (1991) give various empirical relationships for K_L which vary in their dependence on the diffusion coefficient, the radius of the bubble and on the velocity of the rising bubble, which accounts for the renewal of liquid near the bubble surface. Furthermore, many different relations have been found for the Sherwood number, which is the dimensionless ratio of mass transfer to diffusive mass transfer, and which can be used to calculate K_L (equations (5.11 and 5.21)).

1) Lewis and Whitman (1924) described mass transport as a diffusion process, neglected the convective term across a boundary layer δ , assuming a linear concentration profile:

$$K_L = \frac{ID}{\delta} \quad (5.15)$$

where δ is found to be around 10^{-5} m for oxygen bubbles with a radius of 1 mm, as determined experimentally by measuring K_L and ID .

2) Higbie (1935) developed the penetration film theory, valid for bubbles with a "moving and renewing" interface, where the influence of the bubble velocity is high. With an equation for the penetration into an infinite medium K_L after exposure time t can be described by:

$$K_L = \sqrt{\frac{ID}{\pi t}} \quad (5.16)$$

The exposure time t can be approximated as the bubble diameter divided by the velocity ($\approx d/v$), which, results in:

$$K_L = \sqrt{\frac{IDv_b}{2\pi R}} \quad (5.17)$$

3) A completely rigid interface with no convective transport can be described by :

$$K_L = \frac{ID}{R} \quad (5.18)$$

However, this situation is probably not valid here as there is always convection present in the case of a rising bubble.

4) For intermediate regions of surface rigidity and convective transport, Calderbank and Moo-Young (1961) have found an empirical relation:

$$K_L = \frac{ID}{2R} \left[2 + 0.31 \left(\frac{d^3 \Delta \rho g}{\eta ID} \right)^{0.33} \right] \quad (5.19)$$

Experiments (van 't Riet and Tramper, 1991) show that bubbles with diameter smaller than 1 mm follow the experimental relationship for intermediate rigid surface and convection in equation (5.19) (due to surface tension gradients) and bubbles with diameter larger than 3 mm follow Higbie's theory for freely moving interface (equation (5.17)). In the intermediate range of bubble sizes, a large scatter is found, which is the region where the surface can be either rigid or mobile depending on the liquid and surface properties.

5) A different approach from Griffith (1962) gives for bubbles with a rigid interface for $10 < Re < 10^4$:

$$Sh = 2 + 0.66 Re^{1/2} Sc^{1/4} \quad (5.20)$$

where :

$$Sc = \frac{Pe'}{Re} = \frac{\eta}{ID \rho_l} \quad \text{and} \quad Sh = \frac{\Phi \cdot 2 R M}{\rho_g ID} = \frac{K_L \Delta c \cdot 2 R M}{\rho_g ID} \quad (5.21)$$

6) For a bubble with internal circulation or with a mobile interface (Janssen and Warmoeskerken, 1987):

$$Sh = 5.52 \left[\frac{\eta}{2\eta} \right]^{3.47} \left[\frac{2R\gamma \rho_l}{\eta^2} \right]^{0.056} (Re Sc)^{1/2} \quad (5.22)$$

7) Calderbank and Lochiel (1964) found for a circulating sphere, with intermediate Reynolds numbers, and Péclet > 1:

$$Sh = 1.13 (1 - 2.90 Re^{-1/2})^{1/2} (Re Sc)^{1/2} \quad (5.23)$$

8) Boussinesq (1913) found for a circulating sphere and creeping flow:

$$Sh = 1.13 (Re Sc)^{1/2} \quad (5.24)$$

From these mostly theoretically derived equations an estimate can be made of growth factors of bubbles in well-defined systems. With this estimate the mobility or immobility of the bubble interface can be judged into 3 main categories: rigid, intermediate or completely mobile.

5.3 Experimental

5.3.1 Materials

Beer solution

A casket of beer at 20°C was used for all beer measurements. The CO₂ content was measured to be 4.6 to 4.7 g/kg with an Orbisphere cell, which is equivalent to 0.13 mol/l CO₂ in beer. The surface tension was 34 mN/m and the pH 4.7. The CO₂ concentrations of the beer solutions used are given in Table 5.1.

Buffer solutions

In order to compare with a water system, a gas supersaturated buffer solution was also used: Two solutions were first made and mixed together under pressure before the bubble rise measurements.

Solution A: 10 liters acetic acid solution (100%, Merck) at 2 mol/l, pH measured at 3.9.
 Solution B: 10 liters of 0.26 M Na₂CO₃ (anhydrous, Merck).

Mixing together a liter of solution A and a liter of solution B gives a 4.7 g/kg or a 0.13 mol/l solution of CO₂ in 1M acetic acid buffer, the pH varying between 4.4 and 4.5

Table 5.1 Systems used in the measurement of the rise velocity of bubbles.

system	code	Saturation pressure	CO ₂ Concentration	Temperature	Excess CO ₂ concentration
beer	b1	1 atm	1.4 g/kg	20°C	0 g/kg (1.4-1.4)
	b2	2.7 atm	4.7 g/kg	10°C	3.3 g/kg (4.7-1.4)
	b3	2.7 atm	4.7 g/kg	20°C	2.5 g/kg (4.7-2.2)
buffer	w1	1 atm	1.4 g/kg	20°C	0 g/kg (1.4-1.4)
	w2	2.6 atm	4.7 g/kg	10°C	3.3 g/kg (4.7-1.4)
	w3	2.6 atm	4.7 g/kg	20°C	2.5 g/kg (4.7-2.2)

after the measurement of bubble rise (see section 5.3.2). The surface tension was found to vary between 52 and 64 mN/m after the measurements of bubble rise, probably as a result of contamination from the buffer salts used. The concentrations of the buffer solutions used are given in Table 5.1.

5.3.2 Methods

Measurements

The bubble size, growth and rise velocity of bubbles were measured in two systems, beer and buffer. For both systems the measurements were performed at the saturation level of CO₂ at 20°C and 1 atm (b1 and w1), and at the supersaturation level of CO₂ in water and beer, at 2.7 atm and 20 °C. By measuring at 10°C as well as at 20°C, two different excess concentrations were created, b2 and b3 for beer and w2 and w3 for buffer (see table 5.1).

Experimental set-up

The experimental setup is shown in figure 5.2. The experiments were performed in a glass tank which could be pressurised up to 3 bar. The glass tank is cylindrical and is set in a thermostated plexi-glass container which has a flat glass port hole for recording of the images. Carbon dioxide bubbles are produced from a glass silicon-coated capillary (I.D. 0.16 mm) which is held horizontally ($\phi = 0^\circ$, see chapter 4) in order to produce small bubbles. In this chapter the bubbles are produced by feeding gas from a gas cylinder through the orifice into the liquid. In order to produce bubbles of constant size and at constant pressure, the gas is reduced to a low pressure, passed through a mass flow control cell (Brooks), and then split into two flows: a water manostat and the measuring container. Between the measuring container and the splitter, the pressure is measured. By setting the mass flow controller, the capillary can produce a constant stream of bubbles independent of

the pressure in the measuring vessel. With the manostat, small variations in pressure can be achieved, so that the bubble frequency is can be controlled and kept more or less constant.

The beer was transferred under slight over-pressure (3.1 bar) into the measuring vessel (3 bar). It was found that the bubble formation should not be interrupted at any time in order to keep the inside of the capillary dry. If beer flows back into the capillary it takes a very long time before bubble formation stabilises again. The mass flow was therefore kept at a high level during the pressurised filling of the container. During equilibration (at least 6 hours) the bubble flow was kept at a low rate while the pressure in the vessel was kept constant (atmospheric pressure for the saturation level and 2.3 bar for the supersaturation level of the gas, $T = 20^\circ\text{C}$), in order to have the same starting conditions in all measurements.

The buffer solutions were mixed at atmospheric conditions, and the pressure was set after filling the measuring vessel. Again the system was equilibrated over at least 6

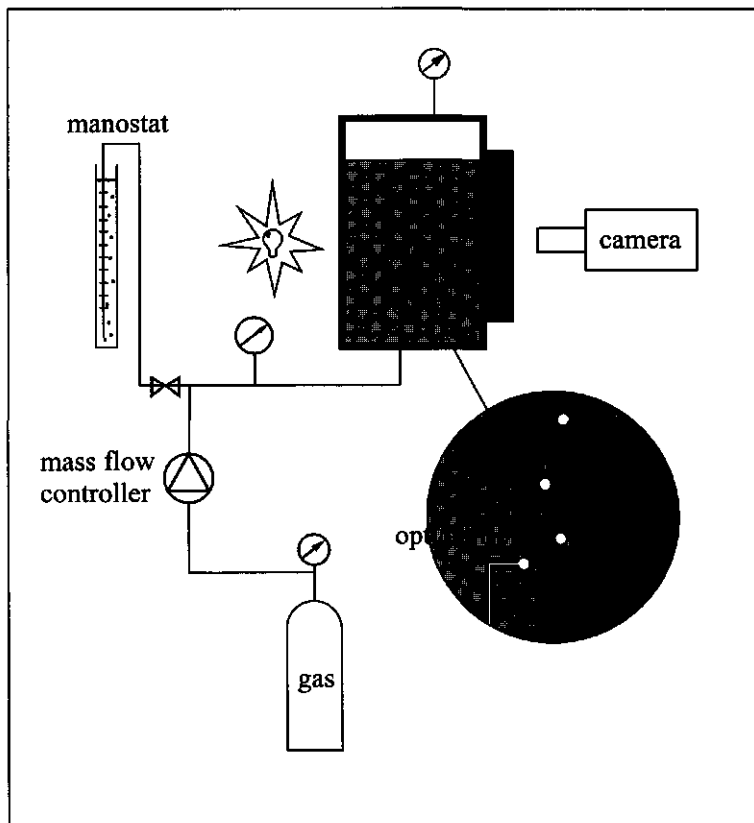


Figure 5.2 Schematic presentation of the experimental set-up.

hours in the same manner as described above. The temperature in the measuring vessel was set at 10°C or 20°C ($\pm 0.5^\circ\text{C}$) with a Haake thermostated water bath. Before measurement the pressure was reduced to atmospheric pressure, and the flow rate set as described with the following settings: the pressure from the cylinder was reduced to 1.6 bar absolute, the mass flow control was set at the lowest setting while still keeping a constant flow of bubbles, and the manometer height was set so that pressure before measuring vessel was 0.05 bar. The manometer was filled to about 40 cm with a soap solution. With the soap, the escaping bubbles in the manometer are smaller (due to the lower surface tension) and the pressure release is controlled in a more subtle manner than if ordinary water was used.

With this set-up, the carbon dioxide bubbles that were produced at the tip of the capillary in the measuring vessel were formed with time intervals of 0.2 to 0.8 seconds. It was found that the interval time between bubbles also influenced the rise velocity of the bubbles, as will be shown in section 5.4.

The bubbles were able to rise over at least 10 cm of liquid. In order to calibrate the height of rise and the size of the bubbles a glass scale of 100 mm was hung besides the capillary orifice.

High speed video measurements

The measurements were performed with a high speed video recorder (Speedcam+, Weinberger, Switzerland, hired from Reinka b.v. in Ettenleur). The CCD camera was equipped with a Nikon C-mount and accessories, and an LCD shutter to increase the resolution of the images. The extension rings between the macroscopic lens and the camera was set between 0.5 and 1 cm for the measurements of bubble rise and for the measurement of bubble size we used a distance of about 4 cm. Back-lighting was performed through a diffusing panel. With the Speedcam+ system 250 to 500 frames per second could be recorded, with the shutter set at 1000 s^{-1} for the velocity measurements and at 5000 s^{-1} for the size measurements during rise.

In this system up to two seconds of motion could be recorded (ample time for the bubbles to rise 10 cm), after which the desired images were saved as bld files. The images (bld) were then converted first to tiff files (Histotif, Weinberger, Switzerland), and then to im files (Image) as the image analysis was performed by a Magiscan (Joyce Loebl) program.

The rise of the bubbles was measured from detachment up to a height of 10 cm. The size of the bubbles were determined at detachment and after rising, at a height of 10 cm. It was not possible to measure the size of the bubbles during rise as the resolution of these images was not high enough.

5.3.3 Theoretical calculations

With the mass transfer coefficients given in paragraph 5.2.2, the increase in bubble size was calculated and compared to the bubble growth as measured and deduced from the measured velocities of the bubbles in beer and in buffer.

Some conclusions could be made concerning the surface velocity of the bubbles rising both in beer and in buffer.

With a set initial radius, the dR/dt was calculated for the mass transfer coefficients given in section 5.2.2, for beer and buffer. These were then compared with the measured values of bubble growth in buffer and in beer.

5.4 Results & Discussion

From the experimental work, we found the values of rising bubbles in the six defined systems. Some calculations were carried out to evaluate the behaviour of the bubble surfaces, in buffer and in beer, as well as the impact of this behaviour on the growth of the rising bubbles in the supersaturated solutions.

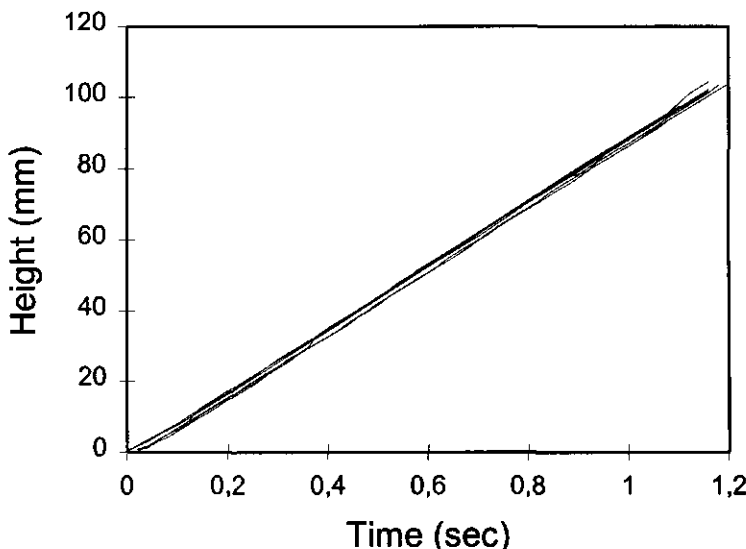


Figure 5.3 The rise of ten individual bubbles in saturated beer solution.

5.4.1 Terminal velocity of bubbles in beer and buffer

In order to measure the terminal rise velocity of the bubbles in saturated beer and buffer, it was necessary to ensure that the bubbles did not grow or shrink. This was realised by standing the liquids with constant bubble flow overnight. In this way, the liquids were given the time to equilibrate to a constant homogeneous mixture of CO₂ and liquid. Figure 5.3 shows the rise of ten individual bubbles in beer, from two different beer samples, saturated with carbon dioxide at room temperature. As can be seen the reproducibility of these measurements is very good, and a linear rise velocity can be easily calculated. The same reproducibility is seen in the buffer solution. The next section will show those results as well as the growth of bubbles as they rise in the supersaturated solutions.

A curious effect which was found was that the frequency of bubbles formed at the orifice could influence the rise velocity. Figure 5.4 shows the effect of the interval time between bubbles detaching from the orifice on the rise velocity.

In the cases where the bubbles do not grow very fast during bubble rise, as is the case in the saturated systems b1 and w1, a shorter interval time (a higher frequency) increases the rise velocity of the bubbles slightly. This is probably due to the lower drag resistance and the upward liquid movement as more bubbles rise in the same path. If the frequency is

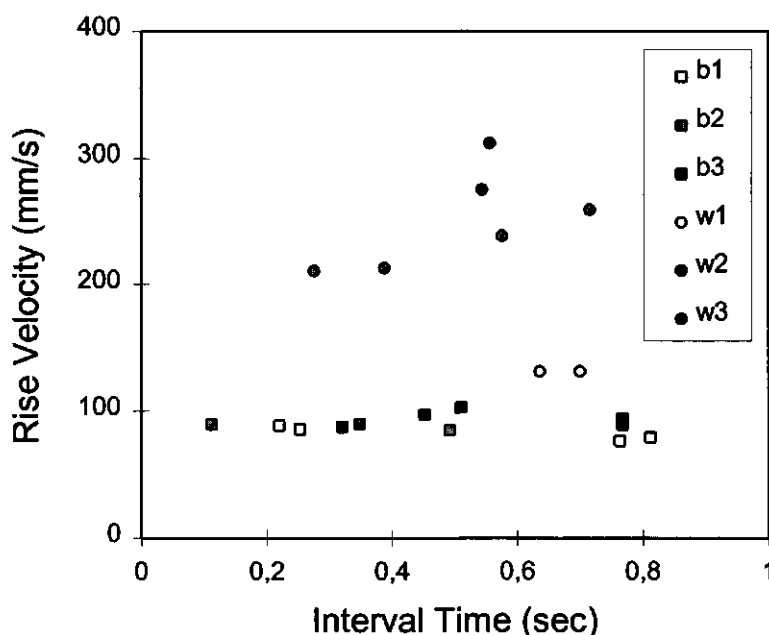


Figure 5.4 The rise velocity of bubbles in the different systems as a function of the interval time between bubble detachment.

reduced or interval time increased, the effect can be neglected and the rise velocity is that of an individual bubble. This has been also seen by Coppock and Meiklejohn (1951), who showed that successive water bubbles induce a higher rise velocity.

In the cases where the bubbles grow considerably during bubble rise, as seen for **w2** and **w3**, a short interval time (high frequency) slows the bubble down. It seems that in this case the mass transport to the bubble is reduced in some way. If the bubbles follow each other quickly, the liquid they pass through will be partly depleted of gas; the growth of the bubbles will be slower and therefore the rise velocity will be reduced compared to the individual rise of a bubble.

Due to these, albeit relatively small, variations in rise velocity, only the data of bubbles with interval time between 0.4 and 0.6 seconds were used in further calculations. The difference seen in figure 5.4 between the bubbles rising in the beer and in the buffer solutions is due to the a small difference in bubble size at detachment, which is a result of the difference in surface tension and contact angle (see section 3.2.1 or and 4.2.2), and due to the different growth velocities of the bubbles in the supersaturated beer and buffer solution.

5.4.2 Rising bubbles in supersaturated beer and buffer solutions

Figure 5.5 shows the rise of bubbles in saturated beer (**b1**), in supersaturated beer at 10°C (**b2**) and at 20°C (**b3**), as well as in saturated buffer solution (**w1**), and in supersaturated buffer solution at 10°C and at 20°C (**w2** and **w3**). The curves in the figure are averages of six data sets from two separate liquid batches. Interestingly, the velocity of the bubbles in the saturated buffer solution **w1** is decreasing with time, whereas all the other curves show a stable or increasing bubble size. Table 5.2 shows the bubble sizes directly measured at height 0 and at height 10 cm, averaged from three measured values, for each experiment. The bubble size in the saturated buffer solution **w1** is indeed found to be smaller after 10 cm of bubble rise, confirming the curve found in figure 5.5. Why this has happened is not known. It is not due to accumulation of contaminants, as that would decrease the pressure in the bubble, and increase the volume. It is also not due to the pressure change during rise of the bubble, as when the bubble rises, the surrounding pressure decreases and therefore the volume of the bubble increases. Finding this reproduced in two different liquid samples, after having equilibrated overnight suggests that something fundamental is happening. One possibility is that the pressure has been building up unnoticed, thereby decreasing the supersaturation, and so making the bubble shrink during rise.

The other curves in figure 5.5 show that the bubbles in beer do not grow so much as the supersaturation is increased, whereas in the case of the buffer solution, the bubble size increases considerably during bubble rise. This is confirmed with the measured size of the

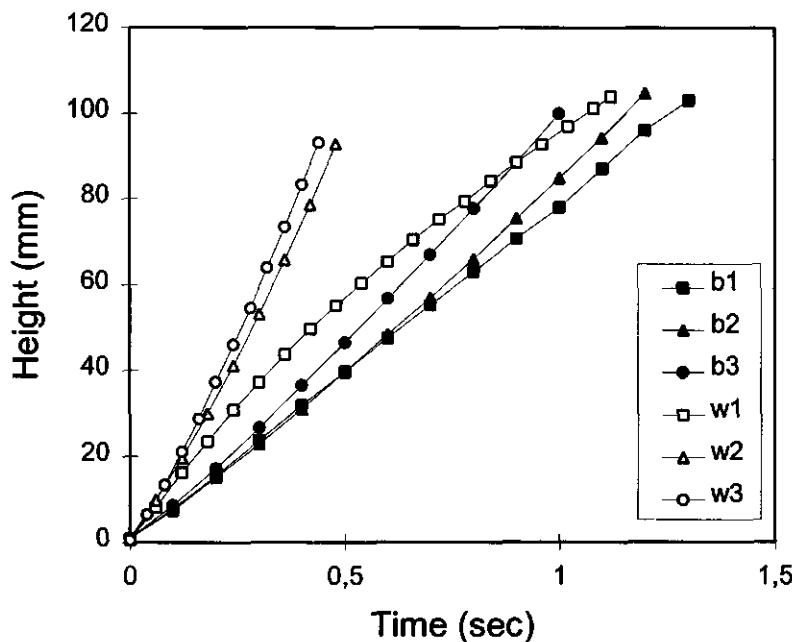


Figure 5.5 The rise of bubbles in the six systems of beer (b1, b2 and b3) and buffer solutions (w1, w2 and w3)

bubbles shown in table 5.2. The inaccuracy of the measured bubble sizes given in table 5.2 is around 0.01 mm.

The reason for the slower growth of the bubbles in beer can be explained by the lower rise velocity, which results in a lower degree of convective transport. However, the rigidity of the surface or the formation of a surface “skin” could be hampering the gas transport (see section 2.7). We will come to this later, in section 5.4.4.

Besides showing that the bubbles in beer do not grow to any considerable degree, table 5.2 shows that the bubble size at detachment in buffer is only a little larger than in beer, confirming the results found in chapter 4, where tilting the capillary angle to 90° gave a bubble size which is much less dependent of the surface tension, than if the capillary was held in a vertical position.

In figure 5.5, the curves b1 and w1 should be fitted with a linear relationship, since the bubbles should not be growing or shrinking in a saturated solution. Curves b2, b3, w2 and w3, however, are fitted with a polynomial function, since a growth in size is found. The resulting equations of the fitted curves $h(t)$, which is the height as a function of the time, are shown in table 5.3. In the next column in table 5.3, the increase in velocity $v(t)$ with time ($=(\delta h/\delta t)$) is also shown. Naturally, the fitted equation $v(t)$ becomes linear for the

Table 5.2 Size of bubbles in mm directly measured in the different solutions at height 0 cm and at height 10 cm. The conditions of b1, b2, b3, w1, w2 and w3 are given in table 5.1.

	b1	b2	b3	w1	w2	w3
h = 0 cm	0.413	0.413	0.395	0.423	0.435	0.439
h = 10 cm	0.424	-	0.495	0.352	0.640	0.714

travelled distance for all the data. In the third column is the empirically calculated linear fit of $R(t)$, where we used the values measured in table 5.2 and the distance of $h = 10$ cm and the velocities of the bubble to check whether the end values measured were correct.

In figure 5.6 the Stokes relation is found to be $v \sim R^2$. Moreover, the standard drag curve will probably show a relation of around $v \sim R^{1.8}$, showing the velocity does not increase linearly with R . In table 5.3 however, we have assumed here that the radius increases linearly with time, and so does the velocity. We therefore now have assumed that $v \sim R$, which is most probably not quite correct. However, for the sake of simplicity, we will stick to these assumptions.

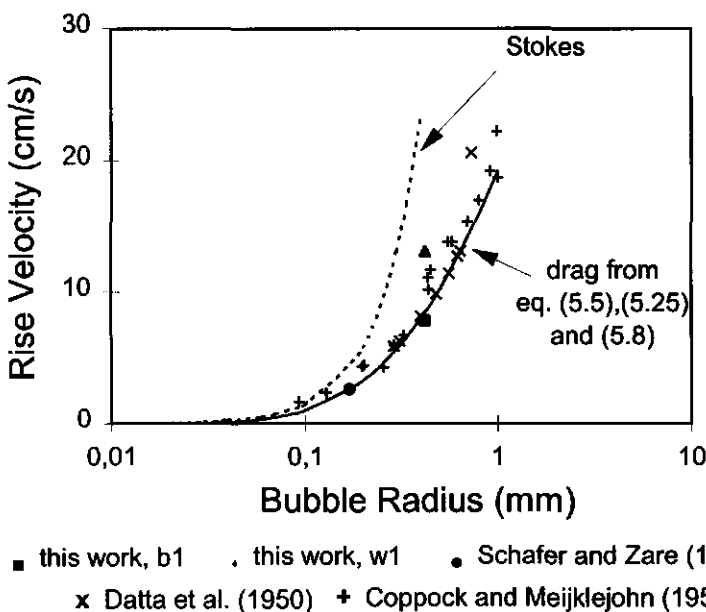


Figure 5.6 The rise velocity of bubbles as a function of the bubble radius. The two curves are theoretical values, the data are experimental values, as described in the legend.

Table 5.3 Fitted equations for the height of rise, the rise velocity and the growth velocity of the bubbles travelling through the different liquids.

	$h(t)$ (mm)	$v(t)$ (mm/s)	$R(t)$ (mm)
b1	$78.99 t$	79.0	$0.100 t + 0.413$
b2	$11.70 t^2 + 73.15 t$	$24.0 t + 73.0$	$0.100 t + 0.413$
b3	$14.80 t^2 + 85.25 t$	$29.6 t + 85.0$	$t + 0.395$
w1	$135.84 t$	136.0	$-0.059 t + 0.423$
w2	$87.40 t^2 + 150.90 t$	$175.0 t + 151.0$	$0.410 t + 0.435$
w3	$118.00 t^2 + 163.50 t$	$222.0 t + 164.0$	$0.550 t + 0.439$

5.4.3 Comparison between the rigid sphere model and experimental results

From the data given in the previous paragraph we can deduce the Reynolds number, and the corresponding theoretical velocity or radius for the rigid sphere model from equations (5.5) or (5.6). If the values fit the measured ones, there is reason to conclude the bubbles have an immobile interface as they rise in the liquid, and the rigid sphere model can be used. However, it is very possible that the bubble interface is partly mobile. In that case, modelling is of no practical use, as the situation at the interface will then be dependent of the history of the surface as well as the shear stresses involved.

Figure 5.6 shows the bubble velocity as a function of the bubble radius. The dotted line shows Stokes law, the full line is calculated from the standard drag curve (figure 5.1) with equations (5.5), (5.25) and (5.8). Inserted are data for water from Datta et al. (1950) and from Coppock and Meiklejohn (1951), as well as data for beer from Schafer and Zare (1991), and our data for **b1** and **w1**. As can be seen the Stokes region is not applicable in our case as the bubbles are too large (and hence the Reynolds number). Our data for **b1** falls on the standard drag curve, suggesting that the bubble in beer behaves like a solid sphere. The bubble in water, however, travels at a faster rate, implying at least part mobility of the surface, as would be expected. The bubbles described by Schafer and Zare (1991) were somewhat smaller in size than the ones measured here, but also followed the rigid sphere model. Interestingly Schafer and Zare found that the bubble showed a considerable increase in bubble size during rise in beer, in comparison to our values. Perhaps they used a type of beer with of lower surface viscosity, which would result in the bubbles having a fluid interface, as opposed to the rigid interface found here. This would explain the fact that their bubbles grow and ours do not.

With the expected radius of the bubble $R(t)$, we can now calculate the dimensionless radius or “Best number” $N_D = C_w Re^2$ according to equation (5.5). With this value the expected Re number can be found from the standard drag curve or from the following approximation for $580 < N_D < 1.55 \cdot 10^7$ and $12 < Re < 6350$ (Clift et al., 1978):

$$\log Re = -1.81391 + 1.34671(\log N_D) - 0.12427(\log N_D)^2 + 0.006344(\log N_D)^3 \quad (5.25)$$

The rise velocity follows from Re and the radius. Figure 5.7 shows the comparison between experiment and theory for the buffer solutions, and figure 5.8 shows the same for the beer. From figure 5.7, it is clear that the predicted velocity from the radius is lower than what was measured. This means that the rigid sphere model does not apply in the case of the buffer solutions, and that therefore it is reasonable to assume that the interface is mobile.

Figure 5.8 shows that the rigid sphere model does apply to the case of the saturated beer solution b1. There is a small difference in bubble radius but that falls within the experimental error. The bubble in solution b2 is found to increase in velocity, but the radius was unfortunately not measured after rise. For b3, however, the experiment gives higher values than the theoretical one, suggesting that at this supersaturation level, the bubble interface is not completely rigid. Perhaps the shear forces from the liquid dragging along the interface have become too large to be completely counteracted with a surface tension gradient.

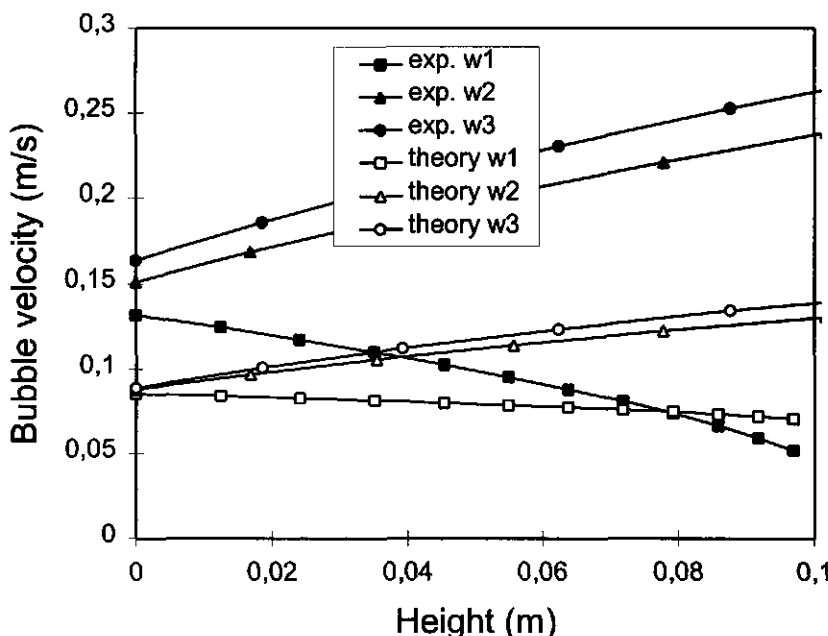


Figure 5.7 The bubble velocity of the bubble in buffer solution as a function of the travelled distance, showing the experimental values as well as those calculated for the rigid sphere model.

A different observation is that the theoretical increase in velocity with the height does not deviate very much from the experimental increase in velocity. The reason for this can be found in the knowledge that the measured radius (experimental) is used to calculate the theoretical velocities. All that is therefore proved with this exercise is that with the measured radii in the buffer systems, we expect a lower velocity if the surface was rigid, and that the measured radii in the beer system fit the measured velocity when we assume that the surface is immobile.

Following Levich's theory, the critical size (for surface rigidity) for bubbles ascending in these beer solution may be roughly calculated using our knowledge of the surface viscosity of the system.

When a bubble rises in a liquid, the surface of the bubble is forced downwards. The rate of downward movement depends on surface properties. Assuming the surface velocity to be equal to the rise velocity of the bubble, v_b , for a freely moving interface, the surface dilation due to the movement of the surface from north pole to equator will be roughly equal to the surface velocity in the direction of the south pole:

$$\frac{dA}{dt} = 2\pi R v_b \quad \text{and} \quad \frac{d\ln A}{dt} = \frac{v_b}{R} \quad (5.26)$$

Error! Not a valid embedded object.

Figure 5.8 The bubble velocity of the bubble in beer as a function of the travelled distance, showing the experimental values as well as those calculated for the rigid sphere model. where A is the area of the bubble surface and $d\ln A/dt$ is the relative deformation rate of the surface.

For systems containing enough surface active material, the shear force F_s acting on half the bubble area along the bubble interface will be counterbalanced by a surface tension gradient over length R , and which can eventually stop surface mobility completely when:

$$\frac{F_s}{A} = \frac{6\pi\eta R v_b}{2\pi R^2} = \frac{\frac{1}{3}\pi R^3 \Delta\gamma g}{2\pi R^2} = \frac{\Delta\gamma}{R} \quad (5.27)$$

where we assume the shear force to be according to Stokes' law, and where $\Delta\gamma$ is the surface tension gradient over length R , so that :

$$\Delta\gamma = 2/3 R^2 \Delta\rho g \quad (5.28)$$

For visco-elastic interfaces, the surface dilational viscosity η_s^d gives the relation between the change in surface tension as a result of the relative surface deformation rate:

$$\eta_s^d = \frac{\Delta\gamma}{d\ln A / dt} \quad (5.29)$$

or

$$\log \eta_s^d = \log \Delta\gamma - \log(d\ln A / dt) \quad (5.30)$$

The surface dilational viscosity is found to be related empirically to $d\ln A / dt$ with a power-law function for various practical systems (Prins, 1976, 1988; Ronteltap, 1989; Kokelaar, 1994):

$$\log \eta_s^d = m \log(d\ln A / dt) + n \quad (5.31)$$

which, with equation (5.30) results in:

$$\log(\Delta\gamma) = (m + 1) \log(d\ln A / dt) + n \quad (5.32)$$

The absolute value of the surface dilational viscosity depends strongly on the value of n . The value of m characterises the "shear thinning" behaviour of the surface. For a large number of practical systems such as beer, coffee, milk, cream and dough suspensions it is found that the value of m is usually a little larger than -1 (e.g. -0.95). This implies strong shear thinning behaviour (Prins, 1990). For more information see section 2.5.

We now make the assumption that the surface may be called rigid when the equator velocity is reduced to less than 0.01 of the bubble rising velocity. With a rigid surface, there is a balance between the shear force and the surface tension gradient balance is valid, therefore equation (5.26) becomes:

$$d\ln A / dt = 1 / 100 \frac{v_b}{R} = 2 / 900 \frac{R \Delta\gamma g}{\eta} \quad (5.33)$$

Inserting this condition into the power-law gives the bubble radius at which the surface can be kept rigid by the balance between the surface tension gradient and the shear stress, for a given m and n .

$$\log R = \frac{(m+1)}{(1-m)} \log\left(\frac{2 \Delta\gamma g}{900 \eta}\right) - \left(\frac{1}{1-m}\right) \log(2/3 \Delta\gamma g) + \frac{n}{1-m} \quad (5.34)$$

For systems with known m and n it is now possible to calculate whether bubbles of a certain size will rise according to the rigid particle mechanism or not.

e.g. For beer, $m = -0.95$ and $n = -1.8$, as calculated for beer, see Appendix III.2. From equation (5.34), we calculate a critical radius of 1.68 mm. With equation (5.9) the

calculated radius where the interface stays rigid is $R < 2$ mm, which is surprisingly close to the critical radius calculated above.

This means that bubbles in beer will stay rigid until the surface viscosity is no longer able to compensate the drag on the surface with a surface tension gradient, or when $d > 3.2$ mm. For contaminated water, the constants m and n will have rather different values, resulting in a smaller critical bubble radius.

In any case, this critical diameter is larger than the bubbles produced in these experiments, which would mean that, according to the above theory, all the bubbles rising in beer should have a rigid interface.

5.4.4 Model calculations for bubble growth during rise

The radii and velocity of the bubbles measured in the solutions **b3** and **w3** were used to calculate the mass transfer coefficients according to equations (5.15)-(5.24) and from this the expected increase in bubble radius from the gas flux was found (equation (5.11)). Table 5.4 shows the calculated linear bubble growth from table 5.3 and the

Table 5.4 *Bubble growth factors according to different mass transfer coefficients valid for different situations of surface mobility and liquid movement, both for beer and buffer solutions.*

equation	region of validity	$dR/dt * 10^4$	$dR/dt * 10^4$
		(m/s) buffer-w3	(m/s) beer-b3
	experiment	5.5	1
1) 5.15	diffusion	9.1	9.1
2) 5.17	fully mobile and renewing interface	17.7	13.4
3) 5.18	rigid interface, no convection	0.2	0.23
4) 5.19	intermediate surface rigidity, convection	4.5	4.5
5) 5.20	rigid interface, convection	1.16	0.9
6) 5.22	intermediate surface rigidity, convection	7.4	5.5
7) 5.23	intermediate surface rigidity, convection	5.2	3.5
8) 5.24	intermediate surface rigidity, convection	6.2	4.7

expected dR/dt at initial growth, when the mass transfer coefficients are used in different regions of validity.

As can be seen in table 5.4, the values found in the buffer solution (with growth) are simulated with the equations valid for intermediate surface rigidity in the presence of convective mass transport. Both equations for fully mobile interface as well as immobile interface give values that are either greater or smaller than the measured growth factor. For the bubbles in beer, however, we find that the measured value is very well matched by the growth factor found in the case of a rigid interface, but with convection.

This confirms the low growth factor seen in the beer bubbles, even at the higher concentrations of carbon dioxide. The bubble interface seems to be too rigid to allow a free transport of gas to take place through the interface. This is confirmed by the findings of various authors. Griffith (1960) along with many others already mentioned that the rate of mass transfer is presumed to decrease as surface active matter is adsorbed from surrounding water. Calderbank and Lochiel (1964) saw a change of the mass transfer coefficient with bubble age in water and with bubble size. Small quantities of surfactant retarded and sometimes eliminated interfacial flow, and thereby reduced mass transfer rates. Meijboom and Vogtländer (1974) have postulated that the mass flux to a bubble covered with surface active material could be less than 40% of the original mass flux to a bubble with a surfactant-free interface. However, they also say that as the viscosity or the bubble size increases, the mass transfer coefficient approaches that of a surfactant free system. In other words, as the bubble size will increase, the bubble interface will become more mobile.

5.5 Conclusions

The results presented in this chapter show that the bubbles detaching from a capillary at inclination angle of 90 degrees are smaller in beer than in buffer solution, as expected and measured in chapter 4. The growth of bubbles in water is considerable, and mass transfer is found to be equivalent to a sphere with intermediate rigidity.

For the bubble sizes encountered in this section, the bubbles were found to rise more or less according to the standard drag curve. The rise velocity for the bubble in water was larger than the rise velocity of a bubble in beer. Presumably this is due to the difference in surface rigidity. The water-bubble interface is probably more mobile than the beer-bubble interface.

The bubbles did not grow to any significant degree during rise in supersaturated beer, which confirms our presumption that the interface is rigid, and that this fact may slow down the growth of the bubble. Whether the reduced mass transfer is due to surface elasticity or due to a mechanical barrier for interfacial diffusion is not known. Bubble growth in water is not reduced at all, as follows from the rise velocity, and the considerable increase in bubble size. We can therefore conclude that the reduction of mass transfer is related to the presence of surface active material at the bubble interface.

5.6 References

Bachhuber, C. and Sanford, C. (1974) The rise of small bubbles in water *J. Appl. Phys.* **45**, 2567-2569.

Beek, W.J. and Mutzall, K.M.K. (eds.) (1975) Transport Phenomena, John Wiley and Sons, London.

Boussinesq, M. J. (1913) Sur l'existence d'une viscosite superficielle, dans la mince couche de transition separant un liquide d'une autre fluide continue *Ann. Chim. Phys.* [8] **29**, 349-357.

Calderbank, P.H. and Lochiel, A.C. (1964) Mass transfer coefficients, velocities and shapes of carbon dioxide bubbles in free rise through distilled water *Chem. Eng. Sci.* **19**, 485-503.

Calderbank, P.H. and Moo-Young, M.B. (1961) The continuous phase heat and mass transfer properties of dispersions *Chem. Eng. Sci.* **16**, 39.

Clift, R., Grace, J.R. and Weber, M.E. (1978) Bubbles, drops and particles, Academic Press, N.Y..

Coppock, P.D. and Meiklejohn, G.T. (1951) The behaviour of gas bubbles in relation to mass transfer *Trans. Instn. Chem. Engrs.* **29**, 75-86.

Datta, R.L., Napier, D.H. and Newitt, D.M. (1950) The properties and behaviour of gas bubbles formed at a circular orifice *Trans. Inst. Chem. Eng.* **28**, 14-26.

Duineveld, P.C. (1994) Bouncing and coalescence of two bubbles in water, Ph.D. Thesis, Twente Technical University, Enschede, The Netherlands.

Edge, R.M. and Grant, C.D. (1972) The motion of drops in water contaminated with a surface active agent *Chem. Eng. Sci.* **27**, 1709-1721.

Griffith, R.M. (1960) Mass transfer from drops and bubbles *Chem. Eng. Sci.* **12**, 198-213.

Griffith, R.M. (1962) The effect of surfactants on the terminal velocity of drops and bubbles. *Chem. Eng. Sci.* **17**, 1057-1070.

Higbie, R. (1935) The rate of adsorption of a pure gas into a still liquid during short periods of exposure *Trans. A.I.Ch.E.* **31**, 365.

Janssen, L.P.B.M. and Warmoeskerken, M.M.C.G. (1987) Transport Phenomena Data Companion, Edward Arnold Delftse Uitgevers Mij, London.

Kok, J.B.W., (1989) Dynamics of gas bubbles moving through liquid, Ph.D. Thesis, Twente Technical University, Enschede, The Netherlands.

Kokelaar, J.J. (1994) Physics of Breadmaking, Ph.D. Thesis, Wageningen Agricultural University, Wageningen, The Netherlands.

Levan, M.D. and Holbrook, J.A. (1989) Motion of a droplet containing surfactant *J. Colloid Int. Sci.* **131**, 242-251.

Levan, M.D. and Newman, J. (1976) The effect of surfactant on the terminal and interfacial velocities of a bubble or drop *A.I.Ch.E. Journal* **22**, 695-701.

Levich, V. (1962) Physico Chemical Hydrodynamics, Prentice-Hall, New York, chapter VIII.

Lewis, W.K. and Whitman, W.G. (1924) Principles of gas adsorption *Ind. Eng. Chem.* **16**, 1215.

Meijboom, F.W. and Vogländler, J.G. (1974) The influence of surface-active agents on the mass transfer from gas bubbles in a liquid II *Chem. Eng. Sci.* **29**, 857-861.

Perry, J.H. (1963) Chemical Engineers' Handbook, 4th ed, Perry, R.H., Chilton, C.H., Kirkpatrick, S.D. (eds), Mc Graw-Hill Book Company, Inc., New York, p5.59-5.69.

Prins, A. (1976) Dynamic Surface Properties and Foaming Behaviour of Aqueous Surfactant Solutions, in *Foams* , Akers, R.J (ed.) Academic Press, London, pp. 51.

Prins, A. (1988) Principles of Foam Stability, in *Advances in Food Emulsions and Foams*, Dickinson, E. and Stainsby, G. (eds), Elsevier Applied Science, pp. 91-122.

Prins, A., (1990) Liquid flow in foams as affected by rheological surface properties: a contribution to a better understanding of the foaming behaviour of liquids, in *Hydrodynamics of dispersed media* , Hulin, J.P., Cazabat, A.M., Guyon, E. and Carmona, F.(eds) Elsevier Science Publishers B.V. , North-Holland, p. 5-15.

Riet, K., Van 't, and Tramper, H. (eds), (1991) Basic Bioreactor Design, Marcel Dekker, Inc, New York, 236-273.

Ronteltap, A.D. (1989) Beer Foam Physics, Ph.D. Thesis, Wageningen Agricultural University, Wageningen, The Netherlands.

Schafer, N.E. and Zare, R.N. (1991) Through a beerglass darkly *Physics Today* **91**, 48-52.

TYVEK: AN IDEAL ACTIVE SURFACE ?

6.1 Introduction

With the knowledge accumulated in the previous chapters, we now aim to find a material on which many bubbles are formed simultaneously and continuously when immersed in a gas-supersaturated liquid. This way, the influences that have been found to affect single bubble formation could be related to the effects found on the formation and stability of foam produced on an active surface (see chapter 7).

We were aiming to find a surface which achieve the production of a reasonable amount of relatively stable foam in a gas-supersaturated solution in a short time (less than 1 minute) constituted of relatively small bubbles ($d = 0.5\text{-}1\text{ mm}$). In figure 6.1 the desired foam properties are related to the corresponding surface properties of the ideal active surface. Apart from these physical properties the material should preferably be easy to handle (cuttable, pliable), light, durable and food-grade, and also not too expensive. Also, an example of an ideal active surface is given in figure 6.1, as well as a practical or non-ideal surface

The active surface we were aiming to find was found mainly by trial and error. The active surface which was eventually used in the foaming experiments (see chapter 7) was a porous spun-bonded fibre material manufactured from polyethylene. The material (Tyvek, Du Pont de Nemours) is essentially hydrophobic, but the external surface is treated with an antistatic coating for printing purposes and is thus wettable. The material holds a large density of active sites, and is easy to cut and fold.

A second material that was used to test our hypothesis was tailored to meet the active surface demands listed in figure 6.1 and for the purpose of comparison is called the model active surface (m.a.s.).

In this chapter, the structure of the Tyvek material was analysed by microscopical means, by BET analysis and by a specially designed wetting method. With this information we try to elucidate the foaming behaviour of the surface. A comparison was made with m.a.s.

Foam properties		Surface properties
bubbles	→	gas in hydrophobic cavities
small bubbles	→	small opening of cavity hydrophilic outer solid surface vertical orientation
narrow bubble size distribution	→	uniform sized cavity openings
large amount of bubbles	→	high density of cavities

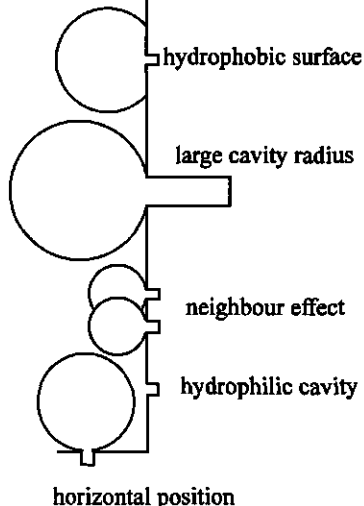
ideal surface		non-ideal surface
		

Figure 6.1 Hypothesis of bubble formation at an active surface from a gas-supersaturated liquid. Relation between surface properties and foaming properties, as well as a sketch of an ideal surface compared to a non-ideal surface.

6.2 Theory

6.2.1 Hypothesis of bubble formation

Gas-supersaturated solutions can foam by inserting an active surface into the liquid. The amount and quality of foam produced depends on certain controllable factors such as the gas concentration, pressure and temperature, but also on the "foam-activeness" of the active surface. At the low carbon dioxide supersaturation level used here (ca 5 g/kg), bubbles can only be formed (without agitation) from surfaces in which gas-filled cavities are present. The gas volume in the cavities grows by diffusional gas transport from the liquid bulk until the gas volume detaches as a bubble from the active surface, rises to the liquid surface and finally forms a part of the foam.

Bubble size and bubble size distribution in a foam formed from an active surface can be partly controlled by the cavity size (see chapter 3) and cavity density on the surface. However, the wetting of the liquid (in this case beer) onto the solid surface can also have a large effect on bubble size at detachment and on the "foam-activeness" of the solid. Increased wetting properties of the liquid onto the solid surface decreases the foam-activeness of individual cavities: if or when (this process is time-dependent) the liquid completely wets the cavity, the gas pocket can be completely expelled or removed, as a result of which bubble formation is deactivated. This means that a non-wetting active surface is preferred for bubble formation. However, if a large contact angle exists between gas and solid surface as is the case for a non-wetting surface, the bubble will grow to a larger size as the contact base spreads beyond the edge of the cavity (see chapter 3). This would result in a larger bubble size than the one formed on a well-wetted surface, as was found by Hey *et al.* (1994) and Lubetkin (1989). The ideal surface should therefore contain hydrophobic cavities situated in a hydrophilic external surface.

In chapter 4 it was shown that the detaching bubble could be decreased in size when inclining the surface to a vertical position or, which is the same, the cavity axis to a horizontal position.

The properties of an ideal active surface, i.e. a surface which stays foam-active for longer periods of time and which produces a reasonably large amount of small equally-sized bubbles over a small period of time, are found in figure 6.1 and summarised as follows. The active surface should have a wettable outer surface, to produce small bubbles; the internal cavity walls situated in the active surface should be non-wettable, to increase the foam-activeness and to ensure that the surface remains active over longer periods of storage; the small equi-sized cavities situated in the active surface should be equally and sufficiently interspaced, to avoid coalescence with neighbouring bubbles before detachment; and the cavities should be positioned horizontally, or the surface vertically, so that both sides of the sheet produce small equally sized bubbles.

6.2.2 Effect of wetting and surface properties on bubble formation

Certain surface properties are important as explained in the former paragraph, when using an active surface to induce bubble formation in a supersaturated liquid. Wetting of the surface is extremely important since the amount of active sites in the surface decreases when the liquid wets the gas-filled voids that are originally available as active sites. Apart from influencing bubble size at detachment (see chapter 3), wetting of the surface can deactivate active sites (Cole, 1974). Hey *et al.* (1994) found an increase in the amount of bubbles formed on a surface with a hydrophobic coating compared to a hydrophilic coating, probably due to the fact that more stable gas nuclei are entrapped at crevices in the surface. Wang and Dhir (1993) found that the fraction of nucleation sites that were active in pool boiling decreased with wettability of the surface. However, Ryan and Hemmingsen (1993) found that with smooth surfaces this difference is less evident, which again can be explained by the fact that there is less chance for gas entrapment in a smooth surface than in a rough surface.

The wetting characteristics of liquids on/in a surface such as Tyvek can be categorised into 3 mechanisms, which not only consist of wetting forces but also of other mechanisms which enable gas to be removed from the voids located inside the material:

- 1) bubble formation, 2) capillary suction and 3) gas entrapment (see also figure 6.2).

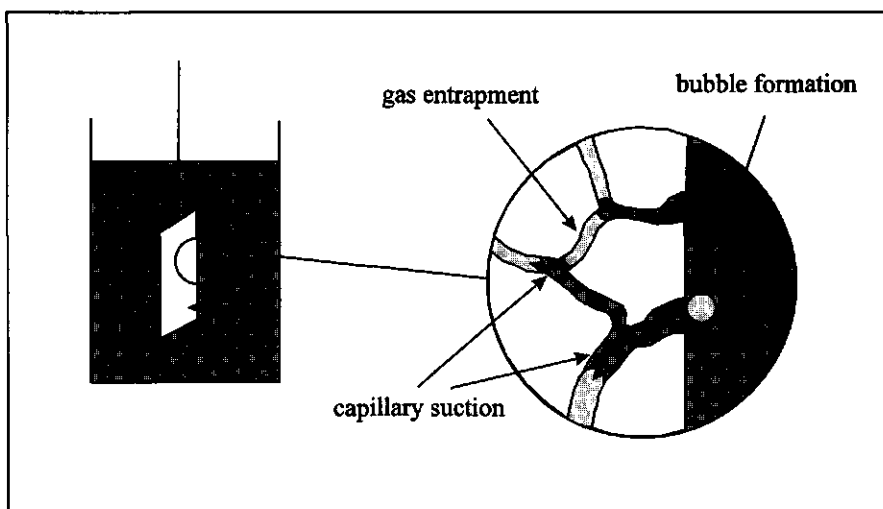


Figure 6.2 Mechanism of Tyvek wetting, showing the process of capillary suction, gas entrapment and bubble formation.

- 1) As a result of the formation of bubbles which escape from the active surface when it is emersed in the liquid, the gas content can be decreased. This effect, however, was only observed in liquids such as alcohol and petroleum ether, both of which have a low surface tension and viscosity and wet the Tyvek material very well.
- 2) A second mechanism, capillary suction of a wetting front, can be described by the capillary pressure and the flow rate, for a tubular pore this is the Poiseuille flow rate (Schwartz, 1969). The capillary pressure is described by:

$$\Delta P_c = \frac{2\gamma \cos\theta}{r_c} = \frac{2\gamma}{r_{curv}} \quad (6.1)$$

where ΔP_c is the capillary pressure (Pa), γ is the surface tension (N/m), θ is the contact angle ($^\circ$), r_c is the radius of capillary (m) and r_{curv} is the radius of curvature of the interface (m).

The Poiseuille flow rate is given by:

$$\frac{dV}{dt} = \frac{\pi \Delta P_c r_c^4}{8\eta L}, \quad \frac{dl}{dt} = \frac{\Delta P_c r_c^2}{8\eta L} \quad (6.2)$$

where dV/dt is the liquid flow rate (m^3/s), dl/dt is the velocity of the liquid front, η is the liquid viscosity and L is the length of the pore.

In most models the radius used is that of the circular cross-section of the tubular pore. Depending on the interfacial radius of curvature the capillary pressure is the driving force for a volumetric flow, which then depends on the cross-sectional area of the pore and the viscosity of the flowing liquid.

- 3) During capillary rise, air may easily be trapped into voids of interconnecting chambers inside the material. This effect is greatly dependant of wetting characteristics (Bankoff, 1958) but also on the amount of intersections and the flow rate of the liquid inside the material (Yu and Middleman, 1993). Furthermore the shape of the pores can play an important role: Princen (1992) showed that angular cross-sections of pores as opposed to circular ones could greatly influence wetting of liquids in pores. Due to an angular cross-section, gas can easily be trapped in the wedge-shaped crevices where for example fibres meet. Wetting liquids, on the other hand, can use these wedges to increase flow rates due to a higher capillary suction. The entrapment of gas in active sites (pores) is probably of essential importance for the foam formation from the surfaces used in this work: if no gas is trapped inside the Tyvek surface when the surface is immersed in the liquid, the bubble formation sites would not be 'active' and no bubbles would grow on the surface at the low gas supersaturations used in this investigation.

In order to estimate the capillary pressure and therefore the flow rate of the liquid into or out of the material, the surface tension, the pore radius as well as the contact angle should be known. The surface tension of the wetting liquid can easily be measured in equilibrium. However wetting action is a dynamic process, where in the case of surfactant solutions in porous media, the surface active components can become depleted and the surfactant coverage decreases at the liquid front (Good, 1992; Yu and Middleman, 1993). The use of the equilibrium surface tension should therefore be cautioned when using solutions other than pure liquids.

The average pore radius can be estimated from BET analysis or other such techniques (Lyklema, 1995). However in a heterogeneous product like Tyvek the pore radius can range over 3 decades (see next paragraph), and only the largest pore sizes will probably be of any importance in the wetting experiment performed in this work, as will be shown.

The measurement of contact angles is usually performed on a flat surface in an advancing, equilibrium or receding situation. The use of this contact angle can however be hazardous due to all kinds of hysteresis factors such as surface roughness, heterogeneity, liquid flow rate, transport rates of surface active material and depletion (Good, 1992). Last but not least is the important effect of the types of curvatures of the solid surface present inside the material. The contact angle is determined by surface and interfacial tensions, but the curvature is also determined by the geometry and shape of the solid surface.

On the whole this means that it is very difficult to assess pore sizes and shapes in a material like Tyvek, and wetting of various liquids can give us only qualitative information about the amount of gas removed or the amount of liquid penetrated into the material. What can be said, however, is that wetting of the active surface will decrease the amount of active sites close to the external surface, thereby decreasing the foamability in a gas-supersaturated liquid. However, the measurement of the wetting properties gives an idea of the amount of active sites left in the material. Furthermore, partly wetting an active surface can also have a positive effect. Due to wetting of the largest macro-pores situated on the outside of the surface, the foam formed should consist of bubbles with a smaller size distribution, resulting in a more homogeneous and thus more stable foam (see paragraph 6.4.5).

6.3 Experimental

6.3.1 Methods

Contact angle measurements

It was found that beer could wet all kinds of surfaces quite well. It was therefore decided to try to relate surface tension of beer on a given surface to the foaming performance of the surface in supersaturated beer. The contact angle measurements were carried out by placing a (sessile) drop of liquid on a given surface, and equilibrate for 10 minutes. The contact angle was measured in equilibrium, and dynamically, by increasing and decreasing the drop volume with a micro syringe. Increasing the volume gives an advancing angle, decreasing the volume gives a receding angle. The foaming was noted visually.

S.E.M. and cryo-S.E.M.

In order to be able to understand the wetting and foaming behaviour of the Tyvek material, an analysis was made of the internal structure of the material by Scanning Electron Microscopy (S.E.M.). This SEM photography was carried out by the TFDL in Wageningen. Mr. Thiel of the ATO-DLO in Wageningen spent many hours attempting to make cross-sections of Tyvek, which failed as the material could not be cut properly without damaging the structure. A normal follow-up procedure is to soak/fill the voids with a type of resin which, after freezing, is easier to cut. Unfortunately the material could not be wetted with any kind of resin. The cross-sectional photographs shown are supplied by Dupont De Nemours. Unfortunately we were unable to find out under what conditions these were taken.

Wetting or weighing method

In order to be able to measure the wetting action or penetration of liquid into a sample of Tyvek, we developed a method of weighing an immersed Tyvek sample as a function of time. Figure 6.3 shows a sketch of the experimental set-up. The Tyvek sample is hung by a piece of steel wire, some rods and extra weight to a force transducer, and the weight of the system was recorded as a function of time. With immersion the weight decreases due to the different density of the liquid surrounding the Tyvek material and because of the trapped gas, but then increases as gas inside the sample is slowly released in exchange for liquid. The change in the volume percentage of gas in the Tyvek sample was then calculated as shown in Appendix VI.1.

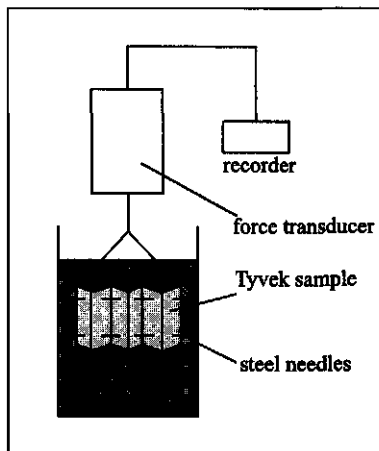


Figure 6.3 Diagram of the wetting method. The Tyvek is held immersed in a wetting liquid while the weight is measured as a function of time.

Foaming method

For the measurement of the effect of wetting of beer on the foaming ability of Tyvek, beer bottles were filled with a Tyvek sample (6x4 cm), resealed and stored upside down during 50 days. Every sampling day three bottles were opened and the foam produced from the Tyvek sample was measured. As the Tyvek sample produces foam from the moment of pressure release, a new method had to be developed to measure foaming ability. Figure 6.4 shows a sketch of the method. During storage the Tyvek samples are held in the neck of the bottle by a polypropylene rod. Positioning the bottle upside down enabled the sample to be completely immersed in beer. Before the foam measurement, the bottle was placed upright, re-emerging the Tyvek sample. After opening the bottle (no foam formed due to the lack of contact between the Tyvek sample and the supersaturated beer) the Tyvek sample was removed. The funnel (a beer bottle from which the bottom has been removed) was positioned and fastened with a clamp mechanism, after which the wetted sample was re-immersed into the beer causing instant foam formation.

6.3.2 Materials

Tyvek

Tyvek material from Du Pont De Nemours, Luxemburg, is a tough micro-porous sheet product made of 100 % high density polyethylene (HDPE) fibres. The sheet is first formed by spinning continuous strands of very fine interconnected fibres, and then bonding them together with heat and pressure. The fibres in type 10 style (Tyvek L-1073-D) which we have used are bonded to form a tough, dense opaque sheet. The dense packing of the

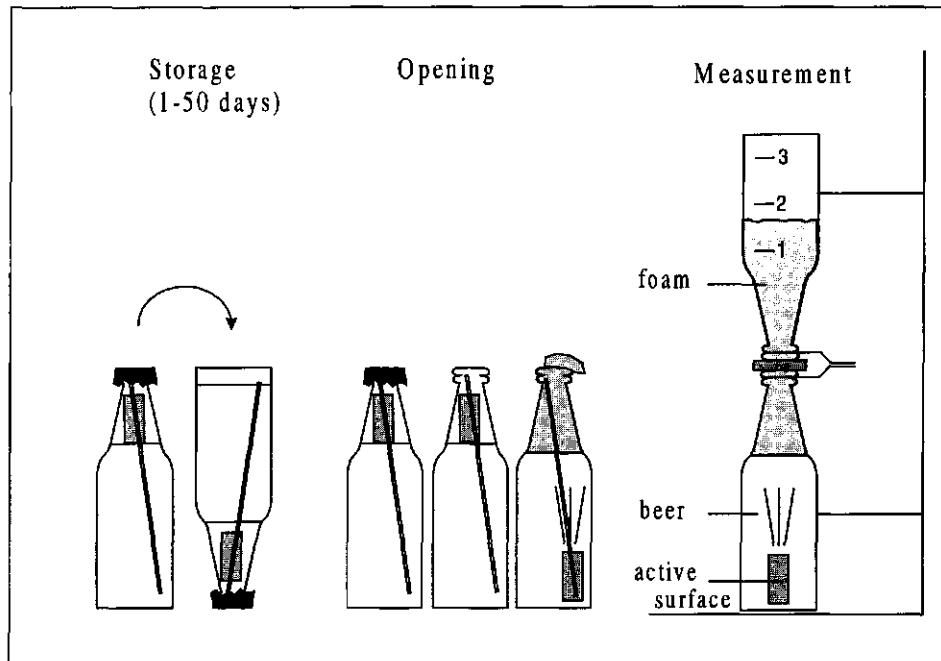


Figure 6.4 Diagram of the experimental set-up used to measure the rate of foam formation from an active surface as a function of wetting period.

fine, interconnected fibres produce a smooth surface, high opacity and whiteness. The large number of bonds per unit area results in a stable and abrasion resistant surface with a stiffness similar to paper. Furthermore the material has been corona treated on both sides (to improve ink adhesion) and is coated with an antistatic agent (to facilitate sheet handling).

The basis weight of the material is around 75 g/m^2 with an average thickness of $186\mu\text{m}$ ($123\text{-}278\mu\text{m}$), as supplied by Du Pont De Nemours. From these values an apparent density can be calculated of 403 kg/m^3 .

From our own measurements we arrived at an average density of about 440 kg/m^3 , and a gas volume content of about 50-55 %. However as seen above, the thickness of the material can vary considerably (up to 50%) which means that the calculation of the gas volume content is subject to a large error. This value must therefore be seen as an estimate of the average Tyvek sample.

Wetting liquids

In the wetting experiments, several liquids of various density, polarity and surface tension are used to give a characterisation of the type of pores that exist in the Tyvek material.

As *water* we used double-distilled water, left to stand one week at ambient temperature and pressure for gas equilibration. The *alcohol* was 96% technical alcohol. The *beer* was stirred overnight for degassing.

The *petroleum ether* (Merck, Darmstadt) boiling range 60-80°C, is a very apolar liquid which should absorb quite readily onto polyethylene.

Teepol (FNZ, Arnhem, 02631-86776) is a commercially available anionic detergent which has to be diluted before use. Teepol contains among other components alkylarylsulfonate, alcoholethersulfate and alcoholethoxylate. The amount of active material is about 15%. As Teepol is a technical product, the contents of two batches may differ slightly.

Alconox powder (Boom, Meppel) primarily consists of a homogeneous blend of sodium linear alkaryl sulfonate, alcohol sulfate, phosphates and carbonates. Alconox is anionic in nature.

K 500 powder (FNZ, Arnhem) is a commercial detergent used successfully in the dairy industry. It consists mainly of the tetra sodium salt of ethylene-diaminetetra-acetic acid with some other components which give a good cleaning and dirt uptake effect.

6.4 Results & Discussion

First of all, different surfaces were wetted with degassed beer, and the foaming achieved after wetting observed visually (section 6.4.1). The structure of Tyvek was then analysed with microscopy (section 6.4.2), and by wetting action of various liquids (section 6.4.3). In paragraph 6.4.4. a relation is found between wetting and foaming ability of pre-wetted Tyvek samples. A different material, named model active surface (m.a.s.), was tested alongside Tyvek in the wetting and foaming test in section 6.4.5.

Section 6.4.6 shows the calculated bubble size distribution of bubbles formed from Tyvek material in beer and in section 6.4.7 several concluding remarks are given concerning the pore size in Tyvek material.

6.4.1 Wetting effect of beer on foamability of different surfaces

The bubble formation on solid surfaces in a gas-supersaturated liquid can be very different depending on surface heterogeneity or roughness and wetting properties. Several types of surfaces (glass, perspex, paper tape and teflon foil, sandblasted glass, and sandblasted perspex) were used to categorise the effect of surface wetting, heterogeneity and roughness on the "foamability" of the material. Table 6.1 gives equilibrium, advancing and receding contact angles of a sessile beer drop on a given surface, measured by increasing and decreasing the drop volume with a micro syringe. In bubble growth on active surfaces the effective angle at which the bubble detaches is probably the receding angle (see chapter 3). Table 6.1 shows that although a surface like teflon shows

Table 6.1 *Equilibrium, receding and advancing contact angle of a degassed beer drop on the given active surface.*

	$\theta_{equilibrium}$	$\theta_{receding}$	$\theta_{advancing}$
glass	9	0	10-20
roughened glass	20-30	0	45
perspex	45	5	90
roughened perspex	30	5	90
teflon foil	90	5	100

“hydrophobic” properties with beer in equilibrium, the receding contact angle is very low. This suggests that surface active components in the beer adsorb onto the “hydrophobic” surface giving the effective surface properties a more “hydrophilic” nature.

A foaming experiment with these “active” surfaces showed that the three smooth surfaces (glass, perspex and Teflon foil) showed different foaming behaviour. Figure 6.5 shows the foam forming on glass and perspex; The glass sample gives off most foam initially but is completely wetted within half an hour. Both the perspex and the Teflon foil showed slow formation of large bubbles so that almost no head was formed. The foam formed with glass was not very stable.

The roughened glass produces an equal amount of foam as the smooth glass. However, the foam formed at a rough surface is more stable and the surface stays foamactive for a longer time. The roughened perspex gives a large foam head which is fairly coarse.

This gives a rough idea of how the type of surface influences foam formation. A hydrophilic or well wetted surface gives small bubbles, as long as it stays foamactive. A hydrophobic surface produces large bubbles and hence is formed at a slow rate but when roughened, the bubbles are smaller and an increase in foamability is seen.

It is not very clear from these experiments whether the receding contact angle is the determining factor in bubble size, since roughening the surface seems to decrease bubble size considerably. Due to the roughening edges in the surface, the local effective contact angles could be both smaller and larger than the (macro scale) contact angles measured and shown in table 6.1.

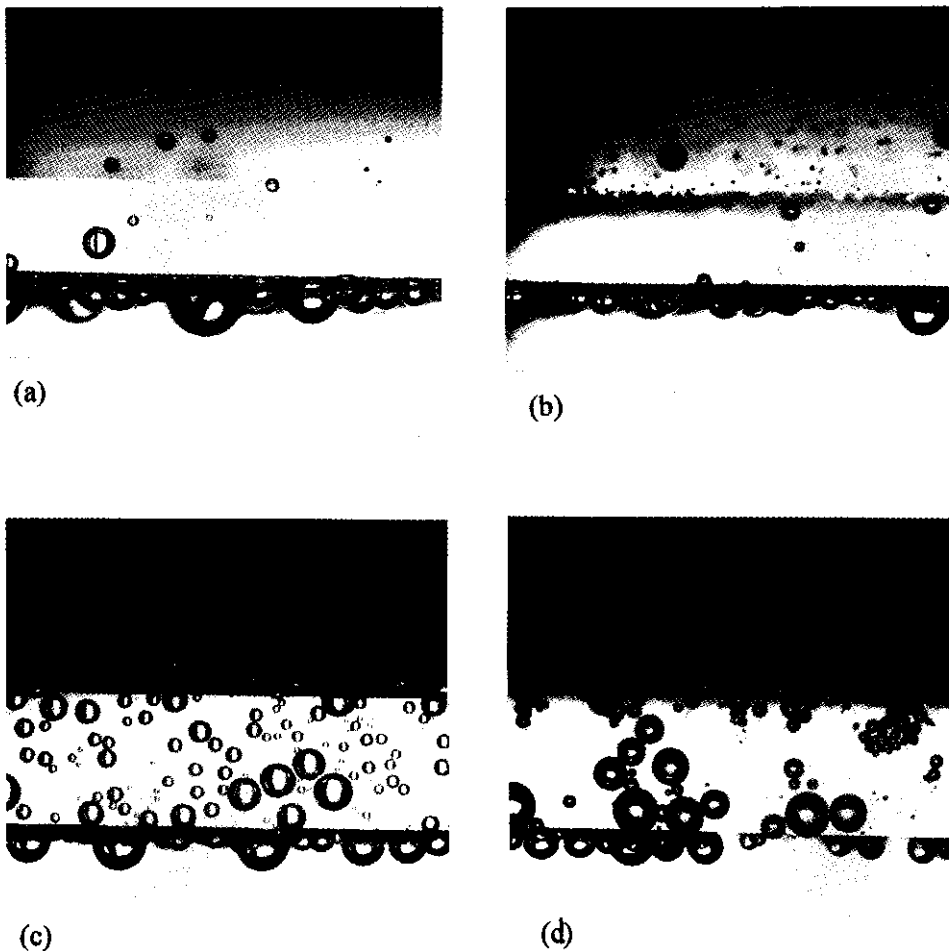


Figure 6.5 Photographs of bubble formation on (a) glass, (b) roughened glass, (c) perspex and (d) roughened perspex.

6.4.2 SEM and Cryo-SEM

Figures 6.6a-d show top views of Tyvek, performed by SEM at various magnifications. As can be seen the surface shows essentially large fibres, but as the magnification increases cracks and cavities can be seen to exist between the fibres as well as cracks in the fibres themselves. Figure 6.7 shows a sketch of the three main types of

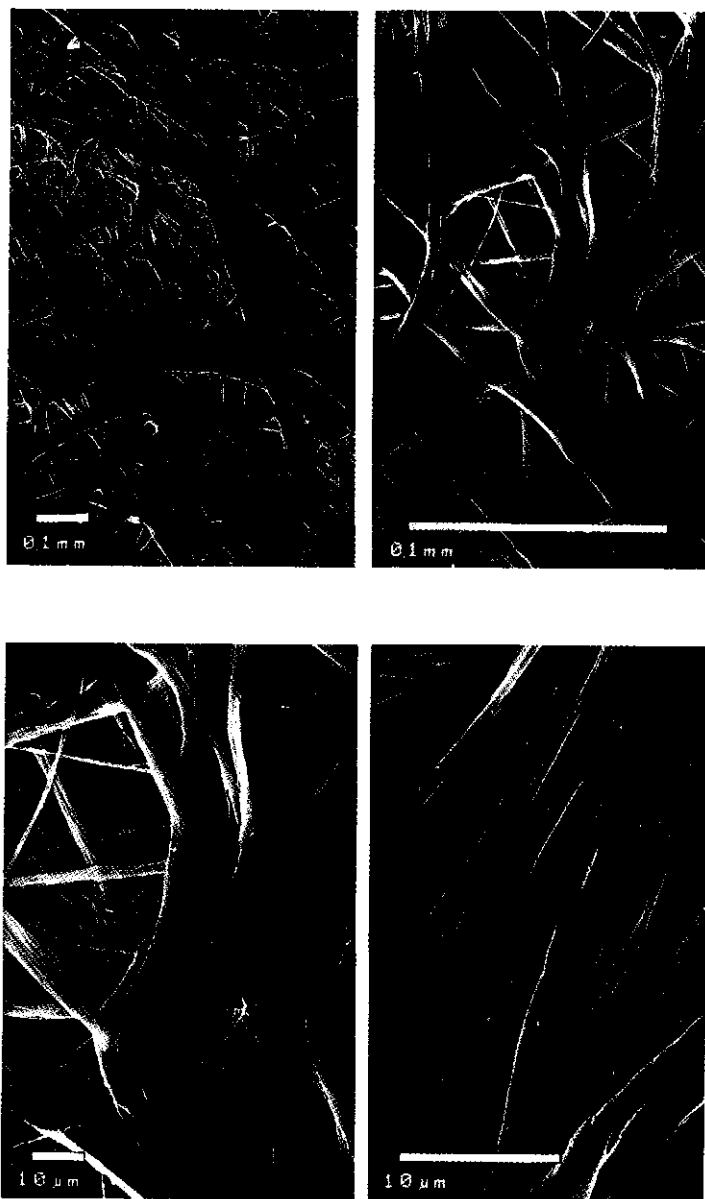


Figure 6.6 SEM photographs of the top view of a sheet of Tyvek material. The magnifications are given as a scale bar in each photograph.

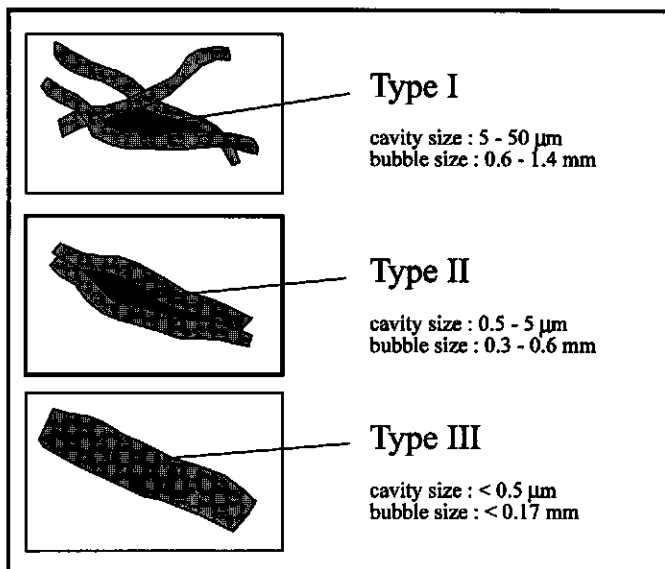


Figure 6.7 Sketch of the range and type of pore sizes estimated from the SEM photo's, as well as the bubble radius that would be expected to detach from these pores using eq.(3.7).

cavities found in the Tyvek material. Type I cavities are pores or voids between secondary fibres; type II are cavities between primary spun-bonded fibres and type III are cracks in the primary fibres. In a dry state all three types of cavities will be actively producing bubbles in a supersaturated solution; if the surface is wetted with a liquid, type I pores could become filled with liquid, and stop being foamactive. This means that the gas molecules have to diffuse further into the material to produce gas bubbles at type II and type III cavities. Another result of the elimination of type I cavities is that the bubble size distribution from a wetted Tyvek sample could be much narrower than from a dry Tyvek sample as will be observed in a later experiment (paragraph 6.4.4).

Figure 6.7 shows the ranges pore sizes for the three cavity types estimated from the SEM images, as well as the estimated bubble size in beer (using eq (3.7), $\gamma = 40 \text{ mN/m}$) when detached from cavities of these sizes.

Various attempts have been made to try to make cross-sectional photographs of the Tyvek material by cryo-SEM. It was found however that the material could not be broken even at very low temperatures, and cutting the material resulted in seeing the effect of cutting technique. As can be seen in figure 6.8(a), the fibres are pressed together and the original spatial structure of the fibres is altered. One thing that can be seen, however, is that very large voids are present within the Tyvek material, as well as very small ones as seen from the SEM photographs. Recently we were sent some photographs from Du Pont

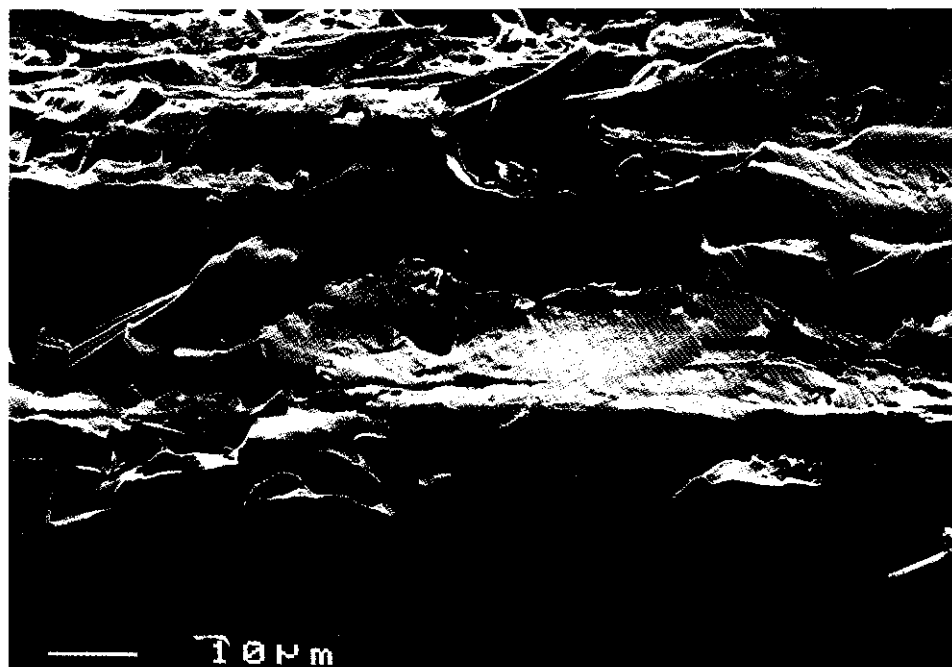


Figure 6.8 Cryo-SEM photographs of cross sections of Tyvek (a) where fibres are pressed together, and (b) from Dupont de Nemours.

(figure 6.8(b)), in which it can be seen that the pores are very heterogeneous (1-30 μm), and show a large degree of interconnection.

The kind of pores found in Tyvek are thus mostly macro-porous ($>=50$ nm), of reservoir type where the mouth is smaller in perimeter than the pore itself (Linsen and v.d. Heuvel, 1967), with mostly slit-shaped voids that are interconnected and mostly positioned in a 2-dimentional structure caused by the manufacturing process.

6.4.3 Wetting of Tyvek in various liquids

A wetting analysis was performed to elucidate the structure of Tyvek in more detail. As mentioned in paragraph 6.2.2, measuring the contact angle between a drop of liquid and Tyvek will not give the full information that we need. The contact angle may be of a certain value but the curvatures of the liquid menisci found inside the cavities of this material may be quite different. By immersing Tyvek into different liquids and analysing the increase in weight as a function of time we aim to find a second estimate of the range of pore sizes (the first being based on the SEM photographs).

Wetting of Tyvek material in various liquids

In order to get a better understanding of the type of material that we are using for foaming experiments, the Tyvek was wetted in liquids of various types of polarity, density and surface activity (surfactant solutions). Table 6.2 gives an overview of the liquids used, their density and surface tension in equilibrium. Paragraph 6.3.2 lists the nature of the liquids used for the wetting test.

Table 6.2 *Density (ρ) and equilibrium surface tension (γ_{eq}) of the liquids used in the wetting experiments at $T = 20$ °C.*

	ρ (kg/m^3)	γ_{eq} (mN/m)
water	998	70
alcohol (96%)	810	23
petr. ether	665	18
beer	1045	40-45
1 wt% Teepol	998	28
1 wt% Alconox	998	30.5
1 wt% K 500	998	31.5

Figure 6.9(a) gives the decrease in vol% gas in the Tyvek sample as a function of time for the liquids water, alcohol, beer and petroleum ether, beginning at around 55 vol% gas in Tyvek. As can be seen in the figure, water and beer slightly wet the Tyvek material, after which a stable situation occurs. Both alcohol and petroleum ether wet the Tyvek so well that the vol% gas becomes negative. This is physically not possible but could be caused by errors in the weighing or in the calculation of the dry gas content. The low values could also be due to the internal swelling of the Tyvek material, as hydrocarbons are found to have this effect on polyethylene (Du Pont de Nemours). The wetting action of petroleum ether and alcohol is very rapid and seems to remove the gas almost completely from the sample.

Figure 6.9(b) shows the wetting properties of three surfactant solutions Teepol, K 500 and Alconox. As can be seen K 500 has a slower wetting action than Teepol and Alconox, but arrives at the same degree of wetting (5 vol% gas) after 15 hours of wetting time. The difference is probably due to diffusion and adsorption differences between the surfactants.

It is noticeable that the degree of wetting increases as the surface tension of the liquid decreases and becomes closer to the surface tension of the solid material which will be around that of petroleum ether.

The Tyvek samples wetted with surfactant solutions were rinsed continuously overnight in double distilled water, after which the wetting in double distilled water was recorded (not shown here). Both the Teepol-treated sample and the Alconox-treated sample were found to have been rinsed properly. The rinsed sample that was initially wetted in K 500 was probably still polluted with adsorbed surfactant, leading to an increased wetting action in water. This experiment strengthens our suspicion that soaking Tyvek into a adsorbing liquid can change its wetting properties considerably and permanently.

If we use the wetting velocity of petroleum ether from figure 6.9(a), we can calculate an average pore size with equations (6.1) and (6.2), assuming a zero contact angle, and $r_c = r_{curv}$: we inserted the equilibrium surface tension given in table 6.2, the viscosity is estimated at $0.8 \cdot 10^{-3}$ Pa.s, and l is taken as 0.1 mm, which is roughly half the thickness of the sample. From figure 6.9(a) we estimate an initial flow rate of petroleum ether of about $0.0833 \text{ mm}^3/\text{s}$. Inserting these values into equations (6.1) and (6.2), the average pore size comes down to about $7.5 \mu\text{m}$, which falls into the lower region of the Type I category described in paragraph 6.3.2. This pore size seems very acceptable, considering only the larger pores are used in the macro scale wetting process measured with the weighing method.

If this calculated pore size is then used to calculate the contact angle for wetting with water, where the initial flow rate is about ten times slower than petroleum ether, the surface tension is 70 mN/m and the viscosity 10^{-3} Pa.s, the calculated angle is 89.3° (for beer the calculated contact angle is 88.8°).

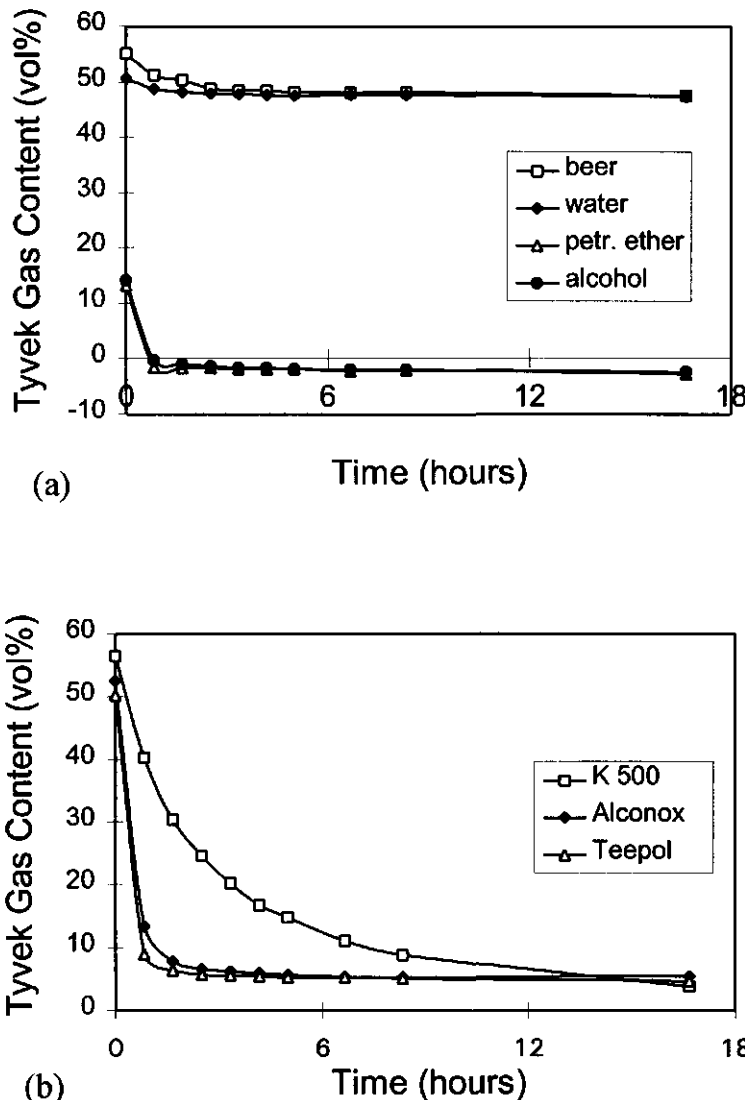


Figure 6.9 Wetting isotherms of Tyvek in (a) water, in beer, technical alcohol and in petroleum ether and (b) in 1% Teepol solution, 1% K 500 solution, and 1% Alconox solution.

As mentioned before and shown in figure 6.9(a) both water and beer do not wet the Tyvek material very well. This is probably due to the large contact angle (non-wetting mode) as a result of which there is no driving force to wet the sample.

6.4.4 Relation between wetting and foaming of Tyvek

We have shown in the previous paragraph that the process of wetting of liquids onto a Tyvek sample can be measured quite accurately. As there was a need to use a pre-wetting treatment before foaming, we investigated the effect of the different degrees of wetting (with penetration of different liquids) on the foaming action of Tyvek in supersaturated beer.

The effect of the wetting of water and a surfactant solution on the foaming ability of Tyvek, compared to a dry sample

Tyvek samples of a constant area were subjected to three cycles of cleaning, wetting, and foaming in beer, where the wetting stage in the cycle was (a) no wetting (dry), (b) wetting in water and (c) wetting in a 1wt% Alconox surfactant solution (and then exchanged with water). After the wetting stage, the samples were placed in supersaturated beer (4g/kg) and the foam height was measured during three minutes. After foaming in beer, all the samples were cleaned with the surfactant, rinsed and dried, and the procedure repeated. The cleaning procedure was necessary to get the sample back into its original condition. The adsorption of beer residue onto the Tyvek surface reduces the foaming ability. Three total cycles were performed in order to observe if the cleaning of the surface had any effect in stopping the reduction of the foamability. It should be noted that Alconox was the most effective in removing beer rests from the Tyvek material, compared to other surfactants and alkaline and acid treatments. In all cases the surface tension of the last rinsing water was checked and found to lie between 69 and 72 mN/m. This at least proved that no surfactant was desorbing from the surface, suggesting a reasonably clean external surface before the start of the next wetting measurement. Also the surface tension of the wetting liquids were measured after wetting the Tyvek samples, and were found to be stable. All the measurements were performed at 23°C.

Figure 6.10(a) shows the foam formation of the dry Tyvek sample in gas-supersaturated beer as a function of time, for the three foaming cycles. The foam is very coarse and rapidly collapses due to the large number of large bubbles. During the last cycle the amount of foam produced is increased. The degree of wetting (D.W.), however, showed no change between cycles (see table 6.3, first column). A change might be expected if the wetting properties were changed due to the contact with beer, but this does not seem to be the case.

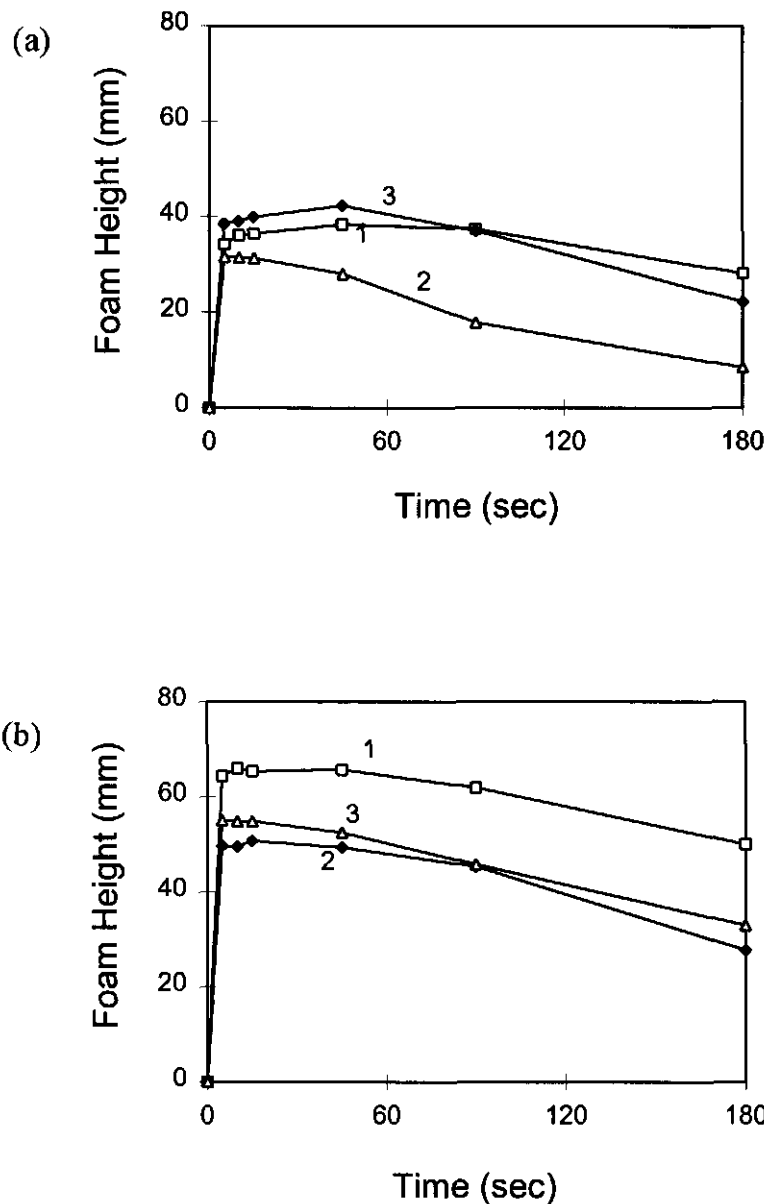


Figure 6.10a,b Foam formation of (a) a dry Tyvek sample in beer, for cycles 1, 2 and 3, (b) a pre-wetted (in distilled water) Tyvek sample in beer, for cycles 1, 2 and 3, and (c) a pre-wetted (in Alconox, and exchanged with water) Tyvek sample in beer, for cycles 1, 2 and 3 (see next page).

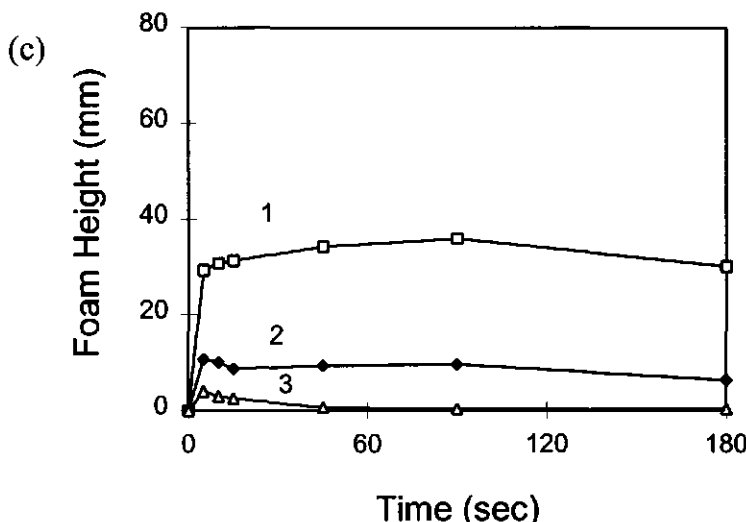


Figure 6.10 c Foam formation of (c) a pre-wetted (in Alconox, and exchanged with water) Tyvek sample in beer, for cycles 1, 2 and 3.

Figure 6.10(b) shows the foam formation of the sample pre-wetted in water. Again a decrease is found in the foaming action after one or two cycles. Again no change in degree of wetting was found preceding the foaming experiment (table 6.3, second column). The amount of foam produced with a water pre-wetted sample is found to be almost twice as high as the dry sample. This could be due to the fact that the foam from the wetted sample is more stable (with smaller bubbles) as a result of less drainage, less coalescence and slower disproportionation.

Figure 6.10(c) shows the foaming of the sample pre-wetted in Alconox solution, and exchanged with water. The foaming decreases considerably with each passing cycle. Looking at the wetting measurements, the wetting with water (after cleaning) changes in time (table 6.3, column 4), whereas the wetting with Alconox is constant and the D.W. high (table 6.3, column 3). As the water penetrates more easily with each wetting cycle, it seems that the Tyvek material is changing in some way. Furthermore, the foam formation is almost stopped completely after three cycles probably due to the high degree of wetting of the surfactant.

It seems as though the wetting with water does not change the surface properties, but the surfactant does. Furthermore, the foaming in beer changes the Tyvek samples in all cases, but does not change its wetting properties. With each cycle the foam formation decreases and, although not shown here, reaches a constant foamability. This suggests that

Table 6.3 *The degree of wetting of Tyvek after 18 hours submerged in liquid, relative to a 50 vol% gas content at t=0.*

cycle nr	Degree of wetting in Tyvek sample (%)			
	dry	water-wetted	Alconox-wetted	water-wetted
1	16	22	96	18
2	16	18	96	26
3	14	24	94	38

some of the surface active components adsorb irreversibly onto the Tyvek material. If the Tyvek material is partially wetted, the beer components can easily adsorb into small niches inside pores where they will be very difficult to remove, if at all. However, this is not reflected in the wetting experiments as the D.W. with water is unaffected after a cleaning and drying cycle.

Concluding, it was found that a pre-wetting of clean water induced more foam formation than when the sample was dry. Furthermore, the foam layer has a more uniform bubble size distribution (not shown here) and is more stable when the active surface has been pre-wetted. A high D.W. with a surfactant reduces the foamability almost to zero, supporting the working hypothesis that active sites (with a certain amount of gas in them) are needed in order to produce bubbles from a solid surface at these low supersaturation levels. The foaming ability of an active surface depends on the amount of available active sites. If all of them are filled with liquid instead of gas (due to wetting) no bubbles may be formed. Furthermore it was shown that Tyvek samples could not be recycled in the foaming experiments using this surfactant as a result of irreversible fouling of surface active material in small pores.

Tyvek wetting and foamability in beer as a function of time

In order to be used as a foaming device, the Tyvek material should have stable active surface properties when immersed in supersaturated liquids over a long period of time. Earlier measurement showed that the degree of wetting of Tyvek in beer decreased somewhat over a period of 15 hours. In this paragraph the degree of wetting of Tyvek in beer was followed for one month. The greatest decrease is found within one day where the D.W. reaches about 12%, after which no further change is seen and the system is thought to be equilibrated.

Attempting to relate the wetting properties to foaming performance, beer bottles were filled with a Tyvek sample, resealed and stored upside down. For 50 days the bottles were opened in triple and the foam formation was recorded.

The maximum foam height was measured roughly with a ruler and plotted as a function of wetting time in figure 6.11. As can be seen, the maximum foam height decreases a little within the first few days of wetting but then becomes relatively stable. This can be well compared with the wetting of Tyvek in beer: it seems as though the amount of foam produced decreases as the active surface is better wetted, and stays constant when the D.W. remains unchanged.

The time taken for the top of the foam to reach point 1, 2 and 3 on the funnel (see figure 6.4) (corresponding to a foam volume of 116 ml, 214 ml and 324 ml) was recorded and plotted for the different wetting times in figure 6.12. As can be seen, the rate of foaming decreases fourfold during the wetting period of a month. From the wetting performance, we know that the volume of gas trapped inside the Tyvek sample does not change. The only possible explanation for the decrease in foaming rate is a rearrangement of liquid and gas phases inside the Tyvek sample during the wetting time. The possibility that the beer bottles leaked gas is small since the bottles were stored upside down.

There are a few possible mechanisms for the rearrangement of the gas inside Tyvek.

1. increase of the diffusion length prolongs the diffusion time and bubble growth.
2. decrease of the amount of active sites reduces the amount of bubbles formed per unit time.

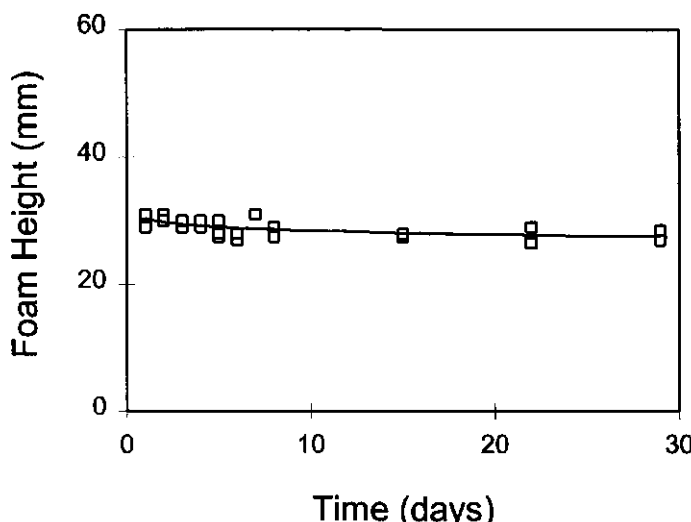


Figure 6.11 Maximum foam height of Tyvek in beer as a function of the wetting period in days.

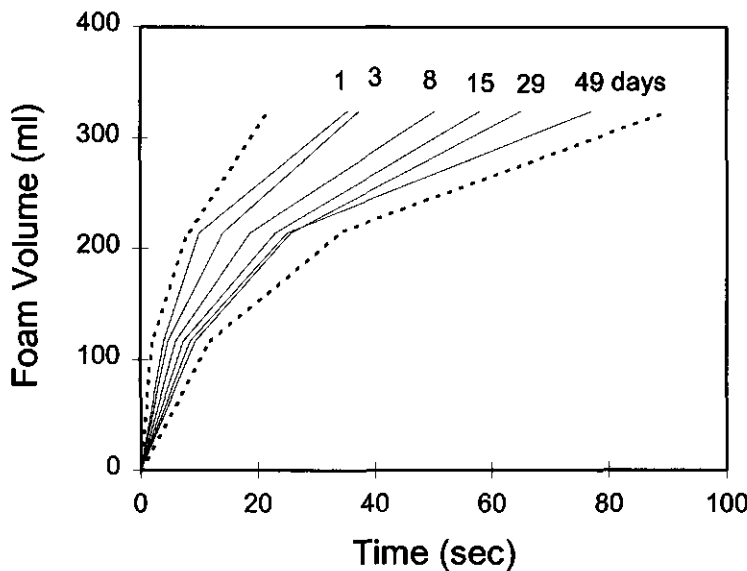


Figure 6.12 Rate of foam formation for Tyvek samples in beer as a function of wetting time.

ad 1) Due to slow wetting of externally situated voids or cavities in Tyvek, the diffusion length increases slowly for the gas transport that needs to take place from the liquid bulk to the bubble interface. This wetting can only take place if the liquid volume inside the Tyvek stays constant. This is only possible when the gas concentrates more in the centre of the sample, and the liquid is more concentrated at the outer edges of the material.

Only a small increase in diffusion length could make the bubble formation slower with the factor found in figure 6.12. The time for the foam layer to build up is increased from roughly 20 to 80 seconds. Assuming that the foam layer will hold about 100.000 bubbles, the difference in growth time per bubble will be 0.2 ms to 0.8 ms.

In order to calculate the diffusion length we can use the penetration theory:

$$l = \sqrt{\pi D t} \quad (6.3)$$

where l is the diffusion length (m), D is the diffusion coefficient (m^2/s) and t is time (s). The difference in diffusion length is then an increase from 0.7 to 0.8 μm in diffusion length, which can be easily produced by a small movement of the gas-liquid interface.

ad 2) The rearrangement could be created by a so-called "proportionation" process, which can occur when the cavities are not well-wetted. Due to the convex curvature of the liquid surface (seen from the gas phase), the pressure in the liquid phase is higher than in the gas phase. When two gas interfaces of different curvature are situated next to each other, shown in figure 6.13, the gas from the gas phase with the largest radius of curvature will diffuse through the liquid to the gas phase with the smallest radius of curvature, where the pressure is lower. With a distribution of larger sites at the external part of the sample and small sites situated internally, this mechanism can rearrange the gas phase in such a way that more gas is concentrated at the centre of the material, or that eventually less active sites remain.

A reduction in the amount of active sites could also be brought about by coalescence of different gas phases within voids, caused by the drive of the system towards the least possible interface and largest curvature of interface. The resulting decrease in the amount of active sites at which bubbles can be formed can result in a foam rate decrease.

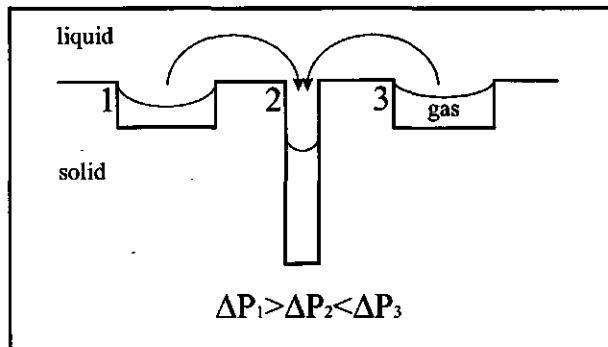


Figure 6.13 Proposed model of "proportionation" process.

6.4.5 Model active surface: wetting and foamability in beer

The so called model active surface (m.a.s.) resulted from integrating the favorable properties of the ideal active surface listed in paragraph 6.2.1 into a practical system. Analogous to the hypothesis this ideal m.a.s. should be foamactive over long periods of time and comparable to the foaming performance of Tyvek material.

Table 6.4 gives a comparison in the active sites and the active site density of Tyvek and the m.a.s.

As a comparison, Tyvek and m.a.s. samples of equal size were submitted to a wetting test and a foaming test (see paragraph 6.3.4). The wetting properties of the m.a.s. were found to be similar to Tyvek. For Tyvek it has been found that the internal dry gas

Table 6.4 *Comparison between Tyvek material and m.a.s. in the amount, the size and the density of active sites*

	Tyvek	m.a.s.
pore diameter:	1-50 μm	30 μm
shortest interval distance:	10 μm	125 μm
sample area (1 side):	19.6 cm^2	19.63 cm^2
number of pores (1 side):	*	125.600
bubble diameter:	0.39-1.44 mm	0.97 mm

* ill defined

content is about 50 vol% in air (see Appendix VI.1). Immersed in beer the D.W. becomes about 15% of the total gas volume originally existing in the Tyvek sample.

The dry gas content of m.a.s. is estimated to be about 25 vol%, which seems to decrease to about 13 vol% when submerged in beer. In other words, the D.W. becomes 48% of the gas volume available.

In both types of material active sites remain present, although Tyvek retains more air than the m.a.s.. This more pronounced loss of active sites in the m.a.s could be interpreted as a loss of foamability of the m.a.s. compared to Tyvek as a result of wetting in beer.

Comparing the foaming behaviour Tyvek foam is formed more rapidly, probably due to the much larger amount of active sites. Therefore a larger maximum foam volume can be reached in the same time. Both types of surfaces produce at least 200 ml foam from 300 ml beer in 10 to 100 seconds.

Concluding, the m.a.s. behaves in a similar way to Tyvek but produces less foam. This is quite understandable since the amount of active sites in the m.a.s. is much smaller than in Tyvek. Although these results can only be interpreted qualitatively, they confirm our hypothesis that inserting hydrophobic cavities into a hydrophilic surface is the key for a stable active surface. Secondly the active surface should hold a high amount of active sites to be able to produce enough bubbles for the formation of a foam layer. The effect of distance between the cavities is still not very clear but the foam which was formed from the m.a.s. seemed finer than foam from a Tyvek surface. This means that the active sites on the m.a.s. probably produce bubbles that are smaller in size. However, the fine foam from the m.a.s. also seemed more sensitive to the process of disproportionation, which seems illogical. Generally, a wide bubble distribution is more sensitive to disproportionation than a narrow bubble size distribution, assuming the bubble sizes are in more or less the same range. When the average bubble size is very small in a narrow bubble size distribution, it is possible that this foam is more affected by disproportionation than a foam with a wide bubble size distribution of relatively large bubbles. The reason for this is that

disproportionation is a process driven by the difference in Laplace pressure between bubbles, which depends on the absolute difference in size. Therefore, the smaller bubbles will have a larger driving force for disproportionation than larger bubbles.

6.4.6 Size distribution of bubbles formed on Tyvek, in beer

The bubbles that were formed on the Tyvek material were analysed by Image analysis (see chapter 3, 4 and 5) just after detachment, in a gas supersaturated beer solution. The bubble size distribution could be obtained from the analysis of about 40 different images each containing about 50 rising bubbles. Figure 6.14 shows the number bubble size distribution, where the number average bubble size is found to be $R_b = 0.2093$ mm, varying from 0.025 to 0.400 mm. Calculating back with equation (3.7), it is expected that the cavity sizes are in the range of 2.6 nm to 10.5 μm . The average capillary radius is 1.5 μm , assuming that the bubbles detach from a horizontal surface, which, presumably, is not very realistic. The cavity size that is active in forming bubbles is therefore probably a little larger than calculated.

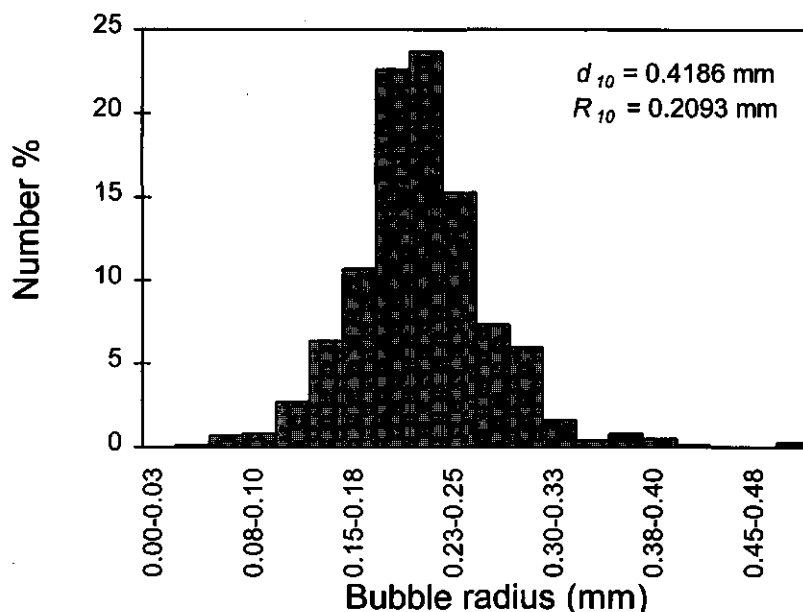


Figure 6.14 Bubble size distribution of bubbles just detached from a Tyvek sample, in a gas supersaturated beer solution, obtained by image analysis.

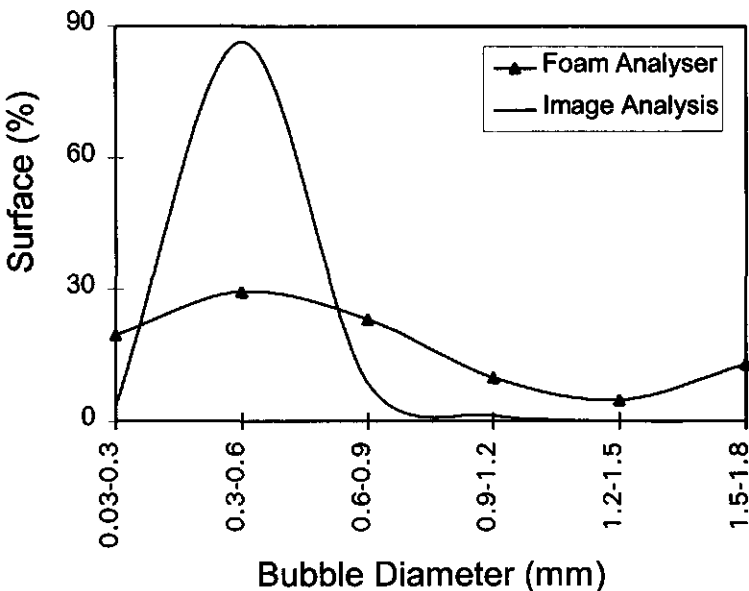


Figure 6.15 Schematic bubble size distribution of bubbles just detached from a Tyvek sample, measured with Image Analysis, and in the foam layer, measured with the Foam Analyser.

It is interesting to compare this bubble size distribution with the one presented of a foam layer formed from Tyvek, given in section 7.4.1. Figure 6.15 shows the schematic distributions for the bubbles rising in the liquid measured by Image Analysis, and for the foam layer, measured with the Foam Analyser. As can be seen the bubble size distribution for the bubbles rising through the liquid is much narrower, than when measured with the foam analyser in the foam. It seems that the size distribution broadens when the bubbles are closely packed together in the foam. This is not strange as the natural process of disproportionation is very quick for carbon dioxide bubbles, when bubbles are situated next to each other in a foam.

6.4.7 Size of active sites in Tyvek material

In this chapter several methods were used to estimate the pore size that is active in the formation of bubbles in the Tyvek material. From the wetting experiments (section 6.4.3), the estimated pore size was $7.5 \mu\text{m}$. From the SEM photographs (see section 6.4.2, figure 6.6) the voids and pores are divided into three possible categories, type I, type II and type III (see figure 6.7), where type I cavities are voids between primary fibres, type II are voids between secondary fibres, and type III are small cuts in the secondary fibres. From

the cross sections (figure 6.8), it seems that the pores/voids vary between roughly 1 μm and 30 μm . Finally, from the bubbles produced on a piece of Tyvek material, the estimated cavity radius (with equation (3.6)) is found to range between 2.6 nm and 10.5 μm , averaging at 1.5 μm . It would seem therefore that the larger cavities (type I) are indeed at least partly filled with liquid as the sample is submerged, leaving the smaller voids between fibres (type II) and small cracks (type III) to be active in foam formation.

6.5 Model calculation of foam produced on Tyvek surface

This exercise is done in order to see if we can predict the amount of foam that can be produced in a few seconds from a certain amount of Tyvek material in a certain amount of supersaturated beer with a certain concentration of carbon dioxide gas.

A few assumptions that are made:

A Tyvek sample measuring 4 x 4 cm has an active surface area of 32 cm^2 when we place it vertically in the liquid. The bubbles grow to an average size of 0.4 mm diameter, which means that the maximum coverage of fully grown bubbles is 10.000 bubbles on each side of the material, assuming there are as many active sites as possible places for bubbles (maximum coverage).

Bubbles growing to a maximum diameter of 0.4 mm, originate from a cavity with internal diameter of around 1 μm (using equation 3.7). Assuming that the supersaturated liquid has a volume of 400 ml with an excess concentration of 3.1 g/kg CO₂, the time of bubble growth can be calculated using Bisperinks model (1994) (see also chapter 3). In a liquid such as beer with a surface tension of around 40 mN/m, the time of bubble growth is estimated to be around 0.07 seconds. Every second, therefore, (1/0.07 x 10.000 x 2 =) 285.714 bubbles are formed on this piece of Tyvek, which amounts to a volume of (0.011 10^{-9} x 285.714 =) 3.14 cm^3 gas /s.

If we assume the gas fraction of the foam layer to be about 70%, this means that every second, (3.14 x 1/0.8 =) 3.92 cm^3 foam is formed. If the container has a cross-sectional area of around 100 cm^2 , this means that every second the foam layer increases by 0.39 mm in height. In order to get a layer of around 4 cm of foam (assuming the foam has no time to break down). The active surface should be active for at least (40/0.39 =) 102 seconds. In these time scales the time taken for the bubbles to rise through the liquid can be neglected.

In order to compare with the a practical situation, we derive the foam height after 180 seconds, which will be around 7.0 cm. The value for the practical situation is given in table 7.1 in column 4, row 2, which is 4.3 cm of foam measured after 180 seconds, for an area of 4x4 cm, in a liquid of comparable supersaturation. The probable reason for the overestimation of the predictive model, is that the concentration is not a constant, but decreases in time, such as will also be explained in chapter 7. Furthermore, we did not

account for drainage processes, which decrease the foam height in time. Concluding, the predictive model is only valid until the concentration is starting to be depleted considerably. In this case, this could be already the case within 1 minute.

For a surface of 2x2, we get for the same situation: 400 seconds for 4 cm foam, 1.8 cm in 180 seconds, which is very reasonable compared to the 2.3 cm given in table 7.1. For a surface of 6x6, we get for the same situation: 44 seconds for 4 cm foam, 16.2 cm foam in 180 seconds, which is obviously not practical as the liquid will be depleted in a very short time.

6.6 Conclusions

In this chapter it was shown that both water and beer do not wet Tyvek material very well, due to the large contact angle with which these liquids enter Tyvek (or, better said, do not enter Tyvek). Other liquids such as petroleum ether or Alconox could wet the material much better due to a lower surface tension and, probably, a smaller advancing contact angle. A complete wetting of Tyvek was not achieved with petroleum ether as expected, probably due to the presence of dead corners in the material. This, of course, is one of the main reasons that the Tyvek material is very suitable for its use as an active surface.

The foaming ability is found to be related to the degree of wetting: a higher degree of wetting results in a lower foamability of the sample in a gas-supersaturated liquid. Keeping the degree of wetting constant results in an equally consistent foamability. Furthermore, the degree of wetting in water or beer does not change after 12 hours. In contrast, however, the rate of foaming (when immersing the sample into gas-supersaturated liquid) is slower when the sample has undergone a longer wetting period. This could be the result of a rearrangement of gas inside the Tyvek material, resulting in a decrease in the amount of active sites in the material.

It is very probable that the structure of the fibrous material Tyvek as well as the hydrophobicity of the material is the key to the low wettability of this surface in beer, as compared to other surfaces. As a result, the foaming behaviour is stable over longer periods of wetting. Presumably, the active sites in Tyvek are type II and type III cavities: during extensive wetting the type I sites are presumably deactivated, leaving type II and type III cavities for the formation of bubbles.

As the amount of active sites is increased, more bubbles per unit time can be formed in gas-supersaturated solutions. The foam formed from the Tyvek material was found to be of a rather coarse nature, probably due to the wide distribution of voids available as active sites. Wetting of the largest cavities situated at the external surface reduced the coarseness of the foam considerably. Hence, an active surface with a more homogeneous distribution of cavities (or fibres) should probably be a more ideal active surface than Tyvek.

The bubble size distribution measured by Image Analysis was compared to the bubble size distribution measured by Foam Analysis in chapter 7. The bubbles rising through the liquid were found to be much more uniform in size than when they are situated in a foam layer. It is clear that the disproportionation process is very fast once the bubbles are closely packed in the foam layer.

Last but not least, a prediction was made of the amount of foam that could be produced from a piece of Tyvek material when submerged in beer with a certain excess concentration. For the initial foam formation this is found to be a reasonable estimate, but as soon as the excess concentration is depleted to a certain extent, or as soon as the foam starts to destabilise in some way, very large errors can be made. It can therefore only be used as a tool to roughly compare different active surfaces.

References

Binas: Informatieboek vwo-havo voor onderwijs in de natuurwetenschappen (1977), Wolters-Noordhof Groningen.

Bisperink, C. G. J. and Prins, A. (1994) Bubble growth in carbonated liquids *Colloids and Surfaces A: Physicochemical and Engineering Aspects* **85**, 237-253.

Bankoff, S.G. (1958) Entrapment of Gas in the Spreading of a Liquid Over a Rough Surface *A.I.Ch.E. 4* (1), 24-26.

Cole, R. (1974) Boiling Nucleation , in *Advances in Heat Transfer 10*, Hartnett, J.P and Irvine, T.F. Jr. (eds), Academic Press, New York, 85-166.

Good, R.J. (1992) Contact angle, wetting and adhesion: a critical review *J. Adhesion Sci. Technol.* **6** (12), 1269-1302.

Hey, M.J., Hilton, A.M. and Bee, R.D. (1994) The Formation of Gas Bubbles at Submerged Orifices *A.I.Ch.E. Journal* **5** (3), 319-324.

Linsen, B.G. and van den Heuvel, A. (1967) Pore Structures, in *The Solid-Gas Interface vol 2*, E.A. Flood (ed), Marcel Dekker Inc. New York, 1025-1053.

Lubetkin, S.D. (1989) The Nucleation and Detachment of Bubbles *J. Chem Soc., Faraday Trans. 1* **85** (7), 1753-1764.

Lyklema, J.(1995) Adsorption at the gas-liquid interface, in *Fundamentals of Interface and Colloid Science, vol II: Solid-Liquid Interfaces* Academic Press, San Diego, 1.1-1.118.

Princen, H.M. (1992) Capillary pressure behavior in pores with curved triangular cross-section: effect of wettability and pore size distribution *Colloids and Surfaces* **65**, 221-330.

Ryan, W.L. and Hemmingsen, E.A. (1993) Bubble Formation in Water at Smooth Hydrophobic Surfaces *J. Colloid Interface Sci.* **157** , 312-317.

Schwartz, A.M. (1969) Capillarity, Theory and Practice *Industrial and Engineering Chemistry* **61** (1), 10-21.

Wang, C.H. and Dhir, V.K. (1993) Effect of Surface Wettability on Active Nucleation Site Density During Pool Boiling of Water on a Vertical Surface *Journal of Heat Transfer* **115**, 659-669.

Yu, M.-C. and Middleman, S. (1993) Air entrapment during liquid infiltration of porous media *Chem. Eng. Comm.* **123**, 61-69.

Appendix VI.1

In the weighing method the volume percentage gas in the Tyvek sample as a function of time is calculated as follows: We estimated that the gas volume fraction of a dry Tyvek sample would be about 50-55 vol% with the following equation:

$$\text{Vol\% gas} = \frac{V_g^{\text{dry}}}{V_T^{\text{dry}}} \times 100\% \quad (\text{VI.1})$$

where V_g^{dry} , V_T^{dry} are, respectively, the volume of gas in the dry sample before immersion and the volume of the total Tyvek sample (including polyethylene and gas). For the gas content in the immersed state, V_g^{dry} is replaced by V_g^{wet} . This value is found with the following measurements and calculations.

We first measured the gas volume of Tyvek by weighing a sample in air ($M_T^{\text{dry}} = \rho_{\text{p.e.}} V_T^{\text{dry}}$) and submerged in water (M_T^{wet}). According to the law of Archimedes for the buoyancy, and neglecting the mass of air, the weight of a Tyvek sample submerged in a liquid will be:

$$M_T^{\text{wet}} = M_T^{\text{dry}} - (V_T^{\text{dry}} + V_g^{\text{wet}}) * \rho_l \quad (\text{VI.2})$$

where ρ_l is the liquid density and

$$V_T^{\text{dry}} = \frac{M_T^{\text{dry}}}{\rho_T} \quad (\text{VI.3})$$

so that equation (VI.2) becomes:

$$M_T^{\text{dry}} - M_T^{\text{wet}} = \rho_l * \left(\frac{M_T^{\text{dry}}}{\rho_T} - V_g^{\text{wet}} \right) \quad (\text{VI.4})$$

where ρ_T is the density of Tyvek (average of $\rho_{\text{p.e.}}$ and ρ_g , following from the volume fraction). From equation (VI.4) we find for the gas volume in a wetted sample:

$$V_g^{\text{wet}} = \left[M_T^{\text{dry}} * \left(\frac{1}{\rho_l} - \frac{1}{\rho_T} \right) \right] - \left[M_T^{\text{wet}} * \frac{1}{\rho_l} \right] \quad (\text{VI.5})$$

The densities of gas, polyethylene (high density) and water were found in literature to be $\rho_g = 1.29 \text{ kg/m}^3$, $\rho_{\text{p.e.}} = 930 \text{ kg/m}^3$, $\rho_{\text{water}} = 998 \text{ kg/m}^3$ (Binas). For the density of Tyvek we took 440 kg/m^3 as a good estimate (see section 6.3.2).

From the vol% in equation VI.1 we can calculate the degree of wetting (D.W.) with the following equation, roughly assuming a 50 vol% gas (should be 47%) content before immersion (dry):

$$D.W. = \frac{50 - \text{vol}\%}{50} * 100\% \quad (\text{VI.6})$$

A D.W. of 0 % means that no liquid has penetrated into the material, whereas a D.W. of 100% means that all the gas is removed from the sample by liquid wetting.

FOAM FORMATION ON TYVEK MATERIAL

7.1 Introduction

In the previous chapter, Tyvek was characterised to be a heterogeneous material containing pores at a total amount of 50 vol%, which act as active sites in the bubble formation in gas-supersaturated solutions. A pre-wetting treatment was necessary to avoid formation of very large bubbles. This way, the foam formed from a sample of Tyvek in beer was relatively stable.

In this chapter, the foam formation from Tyvek in gas-supersaturated solutions is studied in some detail. A standard experiment was developed where the active surface was immersed in the supersaturated solution while keeping the system under pressure. After an equilibration time, the pressure is released and the foam formation from the active surface is recorded as a function of time. Various researchers have investigated the stability of foam once formed (Bhandola *et al.* (1989), Jeelani *et al.* (1990), Bisperink *et al.* (1992a and b), Ronteltap (1989)). The rate of foam formation, however, is not a phenomenon widely studied.

The definition of foam properties can be mainly divided into two parts; foaming ability (foamability) and foam stability; the ability to foam is usually influenced by the type and amount of surfactant in the liquid and the foaming action (for example whipping or gas injection). In our system, the amount and nature of the active sites play an important role, as well as the concentration of supersaturated gas (see chapter 2). Foam stability is influenced by a more than one factors, such as the initial bubble size distribution, the stability of the liquid films between bubbles, the rate of drainage, coalescence and disproportionation (see chapter 2). In our case a further influence is found in the foam formation rate, which can vary for different gas concentrations, temperatures and is also influenced by the amount of active sites in the active surface.

From the foaming measurements, an attempt was made to quantify the factors that cause a head of foam to be formed from an active surface in a gas supersaturated liquid. The bubble size distributions were measured as a function of time with the Foam Analyser; a method by which the measurements can be performed as a function of time without destroying the foam layer. However, different parts of the foam are measured at the different time intervals as a precaution, and therefore the foam must be homogeneous by nature in order to differentiate between similar samples. Unfortunately, the foams were found to be comparatively heterogeneous and the bubble size distributions were not reproducible enough to see differences in bubble size distributions. The effect of

disproportionation and coalescence on the foam stability, although visibly apparent, could therefore not be quantified for the different Tyvek samples used.

This chapter will therefore concentrate on initial foam properties (less than three minutes), where mechanisms such as coalescence and disproportionation have not yet greatly influenced the build-up of the foam. In the relatively short time scale of the foam formation, the most important effect was found to be the initial foam height and the rate of drainage.

Variations in the size and shape of the active surface were found to be able to influence the amount of foam formed and thus also some of the initial foam properties. An increase in the concentration of the supersaturated gas in the liquid (by changing the pressure or temperature) was found, not only to increase the amount of foam formed as would be expected, but also to influence the formation rate and the drainage rate of the foam. Furthermore, changing the shape of the Tyvek sample could influence liquid convection patterns, as well as inducing local depletion of the gas content in the liquid. However, these effects had but a small effect on the foam formation rate at the conditions used here.

7.2 Literature

Gas-supersaturated solutions can foam by inserting an active surface into the liquid. The amount and quality of foam produced depends on certain controllable factors such as the gas concentration, pressure and temperature, but also on the "foam-activeness" of the active surface, as shown in the previous chapter. At the relatively low carbon dioxide supersaturation level used here (ca 5 g/kg), bubbles can only be formed (without agitation) from surfaces in which gas-filled cavities are present. The gas volume in the cavities grows by diffusional gas transport from the supersaturated bulk liquid until it detaches as a bubble from the active surface, rises to the liquid surface and finally forms a part of the foam (see also chapter 3).

In foams comprising carbon dioxide bubbles, small bubbles ($d = 0.5 - 1 \text{ mm}$) in a narrow size distribution are favoured because small bubbles are less sensitive to coalescence (from spreading of lipids and other foam destabilisers) and because a narrow bubble size distribution is less sensitive to disproportionation (Ronteltap, 1989). In theory, both these properties should result in a higher stability of the foam. However, the carbon dioxide gas is highly soluble in aqueous solutions and can diffuse very rapidly across liquid films. If the foam has both larger and smaller bubbles, it will be prone to a faster disproportionation process than when the bubble size distribution is narrow.

In most literature not the formation of the foam, but the decay of foam, is studied. Therefore, articles dealing with foaming are mostly concerned with destabilising effects such as liquid drainage, bubble disproportionation and coalescence (Ronteltap, 1989;

Bisperink *et al.*, 1992a; Bisperink *et al.*, 1992b; Bhandola *et al.*, 1989; Bhakta and Khilar, 1991; Desai and Kumar, 1983; Narsimhan, 1990).

In the foam formation on active surfaces from supersaturated solutions, bubbles are formed during a somewhat longer time than when sparging or agitation is used. After the process of agitation or sparging, the time is set at zero, after which the foam collapse is observed. The time taken for the formation of the foam can in these cases be controlled by changing the rate of agitation or setting the gas flow through the orifice. In our situation, however, the formation rate of the foam depends on the gas concentration, the amount of active sites and of time, and has therefore become a measuring parameter.

In order to avoid foam destabilising effects of drainage, disproportionation and coalescence interfering with the measurements of the foaming rate, a short time scale is used over which foam formation is observed (less than three minutes). In this time, however, already some unavoidable collapse of foam takes place. In our experiments, due to non-constant foam heights and foam rates, it was not possible to compare the drainage and collapse rates.

From literature, it is known that the sparging rate or foaming rate could influence the drainage of the liquid from the foam where a greater velocity of gas results in the entrainment of more liquid into the foam, and therefore in a larger drainage rate (Desai and Kunar, 1983). Confirming this is the result of Narsimhan (1990), where a larger foam head is observed to induce a larger initial drainage rate.

Moreover, the bubble size distribution can greatly affect the stability of the foam. A foam with a wide bubble size distribution drains slowly compared to a foam with a narrow bubble size distribution, but the absolute bubble size also plays a role. A foam containing small bubbles has a larger total bubble surface area, which give more resistance to the drainage of liquid. Furthermore the Laplace suction in plateau borders of newly meeting meeting bubbles is larger, which holds more liquid in the foam, and also slows drainage. The effect on disproportionation is such that the higher Laplace pressure in the gas phase increases the driving force for gas diffusion from small bubbles to larger bubbles (Ronteltap, 1989).

Since the foam formation from an active surface in gas-supersaturated liquids can take a relatively long time, destabilisation processes can attack the first top layer of bubbles before the second layer is formed and so on. This means that apart from having a distribution of bubble sizes due to the properties of the active surface, there is also a gradient in bubble sizes from the top to the bottom of the foam layer. This can range from very fine foam at the bottom to very coarse bubbles at the top. This makes the analysis of the foam stability even more difficult.

In this light the foam formation on active surfaces is measured as the foam height as a function of time, without observing the stability of the foam in great detail.

Literature concerned with investigations of foam formation from supersaturated solutions is very limited. Bhandola *et al.* (1989) looked at beer foam decay after a

standardised pouring method, modelling foam height and gas hold-up with time during foam collapse. The only destabilisation processes taken into account are coalescence and drainage. The initial foam height is derived as a function of temperature and pouring height, at similar supersaturations as used in this work. Lowering the temperature of the solution was found to decrease the foam height by about 20% going from 20°C to 10°C, and by 5% going from 10°C to 5°C. We found decreases of 50 to 75% in foam height lowering the temperature from 20°C to 10°C, depending on the area of active surface. In our work, not only the amount of foam but also the rate of the foam formation was found to decrease with temperature. Our results could therefore not really be compared to Bandhola's work.

Similarly, Jeelani *et al.* (1990) investigated the foam formed during agitation of supersaturated solutions, as a gas desorption process. In their model, again only coalescence and drainage are allowed for. However, the approach used in this article is somewhat similar to the one used in our work, be it that the supersaturation at which the foam was formed was much lower. Moreover, the foam was formed on uncontrolled surfaces during agitation of the liquid, which resulted in a faster and more constant bubble formation rate than used in our experiments. Unfortunately, the authors did not show the dependence of the foam formation rate on the rate of agitation, and the amount of foam did not seem to depend on the initial gas content, such as we found. This could, of course, also be a result of the small differences in gas content used (158 and 174 ml CO₂ gas, compared to 936 and 631 ml in our work). In any case, the rapid form of agitation kept the liquid well mixed so that diffusional gas transport was probably of lesser importance (see paragraph 7.5).

Most importantly, the Jeelani *et al.* noted a foam collapse of 3 cm within the first 3 minutes, which, according to the authors, was a result of coalescence and drainage. In our work we assume no decay takes place within the first three minutes. Whether or not we should take this collapse into consideration is subject to discussion. At least very good care was taken with cleaning of the measuring vessel to avoid coalescence and with keeping a carbon dioxide blanket above the foam to avoid rapid disproportionation.

7.3 Experimental

7.3.1 Methods

Beer equilibration with Foam Generator

The foaming experiments with Tyvek were performed in supersaturated beer in order to have a measurable foam of reasonable stability. In order to be able to create a reference beer of controlled carbon dioxide content (see figure 7.1), the Foam Generator (F.G.) was developed. The F.G. consists of a closed system in which beer or any other

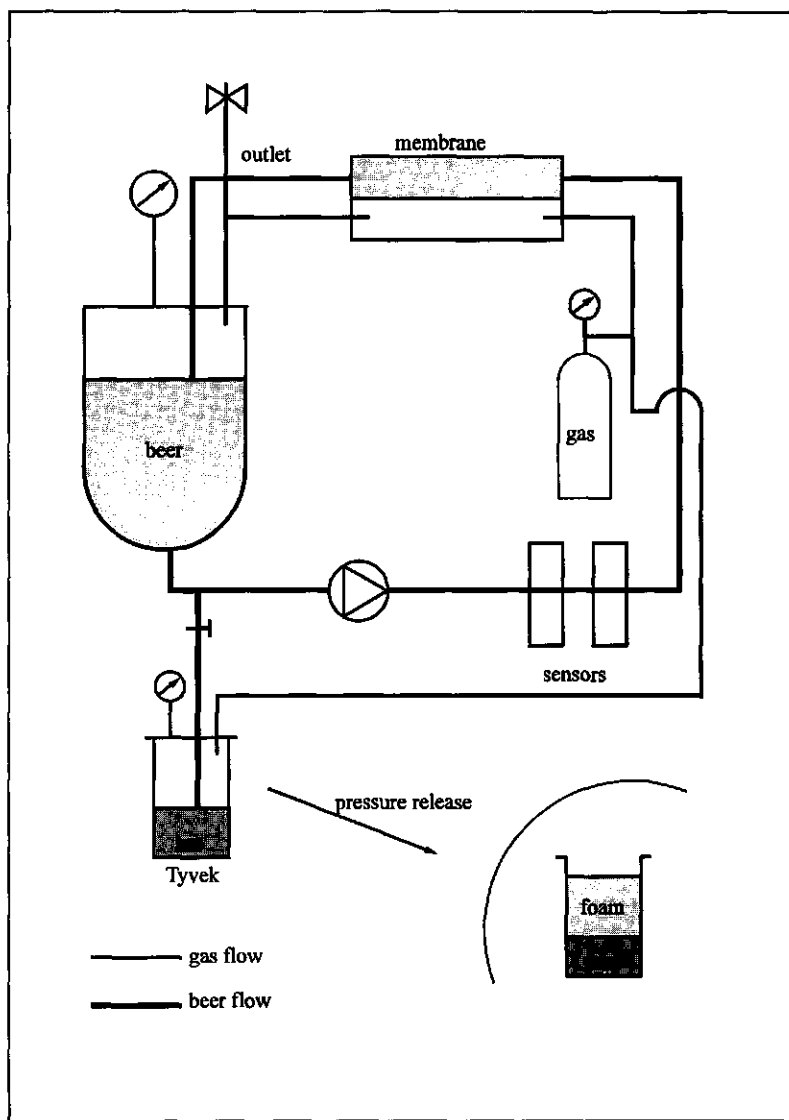


Figure 7.1 Diagram of the Foam Generator.

aqueous system is pumped (membrane pump Prominent Vario, Germany) along a gas-liquid membrane (Liqui-cel 5PCM-102, Hoechst Celanese, Germany) to equilibrate with a given gas. Both pressure and temperature can be set at certain values, resulting in a predictable supersaturation of gas in the liquid (see chapter 2). The carbon dioxide and nitrogen contents are monitored on line with two sensors (Orbisphere, Woerden), that are placed between the pump and the membrane. The whole system can be thermostated with an accuracy of 0.1°C.

One of the advantages of the use of a membrane system is that only a minimum amount of foam is produced in the beer during equilibration with gas. Other methods such as sparging result in the formation of foam and possible loss of surface active material from the liquid.

The membrane used to equilibrate the beer with a given gas consists of two chambers divided by a hydrophobic polypropylene hollow fibre membrane of large contact area (1 m^2). The gas liquid interface is situated inside the micro-pores in the membrane fibres. Due to the non-wetting properties of the membrane the Laplace pressure difference prevents the liquid from entering the gas chamber. The gas is prevented from entering the liquid chamber by a small hydrostatic pressure difference. The rate of gas transfer depends largely on the condition that the liquid and the gas phase stay in their separate chambers. One of the problems encountered is that beer eventually wets the pores and leaks into the gas chamber. This can be prevented by cleaning the membrane with 1 M NaOH after each run, rinsing thoroughly and making sure the membrane is completely clean and dry before repeated use.

When the beer has passed the membrane a number of times, the system is equilibrated as the carbon dioxide content becomes constant. Samples of 400 ml, 500 ml or 600 ml beer are sampled for each foaming experiment. The beer is sampled under pressure into a thermostated container containing an active surface. After the transfer, the beer is equilibrated under pressure for 10 minutes, to allow the foam formed during the transfer to collapse. When the pressure on the container is released with a valve of 1 cm diameter, the gas in the liquid supersaturates and bubbles start to form on the active surface and rise to form a foam layer. This is shown schematically in figure 7.3.

The absolute carbon dioxide concentrations used in the experiments are (a) 6.0 g/kg at 20°C, (b) 6.0 g/kg at 10°C and (c) 4.4 g/kg at 20°C. The saturation concentration c_s of carbon dioxide gas in beer is 1.41 g/kg at 23°C, whereas it is 2.22 g/kg at 10°C (see also chapter 2). In order to compare these three different systems, we calculated the excess concentration c_e with the following equation

$$c_e = c_s (\text{equilibration P,T}) - c_s (\text{measurement P,T})$$

With this calculation, the three supersaturated systems have an excess concentration of (a) C1 = 4.6 g/kg, (b) C2 = 3.8 g/kg and (c) C3 = 3.1 g/kg.

The bubble size distribution

The bubble size distribution in liquid foams measured as a function of time can be used to distinguish between the physical processes that determine the breakdown of foams. A piece of equipment called the Foam Analyser, based on an optical fibre technique (Bisperink *et al.*, 1992a and Bisperink *et al.*, 1992b), was used to measure various foam characteristics e.g. the rate of drainage, the rate of foam collapse, the change in gas

Foam Analyzer

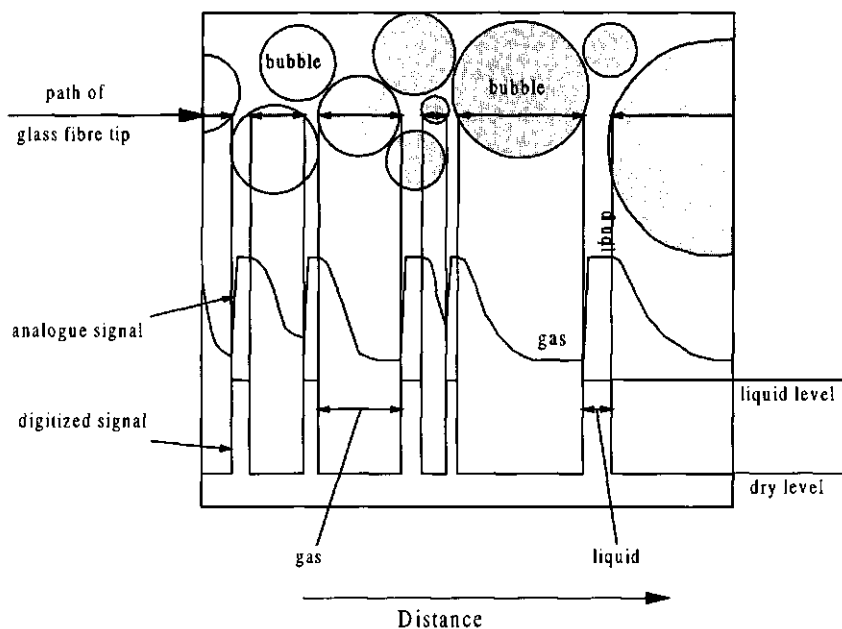
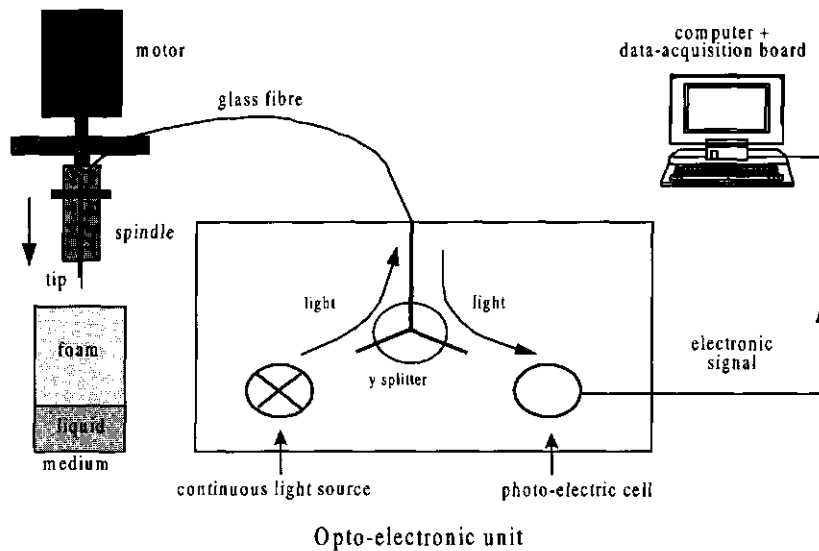


Figure 7.2 Diagram of the Foam Analyser. The top diagram shows a sketch of the whole system, the bottom diagram shows how the analogue signal is obtained and converted to a digital one.

fraction, inter-bubble gas diffusion (disproportionation) and the evolution of the bubble size distribution during the ageing of the foam.

Figure 7.2 shows a schematic drawing of the Foam Analyser (F.A.). A mechanical part is used to move the glass fibre downwards through a foam at a known speed and an opto-electronic part which consists of the optical fibre probe and electronic equipment for signal conversion, data-acquisition and data processing. From the opto-electronic unit, light is sent to the tip of the fibre, where most light is emitted. A part, however, reflects back to the opto-electronic unit. The amount of reflected light depends on the refractive index of the medium surrounding the tip. A medium which has a refractive index close to that of the glass reflects almost no light, whereas a medium of much lower refractive index such as air reflects a considerable amount of light. In this way, a probe travelling through a foam can distinguish between the gas and the liquid phase. At a known sampling rate (frequency is 1 MHz) and with a known downward velocity (ca. 10 cm/s) the signal is sampled every 0.1 μ m and distances between liquid films can be measured. The references given above give a more detailed description of the method.

Foam height measurement with video camera

Measurements with the F.A. are useful if the foam is readily formed. In our case one of the important measuring parameters is the rate of foam formation. In order to be able to register the initial foam formation rate, the foam height was recorded as a function of time with a video camera (Sony CCD V90E). The position of both the top and the bottom of the foam layer were recorded during time. Zero time was taken at the moment of pressure release. Figure 7.3 shows (a) the container before pressure release where L_0 is the initial liquid height, and (b) after pressure release. $H(t)$ is the total height, $L(t)$ is the liquid height in time. $H(t) - L(t)$ is the foam height at time t . The gas height is the increase in total height $H(t)$ from $t=0$ or, $H(t) - L_0$. The foam height subtracted by the gas height gives the amount of liquid in the foam, or the wetness of the foam. The gas height can also be seen as the amount of gas that the Tyvek is able to "release" from the supersaturated liquid. From the initial carbon dioxide content in the supersaturated liquid, the decrease of the gas content in liquid could be quantified and an analysis of the foam formation rate constant could be made, as will be shown in paragraph 7.4.3.

The data resulting from the foaming experiments were calculated to a gas volume, using the initial carbon dioxide content to scale with:

$$N_0 = c_e V \rho_l \quad (7.1)$$

where N_0 is the initial CO_2 content (g) of the beer, c_e is the excess carbon dioxide concentration in g/kg, V is the volume of beer (m^3) and ρ_l is the liquid density (kg/m^3). The absolute amount of CO_2 released from the liquid, $N(t)$ (g), resulting in the foam formation as a function of time, is then:

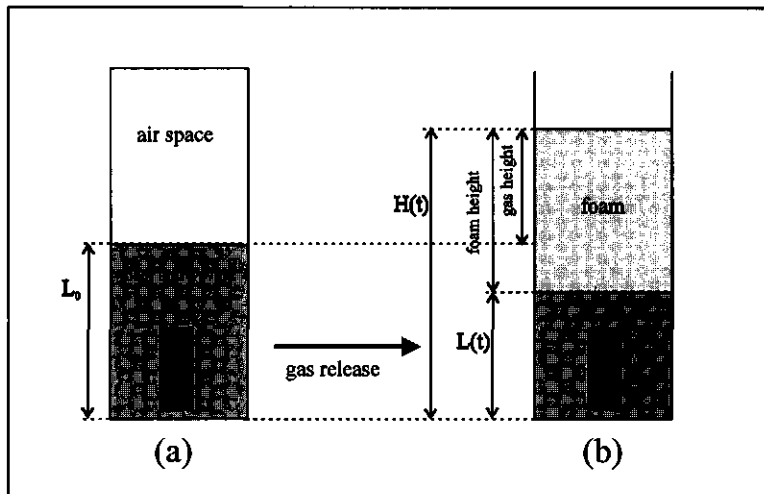


Figure 7.3 Diagram of the measurement of the foam height and gas height. L_0 is the initial liquid level, and $H(t)$ is the total height of foam and liquid. $[H(t) - L(t)]$ gives the foam height, whereas $[H(t) - L_0]$ gives the gas height.

$$N(t) = \left(\frac{(H(t) - L_0)A}{V_{CO_2}^m(T, P)} \right) * m_{CO_2} \quad (7.2)$$

where $H(t)$ is the total height of the liquid and the foam (m), L_0 is the initial liquid height before foam formation (m), A is the cross-sectional area of the vessel (m^2), $V_{CO_2}^m$ is the molar volume of the gas (m^3/mol) and m_{CO_2} is molecular weight of the gas (g/mol).

The relative amount of gas used for the formation of bubbles is defined as the gas yield:

$$Yield = \frac{N(t)}{N_0} \quad (7.3)$$

and the amount of CO_2 left in the liquid, N (g), as a function of time is then:

$$N = N_0 - N(t) \quad (7.4)$$

This way, we can calculate how much of the gas present in the liquid is released towards the formation of foam, and at which rate. Depending on the area and shape of the active surface and the initial gas content, the efficiency of the active surface can be calculated, and so the optimal surface area (shape and size), for a given amount of foam, can be selected.

Measuring procedure of beer foam produced by Tyvek material

The Tyvek samples were cut out and folded from supplied A4 sheets. The samples were pierced through with thin stainless steel needles in order to mould the samples into the desired shapes. The steel rods were also used to attach weights to, in order to prevent the samples from floating around in the liquid during measurements (see figure 7.4).

The samples were treated with alcohol before use, which is a liquid, known from earlier wetting experiments in chapter 6 to penetrate well into the porous material. The samples were then dried in a stove at 40°C and wetted for 2 days at 23°C in double distilled water. This was done in order to create reproducible wetting characteristics of the Tyvek material and a narrow bubble size distribution (see also chapter 6).

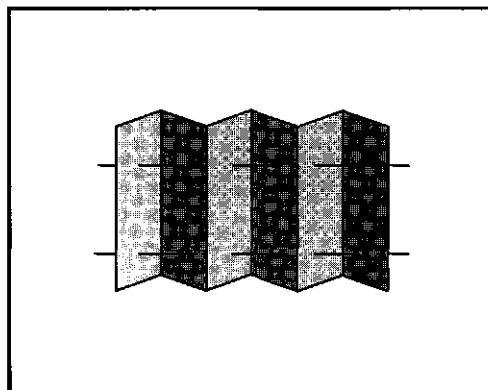


Figure 7.4 Schematic presentation of a Tyvek sample held into shape by two stainless steel rods.

The foaming vessel was wetted with beer during at least one week in order to remove all possible “parasitic” sites from the walls and the bottom of the vessel. After a cleaning procedure the vessel was kept wet at all times. With the Foam Generator, beer was equilibrated with CO₂ gas (Hoekloos, technical) at known pressure and temperature. Samples of 400 ml beer were transferred under pressure into the thermostated foaming vessel containing a Tyvek sample. The foam heights are recorded on video from the moment of pressure release for 3 minutes. The bubble size distribution of the foam was measured with the Foam Analyser 1 and 3 minutes after gas release and compared with tap beer.

7.3.2 Materials

Manipulation of Tyvek material

The Tyvek samples were manipulated in various ways. We first discovered that the surface should be held in an upright position in order to create symmetry of the bubble sizes produced on either side of the surface. Placing the surface horizontally resulted in the production of relatively fine bubbles at the top and of very large bubbles trapped underneath the surface. When these large bubbles ($R > 1$ mm) join the foam layer, they can seriously destabilise the foam as a result of disproportionation with smaller bubbles.

In chapter 4, we have shown that bubbles growing from a horizontally positioned cavity (which is a vertically positioned surface) detach at an earlier stage than bubbles formed at a vertically positioned active site, and are therefore smaller in size. Together, these observations led to the vertical positioning of the surface.

Figure 7.5 shows schematically which variations of Tyvek samples were used in the foaming measurements. The area of the Tyvek samples was varied between 1 and 36 cm^2 . This range was chosen due to the limiting foam height that can be measured with the foam analyser. A larger area of Tyvek material produced more than 10 cm of foam at the highest gas concentration.

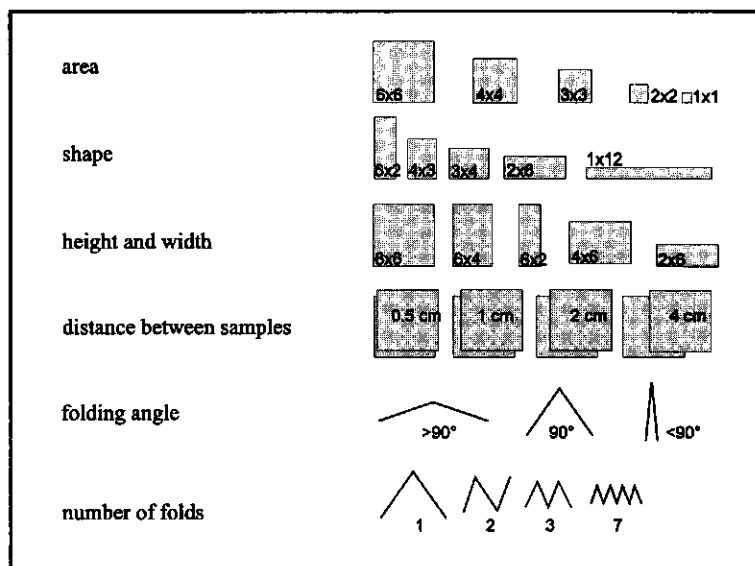


Figure 7.5 Diagram of the shapes and sizes the Tyvek samples used in the foaming experiments.

By changing the surface area, the height h and width w of the samples naturally changed. We therefore also tested the influence of height and width and shape by using samples of 12 and 24 cm² standing up or lying sideways. A third variety was the distance between two samples of equal size, the angle of folding, and the amount of folds in the surface.

Beer volume

Apart from varying the bulk concentration of CO₂ in beer, one experiment was done in order to vary the total amount of CO₂ available in the solution, without changing the driving force of gas transport or supersaturation ratio. This was achieved by varying the volume of beer in the foaming vessel. Apart from 400 ml, foaming was also performed with 500 ml and with 600 ml.

7.4 Results & Discussion

7.4.1 Bubble size distribution

Figures 7.6(a) and (b) show the bubble size distributions of beer foam acquired by foaming with a tap dispenser as well as by foaming with a piece of active Tyvek surface. Fig 7.6(a) shows the bubble size distributions measured with the Foam Analyser based on the percentage surface area of the amount of bubbles per class, 60 seconds after the onset of foam formation, and figure 7.6(b) shows the bubble size distributions, as measured after 180 seconds.

The bubble size distribution measured with Image Analysis in the previous chapter has a maximum (recalculated in surface percentages) at the same bubble size, but a narrower bubble size distribution was found. Presumably this is because only a small amount of bubbles were analysed, furthermore, the bubbles rising in a liquid have not had the chance to coalesce etc, which is the case when the bubble is in a foam.

The bubble size distributions shown in figure 7.6 are originally histograms divided into 36 classes. It must be noted that the largest class also includes bubbles larger than $d = 1.8$ mm, whereas the smallest class does not include bubbles smaller than 25 μm , as this is the lowest range of detection. Furthermore, the curves give a false impression of a continuous distribution, which is not true as the distribution is measured as a histogram. Presenting the distribution into 36 classes would give a more realistic impression of the foam. However, from experience it is known that the presentation in 6 classes, as shown in figure 7.6, gives a good impression of differences between the different foams.

As can be seen the beer foam is naturally heterogeneous with a relatively wide bubble size distribution. The (average) bubble size distribution found in a foam which was formed with Tyvek (6x6 cm, C1) shows that it is as wide as tapped beer. There is,

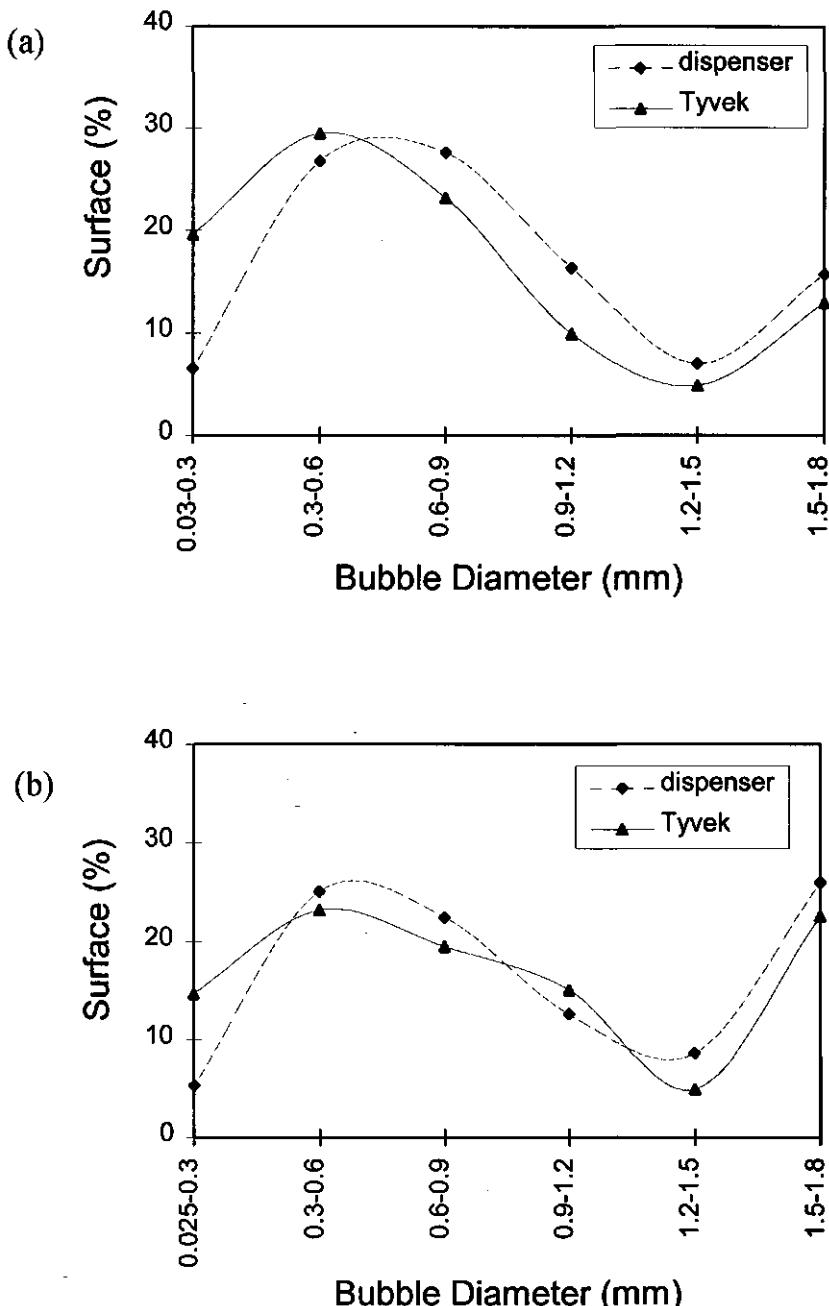


Figure 7.6 Bubble size distribution in beer foam produced with a keg dispenser and with Tyvek, (a) 60 seconds after foam formation and (b) 180 seconds after foam formation.

however, a larger percentage surface area of bubbles in the smallest class. After 180 seconds (figure 7.6(b)), the distribution of the Tyvek foam has become wider than normally measured in tapped beer, suggesting a larger degree of coarsening in the foam. This could be partly due to the fact that a larger number of small bubbles can increase the disproportionation process. However, considering that the foam layer formed with Tyvek is at least 10 cm high whereas a normal head on a tapped beer is no more than 4 to 5 cm high, it is possible that the difference in hydrostatic pressure could play a role in the drainage rate. Such an increase in the drainage would lead to a faster rate of disproportionation as well as coalescence. Moreover, the Tyvek head is formed rather slowly compared to tap dispense, and the foam layer is continuously re-supplied with small bubbles. This last factor could be an additional reason for the presence of a large number of small bubbles after three minutes.

Concluding, the bubble size distribution gives an indication of the good comparison found between the initial Tyvek foam and a normal tapped beer. Foam stability of the two foams, however, cannot be compared so easily, due to the continuous accumulation of small bubbles in the foam and because of the difference in the foam height, which can have a large influence on the rate of drainage, as found from literature.

7.4.2 Effect of Tyvek manipulation

The Tyvek samples that were used in the foaming experiments are organised into 5 categories: area, shape, height and width, distance between samples and folding, all of which are shown in figure 7.5. In this section a general overview will be given of the results, after which we will attempt to quantify the effects in section 7.4.4.

Area

The area of the Tyvek sample was varied in such a way that a large difference was obtained in the amount of produced foam. In order to vary the area, the samples were cut in square-shapes. The effect of the height and the width of the sample is shown in the next section.

In figure 7.7, the gas yield (see equation (7.3)) is plotted against time for 5 Tyvek samples of increasing area, where the excess gas concentration in beer was $C_1 = 4.6 \text{ g/kg}$. The increase of the Tyvek surface area shows an increase in gas yield, which means that more gas is released from the liquid to produce bubbles at the Tyvek surface. This is not unexpected since a larger Tyvek surface means a larger amount of active sites where bubbles can be formed simultaneously. This of course entails that the liquid will be depleted at a faster rate with the large sample than with the smaller samples. In figure 7.7 the largest area reaches an optimal value after 20 seconds, after which the yield will level off (not shown here). The reason for the optimum is because presumably the total of excess gas content of the liquid has been released as foam. The concentration decreases as the

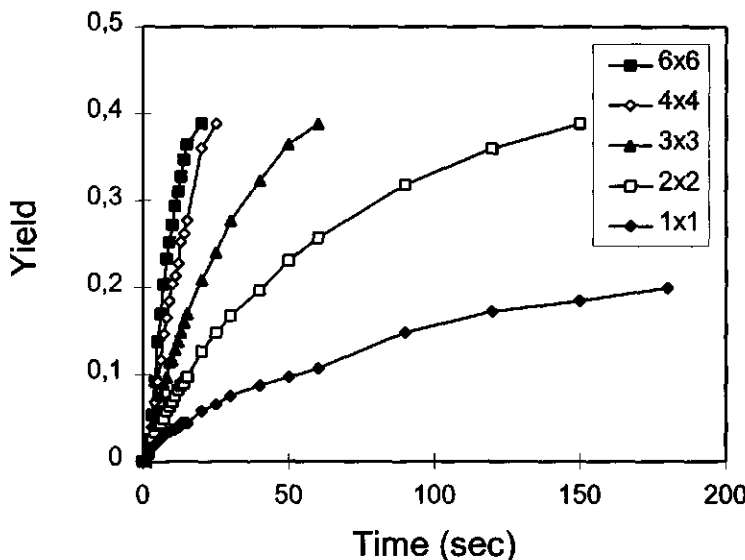


Figure 7.7 Gas yield of various areas (figure 5(a)) of Tyvek, at C1.

Table 7.1 Gas height in cm at $t=180$ seconds for the different Tyvek samples.

$N_0 \rightarrow$	1.84 g	1.24 g	1.52 g
$c_e \rightarrow$	C1 = 4.6 g/kg	C2 = 3.8 g/kg	C3 = 3.1 g/kg
T \rightarrow	20°C	10°C	20°C
6x6	> 8.0 cm	4.3 cm	6.1 cm
4x4	> 8.0 cm	3.8 cm	4.3 cm
3x3	> 8.0 cm	-	-
2x2	8.0 cm	1.1 cm	2.3 cm
1x1	4.1 cm	-	1.0 cm

foam is formed and therefore also the bubble growth rate decreases. This was also found at the other concentrations C2 and C3.

Table 7.1 shows the gas height (in cm) after 180 sec for the three excess concentrations. At lower concentrations, the increase in gas yield is much slower and the total amount of foam after 180 seconds is lower. This result follows the line of explanation

in that, with a lower gas concentration the drive for gas diffusion is lower and the bubbles grow at a slower rate.

From table 7.1, it is seen that at the largest supersaturation C1, the Tyvek samples produce the most foam, at the fastest rates. Moreover, the amount of foam produced depends on the area. With a larger surface area, more bubbles can be formed simultaneously, resulting in a larger foam rate. From figure 7.7, the largest factor in area between sample (6x6) and (1x1) is 36. The initial slope of the curve of sample (6x6) is roughly 12 times larger than the initial slope of the curve of sample (1x1). This means that for these measurements, the initial slope of gas yield is roughly proportional to $A^{0.7}$.

Interestingly, the excess concentration of C2 (larger than C3) produces less foam at a lower foam formation rate than C3. Presumably the supersaturation is now not the only influence on the rate of gas release. The temperature is affecting the diffusion coefficient as well as the liquid viscosity, by which the driving force is naturally decreased, even though the excess concentration is larger. Section 7.4.3 will go into further detail concerning this effect.

Shape

In the previous paragraph the size of the samples was varied without looking at the effect of the shape. Here a Tyvek sample of 12 cm^2 (1 side) was varied in shape, from a height of 1 cm and a width of 12 cm, to a height of 6 cm and a width of 2 cm wide (see figure 7.5). Figure 7.8 shows the effect of this shape factor, for both excess concentrations C1 (full line) and C3 (dotted line). The greatest differences as an effect of the shape are found for the largest concentration, where it is apparent that, as the height of the sample increases (or as the width decreases), the increase in gas yield (or foam formation) is slower.

Although we can only speculate, we believe that the effect found here is caused by local gas depletion. In figure 7.9, the liquid flow that is obtained by the rise of the bubbles to the foam layer is shown schematically. As the liquid flow moves upward, parallel to the vertically positioned sample, the gas flux is horizontal towards the surface where bubbles are formed. It can be argued that a concentration gradient occurs between top and bottom of the active surface. Following this line of argument, a surface with a greater height will cause an effectively larger concentration gradient, and the bubbles formed at the top of the surface will be slower in forming. This effect will be much smaller when the active surface is wide and low.

Unfortunately, it is very difficult to quantify this effect, since we do not know the exact size of the bubbles, the amount of liquid entrained by them, and therefore the velocity of the liquid rising parallel to the surface. This velocity has to be known in order to calculate the time needed for the gas to be depleted, and therefore, to calculate the order of magnitude of this effect. However, making a few assumptions, we can estimate the height at which the liquid is depleted of gas within the correct order of magnitude. In Appendix VII.1, heights in the order of tens of cm's are found at which the volume of

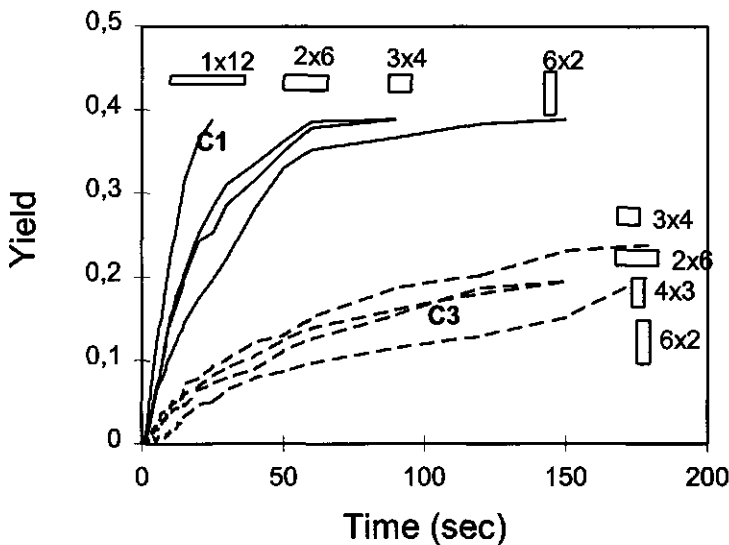


Figure 7.8 Gas yield of various shapes (figure 5(b)) of Tyvek, with an area of 12 cm^2 at C1 (full line) and at C3 (dotted line). The shape corresponding to each curve is shown in the graph.

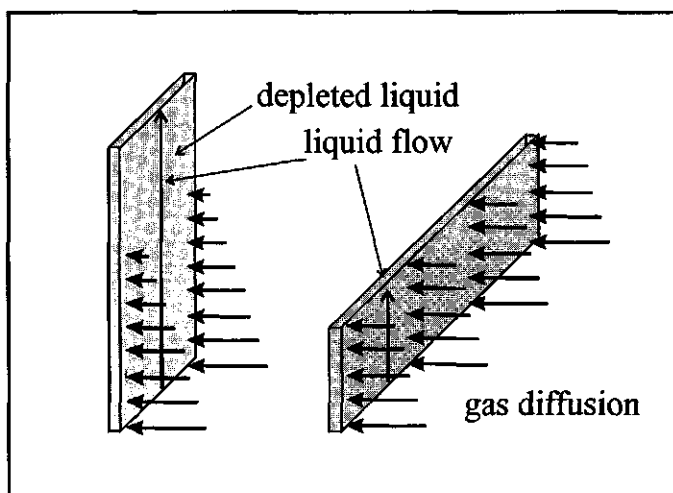


Figure 7.9 Sketch of the liquid flow parallel to the active surface caused by the rise of bubbles. The arrows in horizontal position indicate the driving force of gas transport from liquid to the active surface. After passing a certain height the liquid is depleted of gas and above this point the bubbles formation rate will be much slower.

liquid is completely depleted of the excess gas content, which gives us reason to believe the validity of gas depletion.

Width and height

In the former section, the shape factor was investigated. Here the height and width of Tyvek samples were varied as well as the area. Figure 7.10 shows the gas yield for the different samples, where the full lines represent the short samples (4x6, 2x6 and 1x6) and the dotted lines represent the tall samples (6x6, 6x4, 6x2 and 6x1).

Comparing sample (1x6) with (6x1), the taller sample shows a slower gas yield. The same holds for samples (2x6) and (6x2), as well as for samples (4x6) and (6x4). However, the effect becomes less noticeable as the area is increased, or as the shape becomes a square. Both reasons may be valid, as an increase in area will increase the amount of bubbles formed, and therefore the degree of mixing of the liquid. Less depletion is found to occur when the samples differ less in height, as also found in the previous section.

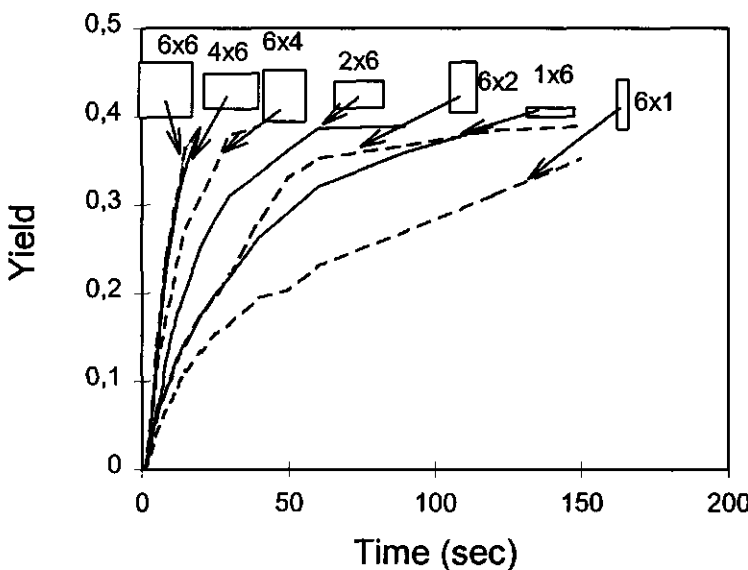


Figure 7.10 Gas yield of various height and width combinations (figure 5(c)) of Tyvek, with various areas ($2 \times 36, 2 \times 24, 2 \times 12, 2 \times 6 \text{ cm}^2$) at C1. The shape corresponding to each curve is shown in the graph, where the dotted curves represent the tall samples and the full curves represent the short samples.

Distance between Tyvek samples and folding

In order to be able to insert larger samples of Tyvek (6x8 cm) into the measuring vessel, the sheets were cut and folded. As we found that the sample shape could influence the foaming characteristics, a check was needed to observe the influence of the folding. To this end, the folding angle was varied roughly between $<90^\circ$, 90° and $>90^\circ$. The folding angle did not give a significant change in foaming properties. Furthermore, the amount of folds (1 to 7) and the distance between two sheets of Tyvek (0.5 to 4 cm) was varied. The amount of folds also showed no effect, except at 7 folds, when the gas yield decreased somewhat and where maybe some of the active sites were shielded off. The distance between the Tyvek sheets did not change the foaming characteristics.

It was expected that folding and changing the distance between samples would affect the liquid movement in such a way that bubble formation would be impeded as a larger portion of the active surface is shielded. However, this expected effect was not found. It must be noted that the experiments in this section were performed using rather large Tyvek samples (6x8), which did cause rather violent foaming. In the previous section, it was observed that the effect of the different shapes became less noticeable as the area of the Tyvek sample increased. It may be that the smaller effects we wanted to observe here were over-shadowed by the large amount of foam formed due to the larger surface area of Tyvek sample used. An effect can be expected to occur when the distance between surfaces is in the order of the bubble size, which was not the case here.

7.4.3 Effect of gas content

Three methods were used by which the gas content was varied: the supersaturation pressure, the temperature of foaming and the volume of supersaturated liquid. In all situations, we made use of the excess concentration, i.e. the concentration of carbon dioxide which does not dissolve at the temperature and pressure of the measurement. This means that a liquid, supersaturated with carbon dioxide at a certain pressure and temperature, will have a larger excess concentration at 20°C than at 10°C . This effectively also means that more foam can be formed in the liquid at 20°C than at 10°C . Furthermore, the saturation pressure can be varied, as well as the volume of liquid used for the foam formation. In the last case, the concentration is not changed (the driving force stays the same), but the total content N increases so that a larger amount of foam can be produced from an active surface.

Figure 7.11(a) and (b) show the decrease of (excess) gas content in the liquid as a function of time calculated from the experimental data with equations (7.1), (7.2) and (7.4). Figure 7.11(a) gives the gas content in the liquid for a Tyvek sample of 2x2, and figure 7.11(b) for a Tyvek sample of 6x6. The full lines are for the experiments performed at 20°C and the dotted lines show results of the measurements at 10°C .

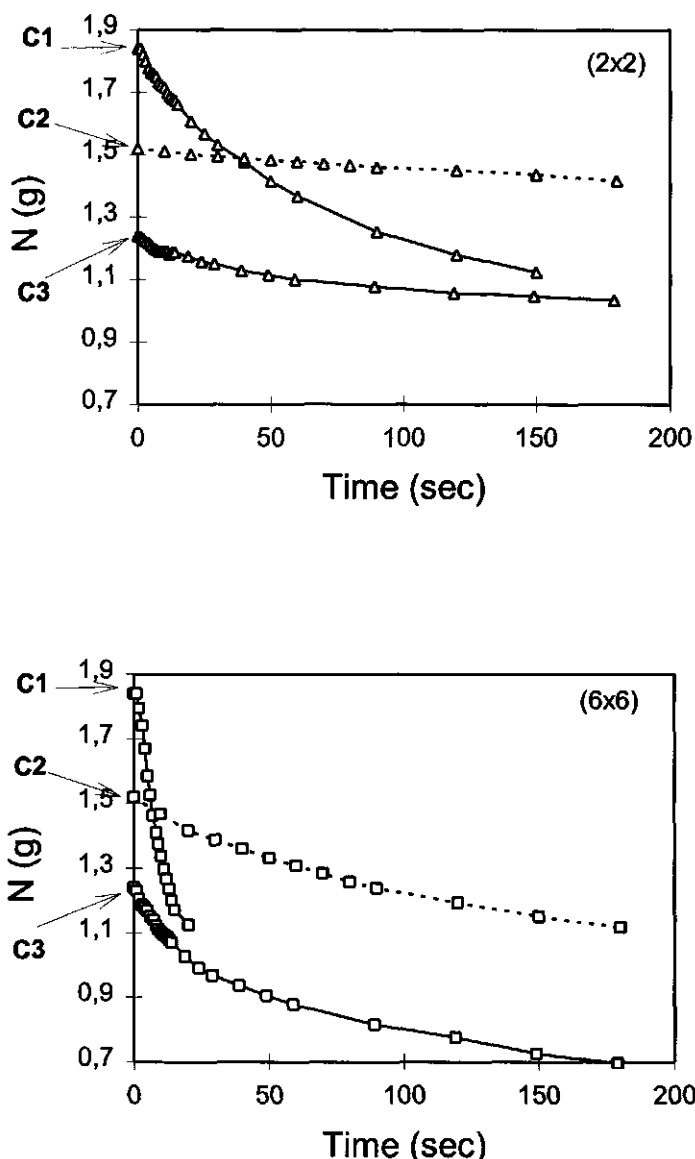


Figure 7.11 Decrease in gas content of the supersaturated liquid as a function of time as a result of the foam formation on two different Tyvek samples (a) for a Tyvek sample 2x2 cm and (b) for a Tyvek sample 6x6 cm. The three initial gas contents are 1.84 g, 1.52 g and 1.24 g which corresponds to the excess concentrations C_1 , C_2 and C_3 . (full lines) 10°C; (dotted line) 20°C.

At 20 °C, the gas content of the liquid decreases to more or less the same value, which differs from the value reached at a temperature of 10°C. Because of this, the curve for C1 passes below C2. The reason for this is that the supersaturation is higher and the saturation concentration is lower for C1. For the larger sample shown in figure 7.11(b), the effect is the same but the decrease in gas content is more rapid. At 10°C (C2), the excess concentration may be higher than with C3, but the foaming and thus the diffusion process is obviously much slower, presumably as a result of the higher liquid viscosity. At a lower temperature, the greater viscosity of the liquid may help to impede the diffusion as well as decrease the convection in the liquid.

Figure 7.12 shows the gas yield of a Tyvek sample (6x8) in different volumes of liquid, containing the same excess concentration, C1. The very fast foaming rates in this experiment (due to large sample area and high excess concentration) made it very difficult to differentiate between the initial foaming rates. It is expected that the initial foam formation rate should be similar for the three liquid volumes, as the driving force (the excess concentration) is the same in all three cases.

However, after a short time, it is clear that the largest amount of foam is formed on the largest volume, and the least amount of foam is formed on the least volume of beer. It is expected that the solutions are equally depleted after 180 seconds, therefore it follows that more foam should be formed in a larger volume of supersaturated liquid.

From these experiments we can conclude that a difference of 10°C in temperature can have a much larger influence on the foam formation in beer than the used differences in excess concentrations. At a larger excess concentration, which is a reasonable gas concentration for a lager beer, but at a lower temperature, the rate of foam formation is considerably reduced.

7.4.4 Quantifying the effect of concentration, Tyvek area and depletion on the foam height formation rate

An attempt was made to quantify the effect of both gas concentration and surface area on the foam formation in supersaturated beer. At a first glance, the foam formation is a first order process: a gas changes from dissolved state to a gaseous phase. The rate is driven by the concentration gradient between the bulk solution and the bubble interface, which depends on the temperature and the saturation, and is limited by the diffusion coefficient. Without the help of the active sites no bubble formation would form, therefore the active surface acts as a “catalyst”. This means that, as long as the gas content is a constant, a first order reaction is expected. It was found however, when fitting the results, that the rate constant is influenced in some way by the concentration. This could very well be due to the convective mixing which occurs in the liquid. An extra effect which we observed was some effect of depletion, as a function of time. We therefore propose the following model which could be applied to the results in this work.

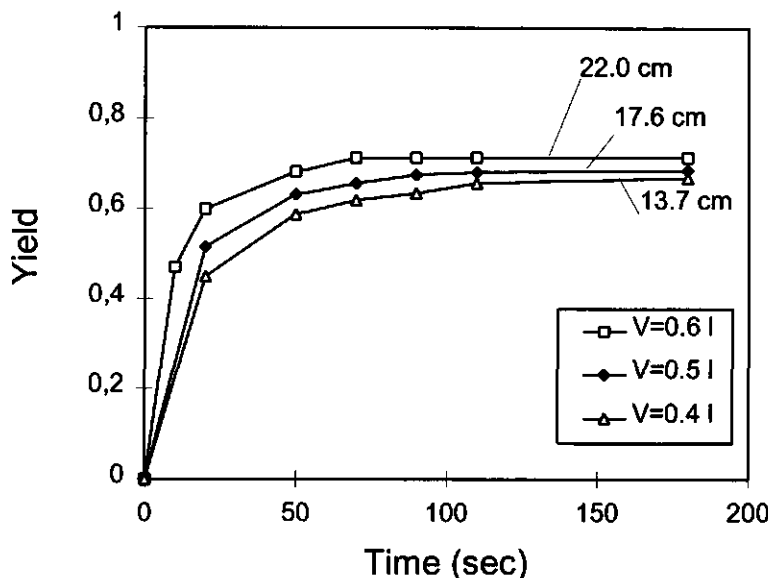


Figure 7.12 Gas yield of a Tyvek sample (6x8 cm) at C1, for three different measuring volumes: 0.4, 0.5 and 0.6 litre beer. The corresponding total initial gas content is 1.84, 2.30 and 2.76 g CO₂. The value shown at the end of each curve is the maximum foam height in the measuring vessel ($H(t) - l(t)$, see figure 7.3).

We start with a second order mechanism, where:

$$-\frac{dN}{dt} = k N^2 \quad (7.5)$$

where N is the CO₂ content in the liquid (g) and k the reaction constant (g⁻¹ s⁻¹).

This gives:

$$1/N = 1/N_0 + k t \quad (7.6)$$

Plotting $1/N$ against t for the linear region of the foam formation, gives plots like the one given in figure 7.13 for C1, where the squares give the measured values and the line is the fitted equation. It is expected that the reaction constant k will be a function of the active surface area A :

$$k = c A^n \quad (7.7)$$

It would be logical for n to be one. At this point, however, the depletion factor has to be taken into account. As discussed in section 7.4.2, the gas depletion is increased when the height is increased. We therefore speculate:

$$k = \alpha \frac{A}{h} \quad (7.8)$$

where α is a constant and h is the height of the sample. Since in this case $A \sim h^2$, equation (7.8) can be rewritten as:

$$k = \alpha A^{0.5} \quad (7.9)$$

The lines shown in figure 7.13 (C1) give the best possible fit when n is taken as 0.65 and $\alpha = 1.10^{-3}$. For C3, reaction constant k is best fitted with $n = 0.65$ and $\alpha = 6.10^{-4}$, and for C2, with $n = 0.65$ and $\alpha = 1.10^{-4}$. This means that for variations in area between 2 and 72 cm^2 , the theory holds quite well, when $n = 0.65$ instead of 0.5; The reason n is found to be a little higher than presumed in equation (7.9) is probably the effect of convective liquid flow. The constant α holds physical parameters such as gas solubility, diffusion coefficient, liquid viscosity and can therefore change with gas content and temperature.

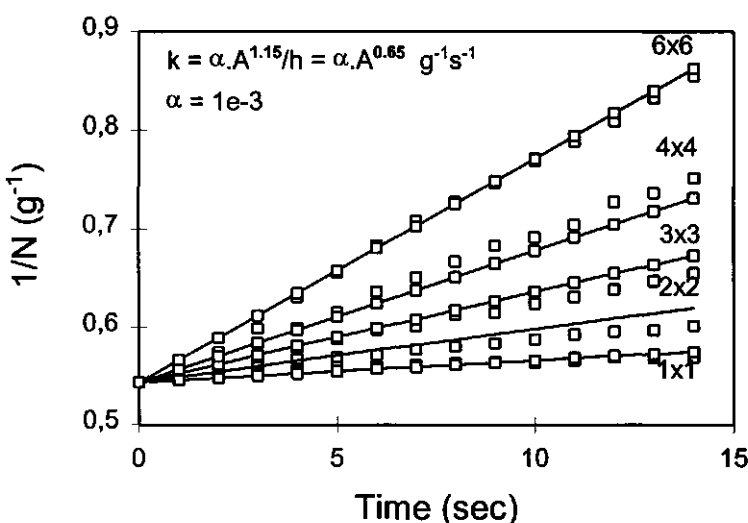


Figure 7.13 The reciprocal gas content of the supersaturated liquid as a function of time as a result of the foam formation on five different Tyvek samples, as given in the graph. The markers show the measured values, whereas the lines are fitted for equation (7.6) and C1.

The fitted values for α show a lower value for C2 than for C3, whereas C2 has a larger gas content. As mentioned earlier, the measuring temperature is probably the main cause for this effect.

The previous exercise was performed, assuming a second order reaction. This is probably not quite accurate, as the kinetics of foam formation will presumably lie somewhere between first and second order. However, further calculation would go beyond the scope of this work, and much more data are necessary to confirm this theoretical approach. In any case it is clear that the gas content is the driving force for the foam formation and that the surface area is a limiting factor for foam formation. Moreover, the temperature decrease from 20°C to 10°C has a very large influence on mass transport, since the rate is found here to be lower even though the gas content is larger. Possibly, n is lower where the temperature is reduced, as less convection takes place, and more depletion. Effects like liquid convection and depletion play a secondary but important factor.

7.5 Conclusions

Foaming by the insertion of an active surface such as Tyvek into a gas-supersaturated solution is found to be very successful. The rate of foam formation as well as the amount of foam produced can be controlled in several ways. By increasing the amount of active sites (by enlarging the area of active surface), the amount of bubbles formed per unit time is increased. By lowering the total amount of available "excess gas", less foam is formed and the rate of bubble formation is reduced. This can be done in several ways: decreasing the concentration, lowering the ambient temperature or by decreasing the volume of the supersaturated liquid.

Different effects are also seen when the shape and size of the sample is varied. Very important is that the samples of Tyvek should be held in a vertical position to ensure that the bubbles detach easily from both sides of the surface with equal size. By increasing the height of the sample in comparison to the width (keeping the total surface area constant), the bubble formation is slowed down obviously due to local depletion of gas from the liquid. With an increase in surface area, the rate of foam formation was increased also. Furthermore, when a larger amount of bubbles are formed per unit time, the liquid could be induced into natural convective flow. This was concluded when the effect of local depletion (due to sample height) became less noticeable at larger surface area. More convection of liquid means the depleted liquid is refreshed continuously and the depletion effect disappears.

We expected that, when the material was folded up, part of the active sites would be shielded from the supersaturated liquid, resulting in a lower rate of foam formation. This expectation, however, was not found in the experiments. It could be speculated that the sample size was too large in these particular experiments.

Concluding, the effect of gas concentration, the amount of active sites (by assuming a constant site density in the surface), the convection and depletion could be fitted with a second order reaction kinetics model. The temperature was found to be of great importance; Although the excess concentration of gas in the liquid was larger in one case than in the other, the rate of foam formation was found to be lower, presumably because the temperature was 10 degrees lower. This lower temperature decreases mass transport by diffusion, and also reduces the viscosity which in turn decreases the convective flow.

References

Beek, W.J. and Mutzall, K.M.K. (eds.) (1975) *Transport Phenomena*, John Wiley and Sons, London.

Bhakta, A.R. and Khilar, K.C. (1991) A network simulation for drainage of static foam columns *Langmuir* 7, 1827-1832.

Bhandola, P.K., Jeelani, S.A.K. and Hartland, S. (1989) Foam Height, Bubble Size and Hold-up in Decaying Gas/Liquid Dispersions *Chem. Biochem. Engng. Q.* 3 (1-2), 1-6.

Bisperink, C.G.J., Ronteltap, A.D. and Prins, A. (1992a) Bubble-size Distributions in Foams *Advances in Colloid and Interface Science* 38, 13-32.

Bisperink, C.G.J., Akkerman, J.C., Prins, A. and Ronteltap, A.D. (1992b) A moving optical fibre technique for structure analysis of heterogeneous products: Application to the determination of the bubble-size distribution in liquid foams *Food Structure* 11, 101-8.

Desai, D. and Kunar, R. (1983) Liquid hold-up in semi-batch cellular foams *Chem. Eng. Sci.* 38 (9), 1525-1543.

Jeelani, S.A.K., Fidi, N. and Hartland, S. (1990) Foam formation during CO₂ desorption from agitated supersaturated aqueous surfactant solutions *Chem. Eng. Sci.* 45 (4), 1043-48.

Narsimhan, G. and Ruckenstein, E. (1986) Effect of Bubble Size Distribution on the Enrichment and Collapse of Foams *Langmuir* 2, 494-508.

Narsimhan, G. (1990) On static drainage of protein stabilised foams, in *Food Polymers, Gels and Colloids*, Dickinson, E. (ed), England, University of Leeds, 207-226.

Ronteltap, A.D. (1989) Beer Foam Physics Ph.D. Thesis, Agricultural University of Wageningen, The Netherlands.

Appendix VII.1

From the results we think that depletion of gas takes place as the liquid travels past the Tyvek sample, entrained by the rise of bubbles to the foam layer. Here we try to estimate the height at which the liquid (with initial gas content, $T=20^\circ\text{C}$ and $P=1 \text{ atm}$) is completely depleted of the excess concentration.

For Fickian diffusion we can formulate a mass balance:

$$\frac{dV}{dt} = \phi A = D \frac{\Delta c}{\Delta x} (b * h) \quad (\text{VII.1})$$

where dV/dt is the volume of gas diffusing per unit time (m^3/s), ϕ is the flux ($\text{m}^3/\text{m}^2\text{s}$), A is the cross-sectional area (m^2), D is the diffusion coefficient (m^2/s), $\Delta c/\Delta x$ (m^3/m^4), is the concentration gradient over a layer of thickness Δx (m) and $A = b \cdot h$, where b and h are the width (m) and height (m) of the piece of active surface considered. d is the diameter of a bubble detaching from the surface. When we estimate Δx to be in the order of the size of the bubble diameter d ($\Delta x \propto d$), see also figure VII.1, equation (VII.1) becomes:

$$\frac{dV}{dt} = D \Delta c h \quad (\text{VII.2})$$

For the rise velocity of a bubble with rigid walls (Stokes):

$$v = \frac{dh}{dt} = \frac{\gamma R^2 \Delta \rho g}{\eta} \quad (\text{VII.3})$$

where v is the rise velocity (m/s) and R is the bubble radius (m). From equation (VII.3) dt becomes:

$$dt = \frac{9 dh \eta}{2 R^2 \Delta \rho g} \quad (\text{VII.4})$$

Inserting equation (VII.4) into (VII.2) we get:

$$\frac{dV}{dh} = \frac{9 D \Delta c \eta}{2 R^2 \Delta \rho g} * h \quad (\text{VII.5})$$

or:

$$V = V_0 - \frac{9 D \Delta c \eta}{4 R^2 \Delta \rho g} * h^2 \quad (\text{VII.6})$$

Here h is the depletion height when $V = 0$.

Assuming a volume of liquid of 1 mm^3 travelling from $h = 0$ upwards with the same velocity as a bubble of that size (diameter 1 mm), with a gas content V_0 of 3 mm^3 gas (C1), we calculate that the gas content of that liquid volume will be zero when $h = 0.6 \text{ m}$. At the lowest gas concentration (C3), V_0 is 1.6 mm^3 and h is around 0.8 m.

When the bubble diameter is smaller than 1 mm, the rise velocity will be lower, so that the depletion height will be smaller. For example when $R = 0.1 \text{ mm}$, $h = 0.15 \text{ m}$, when $R = 0.05 \text{ mm}$, $h = 0.07 \text{ m}$ for C1. Although somewhat higher, these values are in the same order of magnitude as the sample heights used in the experiments.

A few of the assumptions that we have made are of course not correct. If rising bubbles have a certain velocity that does not implicitly mean that the liquid has the same velocity. Richardson and Zaki found that the velocity of a bubble swarm is equal to the Stokes velocity multiplied by the volume fraction taken up by bubbles to the power 2.4 (Beek and Mutzall, 1975). Therefore, in reality, the liquid velocity will be slower than estimated here, as only part of the liquid is entrained, but also because the liquid velocity will be reduced near the wall of the active surface due to friction. This implies that the height at which the gas content in the liquid is depleted will be lower than the estimates for h given above. Concluding, if we know exactly the circumstances of bubble size and liquid flow, more detailed calculations can be carried out. However, a first estimate gives good reason to believe that depletion is certainly an effect worth considering in low gas content systems like this one.

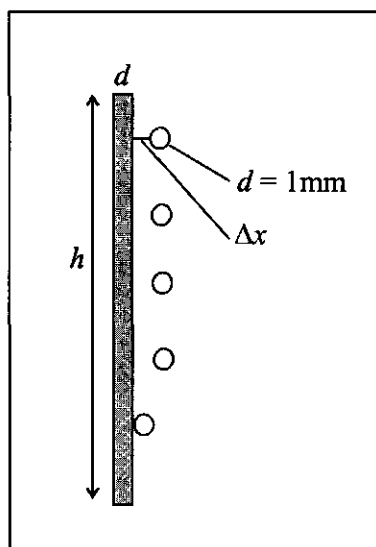


Figure VII.1 A schematic presentation of a bubble rising from an active surface.

GENERAL DISCUSSION AND CONCLUSIONS

The work presented in the last seven chapters is a result of semi-quantitative analysis of quantitative measurements. In order to evaluate the results with a more quantitative method, more and more reproducible results are needed. In this work, however, the decision was made to cover the whole field of processes that a bubble goes through from nucleus to attached bubble and until its arrival in the foam layer. With so broad a field, naturally the results are not as solid as to be able to make hard conclusions. Yet, a wide knowledge has been acquired of the great many processes that influence the formation and growth of a bubble, situated at a solid surface, and rising through the supersaturated liquid.

The main conclusion that can be taken from this work, is that a bubble can be stabilised in a solid porous material over a longer period of time if the contact angle between the liquid surface and the solid surface is large: the surface should be hydrophobic and not well wetted, so that the curvature of the bubble interface is concave with respect to the liquid phase (see also figure 2.4). This is one of the reasons that the selected "active" surface Tyvek is so suitable for a prolonged foam-activeness. The internal pores have such a geometry that the meniscus is concave with respect to the liquid phase, and the liquid cannot wet the pores. Furthermore, the size of the bubbles growing from such a surface can be controlled with the pore size only if the external surface of the site is well wetted by the liquid. The outside of the Tyvek surface is treated in such a manner that it is well wetted, a requirement to ensure the bubbles growing on the surface detach at a relatively small size. An extra advantage of the internal hydrophobicity is that the concave curvature of the liquid-gas interface disables the effect that the relatively large hinterland volume could have on the bubble formation.

Related to the curvature, is the wettability of the surface in contact with a liquid. It has also been shown quite convincingly that the degree of wetting has a large influence on the amount of sites that remain foam-active. A surface wetted with a liquid that permeates into all the pores hardly produces any foam when inserted into a gas supersaturated solution, whereas a surface with a low degree of wetting will produce a large volume of foam within seconds. The working hypothesis that pre-existent nuclei should be present in order to be able to form bubbles is found to be valid for the supersaturation levels used in this work.

The method with which the degree of wetting is measured is designed especially for heterogeneous porous materials such as Tyvek, and is found to be a quantitative tool for the measurement of the degree of liquid penetration into the material. It could, for example, also be used in the research of wetting and cleaning of textiles and other fibrous material.

Insight into the physical structure of the active surface and into the mechanism of foam formation has proven to be able to give valuable information. Comparing the theoretical prediction of foam formation from an active surface (section 6.5) to the practical measurements shows that with insight into bubble formation velocity, into the bubble size at detachment, and into an estimate of the amount of active site density of the material (depending on the degree of wetting) can result in a reasonable prediction of the amount of foam (and qualitatively how stable) that is produced from a sheet of Tyvek at a certain excess concentration of gas in liquid, and at a certain temperature. In reverse order, the surface area needed to produce a certain amount of foam within a period of time can be calculated. It should be noted that this method of making foam stops only then when the active surface is deactivated (taken out of the liquid) or when the liquid is no longer supersaturated.

It is interesting to view the different situations which the bubbles have undergone, as discussed in the various chapters of this thesis: I) In chapter 3 we looked at quiescent bubble growth, in which the bubble surface undergoes slow expansion. Ronteltap (1990(a) and (b)) studied the shrinkage of bubbles, where the bubble surface undergoes slow compression. II) In chapter 4 we applied a high shear deformation onto the bubbles, as a result of which the surface is both compressed and expanded. This is also true for bubble rise, presented in chapter 5, albeit that the deformation is much slower. III) Finally, in the foam layer, the bubbles are also submitted to slow dilation and compression.

When we compare the mass transport (or growth velocity) of gas to or from the bubble in all these situations, there are three situations where growth/shrinkage was hampered in some way. 1) During shrinkage, the bubble size decrease is almost stopped due to, according to Ronteltap, the surface dilatational viscosity. 2) In the case of the bubble rising through a gas supersaturated solution, the bubble in beer hardly grows, whereas the bubble in water grows prolifically. It seems then, that only in situations where only compression occurs, or where a low level of dilation and compression occurs, a barrier is created for gas transfer. For cases of only dilation, or a high level of dilation and compression, this is not the case.

A reason for these phenomena may be found in the “surface skin” theory: This surface skin can be created when a compression occurs, and can be held in place when the shear stress is not too high. This surface skin can perhaps decrease mass transfer, as was found also by Meijboom and Vogtländer (1974). However, when dilation is large, or when no compression at all occurs, the surface skin is continuously broken and gas transfer is not hampered in any way. An analogue can be found in sheets of ice lying on a lake: with large amount of wind, the ice sheets crack, and drift on top of each other at the low bank. With less wind, the ice sheet can become thicker and thicker.

Another important conclusion from this work, is that the reproducibility of the experiments was reduced as a result of effects such as gas depletion, as well as convection. Depletion occurs very quickly if the initial gas concentrations used are low. The first bubble will always be formed more quickly than the next and so forth, which gives a

natural decrease in reproducibility of the results, as shown in chapter 3. Convection is induced when the bubbles detach from the surface, and travel a certain distance through the liquid along that surface. In doing so, they entrain a similar volume of liquid along with them, which results in the movement of liquid. The greater the amount of simultaneously detaching bubbles, the more convection is induced. It is therefore imperative that this effect is accounted for when doing these kind of experiments. Diffusive gas transfer alone will not suffice in describing the mass transfer then.

References

Meijboom, F.W. and Vogländler, J.G. (1974) The influence of surface-active agents on the mass transfer from gas bubbles in a liquid II *Chem. Eng. Sci.* **29**, 857-861.

Ronteltap, A.D. and Prins, A. (1990) The Role of Surface Viscosity in Gas Diffusion in Aqueous Foams. II. Experimental *Colloids and Surfaces* **47**, 285-298.

Ronteltap, A.D., Damsté, B.R., Gee, M. de and Prins, A. (1990) The Role of Surface Viscosity in Gas Diffusion in Aqueous Foams. I. Theoretical *Colloids and Surfaces* **47**, 269-283.

SUMMARY

The amount and size of bubbles in a foam layer that have originated from a solid surface in a gas supersaturated solution is largely determined by the physical properties of that solid and liquid surface and the supersaturation level of the gas in the liquid. The presence of pre-existent nuclei - gas trapped in pores at the solid surface - as well as the wetting properties of the liquid on that surface contribute to the formation of the bubbles. The supersaturation level of gas in the liquid contributes to the rate at which this phenomenon occurs. The main objective of this study is to quantify their contributions in order to establish the relation between a) the physical properties of the supersaturated liquid and solid surface as well as the shapes of the liquid and the solid phases and b) the foam formation in a supersaturated solutions. Therefore: 1) the growth, detachment and rise of individual bubbles forming at an "active" site - a pre-existent nucleus trapped in a cavity in a solid surface - is studied, 2) based on this knowledge the requirements of an ideal "active" surface - a collection of "active" sites - is formulated, and 3) with a selected "active" surface, the hypothesis of the requirements are tested, by determining the foaming properties of the "active" surface in gas supersaturated solution.

In the process of bubble formation at an "active" site in a gas supersaturated solution, the following steps can be distinguished:

1) The growth of a bubble at an "active" site.

By using a model "active" site in the experiments- the tip of a glass capillary which is closed at one end - the following variables have been studied: the mouth radius of the "active" site, the supersaturation of the surrounding solution, the wetting behaviour of the "active" site, the flow of the liquid along the bubble, and dynamic surface properties.

We have observed the effect of the gas supersaturation on the individual bubble growth rate. With three different concentrations of carbon dioxide gas, the growth of individual bubbles on different sized glass capillaries were measured and compared to several growth models. The growth rates of the bubble could be best described by Bisperink's growth model, which takes into account the fact that the bubble is attached to a solid surface, for the movement of the bubble interface into the liquid as well as for the depletion of gas from the layer of liquid surrounding the bubble during growth (chapter 3).

During the experiments, it was observed that the formation of extra, unwanted bubbles, also called "parasite bubbles", influenced the bubble growth rate as a result of the entrainment of liquid. Due to this phenomenon, it was difficult to make a theoretical assessment of bubble growth rates. The opposite effect was also observed, namely at the lowest concentration, where after the formation of a single bubble, the liquid surrounding

the bubbles was so much depleted of gas, that the growth rate of the succeeding bubble was also affected (chapter 3).

The dynamic surface properties were found not to play an important part in the process of bubble formation as the velocity of growth was slow enough to keep the system close to equilibrium (chapter 3).

2) The detachment of a bubble from an “active” site.

By using the same glass capillary as model “active” site the following variables have been studied: the mouth radius of the “active” site, the angle of inclination of the “active” site, the surface tension and the surface rheological properties of the bubble surface, the hinterland effect, the bubble growth rate and the liquid flow around the bubble.

The volume of the detaching bubble has a linear relationship with the internal radius of the “active site”, for a well-wetted surface and as long as the shape of the bubble resembles a sphere (capillary radius < 0.5 mm). For a larger capillary size, and thus a large bubble size, the bubble resembles a pear shape (as shown on the cover of this thesis) and detaches with a smaller volume than predicted theoretically, as a result of mechanical instabilities (chapter 3).

When the capillary or model “active site” is tilted, the bubble size at detachment is decreased as a result of a lower effective adhesive force to the surface. The bubble size as a function of the tilting angle can be predicted theoretically, but experimental assessment of the theory shows some deviation (chapter 4).

To simulate the effect of liquid flow on bubbles attached to a solid surface, a horizontal oscillating movement was imparted to the capillary on which the bubbles grow. Increasing both amplitude and frequency of the oscillation decreases the size of the bubble at detachment. A theoretical examination of this phenomenon is given in chapter 4, and one of the conclusions is that the decrease in bubble size cannot be explained alone with the shear and inertial forces. We have suggested that a “surface skin” is formed, and that the bubble becomes unstable and detaches as soon as the surface skin is mechanically ruptured by shear forces parallel to the surface.

The internal volume of the cavity, also called the “hinterland volume” was found to have less effect on the bubble growth rate than was expected, as the dry internal walls of the cavity behaved more hydrophobically than expected. However, due to a sometimes considerable retreat of the air-liquid interface into the glass capillary after bubble detachment, it was concluded that a large hinterland volume could, in extreme cases, lead to an almost complete stop of bubble formation (chapter 3).

Surface rheological properties were found to be of influence on the detachment of bubbles under the influence of liquid flow. It was found that the bubbles detached at an earlier stage than could be predicted from forces alone. We therefore speculate that due to periodic surface expansion and compression, a “skin” is formed which, when ruptured, unbalances the bubble and induces it to detach (chapter 4).

3) The rise and growth of the detached bubble on its way to the foam layer.

In a model experiment, single bubbles released from a tilted capillary tip were studied during their rise through the liquid. Variables were: the bubble size, the surface rheological properties, the liquid viscosity, the travelled distance, the degree of supersaturation and the distance between two consecutive bubbles.

After the bubbles detach, they rise through the supersaturated liquid to the foam layer. In a gas supersaturated solution relatively free of surfactant, the bubbles are found to grow considerably during the travelled distance, but bubbles rising in a gas supersaturated solution like beer hardly grow during rise. It was therefore speculated that in beer, a surface "skin" could be formed at the bubble interface which is either mechanically too rigid to grow, or is partly insoluble to gas molecules which reduces the mass transfer of gas through the interface to the bubble (chapter 5).

Based on the knowledge obtained in the first part, the second part of this thesis was dedicated to formulating the requirements of an ideal "active" surface, selecting such an "active" surface, and relating the foamability to the material properties of that surface (chapters 6 and 7). From a fundamental point of view, an ideal "active" surface for the production of foam out of a supersaturated solution has to fulfil the following requirements:

- 1) The "active" sites are situated at such a lateral distance from each other that coalescence between neighbouring bubbles is prevented.
- 2) The number of "active" sites is big enough to produce a foam layer of pre-set volume in the required time.
- 3) The "active" surface is situated in a vertical position allowing that bubbles are formed on both sides.
- 4) The outside part of the "active" surface is hydrophilic to ensure a controlled small bubble size.
- 5) The inside surface of the "active" sites are hydrophobic to ensure a long shelf life of such "active" sites.

In an empirical set-up, a variety of surfaces was tested on their ability to produce a foam in a gas supersaturated solution. A suitable and very "active" surface, Tyvek, was selected for further study. The structure of this paper like material is very heterogeneous and porous. It is comprised of polyethylene fibres which are pressed together to form a hydrophobic porous matrix. The outside of this paper is made hydrophilic for printing purposes. This kind of structure could produce a great amount of bubbles simultaneously, and was stable in foamability. The liquid is prevented from entering the pores due to the hydrophobic nature of the material and due to the curvature of the liquid inside the pores, which makes the gas inside the Tyvek material stable over long periods of time, when submerged in the liquid (chapter 6).

The degree of internal wetting of the “active” surface is found to affect foam formation considerably. Almost complete wetting results in almost no bubble formation. When the surface is not previously wetted this may lead to extremely turbulent bubble formation. This proves our hypothesis that pre-existent nuclei are needed to help in the formation of bubbles at the levels of gas supersaturation used in this work. The “active” surface is doubly effective when it is placed in an upright position due to its two sides. A horizontal positioning of the surface leads to the formation of very large bubbles trapped underneath the surface, which help to destabilise the foam as soon as they become a part of that foam (chapter 6).

The surface area of the Tyvek used, and therefore the amount of “active” sites, has a direct effect on the initial rate of foam formation. For example, an area of 16 cm^2 forms a foam layer at a much faster rate than an area of 4 cm^2 . However, this latter surface may stay active for a longer period of time, as the dissolved gas in the solution is not exhausted as rapidly. Eventually, the bubble formation stops when the gas supersaturation in the liquid is exhausted. The surface, however, can be inserted into a fresh supersaturated liquid and the process starts anew (chapter 7).

With this work, we have shown that, in order to enable an “active” surface to foam, it should contain pre-existent nuclei trapped within pores or cavities and these should be stable over a long period of time. This can be accomplished with a material that contains pores or cavities with a hydrophobic internal surface. If this is not the case, the liquid will penetrate into the solid surface and dissolve the gas nuclei within. Without the gas nuclei, no foaming will occur at the gas supersaturation levels observed in this work.

SAMENVATTING

Het aantal en grootte van de gasbellen in een schuimlaag dat gevormd is aan een vast oppervlak in een met gas oververzadigde oplossing wordt grotendeels bepaald door de fysische eigenschappen van dat vaste oppervlak en het vloeistof oppervlak, en door de mate van gas oververzadiging in de vloeistof. De oververzadigingen, die in dit werk zijn gebruikt, zijn vergelijkbaar met die normaliter aanwezig zijn in koolzuurhoudende dranken. De aanwezigheid van reeds aanwezige gaskiemen - gas dat gevangen zit in poriën in het vaste oppervlak - alsook de bevochtigingseigenschappen van de vloeistof op dat oppervlak dragen bij aan de vorming van de gasbellen. De mate van oververzadiging draagt bij aan de snelheid van gasbelvorming. Het doel van dit onderzoek is om deze beide bijdragen te kwantificeren en de relatie te leggen tussen a) de fysische eigenschappen van de oververzadigde vloeistof en van het vaste oppervlak alsook de vorm van zowel vloeibare en gasfase en b) schuimvorming in gas oververzadigde oplossingen. Daartoe werd 1) de groei, het loslaten en het opstijgen van individuele gasbellen, die op een "actieve" plaats - een aanwezige gaskiem die gevangen zit in een vast oppervlak - gevormd zijn, bepaald, 2) op basis van deze informatie, de eigenschappen van een ideaal "actief" oppervlak - een collectie "actieve" plaatsen - geformuleerd en 3) de hypothese van deze eigenschappen getoetst aan de hand van een geselecteerd materiaal, door de schuimeigenschappen van dit oppervlak in een gas oververzadigde oplossing te meten.

Bij het belvormingsproces aan een "actief" oppervlak in een gas oververzadigde oplossing zijn de volgende stappen te herkennen:

1) De groei van een gasbel aan een "actieve" plaats.

Door gebruik te maken van een model "actieve" plaats - het uiteinde van een glas capillair dat aan de andere zijde afgesloten is - konden de volgende variabelen worden onderzocht: de straal van de opening van het capillair, de oververzadiging van de omringende oplossing, de bevochtiging van de "actieve" plaats, de vloeistofstroming langs de gasbel en dynamische oppervlakte eigenschappen van de vloeistof.

De rol van de gasconcentratie bij de groeisnelheid van de gasbellen is onderzocht. De groei van bellen op capillairen van verschillende grootte bij verschillende oververzadiging is gemeten en vergeleken met een aantal groeimodellen. De best overeenkomende was het model van Bisperink, die rekening houdt met het feit dat het belletje aan een wand vastzit, dat het gas-vloeistof grensvlak de vloeistof ingroeit en dat de vloeistofschil om de bel heen langzaam van gas uitgeput raakt (hoofdstuk 3).

Tijdens de proeven is opgemerkt dat extra, zogenaamde parasietbellen ontstaan die een menging van de vloeistof veroorzaken. Hierdoor wordt de toetsing van de theorie, die

aanneemt dat gas transport door diffusie plaatsvindt, bemoeilijkt. Bovendien blijkt dat het tegenovergestelde ook kan gebeuren: bij zeer lage gasconcentratie is de vloeistof rondom de bel zo uitgeput dat de volgende bel er ook last van heeft (hoofdstuk 3).

Bij de vorming van de gasbellen is ondervonden dat de dynamische oppervlakte eigenschappen geen rol spelen, waarschijnlijk omdat bij de relatief langzame belgroei het oppervlak min of meer in evenwicht is.

2) Het loslaten van de gasbel van de “actieve” plaats.

Door eveneens gebruik te maken van het model capillair werden de volgende variabelen onderzocht: de straal van de capillairenopening, de hoek waaronder het capillair geplaatst is, de oppervlaktespanning, de oppervlakte reologische eigenschappen van het oppervlak van de gasbel, het achterland effect, de belgroeijsnelheid en de vloeistofstroming langs de gasbel.

In hoofdstuk 3 wordt de vorming, de groei en het loslaten van individuele gasbellen, gevormd op een capillair, dat aan een zijde gesloten is, onderzocht. Het volume van de loslatende bel is lineair afhankelijk van de interne straal van het capillair, mits de interne wand van het capillair goed wordt bevochtigd, en mits de straal van het capillair kleiner is dan 0.5 mm. Grottere gasbellen worden peervormig (zoals te zien is op de omslag van dit proefschrift), en laten eerder los van de wand dan voorspeld als gevolg van mechanische instabiliteiten.

Als de capillair onder een hoek wordt geplaatst zal de bel een kleiner volume hebben bij het loslaten doordat de adhesiekracht die door de oppervlaktespanning wordt bewerkstelligd kleiner is. Dit volume is theoretisch te benaderen, maar experimenteel is dit moeilijk te bewijzen (hoofdstuk 4).

De vloeistofstroming langs vastzittende gasbellen is gesimuleerd door het capillair waar de bel op groeit een horizontaal oscillerende beweging te geven. Hiermee kan de grootte van de gasbel bij het loslaten worden verkleind. De afname in belvolume is niet geheel te verklaren door afschuifkrachten en traagheidskrachten. De verklaring ligt volgens ons in het ontstaan van een oppervlaktevel, dat bij mechanische breuk door afschuifkrachten parallel aan het oppervlak van de bel een instabiliteit veroorzaakt, waardoor de gasbel bij kleinere volume loslaat dan voorspeld (hoofdstuk 4).

Het interne volume van het capillair, ook wel het achterland genoemd, blijkt minder effect te hebben op de belgroeijsnelheid dan theoretisch verwacht. Dit wordt waarschijnlijk veroorzaakt door een slechtere bevochtiging van het droge interne oppervlak van het capillair dan verwacht. Desalniettemin kan het gas-vloeistof grensvlak zover terugdringen in het capillair na het loslaten van een bel, dat er in sommige extreme gevallen geen nieuwe gasbel meer ontstaat op het capillair (hoofdstuk 3).

3) De opstijging en de groei van de losgelaten gasbel op weg naar de schuimlaag.

In een model experiment worden individuele gasbellen, losgelaten van een onder een hoek geplaatste capillair, gevolgd tijdens hun stijging door de vloeistof. Variabelen

zijn: de belgrootte, de mate van oververzadiging en de afstand tussen opeenvolgende bellen.

Nadat de bellen loslaten, stijgen zij door de vloeistof naar de schuimlaag.

Gedurende de opstijging zullen deze bellen verder groeien. In gas oververzadigde vloeistof waar geen oppervlakte actieve stoffen in zitten, blijken de belletjes flink door te groeien. In het geval van een oververzadigde oplossing van oppervlakte actief materiaal, groeien de belletjes niet of nauwelijks. Dit effect zou eveneens kunnen worden verklaard door het ontstaan van een oppervlaktelevel dat ofwel mechanisch te stijf is, ofwel gedeeltelijk onoplosbaar is voor gasmolekülen waardoor het transport van gasmolekülen door het gasbel-grensvlak geremd wordt (hoofdstuk 5).

Op basis van de opgebouwde kennis uit het eerste deel van dit proefschrift, wordt het tweede deel gewijd aan het formuleren van de eisen die gesteld worden aan een ideaal "actief" oppervlak, aan de selectie van een dergelijk oppervlak en aan het leggen van een relatie tussen de schuim- en de fysische materiaal eigenschappen van dat "actief" oppervlak (hoofdstukken 6 en 7). Vanuit een fundamenteel oogpunt gezien zou een ideaal "actief" oppervlak de volgende eigenschappen moeten hebben om reproduceerbaar schuim te kunnen vormen in een gasoververzadigde oplossing:

- 1) De "actieve" plaatsen zijn op een zodanige laterale afstand van elkaar verwijderd dat buurbellen niet kunnen coalesceeren.
- 2) Het aantal "actieve" plaatsen is groot genoeg om schuim van een vooraf gesteld volume in een bepaalde tijd te kunnen vormen.
- 3) Het "actief" oppervlak is verticaal geplaatst zodat aan weerszijde gasbellen kunnen vormen.
- 4) De buitenzijde van het "actief" oppervlak is hydrofiel om op een gecontroleerde wijze kleine bellen te kunnen vormen.
- 5) De binnenzijde van de "actieve" plaats is hydrofoob om een langdurige activiteit van de plaats te bewerkstelligen.

Met behulp van een empirische methode, zijn een scala aan oppervlakken getest op hun vermogen schuim te vormen in een gasoververzadigde oplossing. Hieruit werd Tyvek als beste geselecteerd voor verder onderzoek. De structuur van Tyvek is heterogeen en poreus. Het bestaat uit fibres van polyethyleen, die samengeperst zijn tot een poreus filter. Deze structuur kan bewerkstelligen dat veel bellen tegelijkertijd geproduceerd worden en bovendien zorgt de hydrofobie en de porievorm ervoor dat het gas in het materiaal stabiel blijft, ook als het materiaal ondergedompeld wordt voor langere tijd (hoofdstuk 6).

De mate van bevochtiging blijkt een grote rol te spelen in de schuimvormings-capaciteit van het materiaal. Een nagenoeg totaal bevochtigd oppervlak blijkt bijna geen schuim te kunnen vormen. Een oppervlak dat niet van tevoren is bevochtigd produceert een kolkende zwerm gasbellen als deze wordt ondergedompeld in een gasoververzadigde oplossing. Dit bewijst dat onze hypothese over de noodzaak van reeds aanwezige gasfase

voor de belgroeい correct is. Het Tyvek oppervlak is zeer doeltreffend mits het rechtop in de vloeistof wordt geplaatst. Als het oppervlak plat liggend in de vloeistof wordt geplaatst, vormen er grote bellen aan de onderzijde, die, eenmaal in het schuim, dat schuim kunnen destabiliseren (hoofdstuk 6).

De grootte van het Tyvek oppervlak dat gebruikt wordt in de proef, ofwel het aantal "actieve" gaspockets, heeft een direct effect op de initiële schuimvormingssnelheid. Bij voorbeeld heeft een oppervlak van vier bij vier centimeter een hoeveelheid schuim gevormd in een veel kortere tijd dan een oppervlak van twee bij twee centimeter. Het kleinste oppervlak blijft dan wel langer actief, aangezien daar de vloeistof minder snel is uitgeput. De schuimvorming houdt uiteindelijk op als de oververzadiging uitgeput is. Toch zal het oppervlak weer actief worden als het in een verse gasoververzadige vloeistof wordt ondergedompeld (hoofdstuk 7).

Met dit werk hebben wij kunnen aantonen dat een actief oppervlak slechts schuimt als het reeds-aanwezige gaskiemen bezit en als deze kiemen stabiel zijn gedurende langere tijd. Dit kan worden bewerkstelligd met een materiaal dat poriën bevat met een hydrofoob intern oppervlak. Als dit niet zo is, zal de vloeistof het materiaal binnendringen en de gaskiemen doen oplossen. Zonder gaskiemen treedt geen schuimvorming op bij de mate gas oververzadiging waarbij in dit proefschrift gewerkt is.

NAWOORD

Nou, dat was het dan, vijf jaar lang zwoegen, en eindelijk is het proefschrift af, tenminste, als het ooit af is. En eerlijk gezegd was dit boekje er nooit gekomen, zonder de hulp van een groot aantal mensen. Bij deze zou ik al diegene willen bedanken die mij hebben geholpen met succes tot deze dag te komen.

Professor Prins, uw altijd positieve instelling heeft mij vaak uit een dal getrokken, en uw altijd constructieve kritiek heeft een bijzondere indruk achtergelaten op dit werk. Altijd was u aanwezig om rare uitkomsten te bespreken, altijd liet u uw eigen mening op de achtergrond- ik moest zelf maar bepalen wat ik wilde doen. De manier waarop u met mensen omgaat heeft mijn bewondering. Door u heb ik geleerd zeer zelfstandig te werk te gaan , maar tevens niet de hulp van anderen te schuwen.

Jan Kempers, ik heb het zeer gewaardeerd dat je tot het einde toe mijn hoofdstukken hebt willen nakijken ook al had je intussen een andere functie.

Hans Bos, jou wil ik graag bedanken voor de zinnige discussies. Het was zeer verhelderend om met iemand die zo'n verschillende insteek heeft te kunnen praten.

Mijn collega's van de - toen nog - sectie Zuivel en Levensmiddelennatuurkunde ben ik erkentelijk voor een ontzettende leuke tijd. Voornamelijk Frank, Marlies, Chris, Coen, Aliza, Arne, Andrea en Martin Bos hebben vaak genoeg mijn frustraties moeten aanhoren, en hebben mij er ook weer bovenop geholpen. De werkgroep Grensvlak Reologie vond ik een zeer nuttige plek om op wat dieper niveau mijn werk te bespreken.

Gerbert, ik ben blij dat je mij een jaartje hebt kunnen helpen, die proeven waaren nooit uitgevoerd zonder jou. Marjo, danzij jou zijn we veel te weten gekomen over belgroei onder invloed van vloeistofstroming.

Verder zijn natuurlijk onontbeerlijk geweest voor dit onderzoek de mensen van de fotolokatie, speciaal Boudewijn en Bo; van de werkplaats, Hans en Eric; en van de glasblazerij, Gert Nieuwboer. Felix Thiel van het ATO-DLO heeft gedurende enkele maanden moeite gedaan om mooie SEM beelden te maken van het Tyvek materiaal. Mijn collega's bij DMV, bedankt voor de extra tijd die mij gegund was om dit proefschrift af te ronden, en voor het getoonde begrip.

Jens, jij bent het laatste jaar degene geweest die mij continu heeft gesteund als ik het niet meer zag zitten; en dat terwijl je het zelf zo druk had met "that damned thesis"! Ik ben blij dat je zulke brede schouders hebt!

Familie en vrienden, het is afgelopen met het eindeloze excuus " ik moet nog wat aan mijn proefschrift werken", vanaf nu kan ik er niet meer onderuit... Ik heb weer alle tijd!

CURRICULUM VITAE

Antien Frances Zuidberg werd op 15 september 1966 te Raamsdonk geboren. In de periode 1977-1984 volgde zij voorbereidend wetenschappelijk onderwijs op de Lycee Français te Antananarivo, Madagascar, Port Moresby International High School te Port Moresby, Papua Nieuw Guinee en op het Vrije Atheneum te Paramaribo, Suriname.

Daaropvolgend, in september 1984, koos zij voor de studie Levensmiddelentechnologie aan de Landbouwhogeschool (thans Landbouwuniversiteit) te Wageningen. Zij koos voor de afstudeervakken Levensmiddelennatuurkunde en Levensmiddelenchemie. Voor de hoofdrichting levensmiddelennatuurkunde is in 1990 een stageperiode gevolgd bij het Unilever Research Laboratorium, Colworth House in Engeland. In juni 1991 slaagde zij voor het doctoraal examen.

In augustus 1991 is zij aan een promotieonderzoek begonnen bij de sectie Zuivel en Levensmiddelennatuurkunde (vakgroep Levensmiddelentechnologie) aan de Landbouwuniversiteit. Het onderzoek is gefinancierd door een zogenaamde "derde geldstroom" financier, waarvan dit proefschrift het resultaat is.

Vanaf 1 mei 1996 is zij werkzaam bij DMV International, een divisie van Campina Melkunie, te Veghel.